Department of Geosciences
University of Fribourg (Switzerland)

A novel approach to estimate glacier mass balance in the Tien Shan and Pamir based on transient snowline observations

Thesis

presented to the Faculty of Science and Medicine of the University of Fribourg (Switzerland)
in consideration for the award of the academic grade of Doctor of Philosophy in Geography.

by

Martina Barandun

from

Feldis, Graubünden

Thesis Number 2099
Printed at Uniprint, Fribourg
2018

Accepted by the Faculty of Science and Medicine of the University of Fribourg (Switzerland) upon the recommendation of Dr. Matthias Huss (supervisor), Prof. Dr. Martin Hoelzle (supervisor), Dr. Tobias Bolch (external expert), and Dr. Antoine Rabatel (external expert) as well as the jury president Prof. Dr. Bernard Grobety.

Fribourg, 25 September 2018

Thesis supervisors

Prof. Martin Hoelzle

Dr. Matthias Huss

Dean

Prof. Christian Bochet

Summary

Glaciers are recognised as an excellent proxy for climate change and their centennial mass loss has accelerated during the past decades. The Central Asian mountain ranges Tien Shan and Pamir host over 25,000 glaciers that have been observed to respond heterogeneous to climate change. Glacier changes in the region have very important consequences on the water availability for the densely populated lowlands. Despite the significance and severity that climate change exerts on the Central Asian water towers, the glacier response is still poorly understood, hampering sound interpretations and predictions of future threats and opportunities. A significant data gap in the field measurement series from the mid-1990s to around 2010, limits the analysis of long-term trends. Despite the recent efforts to re-established the historical cryospheric monitoring network, continuous long-term glacier mass balance time series remain sparse for Central Asia. Thus, improved temporal and spatial coverage of glacier monitoring is essential.

Remote sensing techniques are a powerful tool to study a large number of remotely located and unmeasured glaciers and provide a possibility to partly bridge the aforementioned deficit in data availability. However, the coarse temporal resolution of geodetic mass balance assessments is not suitable to improve the understanding of ongoing processes. This accentuates the indispensable need for improved and extended annual to seasonal observations of mass change of inaccessible and remote glaciers on a cost and labour effective basis as well as for a more elaborated and enhanced, process-orientated methodology.

This work provides a combination of detailed in situ measurements and remote sensing based glacier mass change observation from local to regional scale. A multi-level strategy is applied to complement data from long-term glaciological surveys and remote sensing (snowline observations and geodetic mass balance measurements) with numerical modelling to obtain information at high temporal and spatial resolution for individual glaciers. Through modelling constrained with transient snowlines, annual mass balance time series for a large amount of glaciers located in the Tien Shan and Pamir were made available. Such mass balance estimates provide valuable baseline data for climate change assessments, runoff projection, hazard evaluation and enhance process understanding. A better understanding of the regional annual variability of glacier response to climate change in the Pamir and Tien Shan became possible based on the outcome of this thesis.

In the presented thesis the results are discussed in detail, the weaknesses and strengths of the developed methodology are unfolded and the relevant perspective and future research outlined.

Zusammenfassung

Gletscher sind ausgezeichnete Indikatoren für den Klimawandel. Ihr langjähriger Massenverlust hat sich in den letzten Jahrzehnten weltweit akzentuiert. Die zentralasiatischen Bergketten Tien Shan und Pamir beherbergen über 25'000 Gletscher. Studien zeigen, dass diese Gletscher heterogen auf den Klimawandel reagieren. Gletscherveränderungen in der Region haben wichtige Auswirkungen auf die Wasserverfügbarkeit für das dicht besiedelte Flachland. Trotz den bedeutenden Konsequenzen welche durch den Klimawandel auf diese regionalen Wasserspeicher ausgeübt wird, ist die Veränderung der Gletscher im Tien Shan und Pamir immer noch relativ unbekannt, was fundierte Interpretationen und Vorhersagen zukünftiger Gefahren und Chancen erschwert. Eine prägnante Datenlücke in den existierenden Messreihen von Mitte der 1990er Jahren bis ca. 2010 schränkt eine detaillierte Analyse langfristiger Entwicklungen weiter ein. Trotz der jüngsten Bemühungen, das historische Kryosphäremessnetz wieder herzustellen, bleiben kontinuierliche Langzeitmessungen für die Gletscher in Zentralasien limitiert. Eine verbesserte zeitliche und räumliche Abdeckung der Gletscherbeobachtungen ist daher unerlässlich.

Fernerkundungstechniken sind gängige Methoden, um eine große Anzahl abgelegener und unerforschter Gletscher zu untersuchen. Mit solchen Methoden kann das Defizit an Datenverfügbarkeit der Region teilweise kompensiert werden.

Die grobe zeitliche Auflösung der geodätischen Massenbilanzberechnungen und das somit limitierte Prozessverständnis unterstreichen jedoch den unabdingbaren Bedarf nach verbesserten und erweiterten jährlichen bis saisonalen Massenbilanzbeobachtungen. Abschätzungen auf ausgedehnter räumlicher Skala, sowie eine stärkere Prozess orientierte Forschung sind nötig.

Die vorliegende Arbeit beschreibt eine Kombination aus detaillierten Feldmessungen und Fernerkundungsbeobachtungen der Gletschermassenänderung im Tien Shan und Pamir. Die angewandte Strategie basiert auf mehreren Ebenen aus lokalen bis regionalen Studien. Mit dieser Strategie werden Daten aus langzeit-glaziologischen Feldmessungen und aus der Fernerkundung (Schneelinienbeobachtungen, geodätische Massenbilanzmessungen) mit numerischen Modellierungen komplementieren. Dabei werden Informationen für ausgewählte Gletscher mit hoher zeitlicher und räumlicher Auflösung extrahiert. Durch das Modellieren mit wiederholten Schneelinienbeobachtungen, welche zur Kalibrierung verwendet werden, konnten jährliche Massenbilanzzeitreihen für eine große Anzahl von Gletschern im Studiengebiet berechnet werden.

Solche grossräumigen und zeitlich hochaufgelösten Abschätzungen liefern wertvolle Grundlagen für detaillierte Studien über die Auswirkungen des Klimawandels, ermöglichen fundierte Abflussprojektionen und erlauben verbesserte Gefahrenanalysen. Basierend auf

den Ergebnissen dieser Arbeit, wird ein besseres Verständnis der regionalen jährlichen Variabilität der Gletscherreaktionen auf den Klimawandel im Pamir und Tien Shan ermöglicht.

In der hier vorgelegten Arbeit werden die Resultate im Detail diskutiert, die Schwächen und Stärken der entwickelten Methodik offengelegt und die relevanten Perspektiven abgefasst.

Contents

List of Abbreviations

AAR	Accumulation Area Ratio
ALOS	Advanced Land Observing Satellite
ASTER	Advanced Spaceborne Thermal Emission and Reflection Radiometer
AWS	Automatic Weather Station
CAIAG	Central Asian Institute for Applied Geosciences
CATCOS	Capacity Building and Twinning for Climate Observing Systems
CAWa	Central Asian Water
CHARIS	Contribution to High Asia Runoff from Ice and Snow
CICADA	Cryospheric Climate Services for improved Adaptation
DDF	Degree Day Factor
DEM	Digital Elevation Model
dGPS	Differential Global Positioning System (dGPS)
ECV	Essential Climate Variables
ELA	Equilibrium Line Altitude
ERA-Interim	European Centre for Medium-Range Weather Forecasts Reanalysis
ETM+	Enhanced Thematic Mapper Plus
GCOS	Global Climate Observing System
GFZ	Geoforschungs Zentrum Potsdam
GHOST	Global Hierarchical Observing Strategy
GLIMS	Global Land Ice Measurements from Space
GLOF	Glacier Outburst Flood
GPR	Ground Penetration Radar
GTN-G	Global Terrestrial Network for Glaciers
HMA	High Mountain Asia
HMM	Hidden Markov Model
IceSat	Ice, Cloud, and land Elevation Satellite
IRH	Internal Reflection Horizon
LiDAR	Light Detection and Ranging
MAAT	Mean Annual Air Temperature
MEERA	Modern Era Retrospective-analysis for Research and Applications
MMASTER	MicMac for ASTER
MSS	Multispectral Scanner System
NCAR	US National Center for Atmospheric Research
NCEP	US National Centers for Environmental Prediction
NEESPI	Eurasia Earth Science Partnership Initiative

NDSI	normalized difference snow index
NIR	Near Infrared
NSIDC	US National Snow and Ice Data Center
OLI	Operational Land Imager
RMSE	Root Mean Square Error
SANIGMI	Central Asian Hydrometeorological Institute
SAR	synthetic aperture radar
SCAF	Snow-Covered-Area Fraction
SDC	Swiss Agency for Development and Cooperation
SfM	Structure-from-Motion
SMB	Surface Mass Balance
SNSF	Swiss National Science Foundation
SPOT	Satellite Pour l'Observation de la Terre
SRTM	Shuttle Radar Topography Mission
SVM	Support Vector Machine
SWIR	Shortwave Infrared
TanDEM-X	TerraSAR-X add-on for Digital Elevation Measurement
TI-model	Temperature-Index Model
TIR	Thermal Infrared
TM	Enhanced Thematic
TSL	Transient Snowline
UAV	unmanned airborne vehicles
VIS	Visible Light
VNIR	Visible and Near Infrared
WGMS	World Glacier Monitoring Service
WSL	Eidgenössische Forschungsanstalt für Wald, Schnee und Landschaft

Part I

Thesis Synopsis

Chapter 1

Introduction

1.1 Significance and state of glacier mass balance observations in Central Asia

Glaciers are reliable indicators for climate change (Bojinski et al, 2014). Most glaciers around the world are in retreat and mass loss has accelerated during the past decades (Zemp et al, 2015). Glaciers in High Mountain Asia (HMA) have been observed to respond heterogeneously to climate change (Scherler et al, 2011; Bolch et al, 2012; Kääb et al, 2012). This is not only connected to diverging climatological settings, including very humid conditions as well as extremely arid, continental environments (Schiemann et al, 2007; Yao et al, 2012; Maussion et al, 2014; Sakai and Fujita, 2017), but also relates to a contrasting glacier area-altitude distribution (Fujita and Nuimura, 2011). The Central Asian mountain ranges Tien Shan and Pamir form the north-western margin of HMA. There, glacier change assessments are comparably sparse but indicate a similarly complex and diverse pattern (Gardner et al, 2013; Farinotti et al, 2015; Brun et al, 2017; Wang et al, 2017).

Under a continental and arid climate regime, glacier and snow melt, are important water resources for the highly populated lowland (Konovalov and Shchetinnicov, 1994; Schaner et al, 2012; Chen et al, 2016). Ice melt contribution to runoff is especially relevant for years of droughts, as it bridges water shortage during precipitation-poor periods (Kaser et al, 2010; Pohl et al, 2017). Under a changing climate, accelerated glacier mass loss causes a peak discharge followed by decreasing glacier melt input to the river systems during the consecutive years. In Central Asia peak water is expected to occur within the next few decades (Duethmann et al, 2015; Huss et al, 2017). Huss and Hock (2018) showed that changes in glacier melt contribution to runoff affects the major Central Asian river basins severely. The uncertainty of water availability in the context of a changing climate creates a major potential for political tensions and builds a complex set of future threats, affecting different domains such as water management, energy production and irrigation (Stocker et al, 2013; Varis, 2014). The situation is specifically critical when water resources are shared over national borders (Munia et al, 2016) as for instance in Central Asia.

Glacier mass balance time series are eminently used for the assessment of the relation between mass balance and climate (e.g., Dyurgerov and Meier, 2000; Kaser et al, 2006)

but also to investigate the climate impact on runoff (e.g., Konovalov and Shchetinnicov, 1994; Immerzeel et al, 2010; Huss and Hock, 2018), glacier related hazards (e.g., Kääb et al, 2005b) or sea level rise (e.g., Meier et al, 2007). In the 1950s, an extensive system of cryospheric monitoring was launched under the auspices of the USSR committee for the international hydrological decade and the measurements were intensified during the following decades (Dyurgerov et al, 2002; Kuzmichenok, 2009). The majority of these in situ monitoring programmes stopped with the breakdown of the USSR. Data originating from the monitoring activities are usually published in Russian language. Most of the data is not digitally available, and access to archives is often politically restricted. Only on two glaciers in the Tien Shan, monitoring activities were maintained after the decay of USSR in the mid-1990s: Tuyuksu Glacier, Kazakhstan, and Urumqi Glacier (No. 1), China. For this two glaciers almost continuous mass balance series exist since the Mid-1950's (WGMS, 2017). Efforts to re-establish in situ glacier monitoring on other formerly monitored glaciers have started since around 2010.

To fill the gap of missing glaciological observations, alternatively, several studies employed remote sensing techniques to map glacier area fluctuations (e.g., Bolch, 2007; Khromova et al, 2003; Shangguan et al, 2006; Khromova et al, 2006; Narama et al, 2010; Ozmonov et al, 2013) and assessed glacier volume changes on catchment scale (e.g., Aizen et al, 2007; Bolch et al, 2011a; Pieczonka and Bolch, 2015; Holzer et al, 2015; Li et al, 2017; Goerlich et al, 2017) or more regionally (e.g., Gardner et al, 2013; Gardelle et al, 2013; Lin et al, 2017; Brun et al, 2017; Wang et al, 2017). Furthermore, a few annual mass balance series are available from modelling studies (Li et al, 2011; Farinotti et al, 2015; Liu and Liu, 2016). Detailed region-wide mass balance time series with a high temporal resolution are still lacking for Central Asia.

1.2 Research state in glacier mass change observations

Pioneer mass balance observations reach back to the late 19th century and a first worldwide collection of information about ongoing glacier changes was initiated in 1895 (Hall, 1895a; Forel, 1895). With the establishment of the International Geological Commission, annual reporting on glacier variations became systematic and moved from more qualitative assessments (e.g., Forel, 1881, 1892; Hall, 1895b; Reid, 1895; Forel and Du Pasquier, 1896; Muret, 1900; Brückner, 1907; Reid, 1911; Mercanton, 1916a) to quantitative analysis of glacier changes (e.g., Ahlmann, 1922; Mercanton, 1932, 1948; Mercanton and Renaud, 1951). After the late 1940's the focus shifted from glacier front and area change observations to mass balance assessments (Haeberli, 1998). With the International Hydrological Decade (1965 to 1974), glacier monitoring was connected to energy balance and hydrological observations and Hoinkes (1955) and Hoinkes (1968) proposed specific methods to investigate glaciers systematically. Guidelines concerning data acquisition were published by the United Nations Educational, Scientific and Cultural Organization (UNESCO) within the same decade (Haeberli, 1998) and with the introduction of the report series "Fluctuation of Glaciers" in the late 1960's standardised data on glacier length, area, volume and mass changes have since been published on regular basis (e.g., Kasser and Muller, 1967; Muller et al, 1977). Observation techniques have evolved into standardised and computer-based procedures, applied on glaciers in a wide range of different mountain ranges. With the establishment of the World Glacier Monitoring Service (WGMS) in the mid-1980s, an institution aiming on the collection and provision of glacier fluctuation and inventory data was born. Efforts emerged in the 1990s to develop a tiered observation strategy for glacier monitoring that ever since has regularly been updated to include recent technical and methodological advances (Haeberli et al, 2000; Haeberli, 2006; GCOS, 2010, 2016). Today, Tier 1 refers to multi-component observation systems across environmental gradients. Tier 2 addresses detailed process-oriented studies and model calibration. Tier 3 incorporates the collection of long-term annual mass balance measurements within the major mountain systems, Tier 4 addresses long-term observations of glacier length change and Tier 5 aims on the establishment of glacier inventories from remote sensing imagery (Haeberli, 2006). The for this thesis most relevant state-of-the-art research on glacier mass balance, contributing to the gradual improvement of the aforementioned strategy is outlined hereafter.

1.2.1 Direct and indirect methods

Glaciological measurements

The procedures of glaciological field measurements have been developed in the 1940's and changed only little since. Glaciological surveys, consisting of point measurements, provide typically results at seasonal to annual resolution, and deliver valuable datasets even if tied to only a few samples (Zemp et al, 2015). Main weaknesses of the method are the labour and cost intensity. Remote locations remain often unmeasured, and selecting suitable and representative glaciers is challenging (Hoelzle et al, 2003; Fountain et al, 2009). To obtain a glacier-wide surface mass balance (SMB), the point measurements need to be inter- and extrapolated over the entire glacier area. Essential uncertainties are related to the spatial distribution of the in situ observations and results are sensitive to the choice of an adequate extrapolation method (Hock and Jensen, 1999; Escher-Vetter et al, 2009). Under-sampling of inaccessible glacier areas (i.e. due to crevasses, steep slopes or avalanche zones) can lead to high and often poorly assessed uncertainties (Zemp et al, 2013). Such

under-sampling is usually more important for the accumulation zone (Escher-Vetter et al, 2009), causing often a disequilibrium of measurement densities between regions of mass gain and loss within the same survey. Recent studies couple the traditional techniques to modern technologies (i.e. ground penetration radar (GPR) surveys (Machguth et al, 2006a; Sold et al, 2016), Light Detection and Ranging (LiDAR) surveys (Helfricht et al, 2014a; Fischer et al, 2016), cosmic ray neutron sensing measurements (Howat et al, 2018)) to integrate more detailed seasonal to annual snow accumulation data. However, most of these techniques still require elevated costs and labour, and so far, are not established in mass balance monitoring. Alternatively, high resolution remote sensing stereo-images might have the potential to monitor seasonal to annual snow accumulation on a low-cost and labour base (Shean et al, 2016). Nonetheless, reliable high temporally resolved spaceborne surveys are yet hampered through limited sensor repeat cycles.

Geodetic method

Comprehensive monitoring programmes include periodical geodetic surveys of changes in glacier surface elevation based on topographic maps and space or airborne digital elevation models (e.g., Kuhn et al, 1985; Miller and Pelto, 1999; Kuhn et al, 1999; Cox and March, 2004; Azam et al, 2016; Wang et al, 2014a). Periodic validation and calibration of annual glaciological time series with decadal geodetic estimates significantly improved the robustness and uncertainty estimates of long-term series (e.g., Thibert and Vincent, 2009; Andreassen and Engeset, 2016). With increasing availability and quality of remote sensing products, the methodology will certainly advance in the future. However, survey and generic differences (i.e. internal and basal balance) impede direct comparison of the two approaches (Cogley, 2009; Zemp et al, 2013). Zemp et al (2013) recommended a systematic re-analysis of glaciological mass balance series in combination with geodetic assessments as a standard procedure for every monitoring programme and proposed a conceptual framework. Thibert et al (2008a) provides a comprehensive overview of random and systematic errors connected to both methods.

Today the indirect (i.e., without direct access to the glacier) geodetic method of remote areas has found widespread applications for regional assessments (e.g., Gardner et al, 2013; Gardelle et al, 2013; Brun et al, 2017). Most geodetic mass balance calculations, however, are typically limited to a decadal to semi-decadal temporal resolution and thus, fail to capture seasonal to annual mass balance variations. Next to a range of technical limitation related to sensor characteristics such as unknown penetration depth of radar systems (e.g., Berthier et al, 2006; Dehecq et al, 2016) or errors of image geometry related to sensor motion (jitter) (Girod et al, 2017b), the volume-to-mass conversion can introduce important bias (Zemp et al, 2013). Huss (2013) suggested a conversion factor of $850 \pm 60\,\mathrm{kg\,m^{-3}}$. A value that is forthwith frequently adopted without further consideration for a wide range of different conditions, besides the author's statement that this factor is not constant over space and time, and might vary considerably due to changes in firn layers and the density profile. At the current stage of research, remote sensed mass change observations are generally limited to relatively coarse temporal resolution, and large discrepancies between the results of different studies which is particularly the case for HMA (e.g., Gardner et al, 2013; Gardelle et al, 2013; Kääb et al, 2015; Brun et al, 2017) implies important uncertainties and limitations. Paul et al (2017) gives a comprehensive overview of potential error sources and a strategy to assess the quality of area, velocity and elevation changes derived from different remote sensing products.

1.2.2 Mass balance modelling

Glaciological measurements have frequently been used for mass balance model calibration in order to reconstruct past SMBs (e.g., Vincent, 2002; Azam et al, 2014) or to project future changes (e.g., Radić and Hock, 2006). Further, model simulations might help to interconnect different levels of observations such as point measurements of mass balance or runoff data and are useful for mass balance extrapolation in space and time (Machguth et al, 2006b). Thereby, they provide valuable data for regions and periods where glaciological surveys are sparse (Braithwaite, 1981) and help to improve detailed process understanding (Machguth et al, 2006b). Thus, glacier monitoring and modelling are closely interconnected (Machguth et al, 2006b). Whereas the main purpose of mass balance modelling has been connected to the understanding of the climate and its changes (e.g., Male and Granger, 1981; Pelto et al, 1990; Oerlemans and Fortuin, 1992), water resource management provided the overall motivation for snow and ice melt simulations at an early stage of the modelling history (e.g., Braithwaite, 1981; Lang, 1986). The first accumulation and ablation models operated on a point scale and coarse temporal resolution (Hock, 2005). Today, distributed mass balance models with different complexity on enhanced temporal resolution found widespread use for various purposes, such as sea level rise estimates (e.g., Huss and Hock, 2015; Jackson et al, 2018), runoff (e.g., Immerzeel et al, 2015; Huss and Hock, 2018) and climate change assessments (e.g., Marzeion et al, 2018), or for glacier dynamic investigations where they are coupled to flow models (e.g., Clarke et al, 2015; Pope et al, 2016). However, such distributed models demand the extrapolation of the meteorological input variables that can provoke significant uncertainties.

In recent years, the integration of remote sensing data into mass balance modelling, regarding both calibration (Huintjes et al, 2016) and validation (e.g., Azam et al, 2014; Kronenberg et al, 2016), became increasingly popular. Nevertheless, spaceborne data, so far, could not compensate the use of glaciological measurements for model calibration.

Huss et al (2008) pointed out the value of a model-based extrapolation of point measurements to calculate glacier-wide seasonal to annual SMBs, and to re-analyse existing long-term series. The authors use a distributed mass balance model that is automatically optimized to best reproduce all glaciological measurements, which are available within an extensive monitoring program. Using this method, glacier-wide SMBs remain closely tied to the observation. Through the close link to the mass balance survey, the model is relatively insensitive to meteorological input and model parameters. The same approach has further been used to correct for heterogeneous survey periods, facilitating comparisons to decadal geodetic mass changes (Huss et al, 2009) for re-analysis of glaciological time series as proposed by Zemp et al (2013).

1.2.3 Including snowline observations

A range of other indirect methods that allow mass balance assessments from air- and spaceborne platforms, have been developed to bridge the disadvantages of the above-mentioned methods. Glacier changes of remotely observable quantities such as variation in the extent of the accumulation area (e.g., Dyurgerov et al, 2009; Bahr et al, 2009), alteration in median glacier elevation (e.g., Sakai et al, 2015; Sakai and Fujita, 2017) or in the area altitude distribution (e.g., Tangborn, 1999) have been used to predict glacier response to recent climate change. Rabatel et al (2017) provides a review of three alternative optical remote sensing methods based on snowline, albedo and snow cover mapping, developed to quantify seasonal and annual SMBs. In particular, the mapping of the end-of-summer snowline on optical remote sensing imagery as a proxy for the equilibrium-line altitude

(ELA) and/or the accumulation area ratio (AAR) found widespread use to reconstruct SMB series of individual glaciers (e.g., Kulkarni, 1992; Rabatel et al, 2005, 2012) or of entire catchments (e.g., Kuhn, 1989; Zemp et al, 2007; Rabatel et al, 2016; Tawde et al, 2017). The use of ELA / AAR to predict the mass balance is hereinafter referred as the ELA / AAR - method.

ELA / AAR - Method

The ELA-concept is a theoretical concept indicating the position of zero mass balance along a glacier (Oerlemans, 2001). The ELA cannot be observed directly. However, it can be approximated through observations of the snowline on a glacier surface at the end of the balance year. Pioneer work such as by Lliboutry (1965) and LaChapelle (1962) investigated in detail the relationship between the end-of-summer snowline observed on remote sensing imagery, the ELA and the SMB. Repeated snowline observations using aerial photographs (e.g., Chinn and Whitehouse, 1980; Chinn, 1995; Kaser and Georges, 1997; Chinn et al, 2005) or satellite imagery (e.g., Fujita and Nuimura, 2011; Rabatel et al, 2012; Guo et al, 2014) have since been used to relate year-to-year snowline elevation variability to changes in climate.

Kulkarni (1992) established a simple linear regression between the ELA and observed annual SMBs. Dyurgerov et al (1992), however, showed that the ELA to SMB association is more accurately approximated with the hypsographic curve, than with a simple linear function, and Mikhalenko (1990) explained that the AAR to SMB relation is approximately linear for a majority of glaciers. The robustness of the AAR method was underlined by Kamniansky and Pertziger (1996) through detailed investigations on Central Asian glaciers.

Braithwaite (1984a) quantified the glacier surface mass balance from the altitudinal difference between the ELA for a given year and the balance-budget ELA multiplied by a time- and space-average of the mass balance gradient around the ELA. This gradient was determined from long-term in situ measurements. The authors, however, pointed out the problem of regional application due to the highly variable gradient used as a region-wide constant in their study.

Based on Braithwaite (1984a), Rabatel et al (2005) quantified annual SMB using remotely observed end-of-summer snowlines. Mass changes derived from geodetic methods in combination with long-term ELA and observed balance gradients are used to estimate the steady-state ELA. Hence, the method reduces the need of direct measurements to a minimum. The authors acknowledge a high spatial and temporal variability of the mass balance gradients but showed that results did not significantly decline when using a regional average, and consequently concluded a region-wide application for valid. Rabatel et al (2008) reconstructed the SMBs for a glacier in the French Alps from 1981 to 2005 through a combination with modelling constraint to direct measurements and Rabatel et al (2016) calculated SMBs for 30 glaciers without direct observations in the French Alpes for an even larger time period. The mass balance gradient was adopted for both studies from Rabatel et al (2005) and held constant over space and time. For a basin-wide assessment, Kulkarni et al (2004) replaced the earlier proposed ELA with the AAR to establish a linear function to annual SMB summarized for two glaciers of the basin. The authors used remotely sensed end-of-summer snowlines for the extrapolation to basin scale. A temporally and spatially constant relationship was assumed. Whereas basin wide application might be pertinent as shown in Letréguilly and Reynaud (1989) and Rabatel et al (2005), extrapolation over long time intervals might not strictly hold, due to possible

mass balance regime shifts under ongoing climate change and changes in the glacier geometry that can influence the relation between the SMB and ELA / AAR on a long-term (Braithwaite, 1984a; Dyurgerov and Dwyer, 2000).

An acknowledged limitation for using the end-of-summer snowline as a proxy for ELA / AAR relates to the restricted image acquisition and quality, so that available snowline observations do not always conform to the end of the ablation season. Kulkarni et al (2004) mapped transient snowlines (TSL) on a weekly basis on low-resolution satellite scenes in order to avoid such misinterpretations. However, the coarse resolution might introduce additional uncertainties when used for individual glaciers. Molotch and Margulis (2008) argued that use of higher resolved data with lower repeat cycles is preferential for snow cover mapping. Tawde et al (2017) tried to overcome the same problem by using a mass balance model calibrated with TSL to predict end-of-summer snowlines. In their study, TSL observations are simultaneously used to calibrate and validate the model, and calibration is restricted to a few glaciers of the basin only. Hence, predicted snowlines might be subject to large uncertainties related to the mass balance modelling. Rabatel et al (2016) conversely avoids an inter- and extrapolation of the TSL observations arguing that the uncertainties introduced with modelling are similar to the misjudgement of the end-of-summer snowline elevation due to limited image availability. Mernild et al (2013b) used a second-order polynomial regression to predict the highest point of the TSL to estimate the ELA. The TSL rise might follow such a function. However, a decrease of the snowline is usually related to sudden snowfall events, and thus the proposed function might not be accurate. Shea et al (2012) extended the approach by Rabatel et al (2005) and quantified the annual glacier-wide SMB by combining the altitude of regional end-of-summer snowlines with the glacier hypsography and different SMB gradients above and below the ELA. However, the time-space dependent gradients and limited image resolution and availability remained an issue. Wu et al (2014) tested comprehensively the assumption of the end-of-summer snowline as a proxy for the ELA and highlights two additional concerns: (1) detection is not straightforward when the snowline rises above the firnline; and (2) no theoretical relation to the ELA exists when the snowline rises above the upper glacier edge.

The use of transient snowlines

Dyurgerov et al (1994) suggested replacing the ELA to SMB relation with observations of transient ELA and transient SMB. Consequentially, extensive mass balance surveys during one summer season might be sufficient to cover the entire range of functions between SMB and ELA. The authors also showed that the relation is valid for transient ELA along most of the altitudinal profile for glaciers with summer accumulation. The applicability of the method was found to be critical for years with very low equilibrium lines (Kamniansky and Pertziger, 1996), and Hock et al (2007) identified a sensitivity to variations in quantity of winter accumulation.

Østrem (1973) proposed a defined relationship between the transient ELA and the TSL, and highlighted the regular depletion pattern of the snowline for many glaciers following nearly the elevation contours. The benefit of the information content stored in the rate of change of TSL has found recognized utility since. Applications of temporal changes of the snowline / snow cover observed on time-lapse photography and / or repeated satellite imagery were most frequently used for snow depletion monitoring (e.g., Parajka et al, 2012), model validation (e.g., Miller and Pelto, 1999) or model calibration (e.g., Turpin et al, 1997; Rott et al, 2007). Pelto et al (2013) and Huintjes et al (2015b) suggested to

estimate the elevation of the ELA at the end of the mass balance year, by extrapolating the rate of change of the TSL observed on Landsat images during the summer months to the climatically defined end-of-ablation season and Miller and Pelto (1999) used the rate of change of rise in TSL to reconstruct annual ablation rates for years with missing field data. Thereby, the snow depletion pattern during the summer months was related to measured snow ablation from other years, and under the assumption of a relatively constant relationship between ice and snow depletion over time, the SMB was estimated based on TSL observations. Mernild et al (2013b) validated the use of the TSL changes as a measure for the quantity of winter snow melt with a known mass balance gradient and Pelto (2011) suggested the extrapolation of the observed relation between TSL rise and winter snow depletion to nearby glaciers with presumably similar balance gradients but missing glaciological measurements.

Snow cover observation on multiple optical sensors in combination with snow melt modelling was used to estimate snow accumulation on non-glaciated catchments (e.g., Mittaz et al, 2002; Molotch and Margulis, 2008; Farinotti et al, 2010). The applied method assumes that at the location where the snow cover has depleted, the modelled melt is equal to the accumulated snow during winter. This backward modelling concept was retaken by Huss et al (2013) and Hulth et al (2013) to infer winter snow accumulation along repeated TSL observations over the glacier surface, assuming that at the TSL position all winter snow has melted but ice melt did not yet start. Whereas Hulth et al (2013) calibrated a melt model using direct ablation measurements and emphasized the use of the remotely sensed TSL to infer a correct winter accumulation, Huss et al (2013) resigned completely from the use of field observations. The authors relied on the combination of a relation between the transient SMB and the TSL to infer the sub-seasonal mass balances based simply on the information content stored in the rate of change of the TSL and its position on repeated oblique photography.

1.3 Motivation and project context

The recommended multi-level strategy for glacier monitoring provided within the framework of the Global Climate Observing System (GCOS) (GCOS, 2010, 2016) aims at connecting intense local studies with glacier observation at a regional to global scale (Haeberli et al, 2007). The strategy attempts to integrate detailed in situ mass balance measurements on individual reference glaciers, long-term observations of glacier length changes on an extended number of glaciers and repeated inventories at decadal intervals based on remote sensing. So far, however, no suitable methodology that combines observations of glacier mass changes at high temporal and spatial resolution could be incorporated into the described strategy. In order to extend glacier monitoring to a larger sample, new methods are required that allow a remote determination of the seasonal to annual SMB and deal with limited input data but still meet the expected level of reliability and spatial / temporal resolution. The combination of different well-established concepts is needed to develop new schemes for improved regional estimates and to assess so far unmeasured glaciers.

Glacier mass changes in the Tien Shan and Pamir have very important consequences on the water availability for the densely populated lowlands. Despite the significance and severity climate change exerts on the Central Asian water towers, the heterogeneous glacier response is still poorly understood, hampering sound interpretations and predictions of future threats and opportunities. Extensive research is needed to improve the current knowledge about spatio-temporal changes in the water cycle of Central Asian headwater catchments (Sorg et al, 2012; Unger-Shayesteh et al, 2013; Gan et al, 2015). Improved temporal and spatial coverage of glacier monitoring is thus essential. Notwithstanding, a significant data gap in the field measurement series from the mid-1990s to around 2010 impede sound interpretations of long-term trends. So far, on a global scale, glacier monitoring is relatively under-represented in Central Asia (Dyurgerov et al, 2002; Zemp et al, 2015). The scarcity of reliable and appropriate meteorological and glaciological datasets, as well as the heterogeneity of both, their spatial and temporal extent, hamper a sound synthesis of a regional picture (Unger-Shayesteh et al, 2013). Bolch (2017) stressed the demand for improved monitoring of meteorological variables in high altitudes for HMA and the necessity of more remote sensed glacier mass change observations. Remote sensing techniques are a powerful tool to study a large number of remote and unmeasured glaciers on a cost-effective basis, and can partly bridge the aforementioned deficit in data availability (e.g., Kääb et al, 2015; Brun et al, 2017; Wang et al, 2017). However, the discrepancy and disagreement between region-wide assessments presented for HMA in literature (e.g., Gardelle et al, 2013; Kääb et al, 2015; Farinotti et al, 2015) as well as the coarse temporal resolution accentuate the indispensable need for (i) improved and extended ground measurements, for (ii) a more elaborated and enhanced methodology to observe mass change on elevated temporal / spatial resolution on a regional scale and (iii) for more process-based research.

A comprehensive insight into glacier mass changes in Central Asia is thus required. A combination of intense in situ studies with glacier observation at a regional to global scale enables to bridge weaknesses and shortcomings of a single method and provides accurate and reliable baseline data for climate change assessments, runoff projection and hazard evaluation. In the framework of this PhD project, a multi-level strategy is applied combining data from long-term in situ measurements and remote sensing (snowline observations, geodetic mass balance measurements) by numerical modelling, to obtain information of glacier mass change at high temporal and spatial resolution on a regional scale. With the

approach developed within the framework of this thesis, the quantification of the accumulation and ablation rates with seasonal to sub-seasonal resolution for unmeasured glaciers is targeted. The project aims to provide a contribution to overcome some of the basic problems of accurate water resource management in this region by providing an in-depth understanding of one of the most important components within the water cycle in the arid parts of Central Asia. Results will be relevant for a better understanding of the regional, annual variability of glacier response to climate change in the Pamir and Tien Shan.

Besides the scientific work of this thesis substantial efforts have been put into activities promoting the re-establishment of glacier monitoring in Central Asia which started eight years ago and evolved substantially throughout the duration of this thesis. In situ data necessary for this work were acquired only thanks to this joint monitoring effort by local and international scientists. Independently from the scientific objectives and results of this work, the scientific collaboration and exchange between the Universities of Fribourg as well as the University of Zurich and the Central Asian research institutions will further improve the urgently needed knowledge transfer and will provide a sustainable capacity building in glacier monitoring, which has suffered after the collapse of the former Soviet Union.

This thesis is conducted in the frame of the project "Snowline observations to remotely derive seasonal to sub-seasonal glacier mass balance in the Tien Shan and Pamir Mountains", a study supported by the Swiss National Science Foundation (SNSF), grant 200021_155903. The Capacity Building and Twinning for Climate Observing Systems 1 & 2 (CATCOS: 2011-2017) as well as the follow-up project Cryospheric Climate Services for improved Adaptation (CICADA: 2017-2021) together with Central Asian Water (CAWa) aimed at the re-establishment of modern glacier monitoring in Central Asia after a 15 year measurement gap. The related activities were connected to intense capacity building programmes to raise a sound basis for fundamental scientific research (e.g., Schöne et al, 2013; Hoelzle et al, 2017). The projects are based on a close cooperation between local scientists (Central Asian Institute for Applied Geosciences (CAIAG) and Kyrgyz Hydromet, Kyrgyzstan; UZHydromet, Uzbekistan and Centre for Cryosphere, Institute of Water Problems, Hydropower Engineering and Ecology, Tajikistan) and multinational actors from the University of Fribourg, the GFZ Potsdam (GeoForschungsZentrum), and the WGMS. The here presented thesis is fundamentally interconnected with the mentioned projects and builds on mutual exchange of knowledge, data and funding.

1.4 Thesis objectives and structure

1.4.1 Objectives

The main aim of the thesis is to develop a methodology, which would provide an automated, low cost and effort solution for calculating mass balance for large amount of glaciers located in the Central Asian mountain ranges on annual time scales.

This leads to the following main research questions:

- What is the past and current rate of mass change of selected reference glaciers in the Tien Shan and the Pamir?
- How can the monitoring of changes in the TSL position based on terrestrial cameras or satellite images support the re-establishment, reanalysis and reconstruction of long-term mass balance measurement series in Central Asia?
- Is it possible to obtain seasonal to annual glacier-wide SMB estimates from modelling constrained with remote observed snowlines throughout the melting season for the Tien Shan and Pamir?
- What is the accuracy of the snowline-based determination of the SMB in comparison to direct glaciological measurement and geodetic surveys?
- Is repeated satellite imagery suitable to monitor the snowline evolution for a large number of glaciers, i.e. to determine region-wide SMB at high temporal resolution?

Figure 1.1 schematically illustrates how a chain of methodological developments have been linked to finally tackle the main research question. The chosen strategy moves stepwise from a local to a more regional assessment, with a strong focus on enhanced temporal / spatial resolution of the outcome. To accomplish the above outlined objectives, efforts to re-establish sustainable and modern glacier monitoring on five selected glaciers in Central Asia have been supported throughout the entire duration of the PhD project (**Paper I**). Historical long-term mass balance series available for the region have been re-analysed and data gaps were filled for Abramov Glacier (**Paper II**), and for Golubin, Batysh Sook and Glacier No. 354 (see Appendix A) for which mass balance monitoring were resumed within the CATCOS project. A novel TSL constrained modelling approach has been tested and refined on three Kyrgyz glaciers (**Paper III**) and was applied in combination with multi-annual geodetic surveys on regional scale to estimate the annual mass balance of a large amount of glaciers in the Tien Shan and Pamir (**Paper IV**).

1.4.2 Outline of the thesis

This thesis is divided into three parts: **Part I** constitutes of four chapters forming the synopsis of the thesis. *Chapter 1* gives an introduction into the significance of mass balance measurements in Central Asia, the current state of research, outlines the motivation of the project and introduces the study site. In *Chapter 2* a short thematic and methodological background is given and in *Chapter 3* the research papers as part of this thesis are summarized. A synthesis of the obtained results is provided in *Chapter 4*. This chapter aims to relate the outcomes of the research papers to the scientific context described in the previous chapters. The chapter ends with concluding remarks retaking the main research questions of this thesis and provides an outlook on potential future research. **Part II**

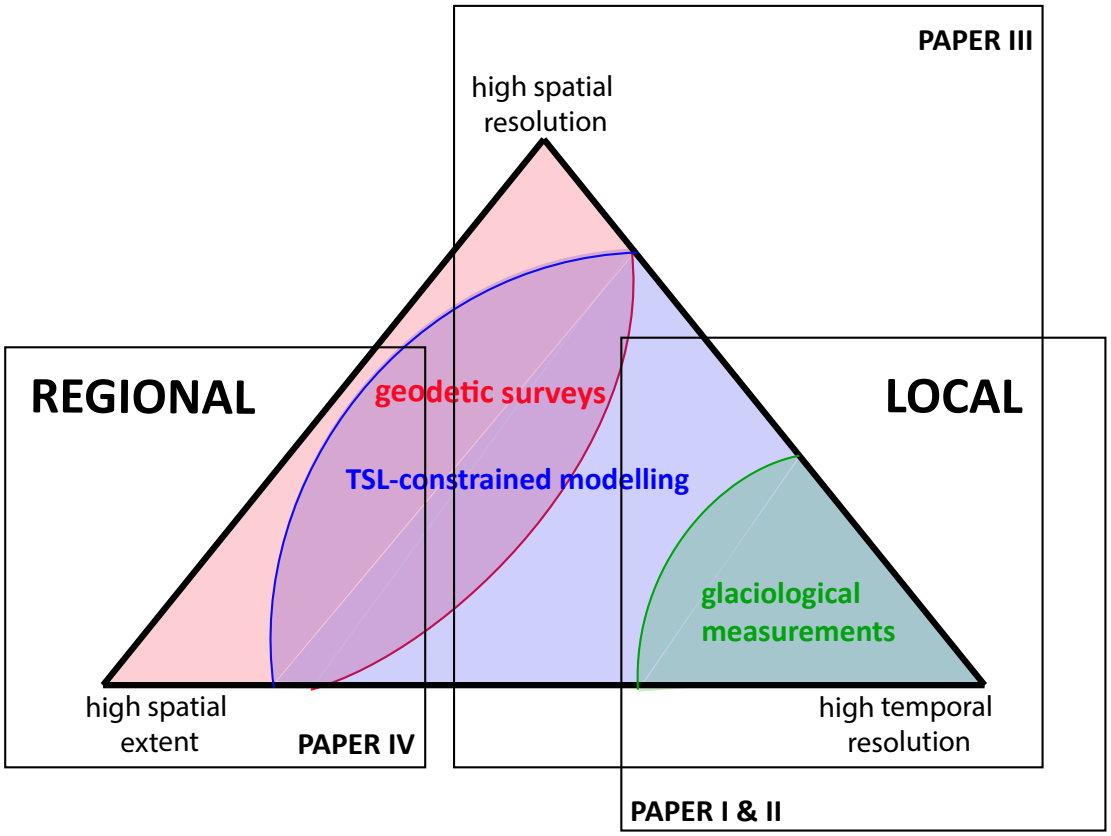

Figure 1.1: Summary of research structure, following from a local to regional scale with the aim to improve temporal / spatial resolution of the mass change observations of glaciers situated in the Tien Shan and Pamir.

contains full versions of the four research papers that are either published or in preparation for peer-reviewed journals and compose the main part of this thesis. In the papers, methodological details, extended data and study site descriptions as well as detailed results and their discussions in the light of certain aspects of the thesis objectives can be found herein. In **Part III** the appended material is provided. This includes the supplementary materials describing all additionally conducted research related to this thesis, curriculum vitae and the personal bibliography.

1.5 Study site

1.5.1 Climatic setting

Central Asia forms part of High Mountain Asia and is a mostly semi-arid region (Barry, 1992). The principal mountain systems are the Tien Shan and the Pamir (Fig. 1.2). Synoptic large-scale meteorological conditions over Central Asia are influenced by the main direction of the zonal flow of the air masses from west to east. According to Schiemann et al (2008) also meridional airflow can occur either in situations when tropical air masses enter from south and south-west or when north-westerly, northerly and sometimes even north-easterly cold air masses intrude into Central Asia. A deflection of trade winds at the western orogen margin to the north and to the south cause intense precipitation (Pohl et al, 2017). Due to a barrier effect, arid and cold conditions dominate in the eastern part of both the Tien Shan (Dyurgerov et al, 1994) and Pamir (Glazirin et al, 1993; Fuchs et al, 2013; Pohl et al, 2017) with precipitation maxima towards the summer (Barry, 1992, Fig. 1.3). A pronounced west to east gradient in seasonal precipitation distribution for the Tien Shan (Dyurgerov et al, 1994) and the Pamir (Glazirin et al, 1993), produces regional variable accumulation and ablation regimes and mass balance gradients. Figure 1.3 summarizes the long-term monthly precipitation sums and the monthly mean annual temperature for three meteorological stations located in the Pamir-Alay (Abramov), the Central Tien Shan (Alplager) and the Northern / Western Tien Shan (Tien Shan (Kumtor)).

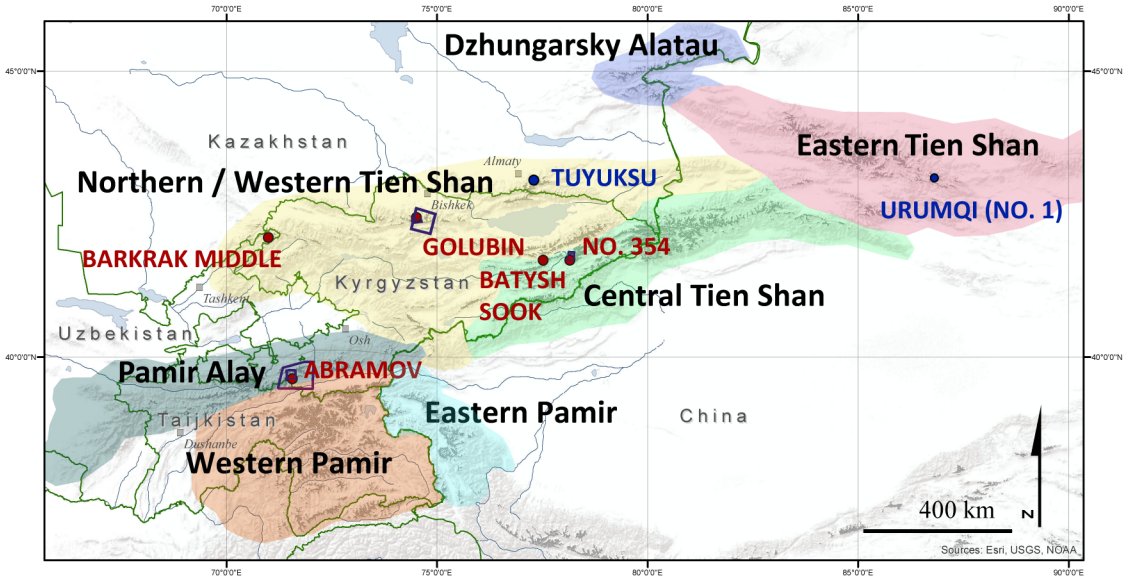

Figure 1.2: Overview map of the study region. The subregion of the Tien Shan are shown in blue (Dzhungarsky Alatau), red (Eastern Tien Shan), yellow (Northern / Western Tien Shan), in light green (Central Tien Shan) and of the Pamir in dark green (Pamir-Alay), in orange (Western Pamir) and in light blue (Eastern Pamir). The locations of all glaciers with long-term mass balance series used in this thesis are indicated in blue and red. The glaciers monitored within the CATCOS and CICADA project are shown in red. The footprints of the high-resolution images available are indicated in purple.

A consistent temperature increase of about 0.1 to 0.2° C per decade during 1960 to 2007 with more pronounced warming in the winter months and a rise in precipitation was

reported for the Tien Shan (Aizen et al, 1996; Kutuzov and Shahgedanova, 2009; Kriegel et al, 2013). For the Pamir, Pohl et al (2017) detected a temperature increase from 0.07 to 0.11° C per year for the last decades but could not identify a clear precipitation trend. As a consequence of increasing air temperature and decreased fraction of solid precipitation with ongoing climate change, snow cover and glacier area decrease was reported for large parts of Central Asia (Bolch et al, 2012; Sorg et al, 2012; Unger-Shayesteh et al, 2013). This was accompanied by a shift in the timing of the onset of the melt season towards the earlier spring (Unger-Shayesteh et al, 2013). Aizen et al (1997) reported a reduction of the maximum snow thickness and snow cover duration over the entire Tien Shan from 1940 to 1991 by 0.1 m and 9 days, respectively. However, certain regions in the Eastern Tien Shan and Pamir tended to have increased average snow cover duration due to altered solid precipitation amounts and distributions that counter balanced the effect of the air temperature increase (Dahe et al, 2006; Sorg et al, 2012; Zhang and Kang, 2017).

Temperatures measurements in a 90 m borehole in the accumulation area of Gregoriev Glacier located in the Central Tien Shan showed negative temperatures throughout the entire profile with a maximum close to −4° C at the bottom (Takeuchi et al, 2014). Recent ice temperature measurements at the tongue of Batysh Sook (Central Tien Shan) also showed temperatures well below zero degrees (see Appendix A). Measurements from firn pits and ice cores at Abramov (Pamir-Alay) from the 1970s indicated similarly a polythermal state of the glacier (Kislov and Nozdryukhin, 1975; Suslov et al, 1980). However, currently available data of Abramov suggested ongoing changes of the thermal regime (personal communication M. Kroneneberg, H. Machguth and I. Lavrentiev). Further studies are however needed to investigate such possible regime shifts in more detail.

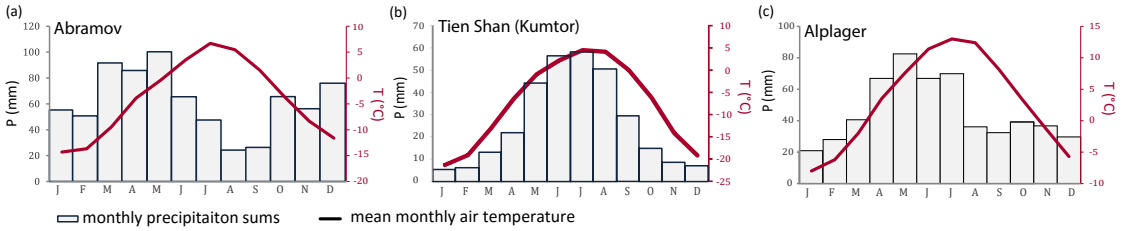

Figure 1.3: Mean monthly air temperature (T) and monthly precipitation sums (P) for the meteorological station at Abramov (1968-1994) at 3837 m a.s.l., for the Tien Shan (Kumtor) station (1997-2014) at 3660 m a.s.l. and the Alplager station (1992-2010) at 2145 m a.s.l.

1.5.2 Glacierisation in Central Asia

The Tien Shan hosts almost 15'000 glaciers, covering a surface area of 12'385 km^2 (according to the Randolph Glacier Inventory Version 6.0 (RGIv6.0; RGI-Consortium, 2017). The mountain range is conventionally divided into Western / Northern Tien Shan (glacierised area: 2265 km^2), Eastern Tien Shan (glacierised area: 2209 km^2), Central Tien Shan (glacierised area: 7269 km^2) and Dzhungarsky Alatau (glacierised area: 520 km^2; Fig. 1.2; Bolch et al, in press). Median glacier elevations is highest for Central Tien Shan ($\approx$ 4200 m a.s.l) and ranges from 3700–4200 m a.s.l. for the other subregions (based on RGIv6). Glaciers in the west are usually of winter-accumulation type, whereas summer accumulation regimes become more frequent towards the east (Dyurgerov et al, 1994) where a combination of low temperature and summer precipitation maximum is more common (Kutuzov and Shahgedanova, 2009). Region-wide geodetic mass balance assess-

ments agree on a glacier mass loss for the Tien Shan during the past two decades (results range between ≈−0.3 to −0.7 m w.e. yr^{-1} for different subregions and periods Gardner et al, 2013; Farinotti et al, 2015; Brun et al, 2017) and accelerated mass loss since the 1970s was reported (e.g., Sorg et al, 2012; Farinotti et al, 2015).

The Pamir is commonly separated into the Eastern Pamir, Western Pamir and Pamir-Alay (Fig. 1.2; Bolch et al, in press). Pamir-Alay contains over 3'000 glaciers (1848 km^2; based on RGIv6.0; RGI-Consortium, 2017). Western Pamir is much larger, hosting almost 10'000 glaciers that span an area of about 8'461 km^2 (based on RGIv6.0; RGI-Consortium, 2017). The median glacier elevation in Western Pamir (≈ 4800 m a.s.l) is almost 1000 m higher than the median elevation of glaciers in the Pamir-Alay. The highest median glacier elevations are found for the Eastern Pamir (≈5000 m a.s.l). Mass change assessments show quite large divergence and range from a close to balanced budget (≈+0.14 to −0.13 m w.e. yr^{-1}; Gardelle et al, 2013; Gardner et al, 2013; Brun et al, 2017) to strongly negative mass balances (≈−0.48 to −0.52 m w.e. yr^{-1}; Kääb et al, 2015; Pohl et al, 2017).

1.5.3 Monitored glaciers

Most historical long-term glacier monitoring programmes distributed through the Tien Shan and Pamir-Alay (Fig. 1.2) were interrupted in the mid-1990. A part of the detailed and extensive historical measurements could be collected and digitized. However, there is still a vast amount of data to be rediscovered and saved from oblivion. A systematic digitizing and storing of the data collected during the former Soviet Union in regional and open-accessible data centers is needed. Since 2010, several monitoring sites have been (re-)established and thereafter continuously measured (Fig. 1.2). The glacier monitoring networks on five glaciers, re-established within the CATCOS and CICADA, and relevant for this thesis, are portrayed hereafter. A more detailed description can be found in the individual publications.

Barkrak Middle Glacier

Barkrak Middle is located in the Oygaing valley in the Pskem catchment in the Western / Northern Tien Shan, Uzbekistan (Fig. 1.2). Between 1960 and 2010, the glacierised area decreased by 23% in the Pskem River catchment (Semakova et al, 2016). The area of Barkrak Middle is ∼2.18 km^2 (Semakova et al, 2016) and spans an elevation range of 3500 to 4100 m a.s.l. (as of 2017). The glacier has three tributaries. Length change observations exist from 1971 to 1990 and glaciological measurements were carried out in the 1960's but were not available for this work. There are two meteorological stations in the valley at different elevations, which have been operated since 1930's. The Oygaing avalanche station (2200 m a.s.l.) conducts daily measurements of air temperature, soil temperature, air moisture, atmospheric pressure, precipitation, wind direction and wind speed. Additionally, daily runoff measurements from March to September are measured at two locations. Maidantal hydrological station (1500 m a.s.l.) conducts runoff measurements at three points. The daily measurement period is from March to September, when, apart from river level, water and air temperature is measured. In 2016, a modern glacier monitoring network was emplaced including, an Automatic Weather Station (AWS), an automatic terrestrial camera and a dense ablation stake network of 11 stakes on the orographic left and middle tributary (Fig. 5.11). In 2017, the stake network was extended to the orographic right part with an additional four stakes. Annual snow profiles and snow probings were carried out on the middle and left tributary of Barkrak Middle. Semakova

et al (2016) proposed a geodetic mass change of -0.82 ± 0.36 m w.e. yr^{-1} from 2000 to 2012 based on DEM differencing from SRTM and TanDEM-X data.

Golubin Glacier

Golubin is located in the Ala Archa valley in the Kyrgyz Ala-Too in the Western / Northern Tien Shan (Fig. 1.2). The glacier has an area of $\sim$5 km^2 (as of 2016) and spans an elevation range of about 3400 m a.s.l. to 4300 m a.s.l. There are several meteorological stations located in the valley and measurements reach back until 1930's (i.e. Baitik at 1200 m a.s.l., Alplager station at 2145 m a.s.l.). Intense glacier and meteorological monitoring started in 1958 and continued until 1994 when the monitoring programme was stopped (Aizen, 1988). Front variations reach back until the 1860's and have been re-analysed in Aizen et al (2007). In summer 2010, surface mass balance measurements were re-initiated and a fully equipped monitoring network including an AWS ($\sim$3300 m a.s.l.), an extensive mass balance network (13 ablation stakes and 1-4 snow pits) and two snowline cameras emplaced in 2013 (Fig. 5.8). For Golubin, the geodetic mass loss reported by Bolch (2015) was -0.46 ± 0.24 m w.e. yr^{-1} from 1964 to 1999 and -0.28 ± 0.96 m w.e. yr^{-1} from 2000 to 2012, whereas Brun et al (2017) found a geodetic mass balance of -0.04 ± 0.19 m w.e. yr^{-1} for the period $\approx$2002 to 2013. Reconstructed mass balance from 1901 to present reveal a mass loss of -0.17 ± 0.45 m w.e. yr^{-1} (see Appendix A).

Glacier No. 354

Glacier No. 354 is situated in the Akshiirak massif in the Central Tien Shan (Fig. 1.2). The glacier covered a surface area of about 6.4 km^2 in 2016. The accumulation zone comprises three basins. The glacier spans an elevation range of $\sim$3750 to 4680 m a.s.l. An AWS, today owned by the Kumtor Gold Mine, installed at an elevation of $\sim$3660 m a.s.l. and a distance of approximately 10 km to the glacier, recorded continuous meteorological data since 1997 (Fig. 1.3b). Before, a meteorological station close to the meteorological station delivered data since 1930 (Kutuzov and Shahgedanova, 2009). No historical glaciological measurements are available for this glacier. Since 2010, in situ mass balance measurements have been obtained for Glacier No. 354 annually in late summer and an automatic camera enables snowline monitoring since 2014 (Fig. 5.10). Kronenberg et al (2016) provided the reconstructed mass balance for the past decade and revealed a mass loss of -0.43 ± 0.09 m w.e. yr^{-1} from 2003 to 2014. Goerlich et al (2017) reported a mass loss of -0.30 ± 0.1 m w.e. yr^{-1} from 1964 to 1980, Pieczonka and Bolch (2015) provided an estimate of -0.79 ± 0.25 m w.e. yr^{-1} from 1975 to 1999 and Brun et al (2017) of -0.46 ± 0.19 m w.e. yr^{-1} from $\approx$2002 to 2014. Glacier No. 354 was selected to replace the previously monitored Sary-Tor glacier due to access restrictions due to mining activities. Sary-Tor has historical mass balance observations from 1985 to 1989 (Dyurgerov et al, 1994), and its mass balance was reconstructed for the period 1930 to 1988 by Ushnurtsev (1991). In recent years, joint efforts between Kyrgyz and Russian scientists led to the re-initiation of the monitoring on Sary-Tor.

Batysh Sook Glacier

Batysh Sook (also named Suyok (Suek) Zapadniy or Glacier No. 419 in earlier studies) is located in the Sook range in the Central Tien Shan in Kyrgyzstan (Fig. 1.2). The small glacier covered an area of $\sim$1 km^2 (as of 2016) and an altitudinal range of 3950 to 4450 m a.s.l. Sporadic mass balance measurements have been carried out between the

1970s and 1980s. The Tien Shan (Kumtor) AWS is located in a distance of ∼32 km. The re-establishment of the glacier long-term monitoring program in 2010 included an observation network of seven stakes and two snow pits measured at annual visits in late summer (Fig. 5.9). The monitoring network has been improved in the following years to increase the representativeness of ablation and accumulation measurements to a total of 14 ablation stakes and four snow pits. The observed cumulative glacier frontal retreat since 1975 summed up to around 0.32 km. Kenzhebaev et al (2017) reconstructed a mass balance of -0.39 ± 26 m w.e. yr^{-1} from 2003 to 2016. A volume change for the entire Sook range of −21% was reported by Hagg et al (2013). The glacier additionally is subject for the location of an annually repeated summer school for local and regional young scientists organized in the framework of the CATCOS and CICADA projects since 2015.

Abramov Glacier

Abramov is located in the Pamir-Alay (Fig. 1.2). The glacier has an area of about 24 km^2 (as of 2016) and ranges from 3650 m a.s.l. to nearly 5000 m a.s.l. Various meteorological variables were measured at a glaciological station located at 3837 m a.s.l. from 1967 to 1998 (Fig. 1.3a). A modern AWS was installed in 2011 (Schöne et al, 2013) within the framework of the CAWa project (GFZ Potsdam, Germany). This station is located at an elevation of 4100 m a.s.l. at a distance of about 1.5 km from the glacier terminus. At the same time, two terrestrial cameras have been mounted to monitor the TSL over the glacier surface (Fig. 5.6). Among a large and detailed scientific programme (Suslov et al, 1980; Glazirin et al, 1993; Kamnyansky, 2001), surface mass balance was measured intensively from 1967 to 1998 (Pertziger, 1996) and the mass balance monitoring was re-established in 2011 with 20 ablation stakes and three to four annually measured snow pits. Since then, annual glaciological surveys were continuously carried out in late August. Brun et al (2017) reported a mass loss of -0.38 ± 0.10 m w.e. yr^{-1} for Abramov from ≈2002 to 2014 and Gardelle et al (2013) presented a mass loss of only -0.03 ± 0.14 m w.e. yr^{-1} from 1999 to 2011.

Chapter 2

Thematic & Methodological Background

2.1 Fundamentals of glaciers

A common understanding of (1) the glacier mass balance processes and (2) their interaction with climate, (3) ways to measure as well as (4) to estimate mass balance changes are required. In the following, a brief introduction is given on the three topics with a focus on mountain glaciers. The content of this chapter is based on the textbook Cuffey and Paterson (2010) and Hooke (2005) that provide a more detailed and comprehensive background on the here outlined topics.

2.1.1 Glacier mass balance

Mass balance processes

Glacier form under cold and wet environments due to persistence of snow and ice, such as in high altitude or latitude. When fresh snow is continuously added and accumulated at the surface (Fig. 2.1), the pressure increases on the buried layers and a complex transformation of the snowflakes into firn takes place. The firnification process continues for several years, increasing gradually the density of the matter to finally form solid ice. The time needed to transform snow into ice depends mainly on temperature, the amount of refreezing and the accumulation rate. A continuous addition of mass through processes such as snow fall, avalanches or wind redistribution results eventually in an overload at the upper part of the glacier. The excess mass is then moved downwards due to gravity (Fig. 2.1). At lower elevations, mass loss starts to exceed mass gain (Fig. 2.1). Glacier mass is primarily removed through melt, sublimation or evaporation, wind redistribution or calving. On a typical mountain glacier of the mid-latitudes, the processes adding mass outweigh the processes that remove mass above a specific altitude. This altitude is called the equilibrium line altitude (ELA, Fig. 2.1). Below the ELA ablation is dominant. In practice there is a significant spatial variability in accumulation and ablation and the equilibrium line (the line of zero mass balance) can have a more complex pattern (Oerlemans, 2001). The mass balance on most mountain glaciers correlates with elevation. The rate of mass

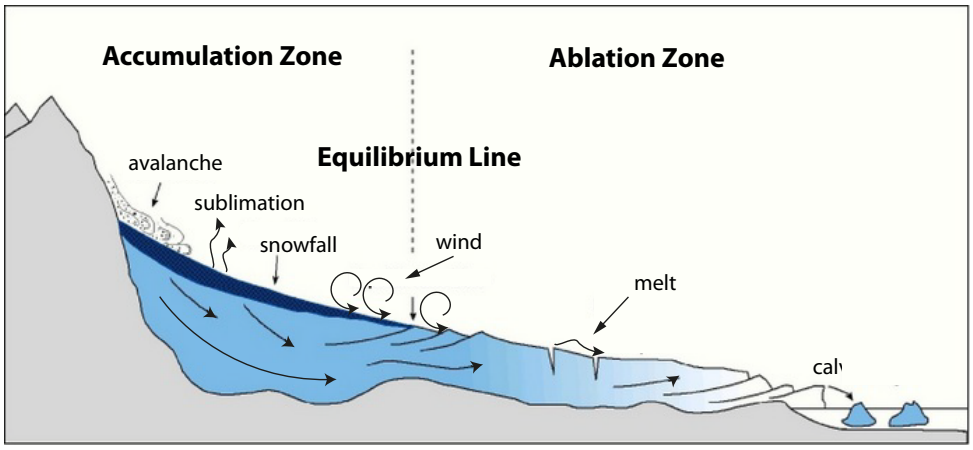

Figure 2.1: A schematic view of a mountain glacier illustrating most relevant components of the surface mass balance (*modified from https://garingerearthsci.weebly.com)*.

balance changes with altitude, is termed the mass balance gradient and may be related to systematic vertical variation of meteorological factors.

Aside from the surface components that in general dominate the glacier mass budget, different processes within and at the bottom of the glacier cause additional mass loss and gain. While at the surface, the major control of the mass balance is the heat and mass exchange with the atmosphere, the geothermal heat flux and friction cause basal melt. Ice deformation, refreezing and advective heat transfer through ice movement and water flow modify the glacier mass from within. Whereas basal melt can be considered negligible for this thesis, the processes of retention and refreezing of liquid water might have strong implications for the glaciers studied here. Both of them are key processes occurring in the accumulation area where they affect snow and firn properties. Water originating from snow melt or liquid precipitation percolates through near-surface snow and through firn layers where it can be retained in its liquid form by capillary forces or in firn aquifers and can refreeze in pore space forming ice lenses. For refreezing to occur, firn cold content and available firn pore space are preconditions. The refreezing of water between the last year's summer surface and the bed is referred to as internal accumulation and contributes positively to the overall mass budget of a glacier (Fujita et al, 1996; Woodward et al, 1997; Fujita and Ageta, 2000). This process can act as a considerable mass loss buffer (Machguth et al, 2016). The firn area is commonly divided into the recristallisation zone, where no melt and thus no percolation occurs; the recristallisation-infiltration zone, where melt water infiltrates to typically a restricted depth of the annual snow layer, the cold infiltration zone, that might reach deeper as the annual layer and the temperate firn zone. The latter is a zone substantially affected by melt and refreezing processes and melt water percolates through the entire firn layer (Shumskiy, 1964). The limit between the recristallisation zone and the infiltration zones is marked by the wet snowline. Below this border, all the snow deposited since the end of the previous summer has been raised to the melting temperature. An entirely water saturated snow and firn pack might be observed at the lower border of the accumulation area. Superimposed ice can form when melt water is prevented from draining by an impermeable underlying ice layer and usually accumulates at the lower limit of the accumulation area where it refreezes.

Refreezing processes in the accumulation area redistribute a significant amount of mass

within the glacier, affect the cold content of the surrounding material by the liberation of latent energy and alter the density of the snowpack / firn (Braithwaite et al, 1994; Humphrey et al, 2012; Machguth et al, 2016). This complex scheme of mass redistribution potentially masks mass balance changes (Pfeffer et al, 1991; Parry et al, 2007). Refreezing processes are important in cold and dry regions such as the Eastern Pamir and the Central and South Eastern Tien Shan.

A glacier in equilibrium has a balanced mass income and outgo, and the glacier geometry remains constant. After a mass balance perturbation, the glacier is in imbalance, either expressed through a positive or negative mass budget at the end of the balance year. The glacier geometry will adjust to reach a new equilibrium. However, such an adjustment is not immediate, taking many years and depends on the initial geometry. Glaciers with large balance gradients and steep bed topography respond faster to a perturbation than flat, inactive glaciers. The dynamic response time, thus, depends on the characteristic ice velocity (Oerlemans, 2001) and can be estimated using the maximal ice thickness around the equilibrium line and the ablation rate at the terminus (Nye, 1960; Jóhannesson et al, 1989). With a known response time, mass balance perturbations can be related to cumulative front changes and the latter might be used to reconstruct mass balances for secular times scales (e.g., Jóhannesson et al, 1989; Hoelzle et al, 2003).

Mass balance formulation

The mass balance m of a glacier can be expressed as the sum of the added c and removed water, snow, firn and ice material a at the surface sfc, the bed *bed* and within i the glacier over a specific time period (Cogley et al, 2011) and can be described as:

$$m = c + a = c_{\mathrm{sfc}} + c_{\mathrm{bed}} + c_{\mathrm{i}} + a_{\mathrm{sfc}} + a_{\mathrm{bed}} + a_{\mathrm{i}}. \tag{2.1}$$

The total mass balance ΔM of a glacier can be described through integrating the sum of all incoming and outgoing mass fluxes m through a vertical column over the entire glacier area S plus the mass loss through calving at the glacier front during a specific time interval t_1 to t_2:

$$\Delta M = \frac{1}{S} \int_S m \, dt \, ds + \frac{1}{S} \int_P d \, dt \, dp \tag{2.2}$$

For a more detailed review of all components and formulations of the mass balance equation Cogley et al (2011) might be consulted.

Mass balance regimes

Mass changes follow a systematic cycle throughout the year, depending on the seasonal distribution of accumulation and ablation. The duration from a minimum of the total mass of a glacier to the consecutive minimum state, occurring approximately one year later, is termed the *balance year*, and often used as reference period for observation. Characteristics of the balance year depend to a great extent on the seasonal distribution of the energy balance components. For this work, two types of mass balance regimes are of particular importance: (1) winter-accumulation type glacier with distinct winter accumulation and summer ablation periods and (2) summer-accumulation type glaciers with a maximum in accumulation and ablation occurring more or less simultaneously during the summer months. Preconditions for a dominant summer accumulation are a pronounced

summer precipitation maxima and cold, dry winters (Naito, 2011). Mass turnovers and inter-annual variability are generally reduced in comparison to winter-accumulation type glaciers (Ageta and Higuchi, 1984). This low activity is connected to a low ice flux due to lower rates of accumulation and ablation. Summer-accumulation type glaciers appear mainly under dry, continental conditions, whereas winter-accumulation type glaciers are observed in more maritime settings (Shumskiy, 1964).

2.1.2 Transient snowline

The TSL marks the border between this year's accumulated snow and the bare ice or firn surface (Cogley et al, 2011). At the snowline position, all snow has melted but ice / firn melt did not yet start, consequentially the balance along the TSL is approximately zero. The TSL is often rather a transition zone where the glacier surface grades from snow, to snow patches, to bare ice. Typically, slush or soaked snow mark the transition (Cogley et al, 2011). The snowline rises with the onset of the melt season continuously until the end of the ablation period. At the end of the summer, when melt has stopped, the snowline is close to the position where accumulation balances ablation, thus approximates the equilibrium line (Østrem, 1975; Oerlemans, 2001). The snow cover might be easy to detect due to the brightness in contrast to the underlying firn and ice layer. However, misinterpretations may result when the snowline is lowered by summer and early autumn snowfall. For summer-accumulation type glaciers where accumulation and ablation seasons are not strictly separated, the end-of-summer snowline still indicates the line of zero mass balance, however, its position might be blurred by individual fresh snow fall events. The snowline does not represent zero mass balance when a significant amount of meltwater refreezes within the snowpack to form superimposed ice. In this case the line of zero mass balance is shifted to the lower boundary of the superimposed ice, thus somewhat below the observed snowline (Cogley et al, 2011). Similarly, to the AAR, the transient snow covered area on a glacier can be related to the total glacier area by the snow-covered-area fraction (SCAF). The SCAF in contrast to the snowline can be patchy and including outliers as well as excluding inlayers (Cogley et al, 2011).

2.1.3 Interaction with climate

Meteorological processes, along with the physical properties of the ice, determine the extent and behaviour of a glacier. Even though influences of large-scale atmospheric circulations on the mass balance variability have been shown (e.g., Vuille et al, 2008; Huss et al, 2010; Mölg et al, 2014), every glacier is exposed to a local or micro-climate. This smaller scale characteristics depend on a combination of the location, morphology and topography, reshaping the influence of the dominant mesoscale and synoptic climate regimes (e.g., Hannah et al, 2000; Mölg et al, 2012). The alliance between climate and glaciers can thus become very complex. Figure 2.2 illustrates a simplified relation between climate and glaciers showing that the mass balance is one element of a chain of processes with inherent feedback mechanisms. For a typical mountain glacier, however, feedback on the concerning meteorological conditions are small (Machguth, 2008). Mass balance can thus be directly related to meteorological conditions and is often used as a proxy for climate change observations.

The atmosphere acts on a glacier through adding and removing heat and mass at the surface. The mechanisms of heat and mass transfer that are relevant for glaciers are shown

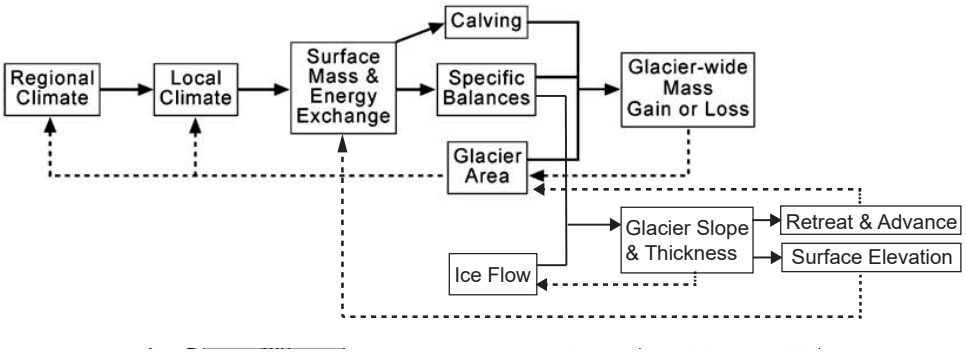

Figure 2.2: The chain of processes describing the relationship of glaciers and climate. Feedback mechanisms are indicated by dotted lines. *(Figure modified from Cuffey and Paterson (2010)).*

in Figure 2.3. Deposition of solid precipitation is closely linked to synoptic airflow and orographic settings, whereas the surface energy budget at the glacier-atmosphere interface is decisive for ablation processes (Kuhn, 1984, 1993; Oerlemans, 2001). For most glaciers, the dominant ablation process is melt. The sum of all energy fluxes at the glacier surface is zero. Thus, when the glacier surface has been heated to 0° C, any surplus of energy is used for melt M or sublimation. The melt process is formulated as:

$$M = \frac{Q_{\mathrm{M}}}{\rho_w * L_f} \tag{2.3}$$

where Q_{M} is the energy available for melt, ρ_w is the density of water and L_f is the latent heat of fusion ($334\,\mathrm{kJ\,kg^{-1}}$). In case of a large vapour pressure gradient at the glacier-atmosphere interface and a large amount of available energy, sublimation replaces melt (e.g., Kaser et al, 1990; Wagnon et al, 1999). Thus, snow or ice is directly vaporized without going through a liquid state. The latent heat of sublimation ($2838\,\mathrm{kJ\,kg^{-1}}$) is substantially higher than L_f and sublimation is consequentially a much more energy intense process. Conditions for sublimation are in general favourable for high-latitude and also for high-altitude glaciers where the scattering and filtering of the incoming solar radiation is low, providing a large energy surplus at the glacier surface (Dozier, 1980). Moreover, dry environments favour a strong vapour pressure contrast between the surface and the air. The vapour pressure gradient is controlled by a range of different factors. Wagnon et al (1999) showed the importance of seasonal humidity distribution for tropical glaciers, whereas Bliss et al (2011) points out accelerated sublimation under conditions of strong winds. Under favourable conditions, sublimation has been shown to be the dominant ablation process (e.g., Huintjes et al, 2015a; Ayala et al, 2017).

From equation 2.3, it is evident that Q_{M} is decisive for the quantity of ablation. Q_{M} depends on the energy budget at the glacier-atmosphere interface. For a melting surface the energy balance can be solved for Q_{M} as:

$$Q_{\mathrm{M}} = Q_{\mathrm{N}} + Q_{\mathrm{H}} + Q_{\mathrm{L}} + Q_{\mathrm{G}} + Q_{\mathrm{R}} \tag{2.4}$$

where, Q_{N} is the net radiation, Q_{H} the turbulent sensible heat flux, Q_{L} the turbulent latent heat flux, Q_{G} the ground heat flux, Q_{R} the heat flux of rain. Q_{G} and Q_{R} are usually small. Q_{H} and Q_{L} are determined by the temperature and mean specific humidity gradients between the surface and the air, and by turbulence in the lower part of the atmosphere. For typical alpine glaciers, Q_{L} is smaller than Q_{H} (Kuhn, 1979). Both

components are in general smaller then Q_N (Kuhn, 1993; Oerlemans and Klok, 2004; Hock, 2005). The turbulent heat fluxes (Q_L+Q_H) become more important in humid environments (Hock, 2005). Q_N is the sum of the incoming and outgoing shortwave S_{in} and S_{out} and longwave L_{in} and L_{out} radiation fluxes:

$$Q_N = S_{in} - S_{out} + L_{in} - L_{out} \tag{2.5}$$

L_{in} and L_{out} depend on the temperature and the emissivity of the surrounding medium, thus include mainly thermal radiation of terrestrial or atmospheric origin. L_{out} is approximately constant over the glacier surface when melting conditions are prevailing, whereas L_{in} varies with cloudiness, air temperature and air water vapour content (Oerlemans, 2001). Incoming long-wave radiation is steadily absorbed and emitted at different levels of the atmosphere and tends to decrease with altitude. At the glacier surface L_{in} and L_{out} compensate each other to a large degree (e.g., Oerlemans, 2001; Klok et al, 2003). Considerable variations of the longwave radiation budget at the glacier surface can be related to longwave radiation emitted from rockwalls (e.g., Aubry-Wake et al, 2017), changes in cloud cover and humidity (e.g., Mölg et al, 2009).

The relative importance of the individual components of the surface energy balance varies temporally and spatially. However in general, the net shortwave radiation S_{net} is the dominant energy flux (e.g., Oerlemans, 2001; Bliss et al, 2011; Azam et al, 2018) and can be expressed as:

$$S_{net} = S_{in} - S_{out} = S_{in} * (1 - \alpha) \tag{2.6}$$

where α is the albedo. The incoming shortwave radiation S_{in} is also denoted as global radiation consisting of direct and diffuse solar radiation. Cloudiness acts as a main control on S_{in}. The more clouds the higher is the share of diffuse S_{in} due to an increased scattering and the lower is the total S_{in} as the clouds absorb S_{in}. More clouds furthermore imply more long-wave radiation (Oerlemans, 2001). The incoming solar radiation is partly reflected depending on the local topography and glacier surface characteristics. Reflected solar radiation from surrounding terrain directed to the glacier surface can be a significant share of S_{in} at the glacier surface in mountain regions, where reflective snow often mantles steep valley walls and peaks.

The shortwave radiation balance at the glacier surface is governed by the albedo α. The albedo is the ratio of the reflected flux density to the incident flux density (Cogley et al, 2011) and is generally higher for snow (0.40 to 0.85) than for ice (0.20 to 0.65) meaning that more solar radiation is reflected over a snow covered surface than over ice. As indicated by the large range of values given for snow and ice, the albedo varies significantly over the glacier surface and throughout the year (e.g., Paul et al, 2008). The highest albedo values occur for fresh snow. The snow aging lowers the albedo as crystal size and air bubble content evolve. Furthermore, liquid water on the surface increases absorption. Spatial and temporal variation of the albedo might be reduced in winter when the glacier is entirely snow covered, while changes during the summer months are more pronounced through ongoing snow depletion exposing the complex albedo pattern of bare ice (Kuhn, 1984). Impurities such as rock particles and organic material concentrate on the surface and reduce the albedo, leading similarly to enhanced melt. Debris and dust layers have a rather complex effect on the absorption of solar radiation varying from enhanced absorption of S_{in} to complete insulation of the surface reducing ablation considerably (Østrem, 1959). Debris covered glaciers can thus have an extremely heterogeneous melt pattern and their response to climate is masked through feedback processes associated with different surface characteristics (e.g., Ragettli et al, 2016).

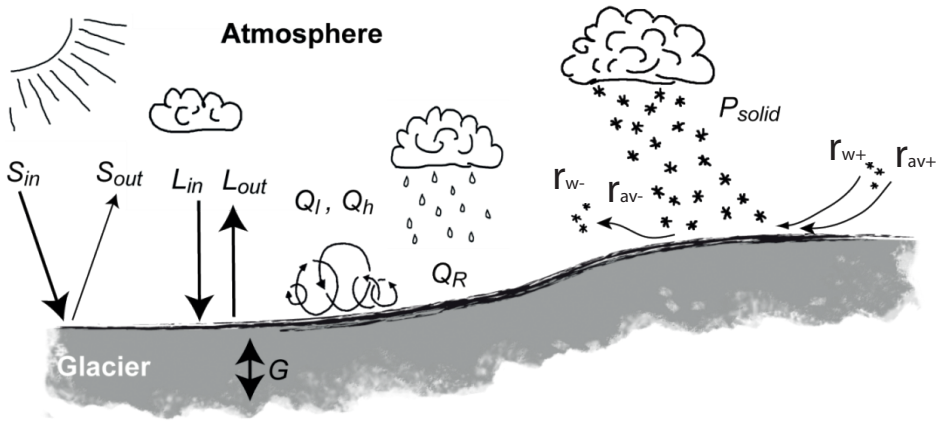

Figure 2.3: A schematic view of the different components of the energy balance acting on the glacier surface. For abbreviation see main text. (*Image Courtesy: H. Machguth*)

.

Mass balance sensitivity

Most effective variables decisive for the mass balance sensitivity to climate are solid precipitation, air temperature, air humidity, solar and terrestrial radiation and surface albedo (Kuhn, 1984). However, it is challenging to dismantle the influence of individual components and the complex relationship is frequently reduced to two parameters, solid precipitation and air temperature (Kuhn, 1993). For many glaciers, a significant relationship between air temperature and melt can be identified and solid precipitation is the major control for accumulation (Ohmura, 2001). Air temperature correlates well to various energy balance terms (Kuhn, 1993). Kuhn (1993) concluded through multi-variance analysis the suitability of air temperature and winter precipitation to investigate the glacier mass balance, but outlined also the importance of the albedo which, however, is more difficult to parameterise.

Fundamental differences of mass balance regimes and sensitivities of glaciers situated in different climate settings are observed due to the variation in annual temperature and precipitation amounts and distributions. Largest sensitivities apply to glaciers in wet climates. Glaciers in such maritime environments can exist at lower altitude due to the large amount of snow accumulation (Oerlemans and Fortuin, 1992; Fujita, 2008a). Maritime glacier reaction is particularly pronounced to solid precipitation and mean summer temperature (Kuhn, 1984). The importance of precipitation decreases with increasing continentality, thus, mean summer temperature is more decisive for glacier located in dry and cold areas. Kuhn (1984) identified that the length of the ablation season is of great importance for the annual balance. Frequent summer snow fall can have significant positive effect on the mass balance (e.g., Ageta and Higuchi, 1984; Oerlemans and Klok, 2004; Fujita, 2008b). Therefore, the sensitivity to summer precipitation is significantly increased for summer-accumulation type glaciers (Fujita, 2008b,a). Two mechanisms are responsible: (1) summer-snow accumulation and (2) reduction of melt rates through an albedo increase even if no significant mass is accumulated. This so called albedo effect, occurring during the summer months is one of the most essential features of summer-accumulation type glaciers (e.g., Naito, 2011; Fujita and Ageta, 2000; Fujita, 2008b). With ongoing climate warming, the duration of ablation seasons extends, and summer snowfall frequencies

decrease so that the bare ice is exposed longer at the surface leading to increased melt (Naegeli and Huss, 2017; Fujita, 2008b).

2.1.4 Methods to determine glacier mass balance

Two well established and complementary methods to observe glacier mass balance found widespread use: (1) the direct glaciological mass balance measurements and (2) the indirect geodetic survey.

(1) The glaciological field survey consists of seasonal to annual point measurements distributed over the accumulation and ablation area. The point sampling sites are chosen to best represent the mass balance pattern of a glacier. For ablation measurements, stakes are drilled into the ice and relative surface elevation changes measured at each stake location after a defined time period indicate the ablated mass at the sample location. The measured elevation difference is converted into water equivalent by using a density assumption for ice of typically $900\,\mathrm{kg\,m^{-3}}$. Accumulation is measured by means of snow depth probing to the last summer horizon in order to survey the snow distribution and depth. Snow density is measured at a few sites only. Thereby, snow pits are dug at selected sites and measured density is then extrapolated to the probing locations to derive the water equivalent of accumulation for each snow depth measurement. The point measurements represent only the surface component of glacier mass balance, and are extrapolated to the entire glacier area. Extrapolation techniques can range from a simple linear relationship of mass balance with elevation (*Profile method*) (e.g., Kononova et al, 2015) to a more sophisticated model-based extrapolations (e.g., Sold et al, 2016). Most frequently used, however, is the *contour-line method* that is based on manually drawn contour lines of equal mass balance between measured data points (Østrem and Brugman, 1991b). This method incorporates the observer's expertise as well as other mass balance indicators, such as end-of-summer snowline observations (e.g., Hock and Jensen, 1999). The area-weighted mean of the extrapolated point measurements expresses the mean annual surface balance B_{sfc}.

The mass balance is measured within a given time interval, typically chosen to match the hydrological year. For mid-latitude alpine glaciers, the balance year is commonly divided into ablation and accumulation season and measurements are ideally conducted at the end of each (Cogley et al, 2011). However, a strict separation of the seasons is not always possible such as for summer or mixed accumulation-type glaciers, and the exact identification of the end date is not trivial. Hence, two measurement systems have emerged: the stratigraphic and fixed-date system. The stratigraphic system is based on the quasi-annual / seasonal span between successive summer / winter surfaces, hence intents to approach the date of the end of each season, whereas the fixed-date system is tied to a certain field-survey date that does not necessarily represent the actual end of each season but is kept constant over the years (Cogley et al, 2011).

(2) The geodetic method is based on the differencing of two digital elevation models (DEM) from two different moments in time (typically in a range of several years to a few decades). This elevation difference maps over the glacier area provide glacier volume changes that are converted into geodetic mass changes B_{geod} by assuming a bulk density of the lost / gained volume (typically used density: $850\,\mathrm{kg\,m^{-3}}$). All components of mass change (surface, basal, internal) are measured and thus B_{geod} approximates ΔM. Survey periods are restricted to the date of the DEM acquisition and often do not conform to the hydrological year or the glaciological measurement periods.

There are a range of other methods to monitor glacier mass balance such as hydrolog-

ical methods and other indirect approaches derived from glaciological measurements. A comprehensive, detailed review of mass balance measurement techniques and recommendations can be found in Kaser et al (2003). Apart from measuring the mass balance, often laborious and cost intensive, a range of methodologies have evolved that are frequently used to estimate changes in mass balance based on minimal input data, detached from field observations. Such methods allow extrapolation in time and space and are fundamental to extend our understanding of glacier mass changes to a more regionally comprehensive picture and to the future. For this thesis, two of such approaches, namely the ELA concept and mass balance modelling have been of particular importance and are outlined in the following Sections.

2.1.5 Estimating mass balance changes using the ELA concept

The equilibrium line indicates the lowest altitudinal boundary of the climate glacierisation (Brückner, 1887; Ohmura et al, 1992; Zemp et al, 2007) and shifts in its position are a good proxy for climate variations (e.g., Ahlmann, 1924; Braithwaite and Müller, 1980; Kuhn, 1989, 1993). High correlation between the ELA and the surface mass balance was observed for a wide range of glaciers (e.g., Østrem, 1975; Braithwaite, 1984a; Kuhn, 1990). Even though Oerlemans (1991) argues that no clear relationship between the ELA and the meteorological variables prevail, the authors recognize a strong linear dependency between the position of the ELA and the mass balance gradient in vicinity of the ELA. Kuhn (1989) and Ohmura et al (1992) showed that the sensitivity of the mass balance to a shift in ELA can be expressed as a function of the mass turnover (Meier, 1961). The same authors found a close interdependence between the temperature and the precipitation at the ELA and showed that the predictive power of this relation increases by integrating net radiation. Letréguilly (1988) found statistically a high correlation between air temperature and the ELA, however, only poor to no relation with precipitation. Braithwaite (2008) tested in depth the accumulation - temperature relation at the ELA position with a Temperature-Index model (TI-model) for different climate regions and underlined the findings by Ohmura et al (1992) of a strong relationship between summer mean temperature and annual accumulation at the ELA.

The ELA concept is based on the assumption that the ELA position of zero mass balance ELA_0 refers to a steady state of the glacier and moves linearly up- or downwards according to perturbation in climate (e.g., Ohmura et al, 1992). For a simple glacier geometry the relation between annual mass balance B_{sfc} and climate can thus, be described as following:

$$B_{\mathrm{sfc}} = \delta b/\delta z * (ELA_0 - ELA_{\mathrm{t}}) \tag{2.7}$$

$\delta b/\delta z$ is the balance gradient and ELA_t is the ELA position of the considered year. These two parameters vary considerably from glacier to glacier that makes an accurate prediction difficult if no measurements are available (Braithwaite and Müller, 1980; Braithwaite, 1984a). Letréguilly and Reynaud (1989) showed that mass balance variability correlates over distances of a few hundred kilometers and holds for glaciers that are located under fairly different climatic settings. Kuhn (1984) found that the mass balance gradients can vary significantly from year to year depending on the climate region and the meteorological condition of the individual year. Furthermore, the alliance between the different parameters is glacier specific and an extrapolation of an established relationship to other glaciers can lead to large uncertainties. Nevertheless, the prediction of the ELA through temperature and precipitation was proven to be of value in order to investigate

the ELA - climate relationship also on a regional scale (e.g., Zemp et al, 2007; Bravo et al, 2015).
The amplitude of the glacier reaction to changes in ELA depends not only on the perturbation but also on the altitude-area distribution, the mass balance gradient (Dyurgerov et al, 1994) and the relation between accumulation and ablation gradient (Benn and Lehmkuhl, 2000). A glacier with a large portion of its area close to the mean ELA is likely to fluctuate stronger between positive and negative balances as a large portion of the glacier is affected by ELA changes (Tangborn et al, 1990). Hence, the SMB - ELA relation can be associated to the hypsographic curve (Dyurgerov et al, 1994). Whereas continental glaciers are characterised by small accumulation and ablation gradients, glaciers in more maritime climate have higher gradients (Oerlemans, 2001). Dyurgerov et al (1994) argued that, annual changes of the mass balance gradient driven by meteorological conditions for maritime type are reflected through parallel shifts of the mass balance gradient, whereas the year-to-year variability of SMB for the continental type is expressed by rotational changes of the gradient around the ELA. The authors proposed to distinguish between the (1) additive structure for the mass balance for glaciers under maritime conditions and the (2) multiplicative structure for glaciers in continental, arid settings. Considering the relationship between the ELA and the SMB, this suggests that glaciers with a smaller vertical gradient are of multiplicative type. Regarding the climate response, glacier with smaller vertical gradients are hence characterized by slower reaction to climate change (Dyurgerov et al, 1994). Numerous glaciers show a mixed behaviour between the two types described by Dyurgerov et al (1994) and furthermore, regime shifts related to climate change can provoke alteration from one type to the other (Hodge et al, 1998; Dyurgerov and Meier, 2000; Østby et al, 2017).
A similar relationship between the ELA and the SMB can be described between the mass balance and AAR where the accumulation area, thus the area above the ELA, is related to the total glacier area. As a rule of thumb, an AAR of approximately 0.7 indicates a steady state glacier. For high-altitude glaciers Braithwaite (1984a) recommended a relation of about 0.5 to represent a balanced budget. However, this relationship was shown to depend firmly on the vertical elevation range of a glacier (Machguth et al, 2012). Machguth et al (2012) investigated the relationship between different topographic and mass balance parameters such as the steady state ELA, the mass balance gradient or the ablation rate at the glacier terminus. Machguth et al (2012) confirmed strong correlations between steady state ELA and median / mid-elevation glacier elevation and discovered a solid relationship between the ablation rate at the tongue with the steady state AAR due to the influence of the glacier-specific hypsometry (Furbish and Andrews, 1984). Furthermore, the vertical glacier extent is a good measure of the distance between the steady state ELA and the tongue and hence correlates well to the ablation rate at the glacier terminus. This relationship is valid for glaciers in different climatological settings and has a strong predictive potential for corresponding glacier characteristics such as response times and the mean mass balance. The use of known mass balance gradients of measured glaciers, might enable to derive the ablation rate at the terminus for unmeasured glaciers when extrapolated, helping to complement observational datasets to a larger scale (Machguth et al, 2012).

2.1.6 Estimating glacier mass balance from numerical modelling

A wealth of different approaches of glacier mass balance models exist, and a wide range of different degrees of complexity have evolved. Complex modelling approaches generally focus on process understanding, while more simplified mass balance simulations are used

for change assessments of, for instance, runoff or sea level rise. As mentioned in Section 1.2, today, most approaches use fully distributed numerical models solving the mass balance at every grid cell and for every time step (e.g., Machguth et al, 2006b; Huss et al, 2008). In general, mass balance models consist of an accumulation and a melt component. Hereafter, different approaches used to model accumulation and melt are briefly introduced. A more detailed and in-depth discussion of different modelling techniques can be found in Oerlemans (2001) and Hock (2005).

Accumulation models

In general, accumulation processes are difficult to model at high spatial and temporal resolution due to its complex and variable spatial pattern. Most elementary accumulation models use the measured precipitation amounts below a temperature threshold to simulate snow accumulation and apply a linear relation with altitude for spatial extrapolation (e.g., Johannesson et al, 1995). Further, redistribution of mass through wind or avalanches is often ignored. More complex models try to account for such processes (e.g., Mernild et al, 2006; Van Pelt et al, 2016; Laha et al, 2017), however, large biases in precipitation measurements in high mountain areas and the complexity of such processes are impeding. To reproduce snow accumulation more accurately, mass balance studies calibrate accumulation through varying precipitation observations (Gerbaux et al, 2005). More accurate simulations are achieved by including detailed seasonal snow cover observations such as from detailed snow probing (e.g., Huss et al, 2008) or high-frequency GPR surveys (e.g., Sold et al, 2016).

Melt models

So far, melt modelling received much more attention and more sophisticated approaches are available. Numerical melt models can typically be categorized into two main domains, (1) the physically based energy balance model and (2) the empirical TI-model. However, transitions of simple TI-models resembling energy balance formulations are widespread. For many glaciers reliable input data are sparse and often incomplete or only available for short time periods (Hock, 2005). Pre-processing of the datasets is often necessary but not straightforward (e.g., Konz et al, 2007; Nagler et al, 2008). Hence, the choice of the appropriate model depends on the study and the available data, and should be carefully evaluated. Hock (2005), for example, argues that for operational purposes, such as short-term runoff estimates on catchment-scale, simple TI-models on daily time resolution are often sufficient, whereas for higher resolution in space and time, a more sophisticated energy balance model is preferable.

Energy balance models: The energy balance approaches assess the energy fluxes at the atmosphere - glacier interface (see Section 2.1.3), and span various degrees of sophistication, from fully resolved energy balance equation accounting for the totality of fluxes from and to the surface to almost entirely parameterized energy balances. Parameterized models focus only on the dominant components of the energy balance and require meticulous calibration. Complex energy balance models are used to understand detailed processes such as the effect of debris cover (e.g., Reid and Brock, 2010; Miles et al, 2016) or internal accumulation (Fujita and Ageta, 2000). In comparison to TI-models and simple energy balance models, more sophisticated models are more suitable for unmeasured areas since they are less dependent on calibration. Simple models are usually applied locally and over shorter time periods (Hock, 2005). Models resolving physical processes in more

details might be more suitable for future prediction of the mass balance since parameters might change with changing climatic conditions increasing the uncertainties of simulations of strongly parameterized models (Hock, 2005). A detailed discussion on very simple to more complex physically based models is provided in Oerlemans (2001).

Temperature-index models: The TI-models assume an empirical relationship between positive air temperature T_{air} and melt M and they are widely applied despite their simplicity (e.g., Braithwaite, 1995). TI-model performance is attributed to the fact that many components of the energy balance show a strong correlation with air temperature (Kuhn, 1993; Ohmura, 2001), which is worldwide one of the most readily available meteorological variable. However, especially at high-altitude, the relationship between melt and air temperature might be non-linear (e.g., Trusel et al, 2015) which makes the use of a simple TI-model in such environments not always suitable (Oerlemans, 2001).

The classical TI-model statistically links the positive air temperatures T_{air} to the melt rate:

$$Melt = \begin{cases} DDF_{\text{ice/snow}} \cdot T_{\text{air}} & T_{\text{air}} > 0° \\ 0 & T_{\text{air}} \leq 0°. \end{cases} \tag{2.8}$$

The degree-day factor (DDF) for snow and ice, respectively, accounts for various unknown and complex processes of the energy balance. However, the DDF are difficult to appropriately estimate and can vary significantly in space and time. Calibration of this empirical approach is indispensable and extrapolation of the DDF is critical due to the often uknown temporal and spatial variability (Hock, 2005). TI-model parameters are recommended to be adjusted for each site individually (Braithwaite, 1995) as well as for different periods (Huss et al, 2008). Two of the main weaknesses, namely the limited temporal resolution and the reduced spatial variability (Hock, 2003), are connected to such constant held DDFs over space and time. Thus, TI-models also lose the ability to project future responses since initially calibrated parameters may not hold for different future climate scenarios (Kuhn, 1993; Gabbi et al, 2014). These shortcomings are being tried to overcome by strengthening the physical foundation of the method through the incorporation of more variables, such as radiation (e.g., Hock, 1999) and albedo (e.g., Pellicciotti et al, 2005) or through temporally and spatially variable DDFs (e.g., Arendt and Sharp, 1999). Hock (2003) and Gabbi et al (2014) provide a detailed review of different TI-models and enhanced TI-models and their suitability for long-term simulations.

2.2 Remote sensing in Glaciology

Remote sensing in Glaciology builds on the information content stored in the electromagnetic radiation i.e. visible light, near infrared, shortwave infrared or thermal infrared reflected or radiated from the surface or the atmosphere. This information is collected as a function of wavelength with a passive system, relying entirely on natural radiation; or with an active system, transmitting inherent illumination and using advanced receivers to observe the scattered signal from the target. The transmitted energy is sensitive to the spectral properties of snow and ice. These properties decide over the degree of transmission, the reflection and the absorption at different wavelengths (Fig. 2.4). Hence, all materials have their specific spectral signature depending on their molecular make-up (i.e. Fig. 2.4).

A range of remote sensing applications have widened the spatial coverage of glacier observations on a relatively low-cost base. Most of the evolved techniques focus on elevation change assessments, glacier velocity characteristics or on the mapping of glacier extent and surface facies such as snow, ice or debris cover. Two different sensor domains have found established utility, namely optical and radar sensors. Both can be carried on air- or spaceborne platforms but might also be ground based. In this work, passive optical systems used for elevation change assessments and glacier facies mapping are of greatest importance. Nevertheless, a short overview of most frequently used laser and radar systems is given hereafter. Additionally, a more detailed outline of optical systems applied in modern Glaciology is portrayed. If no specific references are given the content is based on Pellikka and Rees (2009).

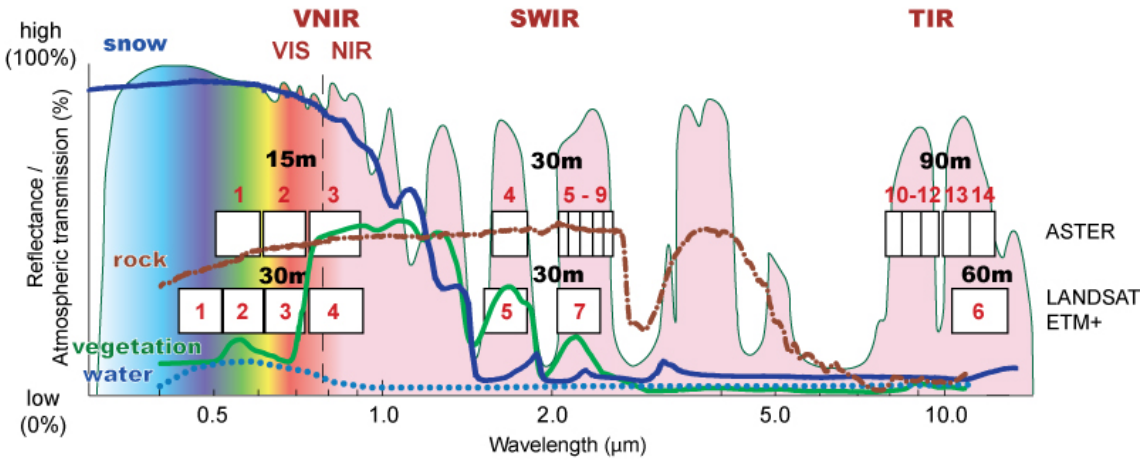

Figure 2.4: Spectral wavelengths and band properties of optical sensors (VNIR: visible and near infrared; SWIR: shortwave infrared; TIR: thermal infrared; VIS: visible light; NIR: near infrared). Reflectance curves of several typical surfaces encountered on a satellite scene (coloured lines). The boxes indicate the wavelength range of different sensors (e.g. ASTER, Landsat ETM+, TM, MSS). (*A. Kääb, University of Oslo*).

2.2.1 Radar and laser remote sensing systems

Most radar systems operate in the microwave spectrum and depend on the dialectic properties of the (near-) surface (Kääb, 2005a). Ground-penetrating radar is today a standardized technique to measure glacier thickness and volume (e.g., Hagg et al, 2013; Petrakov

et al, 2016a). Low frequency GPR are used for bedrock and ice thickness detection (e.g., Collins et al, 1989; Melvold and Rolstad, 2000). Furthermore, GPR has yielded important understanding of the thermal and hydrological properties of snow, firn and ice (e.g., Petrakov et al, 2014; Forster et al, 2014). High frequency GPR measurements, providing a higher resolution, reveal insights into past accumulation rates (e.g., Sold et al, 2015) or the snowpack structure (e.g., Dunse et al, 2009). The benefit of observing winter snow accumulation rates through GPR to derive seasonal snow distribution maps was outlined by Sold et al (2016) and Machguth et al (2006a).

Another radar system used frequently to map glacier topography, velocity and near surface characteristics is the Synthetic Aperture Radar (SAR). The active system can be used to acquire large amounts of images in a relatively short time, independent of daylight and weather conditions. The system led to terrain models on global scale such as provided by the Shuttle Radar Topography Mission (SRTM, Jarvis et al, 2008) or the TerraSAR-X add-on for Digital Elevation Measurement (TanDEM-X, Eineder et al, 2005). These datasets proved to be highly beneficial in various domains in Glaciology and are frequently used for geodetic mass balance surveys (e.g., Gardelle et al, 2013; Pieczonka et al, 2013). However, recent studies accentuate the shortcomings of such applications due to unknown and often highly variable signal penetration depth (e.g., Kääb et al, 2015; Berthier et al, 2016) causing a significant underestimation of the observed surface elevation especially for cold and dry snow in accumulation areas (Dehecq et al, 2016).

Similarly to radar systems, laser scanners such as the spaceborne Ice, Cloud and Land Elevation Satellite (ICESat) or the terrestrial / airborne Light Detection and Ranging send a short pulse and measure the two-way reflection time. These systems operate typically in the near infrared region and are mainly used to create highly resolved terrain models of the glacier surface. Due to the high precision, repeated surveys at relatively short time intervals are used for seasonal to annual mass change detection (e.g., Moholdt et al, 2010; Joerg et al, 2012; Joerg and Zemp, 2014; Treichler and Kääb, 2017).

2.2.2 Optical remote sensing systems

Optical sensors are passive sensors recording reflected solar radiation in the visible to near-infrared (VNIR) and the shortwave infrared (SWIR) spectra (Fig. 2.4). Some sensors also observe emitted wavelengths of the earth (thermal infrared: TIR). Optical sensors are sensitive to weather condition and daylight in the case of reflected radiation. A precise radiometric correction is required before calculating reflectance values due to varying solar incident angles in steep high-mountain topography and due to variable atmospheric conditions (e.g., Hadjimitsis et al, 2004). A wide range of different terrestrial, air- and spaceborne systems frequently applied in Glaciology are available today and the most relevant ones are presented, hereafter.

Spaceborne Systems

Most commonly used optical satellite systems are the freely available Landsat missions, Advanced Spaceborne Thermal Emission and Reflection Radiometer (ASTER) and the recently launched Sentinel-2 platform. The different sensors of Landsat (MSS, TM, ETM+, OLI) have been particularly useful because they collectively cover a long-time span and have a large spatial coverage. The first Landsat platform dates back to 1972 with a spatial resolution of ≈80 m. Since then, the spatial resolution of the Landsat sensors improved and reaches today ground resolution of 10-30 m and repeat cycles of less than 20 days. Whereas earlier Landsat missions only measured VNIR, the today's operating sensors

measure radiance in VNIR, SWIR and TIR that makes it not only useful for automatic mapping of surface characteristics but also for surface temperature observations. ASTER holds similar attributes but additionally has stereo capability and thus is appropriate to create DEMs (see Sec. 2.2.3).

Recent development includes sensors with even higher resolution (<10 m) and faster repeat cycles (e.g. Quickbird, Pléiades). Some of these so-called very high resolution sensors acquire stereo pairs that can be programmed and lead to very precise results (e.g., Berthier et al, 2014; Mukherjee et al, 2017). The main disadvantage is the relatively high costs.

Furthermore, declassified reconnaissance imagery such as Corona or Hexagon data provide a unique dataset, suitable for stereo imaging, reaching back in time to the 1960s and 70s (e.g., Bolch et al, 2008, 2010; Bolch, 2015; Pieczonka and Bolch, 2015).

Sensors with very low spatial resolution, in the order of one kilometer (e.g. Moderate Resolution Imaging Spectroradiometer (MODIS)) are of importance for glaciological studies. The main advantage of these platforms is the correspondingly wide coverage and usually fast repeat cycles (<3 days). Hence, it is possible to cover huge areas in little time on a very low cost base.

Airborne and terrestrial systems

Aerial photography is the longest established technique in remote sensing and operates in the VNIR. They offer flexibility in acquisition and temporal and spatial resolution. However, the data analysis is rather work-intensive and spatial coverage might be inferior to spaceborne data. The airborne platforms are usually mounted on planes or helicopters and more recently, the use of unmanned airborne vehicles (UAV) has become increasingly popular. Overlapping image data allow DEM generation based on a range of stereo-techniques. Today, the improved technique Structure-from-Motion (SfM) has found widespread use (e.g., Piermattei et al, 2015; Girod et al, 2017a). SfM operates under the same basic concept as stereoscopic photogrammetry, resolving three dimensional structures from a series of overlapping, offset images. The advantage of the method in comparison to conventional photogrammetry, is that the geometry of the scene, camera positions and orientation is solved automatically (Westoby et al, 2012). Hence, SfM is especially useful for historical data, when stereo capable satellite sensors were sparse and data quality limited (e.g., Mertes et al, 2017; Mölg and Bolch, 2017). SfM mostly works in a relative coordinate system and projection into a defined system is in general laborious and often relates to important uncertainties.

The essential advantage of terrestrial platforms is the high spatial and temporal resolution and the flexibility of acquisition. However, field access needs to be guaranteed and the oblique view angle makes quantitative analysis laborious and often not straightforward. UAV outperform terrestrial photogrammetry in many aspects (e.g. straightforward data acquisition and improved post-processing, ready-to-use applications (Bhardwaj et al, 2016)). The advantage of terrestrial camera platforms, however, is the unsupervised functioning. This leads to a development of fixed platforms equipped with terrestrial camera sensors for continuous monitoring of temporal and spatial variations for such as snow and ice properties and patterns (e.g., Corripio, 2004; Farinotti et al, 2010; Dumont et al, 2011), calving rates (e.g., Chapuis et al, 2010) and glacier velocities (e.g., Maas et al, 2008).

2.2.3 Satellite stereo imagery and digital elevation model acquisition

Digital elevation models for geodetic mass balance calculations (see Sec. 2.1.4) can be automatically derived from overlapping optical images. Thereby, the elevation of a discrete point on the terrain is determined by the intersection in space of two or more vectors originating from the different image sequences (Fig. 2.5) after they have been corrected for the earths curvature and rotation (Toutin, 2004; Kääb, 2005b). The orientation parameters for each terrain point are computed from a set of ground control points or directly inferred from on-board differential or inertial satellite navigation systems (Kääb, 2005b). However, an accurate co-registration based on a set of tie points on the stereo images guaranteeing the exact overlap of the two DEMs is more important to compute exact elevation differences between two DEMs (e.g., Nuth and Kääb, 2011).

Optical stereo images are usually obtained from scanning or pushbroom sensors (Kääb, 2005b) and consist of images of varying viewing angles. The image sequences are obtained through repeated acquisition of the terrain with different satellites following slightly different tracks (cross-track stereo) or through a single overflight with a nadir-, forward- and/or backward-looking camera (along-track stereo; Fig. 2.5). Generally, along-track systems with a simultaneous stereo channel acquisition are preferable due to the smaller time lag between the images. Hence, changes of the terrain with time are avoided. Kääb (2005b) recommended a combination of both methods to reduce the effects of perspective distortion or hidden terrain sectors and Kääb et al (2002) pointed out the accuracy problems in mountainous and steep terrain using a single system for DEM generation based on ASTER data. A new, improved method MicMac ASTER (MMASTER) to create digital terrain models from ASTER stereoscopic images were presented by Girod et al (2017b). This is an enhanced method to process ASTER data, correcting for jitter-induced cross- and along-track errors.

Berthier et al (2016) used a multi-temporal ASTER DEM strategy to retrieve more reliable elevation data. The authors deduced the elevation change for an averaged time period with a series of ordinary, multi-temporal ASTER DEMs by calculating a linear fit through the elevation time series for each pixel individually. A disadvantage of this method is the not clearly defined time stamp of the derived elevation changes.

2.2.4 Glacier surface classification with remote sensing

Østrem (1975) first described various zones of the glacier (near-)surface, such as snow cover, TSL or superimposed ice based on remote sensing. Different surface types have been mapped manually or with (semi-)automatic segmentation on remote sensing images ever since (e.g., Warren, 1982; Hall et al, 1988; Williams et al, 1991). Today a range of methods for discriminating materials on the basis of their different spectral signatures have found widespread applications, i. e. to map debris free and debris covered glacier extent (e.g., Paul et al, 2002, 2004; Bolch et al, 2007) or to observe surface characteristics (e.g., Fugazza et al, 2015; Naegeli et al, 2015; Winsvold et al, 2018). The wealth of imagery just now becoming available facilitates research on high temporal / spatial resolution and on a large spatial extent. Recent development provides an increased sensor availability with up to daily repeat cycles and on relatively low costs, such as CubeSats (Straub, 2012). However, data management becomes increasingly challenging and automatized tools for glacier mapping, are crucially necessary in order to handle the large amount of data accessible today. In the following, frequently used surface classification methods with a focus on snowline delineation are summarized

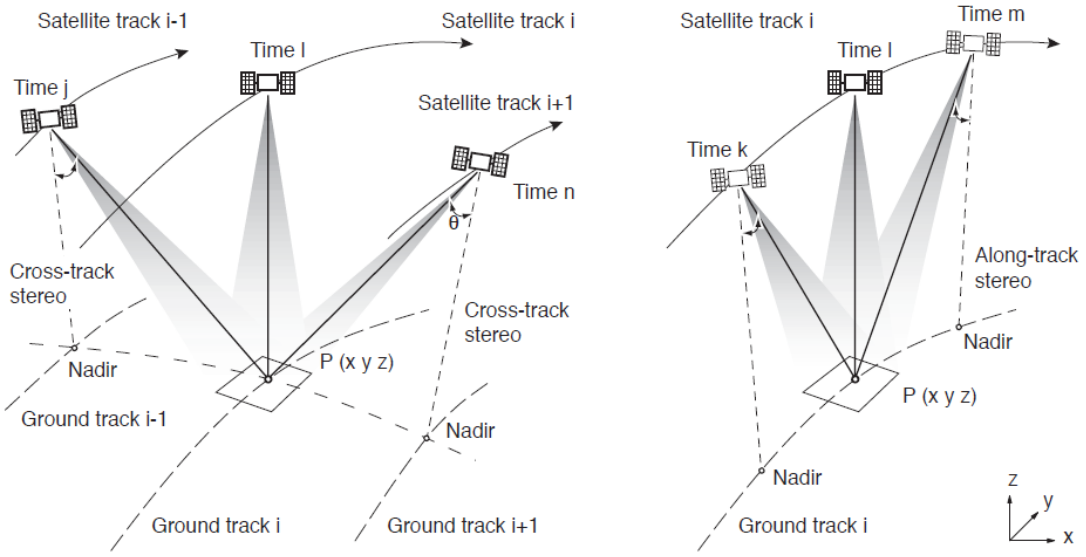

Figure 2.5: Acquisition principal of the two optical satellite stereo modes: cross-track stereo using different satellite tracks with a time differences ranging from days to months (left), and along-track stereo, forward or backward, taken during one overflight (Kääb, 2005b). The along-track images are taken within a time differences in the order of seconds to minutes (right). (*A. Kääb, University of Oslo*).

Surface classification techniques

Manual delineation might be applied for highly complex mapping were expert knowledge is needed. The method is based on combining human interpretation and digitizing (Kääb, 2005b). Such manual delineation is further useful for accuracy assessments, ground truth acquisition, or completion or correction of other classifications.

Semi-automatic supervised classification is an application-driven method. Manually selected training areas of the different surface types are selected in order to define the spectral signatures of these classes (Kääb, 2005b). Each selected signature is then analysed in order to test if the categories are significantly different from the other classes and used to automatically classify every image pixel. Supervised classification often provides accurate results for high-mountain terrain with reasonable spectral discernibility (Kääb, 2005b).

The unsupervised classification is a data-driven method (Kääb, 2005b). During unsupervised classification the image is automatically separated through a range of spectral vectors leading to artificial clusters that have to be assigned to specific surface types of the users interest afterwards. Supervised and unsupervised classifications primarily rely on the spectral characteristics of each pixels.

Image segmentation can also rely on a spatial component using neighbourhood relations of pixels (Kääb, 2005b). This method aggregates areas of the same class membership by region growing algorithms where individual pixels are joint according to algebraic rules. Band ratios using algebraic algorithms, principal components and normalized differences have also been used successfully for surface classification (Kääb, 2005b). Multi-spectral analysis techniques are particularly powerful, if used on a series of repeated images for change detection (e.g., Bishop et al, 2000; Huggel et al, 2002; Kääb et al, 2005a; Round et al, 2017).

Snowline / snow-covered area mapping

Clean ice and snow are well detectable due to their spectral uniqueness in the VNIR-part of the electromagnetic spectrum (Racoviteanu et al, 2008). Manual delineation of the snowlines on optical sensor systems reach far back in time (Rango, 1983; Hall et al, 1987) and proves still to be more robust than automatic classification (e.g., Rabatel et al, 2013; Man et al, 2014; Kienholz et al, 2017) but is disadvantageously very labour-intensive. (Semi-) automatic techniques are often based on similar algorithms as used for glacier outline mapping such as the band ratio method (Winsvold et al, 2015). This method exploits the spectral difference of snow and ice between the wavelengths and is typically based on the VNIR and the SWIR bands (e.g., De Angelis et al, 2007; Barcaza et al, 2009; Rabatel et al, 2012). Another automatic, frequently used method to map snowlines is the Normalized Difference Snow Index (NDSI) (e.g., Hall et al, 1995; Kaur et al, 2009). Thereby the GREEN and SWIR bands are normalized. For both methods, threshold values to separate the different surface materials have to be empirically selected. De Angelis et al (2007) showed that a combination of unsupervised and supervised classification in combination with maximum likelihood classification performs well for cloud free images and allows the classification of different snow and ice types. However, the classification remains sensitive to the experimentally chosen threshold for the different classes (Winsvold et al, 2014) and confusion are often observed between firn and shaded snow (Heiskanen and Kivinen, 2008). Moreover, optical satellite images suffer from frequent cloud cover making parts of the surface invisible to the observer. Cloud masks (e.g., Kruse et al, 1993; Zhu and Woodcock, 2012; Zhu et al, 2015) are used to remove the clouds, however, shadows, unmasked clouds and thin cloud layers affect the image classification.

Sirguey et al (2009) presented a comprehensive method to produce routinely regional maps of seasonal snow cover at subpixel resolution from MODIS data. The computation of ground spectral reflectance enabled the use of image-independent endmembers in a constrained linear unmixing technique to achieve a robust estimation of subpixel snow fractions. This enables snowlines and snow cover monitoring on elevated spatial resolution despite the reduced sensor resolution (e.g., Dumont et al, 2012; Sirguey et al, 2016; Tang et al, 2017; Li et al, 2018).

Alternative methods highlighting promising results are the application of a histogram threshold at the reflectance spectrum over the glacier surface to discriminate the snow covered surface(e.g., Bippus, 2011), or the spectral mixture analysis (e.g., Rosenthal and Dozier, 1996; Klein and Isacks, 1999). The latter examines the reflectance of a pixel with the spectral signature of selected endmember classes. Furthermore, the retrieval of broadband albedo from multi- or hyper-spectral data over the glacier surface to calculate glacier-wide albedo (Naegeli et al, 2017, 2018) or to map transient snowlines (Guo et al, 2014) was shown to provide accurate results.

Other studies outline the potential of SAR data to map transient snowlines and a range of glacier facies (e.g., Adam et al, 1997; Nagler and Rott, 2000) or snow and ice properties (e.g., König et al, 2001). For such applications the radar penetration into the subsurface is used. Through a large back-scattering contrast at the phase change from snow to ice, facies such as wet snow within the snowpack can be detected (Winsvold et al, 2018). Winsvold et al (2018) discussed the potential of SAR imagery to assist glacier-mapping procedures and used dense SAR satellite data time series to map surface and subsurface glacier properties such as the TSL or firn evolution.

A synergistic use of different satellite sensor types (e.g., Thakur et al, 2017; Callegari et al, 2017) show enhanced potential for a more complete and accurate time series of TSL

observations. The optical sensors collect information regarding selective absorption and reflection properties, whereas SAR signals are sensitive to structural shapes and dielectric properties of the objects being imaged (Kumar, 2013). A multi-sensor approach used for cross-comparisons helps to improve classification relying on a single sensor approach only. Winsvold et al (2018) combined optical and SAR data to analyse image time series through chronological gap filling and stack statistics. Thakur et al (2017) retrieved overall aerial extent of snow from SAR image thresholding using self-learning Support Vector Machine (SVM) and refined it with elevation mask from DEMs an optical snow cover maps. Callegari et al (2017) went one step further and developed an approach that can handle classification on different kind of satellite constellations composed of optical and / or SAR platforms automatically. The authors use a Hidden Markov Model (HMM) to improve the SVM classification algorithm. Thereby, a simple membership class estimation from SVM is extended through a probability estimate of the pixel to move to another class on the multi-temporal dataset including all sensors of a virtual constellation with HMM. In this way impossible transitions are identified and reclassified, producing improved multi-temporal and multi-source classifications of the surface type.

Overall, space- and airborne technologies prove to be essential tools for detection of snow and ice facies on the local to regional level but thetr are still challenges and limitations. Crawford et al (2013) gives a comprehensive overview of limiting factors for snow cover mapping and Wu et al (2014) investigates the constraints of snowline detection over glacier surfaces in more detail.

Chapter 3

Research Summary

This thesis consists of four research papers that are either published or in preparation for peer-reviewed scientific journals. The articles consecutively build up on each other and follow the individual research questions to reach the overall aim of the project to improve the knowledge of the state and change of a large amount of glaciers located in Central Asia, on an annual time scale and based on a minimum cost and data effort (Fig. 1.1).

The following chapter is divided into two parts. The first part addresses the past and current state of the glacier monitoring networks for selected glaciers (**Paper I & II**); while the second part focuses on the improvement of the glacier observation system through the development and regional application of a novel modelling approach relying solely on TSL observation for calibration (**Paper III & IV**). Full versions of the published articles can be found in Part II.

During the course of this PhD project, closely linked to the activities of the CATCOS, CAWa and CICADA projects, a rich database and various research products emerged through cooperative efforts between scientists of different national and international research institutions. In the appendix of this thesis, supplementary data acquired in the framework of these cooperative efforts are shortly summarized and brought into context with the thesis. An exhaustive list of data is provided and the data is available at the Department of Geosciences of the University of Fribourg.

3.1 Glacier monitoring in Central Asia

Paper I: Re-establishing glacier monitoring in Kyrgyzstan and Uzbekistan, Central Asia

Hoelzle, Martin, Erlan Azisov, **Martina Barandun**, Matthias Huss, Daniel Farinotti, Abror Gafurov, Wilfried Hagg, Kenzhebaev, Ruslan, Kronenberg, Marlene, Machguth, Horst, Merkushkin Alexandr, Moldobekov Bolot, Petrov Maxim, Saks Tomas, Salzmann Nadine, Schoene Tilo, Tarasov Yuri, Usubaliev Ryskul, Vorogushyn Sergiy, Yakovlev Andrey and Zemp Michael. *"Re-establishing glacier monitoring in Kyrgyzstan and Uzbekistan, Central Asia."* Geoscientific Instrumentation, Methods and Data Systems 6, no. 2 (2017): 397-418.

Paper I introduces the applied monitoring strategy for selected glaciers in the Tien Shan and Pamir-Alay constituted within the CATCOS, CAWa and CICADA projects. The monitoring strategy presented is in accordance with GCOS, and the paper discusses the implementation in the context of Central Asia. The key components to reach a sustainable monitoring programme are (1) the collection, homogenization and securing of historical data, (2) the re-establishment of suitable glacier monitoring sites and (3) the capacity building and twinning activities. The article highlights the value of historical mass balance series and describes most relevant components of resuming discontinuous monitoring sites in detail.

The choice of the to-monitored glaciers was guided by their accessibility, the availability of historical data, the topo-climatic distribution within a mountain range, the suitability for long-term monitoring based on the glaciological feasibility and the availability of other measurements (i.e. length change, meteorological or hydrological observations). Based on a careful evaluation of the aforementioned criteria the modern monitoring network was (re-)established on Abramov (Pamir-Alay), Barkrak Middle, Golubin, Batysh Sook and Glacier No. 354 (Tien Shan).

A detailed review on the individual measurement setups, as well as an overview on the glaciological, hydrological and climatological settings of each selected glacier completes the description of the prevailing topo-climatological characteristics of the Central Asian mountain ranges. Essentially, the authors advocate extending conventional glaciological in situ measurements with remote sensing observations and numerical modelling to generate high quality products relevant to create sound long-term mass balance series for selected benchmark glaciers. Such baseline data is indispensably needed for (1) enhanced process understanding, (2) model validation / calibration, (3) change detection and (4) impact assessments.

The paper highlights the promising results on the re-established observation network but points towards the need of enhanced capacity building as one of the most urgent needs for a sustainable monitoring. Further, continuous long-term support and cooperation among several countries and institutions is required to keep the successfully re-established measurements alive. The paper provides a recommendation scheme for the (re-)establishing of mass balance measurements on either abandoned or unmeasured sites in the context of international collaboration efforts to support sustainable monitoring and the (re-)growth of a scientific community in the cryosphere research domain.

This summary is based on a manuscript **published** in the peer-reviewed journal *Geoscientific Instrumentation, Methods and Data Systems*

Paper II: Re-analysis of seasonal mass balance at Abramov Glacier 1968–2014

Barandun, Martina, Matthias Huss, Leo Sold, Daniel Farinotti, Erlan Azisov, Nadine Salzmann, Ryskul Usubaliev, Alexandr Merkushkin, and Martin Hoelzle. *"Re-analysis of seasonal mass balance at Abramov glacier 1968–2014."* Journal of Glaciology 61, no. 230 (2015): 1103-1117

Paper II built upon the strategy presented in Paper I and combined current mass balance surveys with historical measurements for Abramov Glacier. Glaciological measurements exist from 1968 to 1998 and the mass balance monitoring programme has been re-established in 2011. Existing data was re-analysed and a spatially distributed mass balance model provided continuous daily time series covering the period 1968–2014. For the re-analyses, the model was exclusively used as an extrapolation tool to reach glacier-wide coverage from the direct point measurements. Thus, while strictly referring to the measurement dates, the mass balance is closely tied to the in situ observations and insensitive to the model setup. To reconstruct the mass balance from 1999 to 2011, the model was calibrated with all available seasonal field surveys and used to calculate daily mass balances for the unmeasured years. The reconstructed series were validated through a comparison between simulated and observed TSLs. A parameter re-adjustment was preformed if necessary to provide a best possible estimate. TSL have been delineated manually on optical satellite images and after 2011, photographs from automatic terrestrial camera images were used in addition.

Abramov Glacier exhibited a considerable mass loss from the late 1960s until the end of the 20th century. The results indicate convincing evidence that this trend was continued in the beginning of the 21st century, and inferred a mean annual total mass balance of -0.44 ± 0.10 m w.e. yr^{-1} for 1968 to 2014. The obtained results were compared to geodetic volume changes over the last decade and to a GPR survey in the accumulation zone resolving several layers of accumulation. The at the time available geodetic mass budget for Abramov Glacier from 1999 to 2011 suggested a close-to-zero mass balance for the last decade which contradicts the results provided in the article. However, the accumulation rates estimated from the GPR profiles indicated a low plausibility for equilibrium conditions over the past 15 years.

The ability to adjust the measurement period to the hydrological year and to fill the measurement gaps using a model, enabled the generation of continuous and homogenous time series that facilitated interpretation of annual to inter-annual variability, detection of changes in the mass balance pattern or comparison to other studies and methods. However, as such, the modelled daily mass balance is not strictly representing the observations conducted in the field, and the results might be related to increased uncertainties connected to model parameters, calibration procedure and the input data. The use of a model-based approach, however, proved to be particularly beneficial when the measurement periods are inconsistent or data gaps hamper sound analysis with conventional methods. Importantly, our results show that TSL observations on remote imagery provided essential information to allow model validation when no other data was available.

This summary is based on a manuscript **published** in the peer-reviewed journal *Journal of Glaciology*

3.2 Transient snowlines to support glacier monitoring

Paper III: Multi-decadal mass balance series of three Kyrgyz glaciers inferred from modelling constrained with repeated snowline observations

Barandun, Martina, Huss Matthias, Berthier Etienne, Kääb Andreas, Azisov Erlan, Bolch Tobias, Usubaliev Ryskul, and Hoelzle Martin. *"Multi-decadal mass balance series of three Kyrgyz glaciers inferred from transient snowline observations"*, The Cryosphere, 12:1899-1919.

Paper III dispatched the development of a methodology to include TSL observations for annual model calibration in order to improve the gap filling and the reconstruction of SMB time series for monitored glaciers based on a minimum of input data. The paper proposed the use of TSL throughout the melting season obtained from satellite optical imagery and terrestrial automatic cameras. By combining modelling with remotely acquired information on summer snow depletion, glacier mass changes for unmeasured years were inferred. Multi-annual mass changes based on high-resolution digital elevation models and in situ glaciological surveys were used to validate the results for the investigated glaciers.

The results based on high-resolution geodetic and in situ data confirm a continuous mass loss of the three glaciers found with the TSL constrained model: Abramov, Golubin and Glacier No. 354. Our results suggest slightly less negative SMBs for Abramov of -0.30 ± 0.19 m w.e. yr^{-1} located in the Pamir-Alay than for the Tien Shan glaciers Golubin of -0.41 ± 0.33 m w.e. yr^{-1} and Glacier No. 354 of -0.36 ± 0.32 m w.e. yr^{-1} from 2004 to 2016.

Through the combination of different approaches, it was possible to compensate to some extent the limitations and shortcomings of each individual method. The results indicated that an integration of snowline observations into mass balance modelling significantly narrows the uncertainty ranges of the estimates. Model sensitivity experiments revealed a relatively low sensitivity to the input parameters and the meteorological data used, indicating a considerable advantage in comparison to conventional mass balance modelling that does not include direct glacier-specific observations. Hence, the integration of snowline observations into conventional modelling was shown to be highly beneficial for filling the gaps in long-term SMB series for periods for which direct glaciological measurements were discontinued. Furthermore, the paper highlights the potential of the methodology for an application to unmonitored glaciers at larger scales for which no direct measurements are available.

At present, mass balance observations in the Pamir and Tien Shan are relatively sparse but crucially needed to improve the understanding of glacier behaviour in the context of climate change and of the consequences on future water availability. Direct measurements are important but costly, laborious and require an immense logistic effort. For remote and unmonitored regions and countries, lacking of financial resources and infrastructure to support such monitoring programmes, our proposed approach delivers a tool for investigating and reconstructing the SMBs with minimal efforts.

This summary is based on a manuscript **published** in the peer-reviewed journal *The Cryposhphere*

Paper IV: Region-wide estimate of annual glacier mass balance for the Tien Shan and Pamir from 2000 to 2017

Barandun, Martina, McNabb Robert, Naegeli Kathrin, Huss Matthias, Bunting Pete, Berthier Etienne and Hoelzle Martin. *"Region-wide estimate of annual glacier mass balance for the Tien Shan and Pamir from 2000 to 2017"*, Frontiers in Earth Science: in preparation.

Most regional mass balance assessments for the Tien Shan and Pamir focus on decadal mass changes and only a few consider annual time series, hampering a reliable analysis of region-wide annual variability of glacier response to climate change. In Paper IV, multi-annual glacier mass changes derived from remote sensing are complemented with seasonal to annual mass balance series inferred from modelling closely constrained with TSL observations on a regional scale. The methodology elaborated in Paper III was adapted for region-wide application and extended with a second-order calibration using geodetic mass balances. Thereby, model adjustment was performed until the modelled multi-annual mass change agreed within the uncertainty range of the geodetic estimate. The TSL-constrained modelling approach is applied on all glaciers larger than $2\,\mathrm{km}^2$ situated in the Kyrgyz Ala-Too, the Pamir-Alay and the Akshiirak massif from 2000 to 2017. Geodetic mass changes were calculated for all glaciers larger than $1\,\mathrm{km}^2$ of the entire Tien Shan and Pamir.

To discriminate snow covered and bare-ice surfaces on a regional scale, an automated, multi-step classification scheme to derive spatially distributed shortwave broadband albedo for the glacierised area of each scene was used. The DEMs used to calculate the geodetic mass change were computed with the MicMac for ASTER package using all freely available ASTER scenes with acceptable quality from 2000 to 2017.

A geodetic mass loss of $-0.52 \pm 0.53\,\mathrm{m\,w.e.\,yr^{-1}}$ was calculated for the Tien Shan and $-0.24 \pm 0.43\,\mathrm{m\,w.e.\,yr^{-1}}$ for the Pamir. With the TSL-constrained modelling, a decadal mass loss for the three mountain ranges, the Kyrgyz Ala-Too, Pamir-Alay and Akshiiirak ranging from -0.36 ± 0.32 to $-0.44 \pm 0.32\,\mathrm{m\,w.e.\,yr^{-1}}$ from 2000 to 2017 was confirmed. Annual variability is similar for the Kyrgyz Ala-Too and Pamir-Alay and diverges considerably from the Akshiirak massif, having comparably reduced yearly fluctuations. We could further show that the annual variability of the glaciers increased for the Kyrgyz Ala-Too and the Akshiirak massif but glacier response became more homogeneous for the Pamir-Alay.

The presented mass balance time series annually tied to TSL observations and decadaly tied to the geodetic estimates, enable the analysis of yearly mass balance variability for glaciers in a region with few measurements within the bounds of a multi-annual geodetic estimate and deliver important baseline data for in depth analysis of the glacier response to climate changes on elevated temporal resolution. The presented approach allows, thus, an optimal reconstruction of annual mass balance series of inaccessible and remote glaciers with minimal effort merging information from geodetic mass changes and temporal variations of the snow-cover.

This summary is based on a manuscript **in preparation** for the peer-reviewed journal *Frontiers in Earth Science*.

Chapter 4

Synthesis and Perspectives

4.1 Synthesis

The research on glacier SMB observations in Central Asia from local to regional scale, presented various interesting insights but also revealed challenges and limitations. These are discussed and put into context hereafter, structured along the pathway from a local to a more regional application. First, achievements and major challenges connected to the re-established monitoring on selected glaciers as well as the general findings on glacier changes in the Tien Shan and Pamir are summarized, these are followed by a consideration of the potential, but also of the limitations connected to the use of TSL observations for mass balance estimates. The chapter is closed with a discussion on the applicability of the developed approach in a regional context.

4.1.1 Re-established glacier monitoring in Central Asia - challenges and perspective

After eight years of monitoring efforts in Kyrgyzstan, four glaciers have continuously been measured and data has been delivered to the WGMS through collaborative efforts between national and international institutions. A group of scientists has been trained in data acquisition and analysis and is able to conduct the measurements independently and thoroughly. Collaboration focuses mainly on two institutions, the CAIAG and the Kyrgyz Hydromet. Throughout the project duration, those two institutes collaborated in the field of Glaciology and joint efforts for the establishment of a Cryosphere Science Centre are in process. Through a bottom-up approach, we were able to motivate young scientists and students to find a perspective in Glaciology. We received increased support from the section leaders, head of departments and institutions for our activities related to the glacier monitoring and the capacity building without direct financial benefit. The reward of their collaboration is compensated through knowledge gain and scientific publications as well as increased national and international reputation, facilitating the acquirement of follow-up projects and other collaborations. During the course of the eight years, this is a remarkable development, since institution leaders have been accustomed to projects benefiting infrastructure and salary mostly, and the CATCOS or CICADA approach was new to them.

Uzbekistan looks back on a long history and historical importance of Glaciology. Former Soviet glaciologists are still active today and knowledge was conserved to a certain degree. However, the institutional understanding of the cryosphere research is largely gone, resulting in the fact that the re-establishment of the glacier monitoring was launched much slower in Uzbekistan. After repeated efforts, in 2016 full permissions and support were obtained and together with the Institute of Geology and Geophysics, Laboratory of Glacial Geology a first field campaign could be organised. One of the biggest challenges was the establishment of the contacts to young and scientifically active scientists that are motivated and have the capacity to be involved on a long-term. After two years, we were able to establish profound trust and a close network of collaborators that show motivation and willingness to integrate themselves into the future monitoring activities. In the second year, collaboration was extended to UzHydromet as one of the principal partners. The National University of Uzbekistan and the Tashkent Institute of Irrigation and Melioration show serious interest in participation. The project in Uzbekistan is still very young and has yet to focus on identifying suitable long-term collaboration partners and scientists. Recent efforts within the CICADA project try to extend the monitoring programme to Tajikistan in order to establish a first sustainable glaciological measurement network in the Tajik East Pamir. At current state, collaboration with local institutes and partners has been established and a first field visit is planned for summer 2018.

Kazakhstan is the only Central Asian country for which glacier monitoring has been continued after the Soviet Union. As a consequence, the institutional understanding of cryosphere research as well as knowledge transfer has continued. Activities in Kazakhstan, thus, focus mainly on specific support on modern technology and installations, and on a more advanced level of capacity building.

We could identify an essential advantage in including former Soviet scientists of the different Central Asian countries into the capacity building activities. The presence of a mountain guide to instruct necessary mountaineering techniques and safety skills was found to be of paramount importance for the sustainability of the monitoring. Today, we are able to rely on a team of international and national instructors to accompany the programme activities over the national boundaries. The trans-boundary activities of the project are of great importance to strengthen the relationship and cooperation of the different, usually undermanned local institutions.

The progress made in recent years, promises a future perspective for the glacier monitoring network in Central Asia. However, it is a fragile equilibrium between the cooperation partners, and a complex pattern of political relations influence the sustainability of the programme. The interest and focus of the institutions might change relatively rapid, and as long as no established governmental support is guaranteed, the future of the rebuilt monitoring is delicate. With the applied bottom-up approach, we might fail to reach policy makers and stake holders on the highest level and are unable to transmit the message of value and necessity of the glacier monitoring for their country. For the next three years, funding is guaranteed through the CICADA project to continue the glaciological measurements and to profound the skills of our local partners. During this time, responsibilities, including tasks related to observations and capacity building will be handed over to national institutions step-by-step. Until then, however, the financing of future field campaigns has to be solved from within the countries to guarantee the stability of the glacier monitoring on a long run.

4.1.2 Summary of the detected glacier mass change in the Tien Shan and Pamir

Re-analysed historical glaciological measurements, reconstructed mass balance data and re-initiated in situ measurements provided a comprehensive and complete mass balance time series for Abramov, Golubin, Batysh Sook and Glacier No. 354 (see Paper I, II and Appendix A). The modern direct measurements revealed mass losses ranging from -0.25 to -0.51 m w.e. yr^{-1} (2011-2016) and reconstructed mass balances confirmed the negative signal for the last decades for the aforementioned glaciers (-0.30 to -0.43 m w.e. yr^{-1} from $\approx$2000 to 2014; Paper I, III, Appendix A). First mass balance calculations reported moderate mass loss of -0.10 to -0.25 m w.e. yr^{-1} for Barkrak Middle Glacier since 2017 (unpublished results). Comparison of the reconstructed mass balance time series with published geodetic mass changes showed good agreement for Glacier No. 354 (Brun et al, 2017; Kronenberg et al, 2016) and for Golubin (Bolch, 2015; Paper III). For Abramov, geodetic mass change of -0.36 ± 0.07 m w.e. yr^{-1} derived from aerial photographs and high-resolution optical satellite data for 1975 to 2015 also agreed well with the here presented reanalysed and reconstructed time series (Appendix A) but disagreed with results derived by Gardelle et al (2013), however overlapped within the respective uncertainties (Paper III). The mass balance model calibrated with historical and modern in situ measurements predicted more negative values for Abramov for years without direct observations (Paper II). Contrarily, good agreement was found for the different model setups and the geodetic assessments for Glacier No. 354 and Golubin (Paper III, Appendix A). From the long-term mass balance time series, several short periods of close to zero mass balances (late 1960s / early 1970s and late 1980s / early 1990s) were observed. Overall, mass loss was however dominating (Paper II, Appendix A). Unfortunately, meaningful comparison between the different studies was not always straightforward due to a very limited number of studies assessing the mass change of individual glaciers in the region and due to differences in study periods between the assessments.

Region-wide geodetic estimates based on multi-temporal series of ASTER scenes (Paper IV) agreed with the mass loss observed for the individual glaciers relatively well and hence, underlined the representativeness of the chosen glaciers for the monitoring (Paper IV). Comparison to other geodetic assessments showed good agreement for the Inner and Central Tien Shan (Brun et al, 2017; Farinotti et al, 2015; Gardner et al, 2013) and for the Northern / Wester Tien Shan (Brun et al, 2017; Bolch, 2015; Gardner et al, 2013). For the two aforementioned regions, an ASTER derived average mass loss of -0.48 ± 0.64 m w.e. yr^{-1} and -0.43 ± 0.68 m w.e. yr^{-1}, respectively, was encountered from 2004 to 2012.

Major disagreement between different studies was found for the Pamir / Pamir-Alay (Brun et al, 2017; Pohl et al, 2017; Farinotti et al, 2015; Kääb et al, 2015; Gardner et al, 2013; Gardelle et al, 2013). Figure 4.1 highlights the discrepancy between the assessments leading to ongoing debates over the ambiguous mass balance regime and its change in the region. The TSL-constrained modelled time series are situated somewhere between results of other publications (Brun et al, 2017; Pohl et al, 2017; Farinotti et al, 2015; Kääb et al, 2015; Gardner et al, 2013; Gardelle et al, 2013) and indicated less negative mass balances than the ASTER derived geodetic balance (Fig. 4.1). Important methodological differences, input data quality and inconsistent study periods and spatial divisions might explain the differences between the studies to some extent. Underestimated penetration depth of radar sensors lead to overestimated mass balances (Kääb et al, 2015; Berthier et al, 2016; Dehecq et al, 2016). Pronounced variations of the topographic and meteorological

settings throughout the region are responsible for a locally variable and distinct spatial pattern of the glacier response in the Pamir and Pamir-Alay (Glazirin et al, 1993; Pohl et al, 2017), and inhomogeneous study areas might generate different results. With the help of the annual resolved time series based on the TSL-constrained modelling, differences due to inconsistent time periods and study areas could partly be dismantled. The analysis of IceSat datasets tended to represent a rather negative period from 2004 to 2008. Studies including the early years of the century (2000 to 2003) included more favorable years (Paper IV) and hence led to higher mass balance averages (Fig. 4.1).

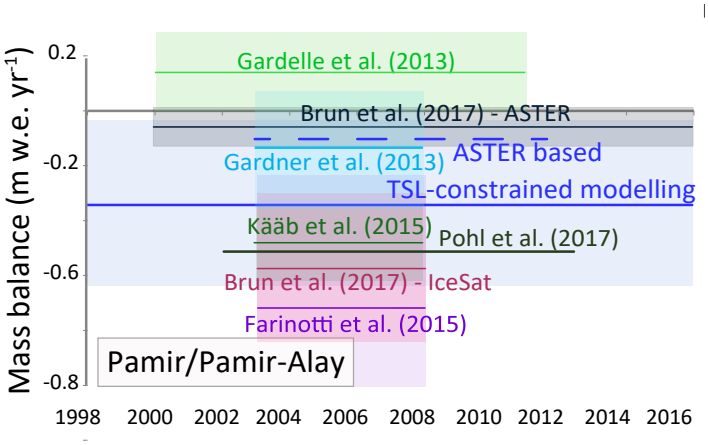

Figure 4.1: Long-term average mass balances from various studies in comparison with the TSL-constrained modelled mass balance for the Pamir / Pamir-Alay. Lines indicate the mean annual mass balance over the respective periods for each study, and shaded squares represent the corresponding uncertainty. For the study by Brun et al (2017) results based on ASTER DEMs and IceSat are presented separately. The results from the TSL-constrained model (blue line) and values derived from ASTER datasets (dashed blue line) for the Pamir-Alay are shown in blue.

4.1.3 Detection of TSL on remote sensing imagery

Space- and airborne observation of the TSL have a long history (LaChapelle, 1962; Meier and Post, 1962; Østrem, 1975; Dozier and Marks, 1987) and more recently ground-based time-lapse photography found increased utility in snow-cover monitoring (Farinotti et al, 2010; Parajka et al, 2012). Paper I promotes the coupling of glaciological measurements with AWS and terrestrial cameras. The terrestrial cameras aim primary on the monitoring of the snow depletion pattern during the ablation season. Most of the here presented glacier monitoring sites are equipped with terrestrial cameras. In Paper II and III, the good agreement between the delineated TSLs mapped on spaceborne and ground based imagery was shown. However, data acquisition and handling is connected to different, source specific limitations and challenges. Figure 4.2 compares the different workflow relevant to achieve data for TSL mapping from a terrestrial camera system to the one of a spaceborne system. In the following the utility of the terrestrial platforms in comparison to spaceborne systems is critically evaluated, highlighting advantages and disadvantages of both systems regarding different aspects. Finally, perspectives to overcome the limitations of the different systems are outlined.

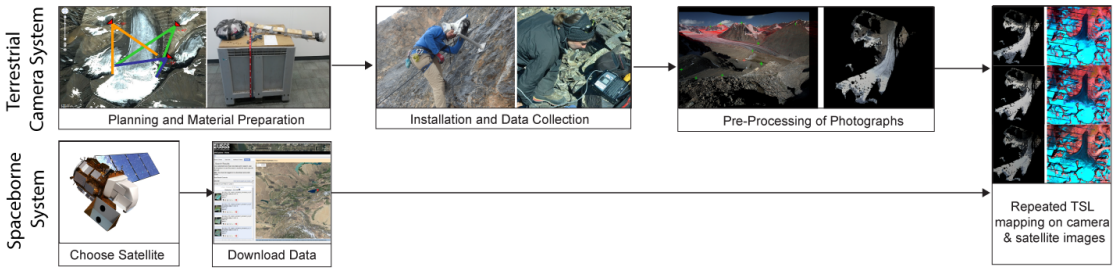

Figure 4.2: Comparison between the process chain of data acquisition and gathering from terrestrial platforms and spaceborne systems.

Data acquisition and gathering

Automatic terrestrial camera setups are flexible and can be designed specifically to retrieve data according to the research objectives. The high temporal and spatial resolution helps to ensure data availability and quality. However, installations of such systems are connected to a rather elevated logistical effort. Site accessibility, in this particular case also restricted through nation's security regulations, complicates the installation and eminently the maintaining. Often, it is necessary to compromise between accessibility, safety, camera setup and image coverage. Frequently, due to the oblique view angle and limited possibilities for a suitable installation site, image framing is not ideal. Data loss due to slowed down commissioning, repeated camera failure or complete platform destruction are common.

Contrasting, for spaceborne systems, these issues are usually not of the researcher's concern, and raw or pre-processed data is accessible on a ready-to-use basis provided through online platforms or databases. Such time-saving data access is very convenient, and allows focusing on the analysis rather than on the acquisition process itself. Further, the extended spatial coverage is a further advantage. Until today, however, repeat cycles for sensors with sufficient high spatial resolution for TSL monitoring of individual glaciers are still limited (Rabatel et al, 2012). With modern development of different new sensors, often related to private earth-observing companies, such constrains might soon be overcome (Popkin, 2017). In particular, the micro / nano satellite technology offers new data sources to monitor TSL on high spatial and temporal resolution, in both the optical and radar domains such as BlackSky, IceEYE, Earth-i, AxelSpace or AstroDigital. Since summer 2017, the PlanetScope CubeSat sensors, for example, deliver daily global coverage in the VNIR on a spatial resolution of 2-4 m (Kääb et al, 2017; Altena et al, 2017). Or similarly, a novel mission concept has been developed by Sarno et al (2018), based on a formation of very low altitude passive small satellites, intercepting the signal transmitted by existing Low Earth Orbit SARs. Most of this very small satellites have still a reduced lifetime and continuity, are commercial or only provide processed data (Popkin, 2017). However, looking back onto the development of the past five years, quantity, capability, repeat cycles and spatial resolution of satellite imagery has immensely increased - a development that will probably continue in an exponential way and challenge the use of terrestrial camera systems in the future fundamentally.

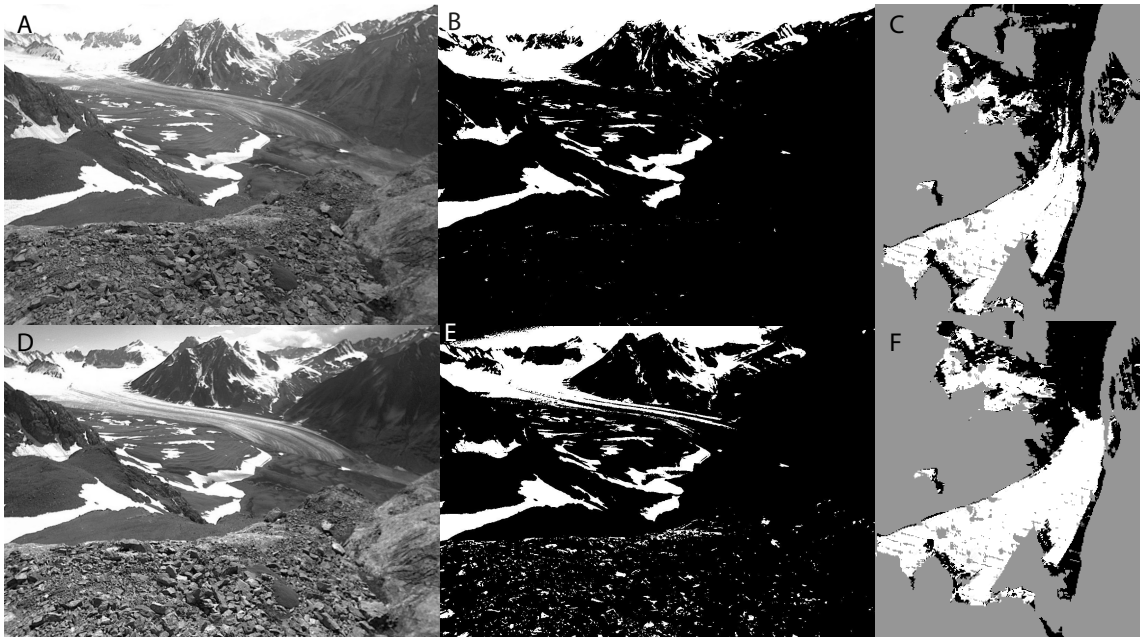

Figure 4.3: Terrestrial camera image from Abramov for **(A)** ideal illumination conditions and with **(D)** over-saturation at the glacier snout of the same day (21/07/2012) but at a different time of the day. The corresponding automatically classified image is shown in **(B)** an **(E)**, respectively. In **(C)** and **(F)** the projected classified images are shown. For image classification a self-adapting histogram threshold algorithm to separate high and low reflectance was used (Otsu, 1979).

Data processing and TSL detection on terrestrial camera images

Terrestrial camera image processing is connected to quite labour-intense pre-processing steps including pre-selection, geometric and radiometric corrections, projection and orthorectification (Corripio, 2004). Most of these steps are not yet fully automatized and are camera related (Lebourgeois et al, 2008). Consequentially, for terrestrial camera images, quantitative data acquisition capabilities might still be limited (Lebourgeois et al, 2008). Probably the most important disadvantage to spaceborne systems, is the oblique view angle of the image framing, making data preparation for quantitative analysis laborious and not trivial. Often the camera view angle is unfavourable to monitor the accumulation area (Huss et al, 2013).

Terrestrial cameras record typically only in the Red, Green and Blue (RGB) channels. Due to the reduced spectral bands, automatic classification of snow-cover, especially over ice is not straightforward (Farinotti et al, 2010; Huintjes et al, 2015b), nevertheless possible (e.g., Huss et al, 2013). Such automatic-classification is found to be very sensitive to illumination and acquisition conditions (Fig. 4.3). For our setup, high-clouds improved conditions for automatized TSL mapping using self-adapting histogram thresholding (Otsu, 1979). Contrary to optical satellite images, high-cloud cover rather attenuates image quality and hence, displays one of the major benefits of the ground-based platforms. However, to avoid misclassification a vicarious pre-selection of the images is necessary to ensure reliable results. In Paper II and III, manual TSL delineation was judged to be more suitable and robust (Fig. 4.4).

To recapitulate the advantages of the flexibility of the camera system, the high temporal and spatial resolution and the reduced sensitivity to high-cloud cover are challenged by

repeated data loss, limited spectral information and laborious pre- and post-processing. Thus, in order for terrestrial camera systems to be able to compete with spaceborne systems in the future, more work is primary needed in the data handling to simplify and accelerate pre-processing and automatic classification procedures.

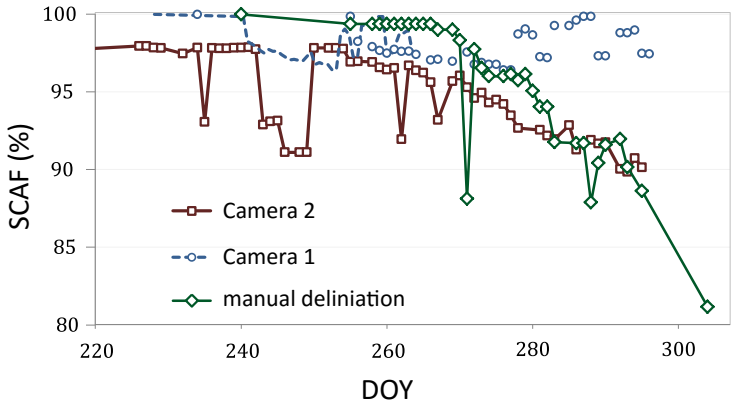

Figure 4.4: Automatic image classification of photographs collected at terrestrial cameras from the Abramov monitoring in comparison to manual delineation (see Fig. 6.3 for camera setup and location). Camera 2 performs better than 1 especially when snowline starts to rise. Contrary, Camera 2 performs worse for the entirely snow covered glacier.

Data processing and TSL detection on satellite images

Pre-processing of satellite images rely on automatized and well-established procedures (Bunting, 2017). Different methods exist to automatically discriminate snow over ice surface and allow effective and fast TSL mapping (e.g., Hall et al, 1995; Barcaza et al, 2009; Rabatel et al, 2012), however accuracy is not always satisfying. The frequently used NDSI or Band Ratio methods use a manually selected threshold value separating the different surface materials. The performance of the threshold depends on the degree of separability of the spectral signatures and is usually empirical (De Angelis et al, 2007). Heiskanen and Kivinen (2008) and De Angelis et al (2007) identified that misclassifications are connected to shadows and debris-cover of ice and snow. Cloud cover and their shadows are still an issue and visual interpretation is often applied to improve results (Zhang and Kang, 2017). Thus, optical thick clouds remain one of the major limitations for optical satellite sensors (Zhu et al, 2015) and automatic filters still show flaws in the processing chain (Irish, 2000) hampering sound automatic classification of TSL on optical satellite images.

In Paper IV, we use broadband albedo maps from Landsat to classify glacier surface characteristics. The separation of snow and ice primary depends on the albedo of the surface classes. The classification from the albedo maps is thus, based on physical parameters, the albedo, unique for both snow and ice (Naegeli et al, 2018). This makes the chosen approach preferable over conventional surface classification algorithms. It is possible to account for fresh snowfall and changes in other surface characteristics due to a physical interpretation of the albedo. However, a range of values for ice and snow can overlap considerably, and a straightforward classification is not always possible (Naegeli et al, 2018). Nonetheless, the transition of the albedo between ice and snow is characterized by

a distinct change (e.g., Hall et al, 1987), and the greatest slope of the albedo-elevation profile approximates the limits between snow and bare-ice surfaces well (Naegeli et al, 2018). Despite the advantage of using albedo maps for surface classification highlighted in Figure 4.5, prevalent problems related to limitated quality of the surface reflectance data (over-saturation), cloud cover and shading have not entirely been resolved yet, and reliable automatic TSL classification on optical multi-temporal satellite scenes still demands improvement.

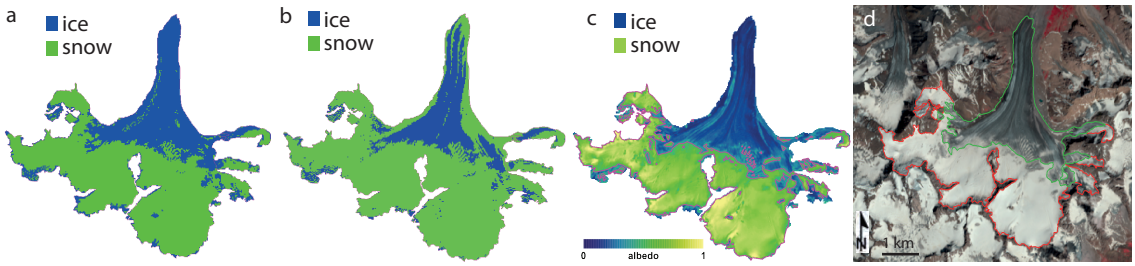

Figure 4.5: Surface type classification based on a Landsat scene for Abramov Glacier using **(a)** Spectral Angular Mapper, **(b)** NDSI **(c)** albedo thresholding and **(d)** manual delineated of the surface types. In comparison to the manual mapping the albedo methods reveals best and most detailed results. (*Figure Courtesy: Kathrin Naegeli*).

Multi-sensor approach for transient snowline mapping

Some limitations using optical satellite sensors (i.e. optical thick clouds, night-time images), can be overcome using SAR data. TSL delineation on SAR images has proofed suitable in the past (Rott, 1984; Hall et al, 2000) and with evolving sensor capability and increased repeat cycles, SAR sensors show the potential of becoming a powerful tool for multi-temporal TSL mapping (Callegari et al, 2016; Winsvold et al, 2018). For, example, the ability to detect superimposed ice zones highlighted in Winsvold et al (2018) and Thakur et al (2017) are of considerable interest for TSL mapping of those Central Asian glaciers for which significant superimposed ice coverage is observed.

Using multi-temporal information from the different and independent satellite sensors in a complementary way, more accurate and complete TSL monitoring is possible. Callegari et al (2017) and Winsvold et al (2018) took first steps towards a multi-temporal and multi-sensor approach for TSL mapping, however more work is needed to develop standardized (semi-)automatic procedures to achieve a more ready-to-use and accessible method for combining both optical and radar systems.

4.1.4 Transient snowlines to support glacier monitoring

Comparison to conventional ELA / AAR - methods

End-of-summer snowlines have frequently been used to calculate annual SMB time series (e.g., Kulkarni, 1992; Rabatel et al, 2005). One of the distinguished values of the method is the close association to the observation and hence the model independence. In Paper III a model constrained with TSL information is used, and the provided annual SMB series cannot be considered as purely observation based. Hence, the approach has lost the model independence and cannot be promoted as a tool to monitor glacier mass balance directly. Yet, Paper III showed that the close tie to TSL observations renders the method relatively

insensitive to model parameters and meteorological input data. It was also demonstrated that the performance drastically increased in comparison to unconstrained modelling or to a model calibrated with available in situ measurements of a distinct time period as used in Paper II.

The ELA / AAR method includes direct glaciological measurements to either establish a relation with the annual balance or by using a measurement based balance gradient (e.g., Braithwaite, 1984a; Dyurgerov et al, 1992). For a regional application, extrapolation in time and space is needed, for which especially the temporal dimension is critical (Braithwaite, 1984a; Dyurgerov and Meier, 2000). For the methodology provided in Paper III, a relation between TSL and SMB is annually recalculated for each glacier individually independent from glaciological observations. Hence, extrapolation of the relationship in space and time is averted.

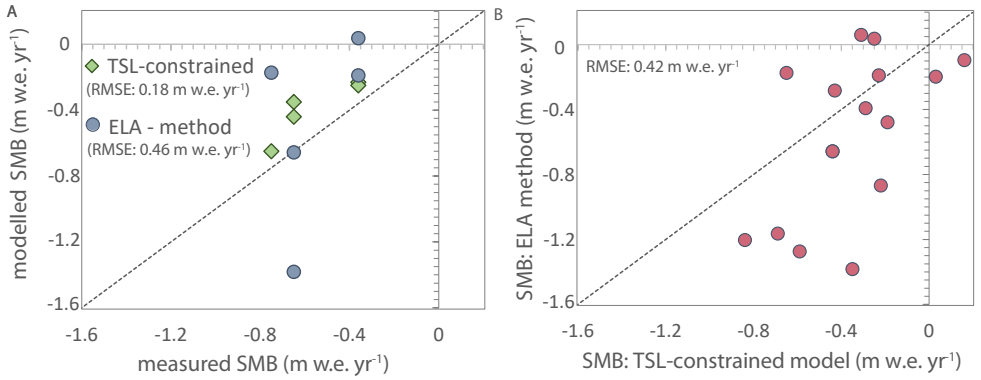

Figure 4.6: (A) Comparison of modelled SMB derived from TSL-constrained modelling and from using the ELA-Method with direct measurements for Abramov Glacier from 2012 to 2016. **(B)** Comparison between SMB derived from TSL-constrained modelling and ELA-method for Abramov Glacier from 2000 to 2016.

A critical limitation of the use of remotely sensed end-of-summer snowlines is the dependence on a single observation dating from the exact moment at the end of the balance year. The results are sensitive to the fact that this observation needs to represent exactly the end of the summer (Rabatel et al, 2016). Though, the limited availability of observations, typically decreasing towards late summer (Wu et al, 2014), and the difficulty to identify the end of the melt season is highly critical. Figure 4.6 compares the annual SMB obtained from the ELA-method, the TSL-constrained model and direct glaciological measurements for Abramov Glacier, underlining the advantage of using the TSL-constrained model. Using a linear relation between AAR and SMB revealed weak agreement with the direct measurements resulting in a RMSE of more than $0.5\,\mathrm{m\,w.e.\,yr^{-1}}$.

The use of the information stored in the temporal change of the TSL to reconstruct annual SMBs was highlighted already by Miller and Pelto (1999) and refined by Huss et al (2013). The methodology developed in this thesis relies strongly on the concept of using repeated information throughout the entire ablation period for calibration to avoid the dependence on a single observation. Sensitivity analysis showed that the image frequency is less important than a good distribution throughout the summer months (Paper III). A well-distributed image sequence captures the depletion pattern over large part of the glacier surface. The test revealed also that the model remains most sensitive towards the TSL observations from the end of the summer. However, in Paper III the dependence on

a single TSL observation could be reduced. An important benefit is, thus, the fact that the TSL observation does not strictly need to represent the end of the balance year to provide reliable results (Fig. 4.7).

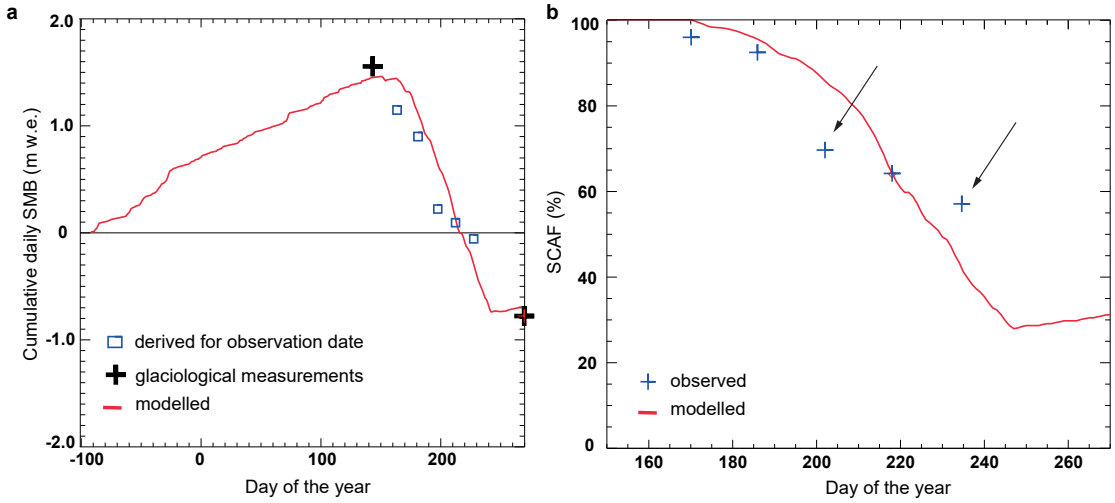

Figure 4.7: Illustrated is the reduced role of a single TSL due to the use of repeated observations for model calibration. **(a)** shows the daily cumulative SMB modelled and calculated from glaciological measurements. The sub-seasonal mass balance for each TSL observation date, derived through an annually derived rating curve between mass balance and the TSL is shown. **(b)** The modelled and observed SCAF is indicated. The total of the SCAF observations were used to calibrate the model. It is visible that a single delineated SCAF does not influence the modelled results notably.

TSL observations to infer surface mass balance on high temporal resolution

Dyurgerov et al (1994) was one of the first to highlight the use of TSL to capture sub-seasonal SMB. Based on his work, Hock et al (2007) used a mass balance model to connect the TSL observations to the SMB. Huss et al (2013) and Hulth et al (2013) went one step further by establishing a relationship between the TSL observations and (sub-)seasonal SMB or winter snow accumulation independent from direct measurements. Whereas Hulth et al (2013) still used ablation and snow density measurements to optimize melt factors to retrieve winter snow accumulation along the profiles of observed TSLs, Huss et al (2013) used exclusively TSL data for model calibration and provided glacier-wide sub-seasonal SMB estimates. Both studies related successfully the information stored in temporal change of the snow-cover pattern throughout the melt season to winter snow accumulation. Huss et al (2013) provided the conceptual idea to develop the approach presented in Paper III. Hereafter, a comparison aims at illustrating the generic and technical differences between the two studies.

Huss et al (2013) proposed a two phase framework that (1) estimated the winter snow accumulation and (2) calculated the glacier-wide mass balance. Phase 1 relied on a backwards modelling approach that couples snow cover depletion pattern with melt modelling. This phase has been adopted similarly in Paper III. Phase 2 addressed the calculation of the SCAF vs. SMB rating curves using the mass balance model. This rating curves can be understood similar to the relationship proposed by Dyurgerov et al (1994) connecting transient ELA observations to measured transient SMB. Whereas Dyurgerov

et al (1994) focused more on the improvement of the conventionally used ELA / AAR method by covering the entire range of possible ELAs over a glacier surface within an annual survey, Huss et al (2013) aimed on establishing a tool to infer sub-seasonal SMB without the use of direct field surveys.

Phase 2 has fundamentally been modified in Paper III with the principal aim of producing annual SMB time series and not sub-seasonal values. This re-orientation was mainly driven through the limited availability of TSL observations for the study region and period. In order to provide a tool to reconstruct mass balance time series and to ensure comparability to other glaciers and methods, the model structure had to be modified to implement a suitable extra- and interpolation between the TSL observation dates and to the end of the balance year. The model alteration bears the consequence of losing a part of the model independence highlighted in Huss et al (2013). Major adjustments of the approach involved the use of meteorological time series throughout the entire modelling procedure instead of the climate long-term mean in order to provide day-to-day variability. Secondly, the long-term climate temperature series were not shifted to represent only the last SCAF observation of each season. Instead all SCAF observations of one summer were used to calibrate the DDFs (Fig. 4.7). In Huss et al (2013) the pre-defined DDFs were held constant over time. The authors identified elevated model sensitivity to the DDFs in comparison to the other model parameters. The increased sensitivity justified to some extend the adjusted calibration scheme in Paper III. A similar test in Paper III revealed, however, that the constant-held ratio between the two melt factors for snow and ice still implies the highest sensitivity. It was also shown that this sensitivity is of half the value found then the one for the DDFs in Huss et al (2013). Thus, not only the importance of the total winter precipitation as indicated in Huss et al (2013) highlight the benefit of annual calibration but also the sensitivity to the DDFs indicate an improvement through their annual optimization. Sensitivities of other parameters are found to be of similar magnitude in both studies.

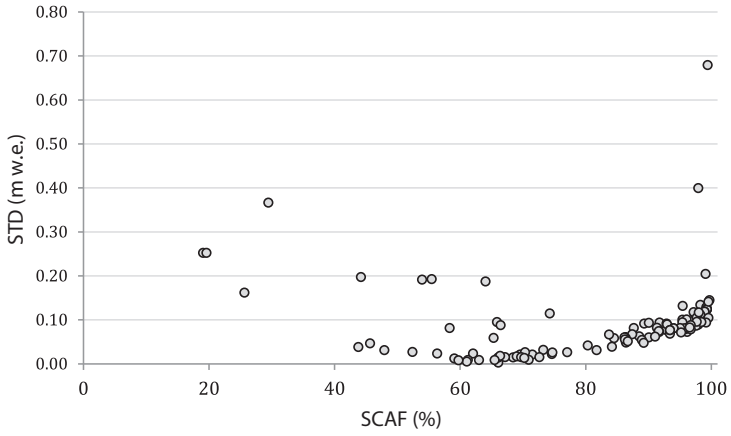

Figure 4.8: Standard deviations (STD) of the sub-seasonal mass balances encountered using different model parameters in comparison to the observed SCAF for the entire study period. Please refer to (Barandun et al, 2018) for details on the sensitivity test.

Using repeated TSL observations to infer sub-seasonal estimates

If the TSL is representative for the SMB, a set of TSL observations covering the full extent of the elevation range of a particular glacier can be linked to a measured or modelled sub-seasonal SMB of the same glacier. In other words, each observed TSL elevation relates to a specific glacier-wide transient SMB. By knowing the relationship between the TSL and the SMB, the SMB can be inferred for each TSL observation throughout the ablation season. Hereinafter, this relationship is referred to as the rating-curve between TSL and SMB. The use of a such rating-curve proposed by Dyurgerov et al (1994) and further developed by Hock et al (2007) and Huss et al (2013), provides an observation based approach to retrieve mass balance on very high temporal resolution for inaccessible and remote glaciers. From the in this thesis elaborated methodology, such a rating curve can be derived for each investigated glacier relatively straightforward. However, for the study region, an establishment of annually resolved rating curves might be hampered by limited frequency and distribution of the TSL observations.

Figure 4.7 shows the sub-seasonal mass balances obtained for each TSL observation through the use of an annual rating curve, indicating fairly good agreement with the modelled result. Even though validation is difficult, the performance of such rating curves is highlighted through the robustness of the derived sub-seasonal values towards changes in the model setup (Fig. 4.8). A sensitivity analysis by changing the constant model parameters by $\pm 25\%$ revealed a sensitivity twice as low for the sub-seasonal SMB than for the modelled annual SMB. Further illustrated is the variability increase for SCAFs close to 100%. This agrees with the findings presented in Hock et al (2007) and Huss et al (2013) that both outlined the influence of the total winter precipitation on the associated rating curve.

Figure 4.9 illustrates the relation between SMB and SCAF for Abramov, No. 354 and Golubin. The modelled SMB vs SCAFs for each TSL observation date of the corresponding study period are compared to the SCAF vs. sub-seasonal SMB derived from the annual rating curves. Overall they agree satisfyingly. However, the spread from year-to-year is much larger for the modelled values, especially for high SCAFs approximating an entirely snow covered glacier. Hence, the relationship from the annual rating curves, closer tied to the TSL observations, is more stable. This highlights the possibility to summarize the different annual curves to one optimal relation and promotes the use of all available TSL observations indifferent of the observation date. The establishment of an optimal rating curve can however become critical for very low SCAFs connected to very negative SMB that are seldom (Hock et al, 2007) and the SMB cannot be derived with the rating curve once the TSL rises above the upper glacier edge. In such cases the model is indispensable. The use of an optimal curve is smoothing out disadvantageously the signal of extreme years to some extent, where annual curves perform better. Nevertheless, the use of rating curves established between TSL and transient SMB carry a large potential to produce reliable time series on extremely high temporal resolution. Considering the increase of available remote sensing sensors for TSL monitoring in recent years and the accelerated tendency for the future seeking daily coverage, such an index allows not only the retrieval of almost daily sub-seasonal mass balances for the last years but also opens the door to an up-to-date estimate of the sub-seasonal glacier mass balance for remote and inaccessible glaciers on a time and cost effective basis.

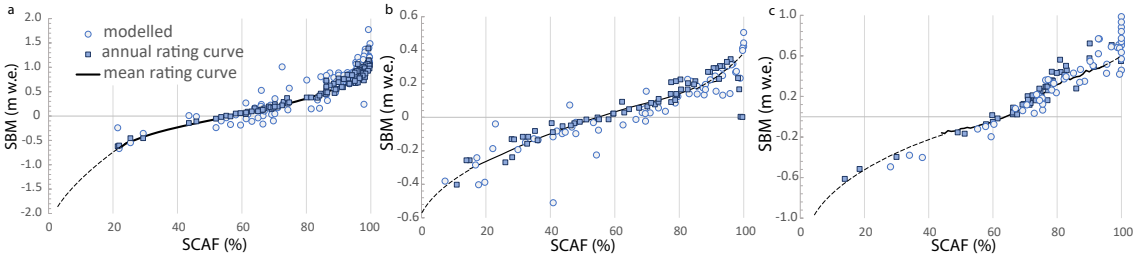

Figure 4.9: SMB versus SCAF for **(a)** Abramov, **(b)** No. 354 and **(c)** Golubin. Shown are the modelled sub-seasonal SMB and SCAF for each observation date (dots) and the SMB calculated using annual rating curves for each observation date (squares). The black line shows the average rating curve using all modelled SCAF vs SMB relations and the dotted line indicates its manual extrapolation to cover the entire range of possible SCAFs.

4.1.5 Applicability to other regions

The applicability of the approach to other regions is primary depending on the representativeness of the TSL for the transient SMB. Thus, the model is in principal applicable on glaciers for which a clear relationship between the TSL and the SMB exists. Such a relationship is found for most winter-accumulation type glaciers and might be questionable for the following cases: (i) presence of superimposed ice, (ii) summer snowfall, (iii) non-winter-accumulation type glaciers, (iv) debris covered, (v) surge-type glaciers and (vi) glaciers with important contribution of internal and basal balances. In the following these cases are discussed and the associated limitations of the model outlined. Figure 4.10 gives an overview for which RGI regions (RGI-Consortium, 2017) the TSL-constrained model might be applied without further adjustments (green) and for which regions one or more of the above mentioned constrains might be encountered and model application is not straightforward (orange). It is also shown for which regions the presented TSL based approach is not recommended (red).

Superimposed ice zones and summer snowfalls

In the presence of superimposed ice, the ELA, in comparison to the end-of-summer snowline, is shifted downwards to the lower limit of the superimposed ice zone (Cogley et al, 2011). Consequentially, the snowline elevation in such cases is typically overestimating the ELA and is hence disconnected from the mass balance. However, the proposed methodology in Paper III does not rely simply on the end-of-summer snowline but uses the information stored in the temporal change of available TSL observations. Consequentially, the influence of such misclassified TSLs on the model performance is reduced, as long as sufficient observation from below and / or above the superimposed ice zone is available. For Abramov Glacier, showing evidences of superimposed ice at the median glacier elevation, the model constrained with TSL performed reasonably well (Paper III) suggesting a possible applicability of the model in the case of superimposed ice (Fig. 4.11).

After a summer snowfall event the TSL can drop considerably during a few days, although the mass balance does not significantly change during this period (Huss et al, 2013). Hence, the link between the TSL and the transient SMB is equivocal during this period and cannot be used for calibration. However, similarly to superimposed ice, sporadic summer snow falls will not influence significantly the modelled results if sufficient other

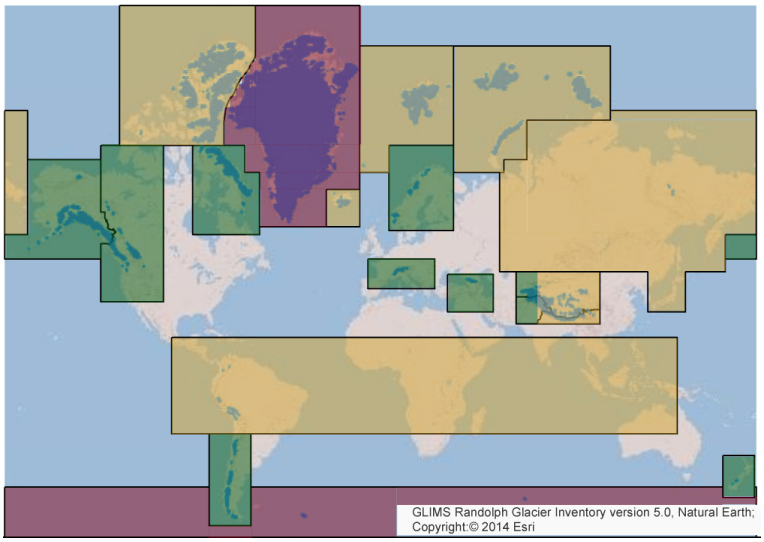

Figure 4.10: RGI regions for which the TSL-constrained modelling approach might be suitable (green). For the once in orange, the approach is principal applicable but might demand sever model adjustment and testing. In red, the regions for which a TSL-constrained model application might be critical.

observations are available for calibration. Nevertheless, it is recommended to discharge scenes with a substantial fraction of fresh snow (Huss et al, 2013, Paper III, Paper VI).

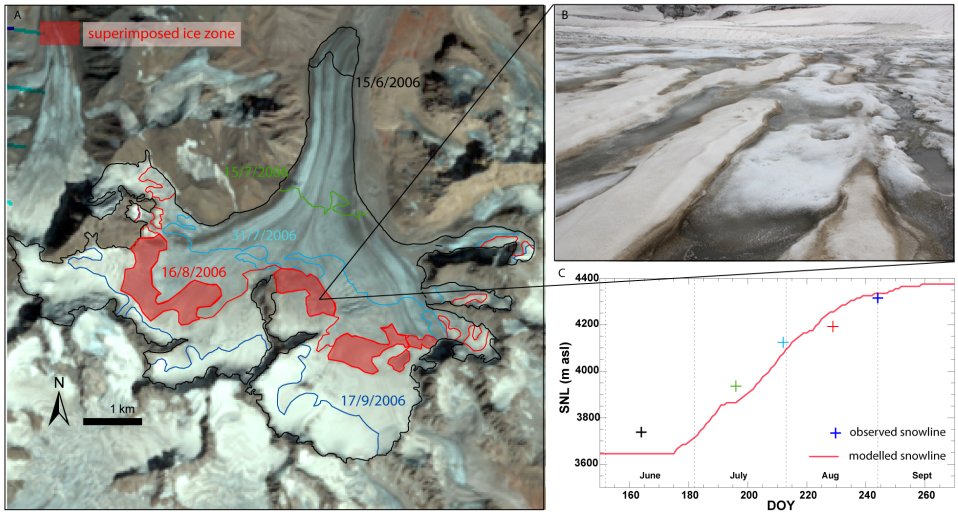

Figure 4.11: Repeated TSL observation on Abramov for the ablation season in 2006 (coloured lines and crosses). **(A)** All mapped TSL from June to September 2006, observing the step wise increase of the snowline, used for model calibration. Satellite image from the 16/08/2006 indicating evidences of superimposed ice, where snowline delineation is not straight forward. **(B)** picture taken of the zone where superimposed ice was observed in 2012. **(C)** comparison of the modelled snowline and the observed TSL. Through the use of several TSLs during one summer, the effect of the superimposed ice such as observed at Abramov can be reduced notably.

Non-winter-accumulation type glaciers

Dyurgerov (1996) shows that a relation between the TSL and the transient SMB exists for glaciers with enhanced accumulation during the summer month. However, Hulth et al (2013) argues that summer snowfalls, lowering the TSL interfere with the concept using TSL observation to constrain winter snow accumulation. Important summer snowfall, contributing significantly to the accumulation, can limit the model performance in the sense that the relationship between the snowline and the SMB is disturbed. This problem is especially pronounced for the TSL rise during the early ablation season where the glacier-wide transient SMBs might still be positive but the TSL already started to raise (Dyurgerov, 1996).

Considering the here used model setup, winter and summer seasons are strictly separated throughout the calibration procedure. Hence, non-winter accumulation is not considered as such. Persistent summer snowfalls are translated in a less rapid increase of the TSL, and reduced melt rates through the summer months or in an overestimated winter accumulation rather than associated to summer accumulation. Thus, despite the ability of the model to predict summer snowfall events, summer accumulation is not involved in the calibration procedure, leading to possible miscalibration of the melt factors and the precipitation correction factor. Consequentially, the representativeness of the seasonal and sub-seasonal components is limited. This, however, does not exclude that the annual SMB of the glacier is reproduced correctly. At the current state of this work more investigation on the model performance and the seasonal distribution is needed to clearly identify the potential and limitations of the presented methodology to simulate the mass balance of summer- and mixed-accumulation type glaciers on seasonal to sub-seasonal resolution. To overcome the limitation connected to the capability to reproduce the seasonal components accurately, adjustments of the model framework are indispensable. Similarly, as for glaciers on which accumulation and ablation occurs all year around the model would need to be able to capture winter ablation and summer accumulation for its accurate calibration.

Debris-covered and surge-type glaciers

The influence of the debris on the glacier mass balance is complex and mantle the climate related reaction of the glacier mass changes (e.g., Ragettli et al, 2016). The presented mass balance model does not account for debris-cover. Nevertheless, the change in TSL over the summer month still gives indication on the interannual variability of the mass balance of debris-covered glaciers. Hence, tied to decadal geodetic changes quantifying multi-annual mass loss, the TSL-constrained model can be used to infer interannual variability for the studied period. For the regional application of the TSL-constrained model, the RGIv6.0 was used. Debris-covered glacier are not signalized and consequentially included in the analysis without further consideration. However, due to the close link to geodetic mass balance estimates, the reliability of the region-wide application may not be affected. Further assessments, nonetheless, are needed to evaluate model performance, especially for the Pamir due to frequent occurrence of debris covered glaciers.

For surge-type glaciers, mass moves suddenly through hydrological or mechanical triggers from the accumulation to the ablation area (Cuffey and Paterson, 2010). The movement is followed by a readjustment of the mass balance to find an equilibrium state for the new geometry. Hence, through this geometrical adjustment the mass balance regime of the glacier might change abruptly due to non-climatic reasons. TSL observations can still be

used to observe the annual SMBs of such glacier types, if the geometry change is adjusted for. However, the observed mass balance cannot be brought in relation to changes in climatic conditions. Surge-type glaciers have been included in the mass balance modelling in Paper IV.

Internal and basal mass balance

The TSL-constrained model, as it is presented here, does not account for internal or basal mass balance, and refers strictly to the surface component. In order to quantify total mass loss of a glacier or a region, this might introduce important uncertainties (Kaser et al, 2006; Cogley et al, 2011; Zemp et al, 2013). Observations showed that refreezing of melt water contributed to the total mass balance of historically investigated glaciers located in the study area (Bazhev, 1973; Glazirin et al, 1993; Dyurgerov et al, 1995; Aizen et al, 1997). In Paper II internal accumulation has been roughly estimated based on calculations of a temperature profile in firn and ice using the heat conduction equation (e.g. Pfeffer et al, 1991). Thereby the refreezing model is calibrated by adjusting firn temperature at the bottom of the profile at model initialization to match repeated firn temperature measurements made in three firn cores in the 1970's (Glazirin et al, 1993). However, this provides only a rough estimate and more accurate quantification is not straightforward. Further, refreezing quantities and pattern might change over time. Miller and Pelto (1999) observed a reduction in internal accumulation, on Lemon Creek Glacier, Alaska having important impacts on the energy balance. During recent field visits, firn temperature measurements at two locations in the accumulation zone at Abramov Glacier (see Appendix A) have shown close to zero degree temperatures during summer field campaign, suggesting that all energy available for refreezing melt water had been used. Additionally, first results from shallow-core drilling indicated substantial changes in the firn stratigraphy in recent years (personal communication M. Kronenberg). These findings point out the need to periodically repeat studies on internal accumulation to identify temporal changes of refreezing processes. So far most attempts to integrate refreezing into mass balance modelling focus on rather short investigation periods (e.g. Schneider and Jansson, 2004; Reijmer and Hock, 2008) and do not evaluate temporal changes in the firn structure over longer time-intervals. Thus, studies focusing on the current state, the past evolution of the firn cover and a sound quantification of refreezing are essentially needed to conclude on the effect of internal accumulation on the total mass balance of the Central Asian glaciers. As suggested by Van Pelt et al (2012) the coupling of a distributed, more process-orientated energy balance model with a snow model that is capable of simulating subsurface temperature, density and water evolution might provide a solution to more accurately account for ice melt, runoff and refreezing. This might enable to study the spatial distribution and the temporal evolution of refreezing on its impacts on the total mass budget of glaciers in Central Asia in more detail.

Basal balance for Abramov has been estimated in Paper II and showed to be small in comparison to the other components. Basal balance is here assumed to not significantly change the total mass budget of the Central Asian glacier. However, this might not be true for glaciers situated in other regions such as Iceland, influenced by high geothermal activities (e.g., Tuffen et al, 2002) or when rapid ice flow drains through the ice streams of the large ice sheets in Antarctica and Greenland (e.g., Fahnestock et al, 2001; Pritchard et al, 2012). Hence in order to apply the proposed model in regions where internal and basal components are contributing significantly to the total mass balance, the here presented

model needs adjustment to account for the non-surface components of the glacier mass balance.

4.1.6 Unresolved technical and methodological issues

Even though the applied methodology showed promising results, some unresolved issues remain. The most important shortcomings and challenges are outlined hereafter.

Image availability

Necessary model input consists of topographic and meteorological information as well as snowline observations. It has been shown in Paper III that the model sensitivity to single snowline delineation is not strong if enough and well-distributed information on the TSL position is available. Considering this study, it was not trivial to find enough suitable data for the early 2000's. For example, in the eastern part of the Tien Shan, where summer snowfall is frequent and clouds and their cast shadows during the summer months hide the TSL, data was sparse. With increasing sensor availability and shorter repeat cycles in the past five years, the availability of usable data has improved considerably. Nevertheless, it is difficult to ensure sufficient continuous image coverage for all glaciers of the study region during the past 20 years, and for the regional assessment incomplete series had to be accepted. Furthermore, accurate TSL monitoring on glacier smaller than $2\,km^2$ was critical due to limited sensor quality, and thus such glaciers were, so far, omitted for the TSL-constrained modelling.

The regional study is currently only based on Landsat data. Further work is needed to include data from different optical and radar sensors such as ASTER or Sentinel 1 & 2. Thereby the results could be improved considerably and individual time series could be completed notably.

Model calibration

The current model calibration is based purely on the information content of the TSL observation. More precisely, winter snow accumulation is optimized using the temporal change of the TSL, whereas summer melt is calibrated with the actual position of the TSL. In order to apply the approach on glaciers without direct measurements, the use of additional ground-based information was avoided. Thus, the two calibrated parameters are not strictly independent meaning that an overestimated accumulation rate can be compensated by a too high ablation rate without degrading the agreement with the TSL observations. Erroneous seasonal components do not affect excessively the calculated annual balance as they equal out but introduce considerable uncertainties for the seasonal to sub-seasonal model outputs. An attempt to overcome this problem was made by iterative calibration, where both parameters were adjusted in parallel (for details see Paper III). With this iterative calibration, the model tends towards an optimal solution for both parameters without the need of additional data. Because winter measurements are sparse for the region a detailed validation of the seasonal components was not possible, however, for the few years and few glaciers for which winter measurements are available, the calibration procedures provided satisfying results (Paper II, Fig. 7.13). Nonetheless, at the current stage of the work, interpretation of seasonal to sub-seasonal mass balance time series have been avoided and more work is needed to properly evaluate the model performance on increased temporal resolution.

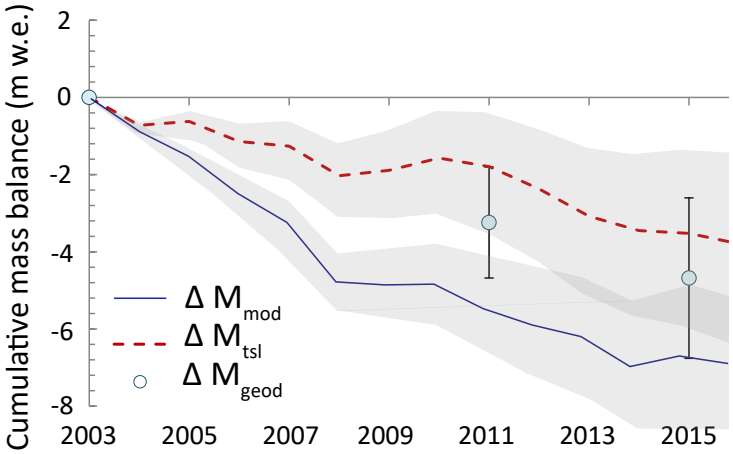

Figure 4.12: Cumulative mass balance for Abramov derived from a mass balance model constrained with historical long-term in situ measurements (M_{mod}), from modelling constrained with TSL (M_{tsl}) and from geodetic surveys based on high resolution images (M_{geod}).

Evaluating different methods against each other

Geodetic mass balances calculated for each individual glacier were used to evaluate and improve the model calibration. Due to the low temporal resolution of the geodetic balances, they have not been integrated directly into the TSL calibration procedures and were only used to readjust the model parameters through a second-order calibration. The model was re-calibrated so that the cumulative modelled mass balance was within the uncertainty range of the geodetic balance. With this second-order calibration, the assumption is made that the geodetic balance provides overall the better estimate than the TSL-constrained modelled mass balance. This is principally justified because the geodetic method is more observation-based than the TSL-constrained results. However, geodetic estimates can be connected to quite large random and systematic errors (Kääb et al, 2015; Paul et al, 2017). Several assumptions introduce important uncertainties that increase with decreasing sensor quality and decreasing spatial resolution. Exactly such sensors are typically used for regional assessments due to cost effectiveness and temporal data continuity (Brun et al, 2017; Yao et al, 2012). Berthier et al (2006) and Dehecq et al (2016) showed that the frequently used SRTM DEM and TANDEM-X datasets have considerable issues with radar penetration depth, and geodetic assessments using ASTER data showed substantial uncertainty (Kääb et al, 2002). Furthermore, the volume-to-mass conversation is still not entirely resolved especially considering short time intervals between the terrain models (Huss, 2013).

In Paper IV, it was shown that the ASTER derived geodetic mass change underestimates the mass balance in comparison to high-resolution data. The method-specific uncertainty estimates are supposedly accounting sufficiently for the uncertainties of the geodetic balances used for the second-order model calibration (Paper IV). However, the approach still prioritizes the geodetic assessment.

Combining different methods

A further limitation of combining different methods of mass balance calculations is related to the difference in the measured quantity. With glaciological observations, surface mass

balance is measured, whereas the geodetic approach examines the total balance, including internal and basal components. The model approaches are more flexible, however, the quantifications of internal and basal components are often not straightforward and for sound determinations, calibration using field data is needed. Such data is often not available and modelling internal or basal processes always demand assumptions and simplifications to a certain degree.

To summarize, combining different approaches to retrieve the best possible mass balance time series is hampered due to the different nature of information collected and it is not trivial to combine the obtained range of results without prioritizing a method over the other. Hence, similarly to the here described re-calibration of a model, re-analysis of direct mass balance measurements (Zemp et al, 2013) is often based on geodetic estimates which are judged to be more accurate. At the current state of research, however, evaluation of the accuracy of the different methods is not trivial and current state-of-the-art estimates may possibly exclude today unknown uncertainties. Therefore, further efforts should be accentuated on finding improved methods to combine different approaches. Such combined approaches can contribute essentially to overcome and avoid any pre-judgment of the used techniques.

4.1.7 Benefit of combining different approaches

This thesis aimed on producing more reliable annual mass balance time series for Central Asian glaciers. A combination of different approaches to retrieve a best estimate on a high temporal and spatial resolution helps to overcome the limitations of using a single method and to reduce the related uncertainties. Glaciological measurements are limited to a few glaciers and are point observations that need to be extrapolated to obtain glacier wide estimates (Escher-Vetter et al, 2009). Nonetheless, they have comparably high temporal resolution that is especially of interest for model calibration related to runoff studies for the continental Central Asian lowland (Unger-Shayesteh et al, 2013) and disposes highly valuable ground-truth for validation of geodetic approaches (e.g., Pieczonka and Bolch, 2015; Bolch, 2015). Geodetic mass balance assessments are spatially better resolved and allow applications on local to regional scale. However, the temporal resolution is limited to five to ten years, hampering inter and intra-annual analysis. Modelled mass balance is more flexible on both temporal and spatial dimension. However, they provide simulated output and do not provide observational data. Model calibration is indispensable to obtain a meaningful output. In contrast to conventional modelling, the TSL constrained model is tied to direct sub-seasonal observations for each glacier individually. This improves the results compared to unconstrained modelling significantly (e.g., Paper III).

In Paper II, in Kronenberg et al (2016) and partly also in Kenzhebaev et al (2017) the mass balance time series was improved through model calibration with in situ measurements, and validated with TSL observations and geodetic mass balances. Paper III highlights the value of TSL observations for calibration and increases the reliability of the estimate through comparison with in situ measurements and geodetic surveys. Comparing the mass balance time series for Abramov presented in Paper II with the one published in Paper III, the benefit of directly integrating annual TSL observations into model calibration, and not only using it for validation becomes obvious (Fig. 4.12). A mass balance model calibrated with long-term glaciological measurements agrees well with the TSL model results for years where it is tied to in situ surveys (Paper II, III). However, for periods without direct observations, significant discrepancies, especially concerning the accumulation rates are found. The comparison to geodetic surveys underline the limited performance of the mass balance model calibrated with long-term glaciological measurements for unmeasured periods that might be explained by the temporal variation of model parameters over time (e.g., Gabbi et al, 2014).

Despite the generic differences, the combination of the three approaches described above is shown to be highly beneficial and provided reliable mass balance time series for a large number of the Central Asian glaciers. Through the combination of the totality of available information, temporally and spatially highly resolved results can be provided on a regional scale with an increased confidence level (Paper IV). Even though the combination is not always trivial and a strict separation between calibration and validation is essential. It was shown that uncertainties of a single method can be overcome to some extent by combining different approaches leading to a more comprehensive mass balance estimate of the studied glacier (Paper III).

4.1.8 From local to regional mass balance observations

Glacier monitoring programmes consider single or a few selected glaciers that are thought to be representative for the corresponding mountain ranges (Haeberli et al, 2000). Intense mass balance measurements (e.g., Dyurgerov et al, 2002) are frequently completed with complementary measurements and research (e.g., Suslov et al, 1980), providing a rich volume of information and knowledge for the specific sites. The research conducted on local scale can be very exact and specific, helping to improve measurement techniques, modelling algorithms and process understanding step by step. The investigators have a high level of control on data state and quality. Efforts outlined in Paper I essentially contributed to re-build a modern monitoring network of Central Asian glaciers, enabling an improved understanding of glacier changes in the Tien Shan and Pamir on a local scale (e.g., Paper II, Appendix A). Through the emplaced programme, important baseline data was generated and made accessible for further applications in manifold domains such as change detection and hazard assessments, typically focusing on a larger spatial dimension (e.g., Appendix A).

Working on regional to global scale involves substantial data quantities and demands automatized procedures in order to manage the load of collected information. Often, one has to rely on pre-processed data or datasets of unknown quality. Uncertainties related to the different input variables are difficult to assess and generally a range of assumption and simplifications have to be accepted. Furthermore, data gaps need to be filled (e.g., McNabb et al, 2017) and data has to be extrapolated (e.g., Huss, 2012) to provide comprehensive estimates. This generally leads to a decreased quality control. Whereas efforts of local studies focus on the understanding of processes, regional to global studies are less process-oriented and challenges relate to data management routines and computational constraints.

Both, local and regional studies are necessary and of great importance to improve the understanding of the undergoing changes in the Central Asian cryosphere. The way of connecting from the local knowledge to a more regional and further to a global view is an asset to produce a sound and reliable analysis of the state, change and impacts of the Central Asian glaciers. Looking back in time, the intense research programmes at specific sites in Central Asia during the Soviet Union were followed by a sheer absence of measurements from the late 1990s to the early 2010s. Today, we reached a point, where the scientific activities are slowly reactivated in the region; however, large data gaps and missing detailed regional assessments hamper sound analysis. In order to estimate past changes and predict futures development, long-term time series are needed. Paper II presented a way to connect historical data to recent measurement and Paper III developed a tool to improve the gap filling of long-term mass balance series. With Paper IV, a regional glacier mass balance assessment on a higher degree of detail than provided by most previous studies (Gardner et al, 2013; Brun et al, 2017) and an innovative connection of the local and regional level was aimed at. Illustrated with the four research articles, this thesis aimed to move step-by-step from a local to a more regional context and provides relevant insights on the glacier mass changes for the main mountain ranges in Central Asia on different spatial scales.

4.2 Conclusions

The conclusions are structured according to the research questions starting at a local scale of glacier mass balance observations that is extended to a regional context.

What is the past and current rate of mass change of selected reference glaciers in the Tien Shan and the Pamir?

Today reanalysed historical glaciological measurements (Paper II), reconstructed mass balances (Paper II, see also Appendix A) and re-initiated in situ measurements (Paper I) complete the time series for Abramov, Golubin, Batysh Sook and Glacier No. 354 for the last decades. The combination with high-resolution geodetic estimates, reaching partly back until the 1970s (see Appendix A) and more frequently available since 2000, enable a profound analysis of the current rate of mass change of the selected reference glaciers. All of the four investigated glaciers show a predominately negative mass balance ranging from -0.30 to $-0.43\,\mathrm{m\,w.e.\,yr^{-1}}$ for the period from ≈2000 to 2014. Since the mid-1960s several short periods of decreased mass loss or slight mass gain have been observed (Paper II and Appendix A), however, mass loss overall outweighs gain for the period 1968 to 2014 (Paper II and see also Appendix A). For example, for Abramov and Golubin glaciers a cumulative mass loss of over $-15\,\mathrm{m\,w.e.}$ and of around $-14\,\mathrm{m\,w.e}$, respectively have been determined since the onset of the Soviet monitoring programme at the end of the 1960s (Paper II and Appendix A). Furthermore, no clear tendency towards less negative or positive mass balances was detected for the here monitored glaciers. Though, a slight shift towards a simultaneous increase of accumulation and ablation is indicated by the reanalysed and reconstructed time series. However, at the current state of this work, time series are still rather short to clearly identify such regime shifts and additional field surveys are essentially needed for sound analysis. Continued field surveys in the upcoming years through the re-established monitoring programme coordinated within the CICADA project will further facilitate research on glacier mass changes and will provide valuable baseline data for validation and calibration for the Tien Shan and Pamir. For the selected monitoring sites, so far, data is continuously submitted to the international data centers since 2010 and the concluding aim of a sustainable and a long-term programme led by local scientists is step-by-step aspired.

How can the monitoring of changes in the TSL position based on terrestrial cameras or satellite images support the re-establishment, reanalysis and reconstruction of long-term mass balance measurement series in Central Asia?

The support of TSL observations for mass balance monitoring has proofed to be beneficial for several applications. To include terrestrial cameras into a glacier-monitoring network can help to improve the coverage of TSL observations during the ablation season for selected glaciers significantly. Despite the disadvantages connected to demanding installation and maintenance as well as the laborious pre-processing, terrestrial camera images can fill data gaps in spaceborne observations, especially for regions with frequent cloud cover such as in the Central Tien Shan. In the case of incomplete or missing glaciological measurements, ground-based and spaceborne TSL observations provide a valuable proxy for the mass balance and can help to reconstruct the missing data through coupling to a mass balance model (Paper III).

TSL observations are beneficially used for model validation when no direct field surveys are available, as shown in Paper II and in Appendix A, and can improve conventional modelling significantly. Nevertheless, the use of TSL positions for validation of modelled mass balances might be restricted to the evaluation of melt rates only. Correct winter snow accumulation cannot be verified, as highlighted through the underestimated winter balances for Abramov presented in Paper II. Withal it has been shown that including TSL observations directly into a model calibration procedure for both melt and winter snow accumulation, improves the mass balance estimates considerably (Paper III). Even though the calibration of the two parameters is interdependent, better estimates of both accumulation and ablation components are obtained in comparison to conventional modelling (Paper III). In Paper III & IV, it is shown that TSL observations can entirely replace direct measurements for model calibration. Hence, the field surveys become available for independent validation. Further, the reduced sensitivity to meteorological input data and model parameters of the TSL-constrained model highlights the capability to reconstruct SMB series for unmeasured glaciers based on a minimum input data (Paper IV). TSL observations support reanalysis of SMB time series as a tool for validation but also improve SMB reconstructions while coupled to a model for unmeasured years and glaciers; thus helps extending the glacier mass change observations spatially and temporally.

Is it possible to obtain seasonal to annual glacier-wide SMB estimates from modelling constrained with remote observed snowlines throughout the melting season for the Tien Shan and Pamir?

Paper III & IV provided annual SMB time series for glaciers located in different mountain ranges in the Tien Shan and Pamir. The approach holds for glaciers with different mass balance regimes on annual time scales, and produced reliable estimates in combination with results from geodetic assessments. Due to the current model setup, however, seasonal to sub-seasonal SMB are linked to increased uncertainties. Especially for non-winter accumulation type glaciers, calibration procedures are less robust. Despite capability of the model to predict summer precipitation, the calibration procedure based on a backwards modelling approach between predicted melt and winter snow accumulation, associates accumulated snow to winter only but not to summer snowfall, provoking a possible miscalibration of both calibrated parameters. Thus, at the current state of this thesis, the mass balance estimates are tied to annual temporal resolutions and more investigation on the model performance for seasonal to sub-seasonal estimates is needed. However, this is not trivial due to the limited availability of validation datasets from direct measurements. The importance of temporally high resolved glaciological measurements including seasonal measurements in order to develop sound and novel approaches to observe mass balance changes needs to be highlighted here.

What is the accuracy of the snowline-based determination of the SMB in comparison to direct glaciological measurement and geodetic surveys?

A detailed sensitivity and uncertainty analysis showed that the uncertainties related to the TSL-constrained modelling are primarily related to the data availability for TSL mapping, and hence depend strongly on distribution and frequency of the images (Paper III). Further, wrong chosen, un-calibrated model parameters can interfere with the model performance. Whereas in Paper III, geodetic assessments were used for validation, in Paper IV, region-wide, multi-annual geodetic estimates are included into the model calibration

directly, in order to constrain the so far unchanged, but not well constrained parameters. Through such a combination, uncertainties could be reduced notably. This highlights the importance of combining different methods and datasets to lower the uncertainty ranges of the mass balance estimate and helps to overcome the limitations tied to a single method.

Noteworthy is that debris covered glaciers in the Pamir and Tien Shan are frequent but have not been addressed specifically in this thesis. Further the contribution of internal and basal components to the total mass balance are not well known for the study region. Mass balance modelling constrained with the TSL observations does not account for alternated melt rates due to debris layers and focus only on the surface component. Hence, for sound regional assessments related uncertainties need to be accounted for.

Is repeated satellite imagery suitable to monitor snowline evolution for a large number of glaciers, i.e. to determine region-wide SMB at high temporal resolution?

Region-wide application of the TSL-constrained modelling in combination with multi-annual geodetic mass changes has shown to be applicable on a large amount of glaciers in Central Asia. The retrieval of results on high temporal / spatial resolution is thus possible and provides insight not only into decadal changes but also highlights annual mass balance variability for a region for which so far only little was known on such time scales.

Results from the Kyrgyz Ala-Too, in Western / Northern Tien Shan show good agreement with semi- to decadal region-wide geodetic mass changes. Results for the Pamir-Alay provided similar accuracy. Both regions are dominated by winter-accumulation type glaciers and subject to dry, cloud-free summers. Hence, image availability is not a limiting factor. Other than for Western / Northern Tien Shan and Pamir-Alay, the Akshiirak massif in Central Tien Shan is influenced by important summer precipitation. This, on the one hand, makes it more difficult to find adequate and sufficient images for TSL observations and on the other hand hides the TSL through fresh snowfall frequently. Nevertheless, the TSL approach revealed annual SMB for most glaciers in the Akshiirak massif with sufficient quality.

4.3 Perspectives

Future valuable investigations to tackle the encountered limitations, challenges and open questions, but also to exploit the full potential of the methodological advancements made in the context of this thesis are listed below:

Improvement of glacier monitoring network in Central Asia

- Improvement of the spatial coverage of the glacier monitoring network: Measurements are needed for the East and South-West Pamir and the South-East Tien Shan.
- Enhance temporal resolution of field surveys for the here monitored glaciers to seasonal resolution in order to enable sound validation of the model performance at resolution lower than one year.
- Include quantification of sublimation, refreezing and superimposed ice to lower uncertainty range of the mass balance surveys, and to guarantee sound estimates of the melt rates and the connected uncertainties. This should further facilitate the comparison between the different methods with generic differences.
- Available meteorological datasets from different stations in the Central Asian mountains need homogenisation, reanalysis and adequate gap filling. A comprehensive, freely available database of the meteorological observations could enable further research on climate and cryospheric change in the region.

TSL observations on remote sensing images

- Using enhanced satellite products (with improved atmospheric and topographic correction) for TSL mapping enable a better narrow-to-broadband albedo conversion, especially regarding over-saturated snow surfaces. Enhanced cloud mask algorithms might facilitate the pre-processing steps of the remote sensing data and reduce misclassification due to unmasked clouds and cloud shadows.
- Multi-sensor approach to detect TSLs to improve quantity and quality of TSL observations. Coupling between optical and radar systems limit issues connected to day light and cloud cover. Furthermore, including all well established, freely available optical and radar sensors (ASTER, Sentinel and Landsat) and extending the automatic surface classifications onto scenes from micro and nano satellites as well as from UAV and terrestrial camera systems with high temporal and spatial coverage will increase image frequency to a close-to-daily coverage. This implies automatized and enhanced data management tools to handle the quantity of collected data.

Including TSL observations for annual mass balance observations

- In detail evaluation of model performance of non-winter-accumulation type glaciers, related to possible model adjustments to account for summer accumulation during calibration procedure. Equally, assessing model adaption to include basal and internal components of the mass balance as well as to include the effect of debris cover on glacier melt. To account for the aforementioned processes, the use of a more physically based energy balance model might be appropriate.

- Extend the TSL-approach to glaciers smaller than 2 km^2 enabled through improved sensor resolution and surface classification algorithms.
- Application of the approach to retrieve annual time series for other regions, for which only sparse and discontinued measurement series are available such as for the Chilean Andes or the Patagonian ice caps.
- Preparation of a fully automatized application to model SMB constrained with TSL observations, that can be provided to national correspondents of the WGMS involved in the glacier monitoring to facilitate glacier mass change observations for inaccessible glaciers on a large spatial scale on cost and labour effective basis.
- To improve assessments on glacier runoff contribution, annual to seasonal melt rates. The TSL-approach to estimate glacier melt can be coupled to a runoff model to significantly improve the knowledge on the glacier melt contribution to total runoff.

Including TSL observations for seasonal to sub-seasonal mass balance observations

- Increasing the temporal resolution of the modelled time series to seasonal / sub-seasonal dimensions. This needs, at first, a profound evaluation of the model performance on glaciers with extensive seasonal to sub-seasonal measurements, i.e. for glaciers in the Swiss Alpes or Scandinavia.

Including TSL observations for real-time mass balance observations

- Developing a new Index approach for real-time glacier mass change observations. Establishing glacier specific rating curves between the TSL and SMB from a total of available observations and modelled transient mass balances to cover the entire range of possible SCAFs. The rating curves need to be validated with glaciological surveys for selected glaciers. Such rating curves might than be established for a large amount of unmeasured and remote glaciers. With the established rating curves and increased image availability during the summer months from modern satellite sensors, a close to real-time mass balance estimate will be possible.
- Real-time estimates can be used to identify extreme meteorological conditions and might be connected to early warning systems to identify potential hazards such as droughts or flooding from remote sensing data and without the need for direct measurements. Thus, the approach can be applied on inaccessible, data sparse regions.
- Dense sub-seasonal mass balance estimates can be used to identify seasonal changes in melt contribution to runoff.

Part II

Research Articles

Chapter 5

Paper I: Re-establishing glacier monitoring in Kyrgyzstan and Uzbekistan, Central Asia

Hoelzle, Martin, Erlan Azisov, **Martina Barandun**, Mathias Huss, Daniel Farinotti, Abror Gafurov, Wilfried Hagg, Kenzhebaev, Ruslan, Kronenberg, Marlene, Machguth, Horst, Merkushkin Alexandr, Moldobekov Bolot, Petrov Maxim, Saks Tomas, Salzmann Nadine, Schoene Tilo, Tarasov Yuri, Usubaliev Ryskul, Vorogushyn Sergiy, Yakovlev Andrey and Zemp Michael. *"Re-establishing glacier monitoring in Kyrgyzstan and Uzbekistan, Central Asia."* Geoscientific Instrumentation, Methods and Data Systems 6, no. 2 (2017): 397.

Abstract

Glacier mass loss is among the clearest indicators of atmospheric warming. The observation of these changes is one of the major objectives of the international climate monitoring strategy developed by the Global Climate Observing System. Long-term glacier mass balance measurements are furthermore the basis to calibrate and validate models simulating future runoff of glacierized catchments. This is essential for Central Asia, which is one of the driest continental regions of the northern hemisphere. In the highly populated regions, water shortage due to decreased glacierization potentially leads to pronounced political instability, drastic ecological changes, and endangered food security. As a consequence of the collapse of the former Soviet Union, however, many valuable glacier monitoring sites in the Tien Shan and Pamirs were abandoned. In recent years, multinational actors have re-established a set of important in-situ measuring sites to continue the invaluable long-term data series. This paper introduces the applied monitoring strategy for selected glaciers in the Kyrgyz and Uzbek Tien Shan and Pamir, highlights the existing and the new measurements on these glaciers and presents an example for how the old and new data can be combined to establish multidecadal mass balance time series. This is crucial for understanding the impact of climate change on glaciers in this region.

5.1 Introduction

Glacier fluctuations in mountain areas have been monitored in various parts of the world for more than a century (Haeberli et al, 2007; Zemp et al, 2015) and glacier changes are considered to be reliable indicators of worldwide atmospheric warming trends (Stocker et al, 2013). Mountain glaciers and ice caps are important for early-detection strategies in global climate-related observations. Hence, glaciers are one of the 'essential climate variables (ECVs)' in the Global Climate Observing System (GCOS). Embedded in GCOS is the Global Terrestrial Network for Glaciers (GTN-G) operated by the World Glacier Monitoring Service (WGMS), the US National Snow and Ice Data Center (NSIDC), and the Global Land Ice Measurements from Space (GLIMS) initiative. These institutions follow the so-called Global Hierarchical Observing Strategy (GHOST) (WMO, 1997b, 2010) forming the base for the strategic observation framework. The main objectives of long-term glacier monitoring are related to (1) process understanding, (2) model validation and / or calibration, (3) change detection and (4) impact assessment. Furthermore, they play a key role for assessing climate change effects such as estimating sea-level rise, regional changes in runoff, and impacts of natural hazards. Especially countries and regions that are vulnerable to climate change rely on a sound and continuous long-term database providing the necessary information to cope with future challenges in different areas such as water management, irrigation for agriculture, disaster risk reduction, and public health.

Continuous in-situ monitoring of glaciers in remote areas is a challenging task, and maintaining the necessary measurements can be both logistically and economically demanding. Reasons include missing long-term financial and / or human resources as well as general political instability, access to remote regions, natural hazards or missing infrastructure. In many countries with glacierized mountain ranges continuous observations are thus lacking. For these reasons, monitoring strategies need to be improved and different techniques such as in-situ measurements, remote sensing and modelling have to be combined to generate high-quality products.

Currently, a re-establishment of historical monitoring sites in Kyrgyzstan and Uzbekistan is jointly developed by different international projects including Capacity Building and Twinning for Climate Observing Systems (CATCOS), Central Asian Water (CAWa),

Figure 5.1: Map of glaciers in Central Asia, where the investigations were gradually re-established starting in 2010. Red symbols show glaciers investigated within the CATCOS/CAWa projects and blue glaciers are covered by other projects such as CHARIS

CryospherIc Climate Services for improved ADAptation (CICADA) or Contribution to High Asia Runoff from Ice and Snow (CHARIS). In the frame of those projects, the measurement series on selected glaciers (see Fig. 5.1) in Kyrgyzstan and Uzbekistan are (re-)initiated. The project CATCOS had two phases, the first phase phase was from 2011 to 2013, which was mainly related to the technical installations and the second phase from 2014 to 2016 was mainly used for capacity building and twinning activites. The project will be continued within the next years in a cooperative effort between Kyrgyzstan, Uzbekistan, Germany and Switzerland.

This paper aims at presenting and discussing the major steps and methodologies developed and applied in Kyrgyzstan and Uzbekistan to (re-)establish glacier monitoring at the most important sites within the two projects CATCOS and CAWa (Fig. 5.1). The described methods and experience might be a blue print for similar cases in other parts of the world. The key steps, around which this paper is centered, are the (1) collection, homogenization and securing of historical data and (2) the re-establishment of glacier monitoring and (3) capacity building and twinning.

5.2 Glaciers in Central Asia

Glaciers in Central Asia constitute an important water storage component (e.g. Immerzeel et al, 2010; Kaser et al, 2010; Duethmann et al, 2015), which is of particular importance for different sectors including agriculture and energy production (Siegfried et al, 2012). With the ongoing climate change the corresponding variations in glacier area and volume in this region are considerable. Most studies agree on the general trend of glacier mass loss, including an acceleration since the 1970s (e.g. Sorg et al, 2012; Farinotti et al, 2015). Regarding seasonal changes, the studies however disagree. In their comprehensive review on past changes in high-altitude areas of Central Asian headwaters, Unger-Shayesteh et al (2013) conclude that there is (i) a lack of reliable data especially for the glacio-nival zone, (ii) methodological limitation in trend analysis, and (iii) a strong heterogeneity in spatial and temporal extent of the available analyses. These restrictions hamper a sound synthesis for the whole region, and limit the understanding of interactions between changes in highly-variable climate parameters, the cryosphere, and the hydrological response of headwater

catchments. Altogether, these shortcomings indicate the importance of high-quality in-situ measurements, which are required for a better calibration and validation of local to regional-scale models for estimating future glacier mass balance and runoff.

5.2.1 Tien Shan

Glaciers in the Tien Shan cover around 12,400 km^2 of which about 7,400 km^2 are situated in Kyrgyzstan according to the Randolph Glacier Inventory Version 5.0 (RGIv5.0) and about 117 km^2 in Uzbekistan (Arendt et al, 2015). In the Tien Shan, only two continuous long-term glacier mass balance series are presently available (Tuyuksu Glacier in Kazakhstan, and Urumqihe Glacier No. 1 in China). Two long-term mass balance measurements in the Kyrgyz Tien Shan were discontinued in the 1990s (Golubin and Karabatkak). Whereas glaciers in the western part of the Tien Shan receive winter accumulation, glaciers in the East are summer-accumulation type glaciers. Furthermore, annual precipitation sums are maximum in the Northwest and decrease south-eastwards (Voloshina, 1988). This shift goes along with an alteration of the annual precipitation maximum which is earlier in the West and in summer in the East (Dyurgerov et al, 1994). Kriegel et al (2013) show a temperature change of 0.1-0.2 °C per decade for the ablation period (April-September) during 1960-2007 for the Naryn station. The same authors indicate an unequivocal change in precipitation across a few stations in the Central Tien Shan. A decrease in snow cover has been observed for the period from 1960 to 2007 in the entire Tien Shan (Chen et al, 2016). Precipitation changes seem to be less important. Higher air temperatures resulted in positive runoff trends in spring and autumn for the Naryn catchment, which is likely to be related to enhanced snow and glacier melt corresponding also to the observed annual area shrinkage rates since the middle of the 20th century (e.g. Sorg et al, 2012). For Small Naryn, significant negative runoff trends were found whereas for Big Naryn a positive but not significant trend were found for August, which is the month with the largest glacier runoff contribution Kriegel et al (2013).

5.2.2 Pamir-Alay

In the Pamir, glaciers cover approximately 12,100 km^2. The sub-region Pamir-Alay has a total glacier area of around 1,850 km^2 (both values are based on RGIv5.0). In the Pamir-Alay, direct mass balance measurements only exist for Abramov Glacier (Fig.5.1). For the Pamir-Alay, a strong gradient in the equilibrium line altitude (ELA) from West to East is observed (Glazirin et al, 1993). This is linked to important differences in precipitation (Suslov and Akbarov, 1973). According to Suslov and Akbarov (1973) and Glazirin et al (1993), the maximum annual precipitation in the Pamir-Alay is about 1900 mm yr^{-1} in the western part at the border between Kyrgyzstan and Tadjikistan, and about 400 mm yr^{-1} in the eastern part. The seasonal precipitation regime also differs from West to East: Whilst the West shows a maximum precipitation during autumn and winter, the East is characterized by a maximum during spring and summer. Therefore, both accumulation and ablation are region-dependent, resulting in different glacier surface mass balance gradients. This also influences total discharge from glaciers, which is estimated as 1.6 km^3 yr^{-1} corresponding to about 8% of the total annual runoff of all rivers in Central Asia (Suslov and Akbarov, 1973). Focusing on a region in the eastern Pamir, Khromova et al (2006) found a reduction in glacier area of 10% from 1978 to 1990, and of 9% from 1990 to 2001. Glacier front variations with annual rates of –11.6 m yr^{-1} for very large glaciers, –7.3 m yr^{-1} for valley glaciers and of –3.3 m yr^{-1} for smaller glaciers were observed. The high sensitivity of glaciers to summer temperatures is assumed to be responsible for the

Table 5.1: Information of observed glaciers and type of measurements currently available from WGMS (2013) for mass balance (mb) and frontal variation, see Fig. 5.1 for location

Glacier	Type	Period	Interval		Re-start
Golubin	mb	32	1968	2016	2010
Golubin	fv	30	1861	2016	2011
Abramov	mb	36	1967	2016	2011
Abramov	fv	17	1850	2016	2011
Batysh Sook	mb	11	1970	2016	2010
Batysh Sook	fv	17	1975	2016	2010
Glacier No. 354	mb	6	2010	2016	2010
Glacier No. 354	fv	14	1972	2016	2010
Barkrak Middle	mb	-	-	-	2016
Barkrak Middle	fv	18	1970	1990	2016

long-term retreat (Glazirin et al, 2002). The negative mass budget of the glaciers in this region indicates that increased winter and summer precipitation cannot compensate for the increase in air temperature (Khromova et al, 2006). A smaller reduction in glacier area of 3 % yr^{-1} for the period 2000 and 2007 was observed by Narama et al (2010) for a region, which is close to the SE-Fergana mountain range situated in the East of the Pamir-Alay.

5.3 Instrumentation, Methods and Data

5.3.1 Monitoring strategy

The applied strategy to re-establish glacier observation networks in Central Asia is partly based on the Tiers 2 and 3 of GHOST (WMO, 1997a,b) and the experience gained in different monitoring projects. For glacier mass balance, the strategy is composed of several components:

1. Mass balance measurements using the glaciological method,
2. observation of the transient snow line on photographs from terrestrial automatic cameras and / or on satellite images during the summer months, and
3. a mass balance model driven by nearby automatic weather station data, reanalysis data, or climate model results (see Fig. 5.2).

As an important additional element, geodetic measurements should be integrated for calibration or validation purposes depending on the given objectives. The combination of the different approaches allows producing accurate mass balance estimates with a high temporal and spatial resolution (e.g. Zemp et al, 2013). An important advantage of the described strategy is that all different components can be used independently (e.g. Huss et al, 2009).

The re-establishment of the in-situ glacier monitoring has to obey certain criteria for the selection of the glaciers. These are based on several pre-conditions such as field-site accessibility, availability of historical data, geo-climatic distribution within mountain ranges, suitability for long-term monitoring based on glaciological feasibility and the availability of other measurements. Based on these criteria, the five glaciers Abramov, Golubin, Batysh

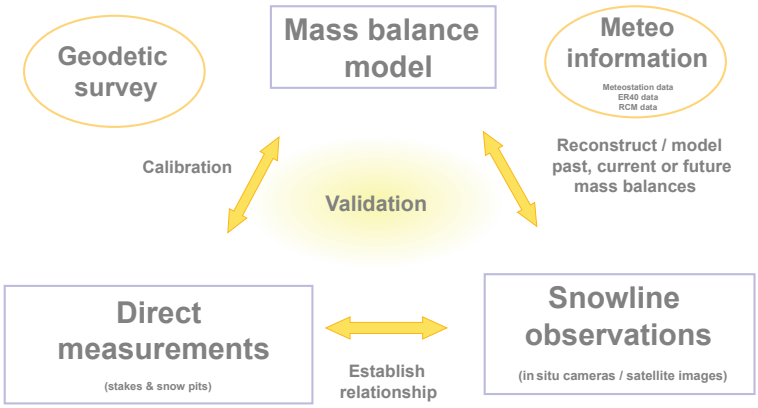

Figure 5.2: Schematic view of the monitoring strategy applied for re-established measurements in Central Asia

Sook, No. 354 and Barkrak Middle were selected within the projects CATCOS and CAWa (see Fig. 5.1 and Tab. 5.1).

5.3.2 Implementation

The implementation of the measurement network within the re-establishing activities (in the following referred to as 'new' measurement network) takes advantage of the concept described above. Our approach is summarised below to clarify the individual steps during the re-establishment of the mass balance series:

1. Finding appropriate collaboration partners.
2. Collection of all historical mass balance data from different sources.
3. Based on a review of these data and expert knowledge, the glacier selection was conducted and accordingly the new mass balance network was designed.
4. Set up of the new glaciological mass balance measurement networks on the selected glaciers in the years 2010 (Golubin, Batysh Sook, No. 354) , 2011 (Abramov), 2016 (Barkrak Middle). In parallel, installation of automatic snow line cameras and new weather stations close to the glaciers in collaboration with partners in the CAWa project from Kyrgyzstan, Uzbekistan, Germany and Switzerland.
5. Selection of satellite images with optimal visibility of melt-out patterns and snow lines.
6. A mass balance model was used as an extrapolation tool to obtain from mass balance point measurements the glacier wide mass balance. Model validation was performed using snow line measurements from the automatic cameras or from satellite images. The model also served for reconstructing mass balance for periods with longer data gaps.
7. Comparison of mass balance retrieved by in situ measurements and geodetic measurements.

5.3.3 Glacier observations

Data from WGMS and literature

Glacier monitoring in Central Asia started more than 60 years ago. During this time, several different glaciological programmes were established in the mountain ranges of Kyrgyzstan, Kazakhstan, Uzbekistan and Tajikistan. We compiled all available glacier data from the WGMS (WGMS, 2013). The total number of past glacier observations are summarized in Tab. 5.2, delivering basic information related to all existing measurements having an observation period longer than two years. For 17 glaciers, mass balance measurements exist with mean observation period lengths close to 20 years. Thickness change measurements for nine glaciers and repeated front variation measurements for 62 glaciers with measurement periods from 9 to 20 years are also available. Most of the mass balance measurements were initiated between 1960 and 1970 and were discontinued in the 1990s. Detailed description of stake and snow pit measurements for Abramov glacier were retrieved from Pertziger (1996).

Glaciological measurements

The determination of the mass balance of a glacier using the so-called glaciological method is the standard method used since the earliest times of mass balance measurements (Mercanton, 1916b). This robust method is widely used to determine the seasonal to annual mass change of individual glaciers. It is based on measurements of ablation at stakes, which are drilled into the ice of the ablation area, and of snow depth and density measured in snow pits in the accumulation area. The advantage of this method is the direct determination of the temporal evolution of mass balance. Calculation of the total mass change derived from point measurements, however, can be challenging since individual stake readings and snow pit data have to be extrapolated over the glacier, thus resulting in considerable uncertainties (for further details, see Østrem and Brugman, 1991a; Kaser et al, 2003; Thibert et al, 2008b; Cogley et al, 2011).

On the (re-)established glaciers the following measurements were carried out:

- For the ablation measurements in late summer, plastic or wooden stakes were drilled into the ice in the ablation area to a depth related to the expected melt rate at the corresponding altitude varying on the observed glaciers between around 2 to 10 m. This was done with an auger or a steam drill.

- In the accumulation area, several snow pits were dug to determine the annual snow accumulation and its density. Additionally, several snow depth measurements with steel or aluminium rods of 2 to 5 m length were performed. Theses were combined with occasional ground penetrating radar (GPR) measurements using a frequency of 800 MHz to detect snow layers of former years. This information allows an improved extrapolation of the highly variable snow distribution on the glacier (Sold et al, 2013) and reconstructing past accumulation rates back to almost one decade (Sold et al, 2015).

- Frontal variations in glacier length were measured at the glacier tongue using handheld GPS and / or were digitised based on satellite images.

The stake and snow pit locations aim at representing the former transects of measurement on the glaciers to allow comparability. The total number of new stakes and pits,

Table 5.2: Information on glaciers before the re-establishment of the measurements was initiated based on WGMS (2013). Abbreviations: KG = Kyrgyzstan, KZ = Kazakstan, UZ = Uzbekistan, TJ = Tajikistan, mb = mass balance measurements, tc = geodetic thickness change, fv = front variations

Country	Meas.	Glaciers observed	Mean observation period	mean start date	mean end date
KG	mb	7	19	1973	1994
KG	tc	2	2	1977	1989
KG	fv	19	9	1954	2002
KZ	mb	9	19	1974	1992
KZ	tc	7	2	1958	1998
KZ	fv	11	16	1957	1987
UZ	mb	0			
UZ	tc	0			
UZ	fv	11	20	1965	1988
TJ	mb	1	3	1983	1985
TJ	tc	0			
TJ	fv	21	11	1968	1989

however, had to be reduced substantially to keep the annual work load on a manageable level.

Geodetic mass balance

Geodetic mass balance measurements are useful to infer mass and volume changes of glaciers over decadal periods (Ahlmann, 1924) providing considerable precision and high spatial resolution. Digital elevation models (DEMs) derived from different sources like topographic maps, GPS-surveys, aerial photographs, satellite images, synthetic-aperture radar (SAR) or Light Detection and Ranging (LiDAR) are compared to each other and the elevation differences over the glacier can be converted into the glacier's mass change over a given time interval (e.g. Bauder et al, 2007; Thibert and Vincent, 2009; Zemp et al, 2013). In general, multi-annual time periods are needed to reach an acceptable level of accuracy (Paul et al, 2013b). The most important uncertainties are due to (i) density conversion (Huss, 2013), (ii) elevation biases and errors in the co-registration of the two DEMs (Berthier et al, 2006; Paul, 2008; Nuth and Kääb, 2011), (iii) data gaps, (Pieczonka et al, 2011; Bolch and Buchroithner, 2008), and (iv) errors and artefacts in the DEMs.

Geodetic glacier volume changes focusing on Central Asia often rely on the Shuttle Radar Topography Mission (SRTM) as a baseline for the year 2000 (e.g. Berthier et al, 2010; Gardelle et al, 2012b, 2013; Surazakov and Aizen, 2006). However, the quality of the SRTM DEM is affected by electromagnetic wave penetration into the snow and ice. This can lead to major uncertainties, especially affecting elevation changes in the accumulation area, for which a corrections have to be applied (Berthier et al, 2006; Gardelle et al, 2012b, 2013; Kääb et al, 2015) These corrections, however, are difficult to quantify as they strongly vary with local conditions (Kääb et al, 2015). Other data sources for the geodetic method applied in Central Asia are topographic maps or stereo imagery derived from several sensors operating in the visible range of the spectrum, such as ASTER (Advanced Spaceborne Thermal Emission and Reflection Radiometer), SPOT (Satellite pour l'observation de la Terre), Cartosat, Corona or Hexagon data (e.g. Hagg et al, 2004b;

Bolch et al, 2011a, 2012; Pieczonka et al, 2013; Gardelle et al, 2013; Pieczonka and Bolch, 2015; Bolch, 2015; Petrakov et al, 2016a). Furthermore, laser altimetry measurements, e.g. from the ICESat satellite mission operated between 2003 and 2009, offer a possibility of mass change computation for mountain glaciers (Kääb et al, 2012; Gardner et al, 2013; Neckel et al, 2014; Farinotti et al, 2015). Elevation differences at points along the repeated tracks are interpolated and converted into volume and mass changes. Due to point measurements and uncertainties associated with interpolation, this method delivers robust results rather on large scales and not for individual glaciers.

Snow line observations

The calculation of glacier-wide annual mass balance from statistical relations using ELA and accumulation area ratio (AAR) is well established (Braithwaite and Müller, 1980; Braithwaite, 1984a; Benn and Lehmkuhl, 2000; Kulkarni, 1992). It has been applied in many different mountain ranges (Kulkarni, 1992; Rabatel et al, 2008; Chinn et al, 2012; Stumm, 2011) and it is often used to relate temperature and precipitation with mass balance (Kuhn, 1984; Ohmura et al, 1992). Generally, ELA and the annual mass balance are well correlated (Rabatel et al, 2005, 2012). The advantage of using ELA and AAR is their straightforward mapping using remote-sensing data (Rabatel et al, 2013). However, this approach relies on the calibration against long-term glaciological in-situ measurements. An interesting alternative is the use of transient snow lines. Their monitoring can be used as a good proxy for the sub-seasonal mass balance (Huss et al, 2013). The distinction between snow-covered and snow-free zones on a glacier can be retrieved by different means such as analysis of repeated images taken by terrestrial cameras and satellites, or by mapping with GPS. This information can be used to establish and analyse snow-cover depletion curves (e.g. Parajka et al, 2012) and in combination with corresponding model approaches, the water equivalent of the winter snow cover can be directly extracted (e.g. Martinec and Rango, 1981; Schaper et al, 1999). Repeated snow line observations during the ablation period are also used for mass balance model validation (Kenzhebaev et al, 2017; Barandun et al, 2015; Kronenberg et al, 2016).

The annual course of the snow line, and the related snow-covered area fraction (SCAF), was recently used in combination with a backward modelling approach to determine sub-seasonal mass balance values (Hulth et al, 2013; Huss et al, 2013). The approach by Huss et al (2013) uses transient snow line observations and meteorological information in combination with a mass balance model. Remote monitoring for glaciers with limited accessibility is thus possible. It offers also an important backup that helps achieving a better coverage with mass balance estimates and thus to reduce future data gaps.

In the framework of the CATCOS project, we installed six terrestrial cameras (Mobotix, M15 and M25) for snow line observation: Two cameras at Abramov glacier, two cameras at Golubin glacier, one camera at Glacier No. 354 and one camera at Barkrak Middle glacier. Every day, eight pictures are taken, transferred to a nearby CAWa meteorological station, and sent via satellite connection to a database (Schöne et al, 2013). For Glacier No. 354 (Kyrgyzstan) and Barkrak Middle glacier (Uzbekistan), data is stored locally and downloaded once a year.

Meteorological Measurements

Meteorological data constitute an important component of a complete glacier monitoring approach as a required input to mass balance models. There has been an extensive network of continuous long-term meteorological time series of air temperature and precipitation

in Central Asian countries during the Soviet times (Aizen et al, 1995b). However, this network thinned out considerably during the recent past (Unger-Shayesteh et al, 2013).

Some new meteorological stations were installed in close vicinity of Abramov glacier in 2011 and Golubin glacier in 2013 by the CAWa project (Schöne et al, 2013). These two stations were equipped with standard meteorological and ground sensors (see detailed description in (Schöne et al, 2013)). Data access is open and facilitated by GeoForschungsZentrum (GFZ) in Potsdam and CAIAG in Kyrgyzstan (http://sdss.caiag.kg). Meteorological information for the glaciers Batysh Sook and Glacier No. 354 are retreived from the nearby Tien Shan meteorological station (3660 m a.s.l.). This station is operational since 1930 but was relocated in 1997. This causes a shift in the data, hampering its use for long-term studies. Data are available from Hydrometeorological Services of Kyrgyzstan. A small meteorological station was installed in the glacier forefield of Barkrak Middle glacier in 2016 by the CATCOS project.

The access to several historical meteorological time series is, for example, provided by the northern Eurasia Earth Science Partnership Initiative (NEESPI). Data sets such as Reananlysis products, e.g. NCEP/NCAR R1 (US National Centers for Environmental Prediction/US National Center for Atmospheric Research), ERA-Interim (European Centre for Medium-Range Weather Forecasts Reanalysis) or MERRA (Modern Era Retrospective-analysis for Research and Applications) can be used to fill data gaps and to extend data records back in time (e.g. Salzmann et al, 2013; Schär et al, 2004; Schiemann et al, 2008; Schmidli et al, 2001).

Establishing multidecadal mass balance series

The combination of the methods described in the above chapters allows fully exploiting the richness of the available data. Our approach is visualised schematically in Figure5.2 and an example is shown in Figure5.4. Establishing multi-decadal mass balance series for data-scarce regions or time periods requires various data sources to be combined in an optimal way. The methodology that has been presented already in different studies (e.g. Barandun et al, 2015; Kronenberg et al, 2016; Kenzhebaev et al, 2017) is shortly summarised hereafter.

The core of the establishment of long-term mass balance series are in situ data (stake and snow pit measurements and meteorological information, such as precipitation and temperature), a mass balance model, and remote sensing products such as optical satellite sensors and terrestrial cameras. The model used can either be a simple degree-day or a more sophisticated energy balance model, which is able to produce sub-seasonal mass balance as an output (e.g. Machguth et al, 2006b; Huss et al, 2008, 2009). Depending on the objective of the application different investigations are possible with the ingredients of the strategy presented in Figure 5.2. In Barandun et al (2015, for details), for example, we reanalysed mass balance data from the period 1968 – 1994 and calculated glacier-wide balances for the years without measurements to establish a continuous series covering the period 1968 – 2014 using a spatially distributed simple energy balance model (Fig. 5.4). The model was calibrated with seasonal mass balance data and was subsequently used to reconstruct the mass balance for the period with no measurements. Model validation was performed by using snowline observations derived from optical satellite images and, when available also from images of an automatic camera. In a final step, the resulting mass balance values covering several years or decades were compared to the geodetic glacier volume change determined based on the comparison of digital elevation models (Barandun et al, 2015).

Table 5.3: Observed geodetic mass balance for Abramov, Golubin, Batysh Sook and Glacier No. 354

glacier	method	source	period	B_a (m w.e. yr^{-1})
Abramov	$B_{\text{glac.-rec.}}$	(Barandun et al, 2015)	2000–2011	−0.51±0.15
Abramov	$B_{\text{geod.}}$	(Gardelle et al, 2013)	2000–2011	−0.03±0.14
Golubin	$B_{\text{geod.}}$	(Bolch, 2015)	1964–1999	−0.46±0.24
Golubin	$B_{\text{geod.}}$	(Bolch, 2015)	1999–2012	−0.28±0.97
No. 354	$B_{\text{geod.}}$	(Pieczonka and Bolch, 2015)	1975–1999	−0.79±0.25
No. 354	$B_{\text{geod.}}$	(Kronenberg et al, 2016)	2003–2012	−0.48±0.07

5.4 Investigations at individual monitoring sites

In the recent past, results of glacier monitoring activities in Central Asia (except Kazhakstan and China) are mainly based on remote sensing techniques with a focus on geodetic area and volume change assessments (see Tab. 5.3) or front variation measurements (Aizen et al, 2007; Konovalov and Desinov, 2007; Niederer et al, 2007; Haritashya et al, 2009; Kääb et al, 2015; Narama et al, 2010; Hagg et al, 2013; Kriegel et al, 2013; Gardelle et al, 2013; Gardner et al, 2013; Ozmonov et al, 2013; Pieczonka et al, 2013; Khromova et al, 2014; Bolch, 2015; Pieczonka and Bolch, 2015; Farinotti et al, 2015; Petrakov et al, 2016b). Between 1994 and 1998, most of the in-situ glacier observation programs were discontinued. The re-initiation of in-situ monitoring activities on five selected glaciers, Abramov, Golubin, Batysh Sook, Glacier No. 354 and Barkrak Middle, now continues the historical measurement series and is described in the following sections with the main findings emerging from the current and historical monitoring. At some other glaciers like Karabatkak or Sary-Tor also a re-establishment programme was developed under the auspice of the Kyrgyz Institute of Water Problem and Hydropower Engineering together with the Moscow State University within the project "Contribution to High Asia Runoff from Ice and Snow" (CHARIS) financed by USAID.

5.4.1 Abramov glacier, Kyrgyzstan

Abramov glacier is a valley-type glacier and is located in the northern slope of Pamir-Alay (Kyrgyzstan) within the basin of the Vakhsh river, which is one of the largest tributary of the Amu Darya river (Fig. 5.1). The glacier drains into Koksu river, which has a hydrological catchment area of 58 km^2 with a glacierization of roughly 51 % (Hagg et al, 2006). Abramov has a surface area of about 24 km^2 (in 2013) and a volume of 2.54 km^3 (Huss and Farinotti, 2012). The glacier is exposed to the North and ranges from about 3600 to 5000 m a.s.l.

Annual mean air temperature at the equilibrium line of the glacier (around 4260 m a.s.l.) is –6.5 to –8 °C (Kamnyansky, 2001). Average annual precipitation measured at 3837 m a.s.l. is about 750 mm (Glazirin et al, 1993). The glacier is assumed to have a temperate accumulation zone with cold ice near the surface in the ablation area, even though slightly negative temperatures were reported in the accumulation area by Kislov et al (1977).

A research station at Abramov glacier was built in 1967 by the Central Asian Hydrometeorological Institute (SANIGMI) in Tashkent, guaranteeing the continuous collection of glaciological and meteorological observations. The station was destroyed in the late 1990s

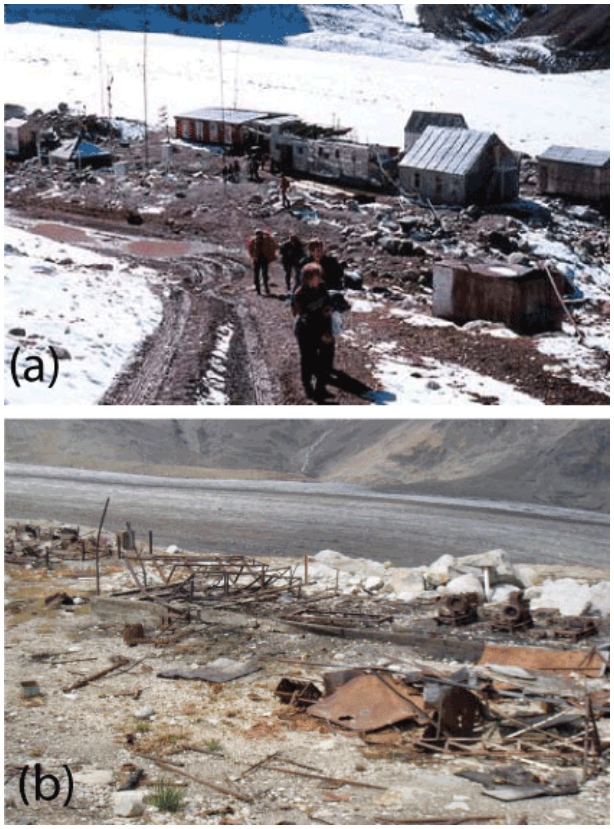

Figure 5.3: (a) Abramov research station in the year 1993 (photo: NSIDC), (b) Ruins of the Abramov research station in 2011 (photo: M. Hoelzle)

during politically unstable times (Fig. 5.3). With the station, also other valuable equipment and the measurement network was lost.

Continuous and detailed mass balance measurements exist from 1968 to 1994 (Pertziger, 1996), whereas from 1994 to 1998 seasonal mass balance values are available from WGMS (2001). Several publications have assessed the long-term mass balance of Abramov glacier. Comparing the results of these studies, differences in the order of ± 0.3 m w.e. yr^{-1} (from 1974-1994) are revealed (Suslov et al, 1980; Glazirin et al, 1993; Kamnyansky, 2001; Pertziger, 1996; WGMS, 2001; Dyurgerov et al, 2002; Barandun et al, 2015). Therefore, the data series were homogenised (Barandun et al, 2015). The historic mass balance measurements on Abramov glacier only show few positive years with mass balances exceeding $+0.3\,\mathrm{m\,w.e.\,yr}^{-1}$, such as 1968/69, 1971/72, 1986/87, 1991/92 and 1992/93. Rasmussen (2013) calculated the Abramov glacier's mass balance sensitivity to air temperature change as $-0.47\,\mathrm{m\,w.e.\,yr}^{-1}\mathrm{C}^{-1}$ using a positive degree-day model driven with NCEP/NCAR Reanalysis data, indicating the highest sensitivity of all studied glaciers in Central Asia.

The mass balance was reconstructed according to the method describe in the method chapter and for the time period for which no direct measurements were available (Barandun et al, 2015). Such reconstructions of past mass balance time series are important to (a) fill data gaps, (b) compare past variabilities with current ones, (c) detect changes in glacier sensitivity, (d) interpret present and future impacts of glacier change. An example of such a reconstruction is shown in Fig. 5.4 for Abramov glacier (Barandun et al, 2015), where mass balance data was homogenised for the period 1968 – 1998 and 2012 – 2015 and reconstructed for the period 1999 – 2011 using a calibrated distributed mass balance

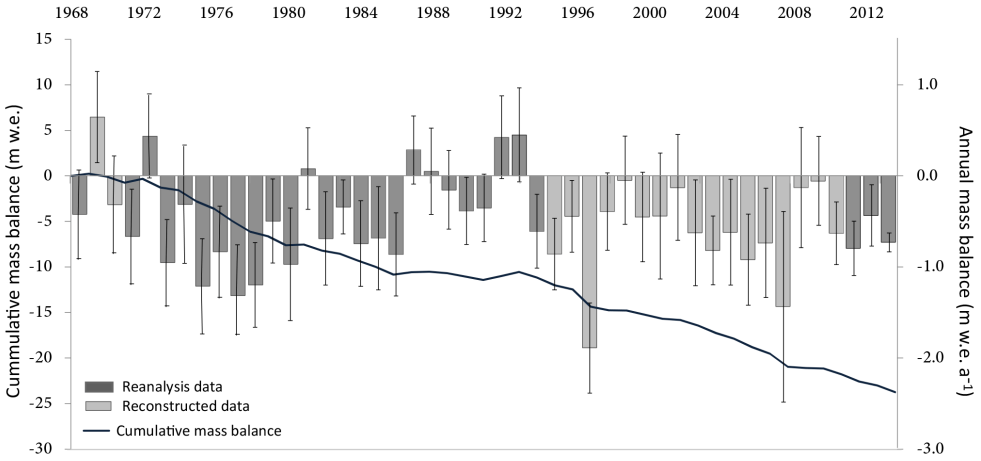

Figure 5.4: Reconstructed mass balance data for Abramov glacier according to Barandun et al (2015)

model. The results of the reconstruction were validated using snow lines digitised from the Landsat images. The mean mass balance for the time period 1998 – 2011 is $-0.51\pm$ $0.17\,\mathrm{m\,w.e.\,yr^{-1}}$ and it is $-0.44\pm$ $0.10\,\mathrm{m\,w.e.\,yr^{-1}}$ for 1968 – 2014 (Barandun et al, 2015).

Maximal discharge of Abramov glacier has been measured in the month of August with around $14\,\mathrm{m^3\ s^{-1}}$ during the first observation years in the 1960/70s (Yemelyanov, 1973). A future change in the discharge pattern based on different climate scenarios indicating an increase in annual runoff. Furthermore the seasonal peak will shift towards May to June and a decrease will likely occur in August (Hagg et al, 2007). Compared to the very high sensitivity of glacial runoff to air temperature, precipitation changes appear to be of secondary importance (Hagg et al, 2007).

A new and fully automated meteorological station was installed in August 2011 at Abramov glacier at an altitude of 4100 m a.s.l. within a distance of about 1 km from the glacier. The station records GPS position, air temperature, relative humidity, atmospheric pressure, precipitation, wind speed and direction, shortwave incoming and outgoing radiation, as well as longwave incoming and outgoing radiation, soil water content and soil temperatures (Schöne et al, 2013). The historical and re-established mass balance networks are shown in Figure 5.5. Field data were analysed by using a distributed mass balance model for extrapolating the point measurements to the entire glacier (Huss et al, 2009; Barandun et al, 2015) and the results are presented in Tab. 5.4. Since 2011, five field campaigns were conducted on Abramov glacier allowing the calculation of glacier-wide mass balance (see Fig. 5.6). Annual mass balance 2012 – 2016, i.e. after the re-establishing the monitoring programme, were negative with a mean of $0.41\,\mathrm{m\,w.e.\,yr^{-1}}$ (Tab. 5.4). The observed cumulative glacier frontal retreat since 1850 sums up to more than 2 km (see Tab. 5.5, Fig. 5.7).

5.4.2 Golubin glacier, Kyrgyzstan

Golubin glacier is situated in the Ala–Archa catchment located in the Kyrgyz Alatoo range in the northern Tian Shan in Kyrgyzstan (Fig. 5.1). The catchment belongs to the larger Chu river basin, which drains into the Kazakh steppe. The Ala Archa catchment contains 48 glaciers. Bolch (2015) reports a total glaciated area in Ala Archa of $40.5 \pm 0.5\,\mathrm{km^2}$ in 1964 and 33.3 ± 0.8 $\mathrm{km^2}$ in 2010. Golubin glacier covers an area of 5.5 $\mathrm{km^2}$ based on a satellite image of 2002, has a volume based of $0.348\,\mathrm{km^3}$ (Huss and Farinotti, 2012), and

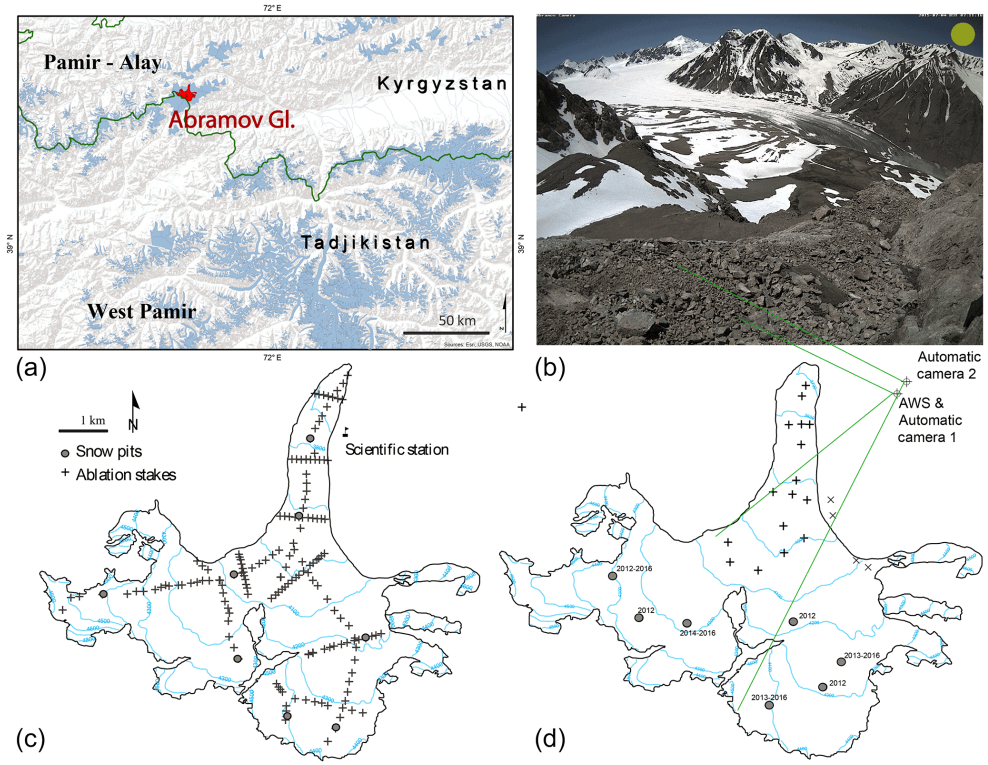

Figure 5.5: Historical and new mass balance network on Abramov glacier (Kyrgyzstan) with corresponding map (upper left) and snow line camera picture (upper right)

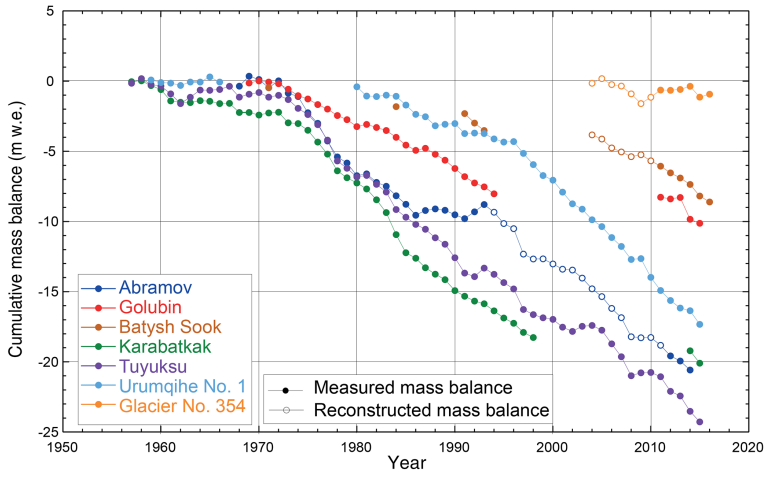

Figure 5.6: Cumulative mass balance measurements for glaciers in Central Asia. Filled dots are direct glaciological measurements, non-filled dots are reconstructed values.

spans over an altitudinal range of 3300 to 4400 m a.s.l. The continental-type glacier has a northern aspect in the accumulation area, and a northwestern aspect in the ablation area.

The climate in the Ala Archa region is chracterised by limited annual precipitation of around 700 mm yr^{-1} mainly during April to June (48%) (Aizen et al, 2006). Mean annual air temperature in the ablation area of the glacier (3450 m a.s.l.) is about 1.5 °C, calculated with a lapse rate of 0.72 °C per 100 m from Baitik station (Aizen et al, 1995a).

Glaciological investigations on Golubin glacier started in 1958 and continued until 1994 when the monitoring programme was stopped (see Tab. 5.1). Between 1958 and 1973, the

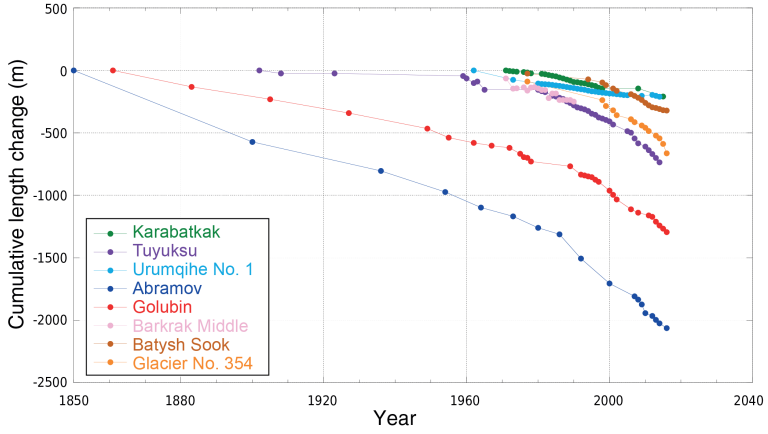

Figure 5.7: Cumulative front variation measurements for glaciers in Central Asia

mass balance was predominantly positive and mainly negative afterwards (Aizen, 1988). Using imagery of several satellites Bolch (2015) determined the geodetic mass change for the periods 1964 to 1999, and 1999 to 2010. A mass balance of –0.46 ± 0.24 m w.e. yr^{-1} for the first period and of –0.28 ± 0.97 m w.e. yr^{-1} for the second period was detected. For the whole Ala Archa catchment, a glacier area change of –5.1% from 1943 to 1977 and of –10.6% between 1977 and 2003 was observed (Aizen et al, 2006, 2007). The mass balance sensitivity to temperature change was determined by Rasmussen (2013) as –0.17 m w.e. a $°C^{-1}$, which is substantially lower than for Abramov glacier.

In summer 2010, mass balance and length change measurements were re-initiated. In Figure 5.8 the former and the new measurement network are presented. Complete information is available for six years now. During this time, the length change measurements were performed by GPS and by analysis of satellite images. The recent observations of the glacier tongue could be connected to earlier measurements by Aizen et al (2006, 2007) (Fig. 5.7). The glaciological measurements were analysed by using a distributed mass balance model (Huss et al, 2009) (Tab. 5.4, Fig. 5.6). The meteorological station, installed in 2013, is situated at an altitude of 3300 m a.s.l. at a distance of 500 m away from Golubin glacier (Schöne et al, 2013). Two further climate stations Alplager and Baitik are located in the Ala-Archa catchment at the altitudes of 2340 m a.s.l. and 1580 m a.s.l., respectively. The re-initiated mass balance measurements since 2010 indicate mostly negative mass changes. In 2010/2011 and 2015/16, a positive mass balance was measured (Tab. 5.4). The observed cumulative glacier frontal retreat since 1861 sums up to around 1.3 km (see Table 5.5 and Fig. 5.7).

5.4.3 Batysh Sook glacier, Kyrgyzstan

Batysh Sook glacier (also named Suyok (Suek) Zapadniy or Glacier No. 419 in earlier studies (WGMS, 1993; Hagg et al, 2013; Kenzhebaev et al, 2017)) is located in the Sook range in the Central Tien Shan in Kyrgyzstan. The range comprises of 44 glaciers with a total area of 30.9 km^2 and volume of 1.2 km^3 in 2007 (Hagg et al, 2013). Batysh Sook glacier (Fig. 5.1) belongs to the Naryn catchment, major tributary of the Syr Darya river. The small glacier covered an area of around 1.2 km^2 in 2005 and covers an altitudinal range of 3950 to 4450 m a.s.l. with an estimated volume of around 0.033 km^3 ±6.5% in 2010 (Hagg et al, 2013). The glacier is assumed to be composed of a temperate accumulation zone and a cold ablation area.

Table 5.4: Glaciological mass balance for Abramov, Golubin, Batysh Sook and Glacier No. 354 after the re-establishment of the measurements, calculated for the hydrological year using a mass balance model

glacier	year	area (km^2)	ELA (m a.s.l.)	B_a (m w.e. yr^{-1})
Abramov	2011/12	24.06	4265	− 0.795 ±0.30
Abramov	2012/13	24.01	4225	− 0.436 ±0.34
Abramov	2013/14	24.01	4245	− 0.730 ±0.10
Abramov	2014/15	23.94	4115	+ 0.171 ±0.30
Abramov	2015/16	23.93	4185	− 0.274 ±0.30
Golubin	2010/11	5.47	3775	+ 0.029 ±0.2
Golubin	2011/12	5.47	3875	− 0.318 ±0.2
Golubin	2012/13	5.45	3835	− 0.251 ±0.2
Golubin	2013/14	5.45	4325	− 0.665 ±0.2
Golubin	2014/15	5.44	4315	− 0.565 ±0.2
Golubin	2015/16	5.44	3745	+ 0.130 ±0.2
Batysh Sook	2010/11	1.13	4255	− 0.375 ±0.17
Batysh Sook	2011/12	1.13	4265	− 0.476 ±0.15
Batysh Sook	2012/13	1.12	4255	− 0.368 ±0.16
Batysh Sook	2013/14	1.11	4265	− 0.463 ±0.16
Batysh Sook	2014/15	1.11	4305	− 0.822 ±0.15
Batysh Sook	2015/16	1.11	4265	− 0.424 ±0.14
Glacier 354	2010/11	6.47	4195	− 0.41 ±0.24
Glacier 354	2011/12	6.44	4205	− 0.46 ±0.26
Glacier 354	2012/13	6.42	4225	− 0.55±0.25
Glacier 354	2013/14	6.41	4275	− 0.64 ±0.22
Glacier 354	2014/15	6.41	4365	− 0.84±0.24
Glacier 354	2015/16	6.40	4155	− 0.23±0.24

According to the Tien Shan meteorological station situated in a distance of around 32 km, the mean annual temperature is –6.0°C. July is the month with the highest temperatures (4.4°C) and January has a mean temperature of –21.7°C (1997 to 2014) (Kutuzov and Shahgedanova, 2009). Mean annual precipitation is 360 mm (1997 to 2014), of which up to 75% was recorded during the summer months (May to September).

Batysh Sook was already monitored during short periods in 1970/71, 1983/84 and from 1988 to 1991 (see Tab. 5.2 WGMS (1993)). Hagg et al (2013) calculated an area loss of around 19.8% and a corresponding volume loss of 12.1% for all glaciers within the Sook range for the time period 1956 to 2007.

Since 2010, several stakes and some snow pits are measured on an annual basis on Batysh Sook glacier. In Figure 5.9 the old and the new measurement networks are presented. The mass balance is analysed using a distributed mass balance model (Huss et al, 2009). The results indicate continuous negative mass balance of about –0.4 to –0.8 m w.e. yr^{-1} since 2011/2012 (Tab. 5.4). The observed cumulative glacier frontal retreat since 1975 sums up to around 0.32 km (see Tab. 5.5 and Fig. 5.7).

A reconstruction of past mass balances for the period 2004 to 2010 was performed by (Kenzhebaev et al, 2017) using a calibrated distributed temperature index mass balance model. For the reconstructed period an average annual mass balance of –0.39 ±0.26 m w.e. yr^{-1} was found. For the direct measured period 2011 to 2016, three different methods

Table 5.5: Length change ΔL measurements for Abramov, Golubin, Batysh Sook and Glacier 354 based on GPS surveys, satellite images and maps

Abramov		Golubin		Batysh Sook		Glacier 354	
Period	ΔL (m)	Period	ΔL (m)	Period	ΔL (m)	Period	ΔL (m)
1850-1900	−572	1861-1883	−131	1975-1977	−25	1972-1977	−89
1900-1936	−232	1883-1905	−100	1977-1994	−47	1977-1998	−148
1936-1954	−169	1905-1927	−110	1994-1998	−24	1998-1999	−47
1954-1964	−125	1927-1949	−125	1998-1999	−22	1999-2001	−35
1964-1973	−70	1949-1955	−72	1999-2001	−27	2001-2002	−39
1973-1980	−92	1955-1962	−42	2001-2002	−18	2002-2006	−33
1980-1986	−52	1962-1967	−22	2002-2006	−27	2006-2007	−23
1986-1992	−193	1967-1972	−17	2006-2007	−15	2007-2009	−27
1992-2000	−201	1972-1975	−47	2007-2008	−14	2009-2010	−18
2000-2007	−102	1975-1976	−26	2008-2009	−18	2010-2011	−25
2007-2008	−27	1976-1977	−6	2009-2010	−23	2011-2013	−36
2008-2009	−39	1977-1978	−30	2010-2011	−20	2013-2014	−22
2009-2010	−69	1978-1989	−39	2011-2012	−15	2014-2015	−45
2010-2012	−22	1989-1992	−65	2012-2013	−6	2015-2016	−76
2012-2013	−32	1992-1993	−7	2013-2014	−9		
2013-2014	−27	1993-1994	−8	2014-2015	−9		
2014-2016	−38	1994-1995	−7	2015-2016	−3		
		1995-1996	−20				
		1996-1997	−16				
		1997-2000	−71				
		2000-2001	−34				
		2001-2002	−37				
		2002-2006	−79				
		2006-2008	−27				
		2008-2011	−22				
		2011-2012	−12				
		2012-2013	−38				
		2013-2014	−32				
		2014-2015	−25				
		2015-2016	−27				

were applied. The first method, profile method, revealed a mass loss of –0.41 ±0.28 m w.e. yr^{-1}, the second method, the contour line, resulted in a negative mean mass balance of –0.34 ±0.20 m w.e. yr^{-1}, and the third method, based on model extrapolation calculated a value of –0.43 ±0.16 m w.e. yr^{-1}.

5.4.4 Glacier No. 354, Kyrgyzstan

Glacier No. 354 is situated in the southern part of the Akshiirak glacierized massif, Inner Tien Shan in Kyrgyzstan (Fig. 5.1). According to Aizen et al (2006), the range contains 178 glaciers (87% of them are valley type glaciers) covering an area of 371 km^2. The Akshiirak glaciers on the eastern and southern part of the mountain range drain into the Saridjaz river, a tributary of the Tarim river via Aksu river and the runoff of the glaciers on the western part contributes to the flow of the Naryn river. The glacier had a surface

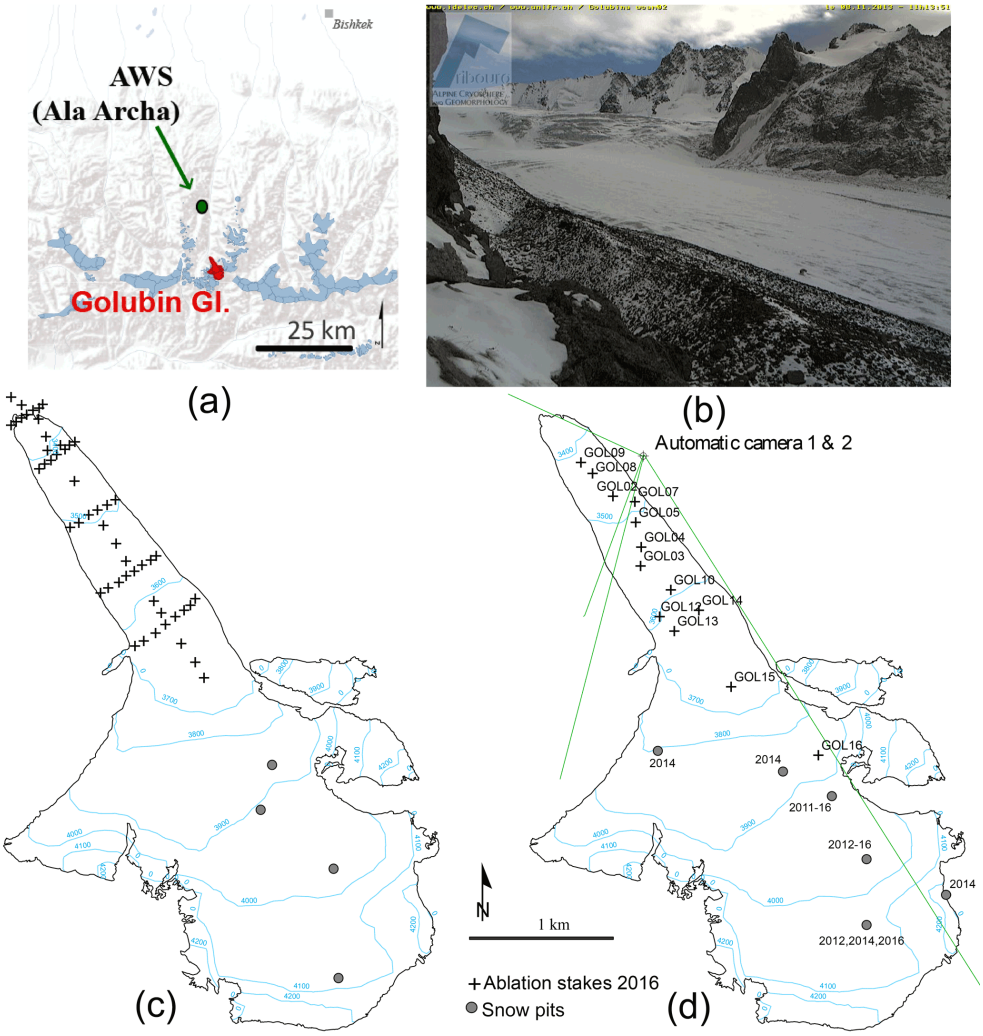

Figure 5.8: Historical and new mass balance network on Golubin glacier (Kyrgyzstan) with corresponding map (upper left) and snow line camera picture (upper right)

area of 6.41 km^2 in 2014 Kronenberg et al (2016). The accumulation area is composed of three basins and the glacier tongue is directed to the Northwest. The glacier covers an altitudinal range of around 3750 to 4650 m a.s.l. Hagg et al (2013) performed GPR measurements on the glacier tongue and used a simplified ice mechanical approach to determine the total volume of this glacier to 0.272 km^3 ± 0.022 km^3. Pieczonka and Bolch (2015) quantified the geodetic mass balance for Glacier No. 354 (Bordu-Yushny in their study) from 1975 to 1999 as –0.79 ±0.25 m w.e. yr^{-1}.

The Akshiirak range is closely situated to the Sook range, and the closest meteorological station is again the Tien Shan station (14 km distance). The climate is similar to the one of Bathys Sook glacier.

Glacier No. 354 was selected to replace the previously monitored Sary-Tor glacier due to current access restrictions because of mining activities. Sary-Tor has mass balance observations based on the glaciological method for the period of 1985 to 1989 (Dyurgerov et al, 1994) and its mass balance was reconstructed for the period 1930 to 1988 by Ushnurtsev (1991). Mass balance measurements were re-initiated in 2013 by a team of Russian and Kyrgyz scientists. The front variations of Sary-Tor indicate a retreat of 70 m

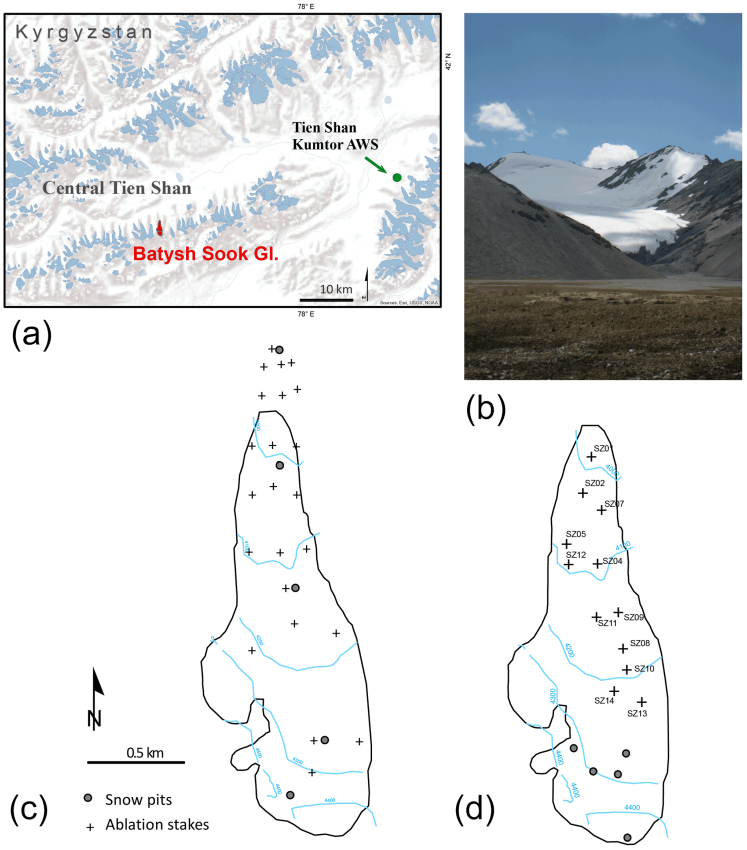

Figure 5.9: Historical and new mass balance network on Batysh Sook glacier (Kyrgyzstan) with corresponding map (upper left) and picture (upper right)

from 1932 to 1943, no changes from 1943 to the mid-1970s, a retreat of 220 m from 1977 to 1995 and of 90 m from 1995 to 2003 (Aizen et al, 2007).

Kronenberg et al (2016) presented a reconstruction of the seasonal mass balance of Glacier No. 354 from 2003 to 2010. This reconstruction is based on an analysis of the annual measurements of stakes and snow pits of the years 2010 to 2014 (Fig. 5.10). The glaciological data was used to calibrate a distributed mass balance model, which was then used to reconstruct the seasonal mass balances since 2003. In addition, winter accumulation measurements were performed in spring 2014 and also used for model calibration. Furthermore, the geodetic volume change was determined based on two high-resolution satellite stereo images acquired in 2003 and 2012 and used to validate the modelled cumulative glacier-wide mass balance. For the period 2003 to 2012, an annual mass balance of -0.40 ± 0.10 m w.e. yr^{-1} was modelled. This result corresponds well with the geodetic mass balance of -0.48 ± 0.07 m w.e. yr^{-1} for the same period (see Tab. 5.4 and Tab. 5.3, Kronenberg et al (2016)). The observed cumulative glacier frontal retreat since 1972 sums up to around 0.66 km (see Tab. 5.5 and Fig. 5.7).

5.4.5 Barkrak Middle, Uzbekistan

Barkrak Middle glacier is located in the Oygaing valley in the Pskem catchment in the western Tien Shan, Uzbekistan (Fig. 5.1). The Pskem river drains into Chirchik river, a tributary of the Syr Darya river. The area of the glaciers in the Pskem river basin including the Oygaing and the Upper Maydan valley (located in Kazakhstan) was 93.6 km^2 in the

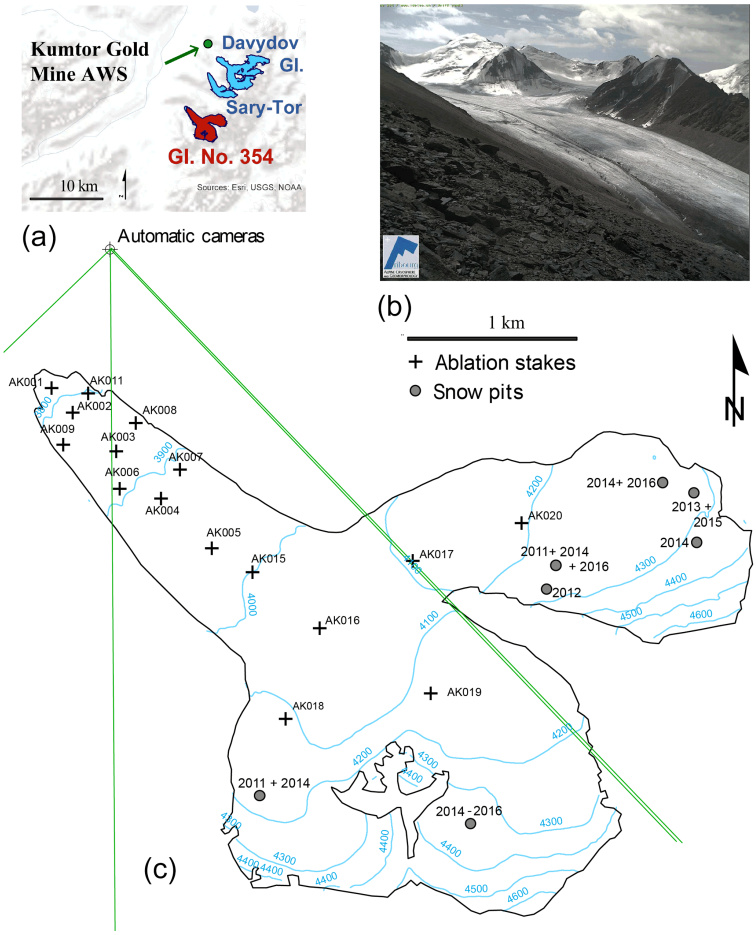

Figure 5.10: Mass balance network on Glacier No. 354 (Kyrgyzstan) with corresponding map (upper left) and snow line camera (upper right)

year 2007 (Semakova et al, 2016). The area of Barkrak Middle is 2.18 km^2 (Semakova et al, 2016) and the volume is 0.087 km^3 (Huss and Farinotti, 2012).

Between 1960 and 2010, the glacierized area decreased by 23% in the Pskem river catchment and more specifically a 16.8% decrease in glacier area was observed from 1980 to 2001 in the basin of the Oygaing river, where Barkrak Middle glacier, is located (Semakova et al, 2016). For Barkrak Middle glacier, observation of length change exist from 1971 to 1990 with a total cumulative retreat of 249 m (see Fig. 5.7).

In 2016, a new mass balance network with a total of 11 stakes was established (Fig. 5.11). In addition, a meteorological station in the glacier forefield and an automatic snow line camera were installed (Fig. 5.11).

5.5 Summary of glacier length and mass changes in Central Asia

The measurements performed on various glaciers in Central Asia show an overall mass loss over the last five decades. There are some individual years with positive mass balances within all decades (Fig. 5.6, 5.12, Tab 5.3). However, the positive mass balances are mostly observed during the beginning of the measurements in the 1960/70s. Long-term trends based on the glaciological, as well as on the geodetic method indicate a mean

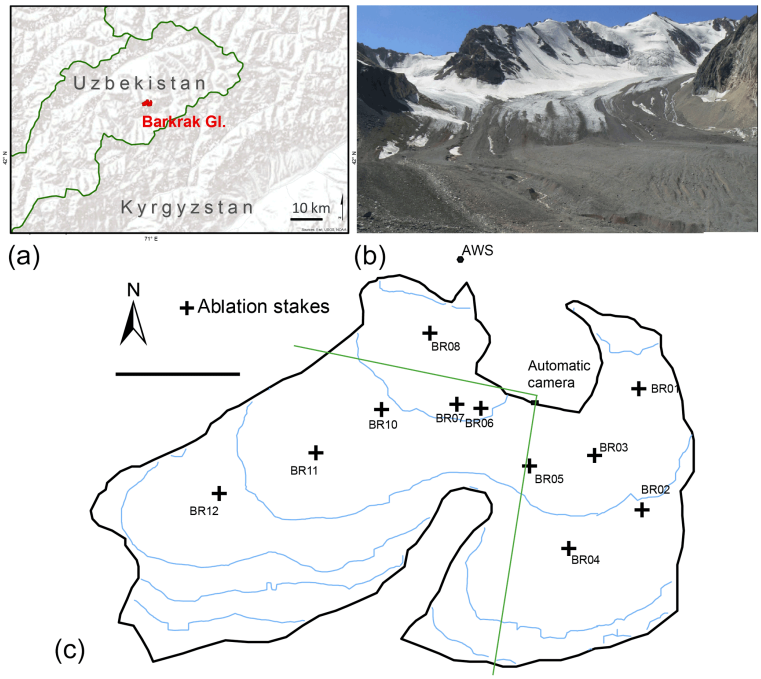

Figure 5.11: Mass balance network on Barkrak Middle (Uzbekistan) with corresponding map (upper left) and picture (upper right)

negative mass balance in the range of −0.3 to −0.8 m w.e. yr^{-1}. Most negative mass balances were observed at Abramov, Karabatkak, Tuyuksu and Urumqihe WGMS (2013), whereas Golubin and Batysh Sook exhibited smaller mass loss. This observation is in line with the mass balance sensitivities of the glaciers in Central Asia as inferred by Rasmussen (2013). The observed cumulative mass balance determined by the glaciological method is supported by several remote sensing studies underlining the findings (Aizen et al, 1995b; Bolch et al, 2011b, 2012; Pieczonka et al, 2013; Gardelle et al, 2013; Pieczonka and Bolch, 2015; Bolch, 2015; Kronenberg et al, 2016).

The network of glaciological and geodetic measurements in the Tien Shan Mountains has been strongly improved by the re-establishment of the monitoring programmes starting in 2010. In the Pamir Mountains, however, glacier mass balance measurements are still sparse as only Abramov glacier in the most northwestern part is monitored. This glacier is not representative for the entire Pamir, also containing glaciers at much higher altitudes that respond differently to atmospheric warming (e.g. Kääb et al, 2015; Kääb et al, 2012; Gardner et al, 2013; Gardelle et al, 2013).

Length changes are an important element of glacier monitoring. Direct measurements extend back into the 19th century in several mountain ranges and some reconstructions based on geomorphological dating go back to the 16th century (Zemp et al, 2015). In general, the cumulative front variation measurements for the investigated glaciers in Central Asia reveal a long-term glacier retreat (see Tab. 5.4, Fig. 5.7). Using a simple parametrisation scheme developed by Haeberli and Hoelzle (1995) and used by Hoelzle et al (2003) to convert curves of cumulative glacier advance and retreat into time series of temporally averaged mass balance by applying a continuity model originally proposed by Nye (1960). This approach considers step changes after full dynamic response and new equilibrium of the glacier based on the assumption that a mass balance change is leading to a corresponding glacier length change depending only on the original length of the glacier and

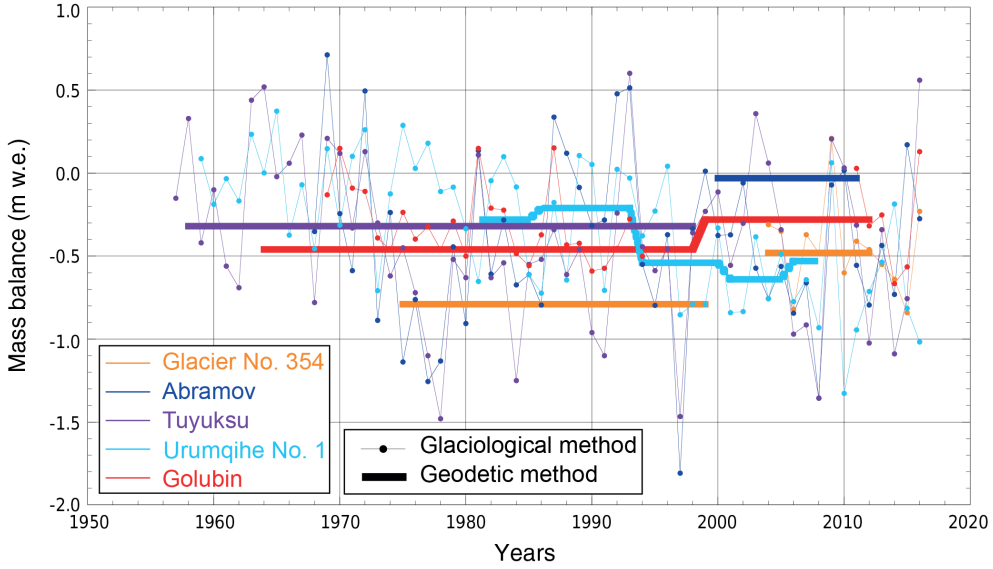

Figure 5.12: Comparison of glaciological and geodetic mass balance for glaciers in Central Asia. The geodetic mass balances are from (Hagg et al, 2004a) (Tuyuksu), (Wang et al, 2014a) (Urumqihe no. 1), (Pieczonka and Bolch, 2015; Kronenberg et al, 2016) (Glacier 354), and (Gardelle et al, 2013) (Abramov). The glaciological data are provided by WGMS (2013).

its annual mass balance (ablation) at the glacier terminus. Calculating these values for Abramov (for the period 1850 – 2016) is resulting in –0.35 m w.e. yr^{-1}, for Golubin (1861 – 2016) around –0.2 m w.e. yr^{-1}, for Batysh Sook (1975 – 2016) and Glacier 354 (1972 – 2016) around to –0.35 m w.e. yr^{-1}.

5.6 Discussion

We demonstrate that, a valuable glaciological dataset is available for the Central Asian mountains, particularly for the Tien Shan, despite of different historical backgrounds and changing methodological aspects. New monitoring networks in combination with historical measurements will generate highly valuable baseline data for future research, climate change observations, assessment of climate change impacts and related adaptation measures, including water resource management. Continuous long-term support and cooperation among several countries and institutions is required to keep the successfully re-established measurements alive. The newly developed strategy and its implementation to connect in-situ measurements with remote sensing and numerical modelling techniques (see Fig. 5.2) will allow the establishment of an efficient glacier monitoring programme. This will guarantee an optimum between available human capacity and efforts, sustainable financial coverage and data quality, offering a feasible way to perform long-term monitoring. Our approach implemented in Kyrgyzstan and Uzbekistan has to be proven during the next years and should be further developed. Over the last years, it delivered promising results, although there are still many improvements possible. One of the most urgent needs is capacity building, i.e. the education of young local scientists being able to continue the monitoring programme independently (Nussbaumer et al, 2017).

Our approach also reveals that on a scientific basis, an in-depth re-evaluation of long-term geodetic mass changes on all selected glaciers is absolutely necessary. Most geodetic measurements (e.g. for Glacier 354, Urumqihe No. 1 and Tuyuksu) match well with the

glaciological mass balances (Fig. 5.12). All these measurements show almost persistently negative mass balances since the mid-20th century. At Abramov glacier, however, considerable differences between geodetic and reconstructed glaciological measurements were found (Fig. 5.12 and Tab. 5.3). For the period 2000 to 2011, Barandun et al (2015) determined a negative value of –0.51 ±0.17 m w.e. yr^{-1}, whereas Gardelle et al (2013) reported a mass balance of –0.03 ±0.14 m w.e. yr^{-1} for the same period. The geodetic measurements are subject to considerable uncertainties that are, for example, related to underestimated penetration of the radar signals into snow and firn in the accumulation areas during the acquisition of the SRTM mission in the year 2000 (Paul et al, 2013b). This is confirmed by other studies using ICESat measurements in the same region (Kääb et al, 2015; Kääb et al, 2012; Gardner et al, 2013) and by ground penetrating radar measurement in the accumulation area of Abramov glacier (Barandun et al, 2015). This shows the need for further analysis of existing aerial and satellite data in order to create additional high-accuracy elevation models. Another problem encountered during the homogenisation process of the mass balance time series was a considerable inconsistency, which is mainly related to different interpretations of the former stake networks or to missing measurements.

Glacier frontal variations complement the mass balance measurements. They show a continuous retreating trend for the last decades and century. The inferred estimates of mass change calculated based on the length change measurements are in quite good accordance with the mass balance measurements.

5.7 Conclusions

This paper demonstrates the richness of historical dataset from the long-term glacier measurements available in Central Asia and particularly in Kyrgyzstan and it introduces the (re)-established glacier measurement network highlighting the importance of capacity building to make the efforts sustainable. In connection with the new glacier monitoring strategy and its current implementation, the long-term in-situ data are fundamental to understand the relevant processes and the impact of climate change on glaciers in the Tien Shan and the Pamir-Alay and the impacts for the people living nearby as well as in far distances downstream. Therefore, the cryospheric ECV 'glacier' is an important variable, for which sustainable long-term monitoring has to be ensured not only in industrial countries but also in developing countries. Without the long-term measurements, questions like the future behaviour of glaciers and their possible disappearance and the impacts for the society cannot be answered comprehensively. Only well-validated and well-calibrated models based on sound process understanding and high quality data will ensure projections with acceptable level of uncertainty. These models and their outputs are the only tools for estimating future runoff evolution in one of the driest continental regions of the northern hemisphere, where future water shortage due to decreased glacierization has the potential to lead to pronounced political instability, drastic ecological changes and might endanger future food security in a highly populated region. This highlights the importance of in-situ monitoring networks of all ECVs within national and international Climate Services and their use together with remote sensing and numerical models.

Author contribution

MHo and MZ conceived of the presented idea. MHo, MZ, HM, MHu and MB conceived the monitoring network and proposed the analytical methods. MB, TS, EA, RK, MK, AG

carried out computation and led the field measurements and capacity building programs. MHo wrote the manuscript with help of DF, MHu, MB, MK, WH and MZ. TS, MB, MHo, RU, AG, YT, AY, AM, MP, BM, WH, DF, HM helped with the planning and execution of the monitoring strategies and took active role in the capacity building. TS, AG and SV completed monitoring with installations of modern automatic weather stations within the Central Asian Waters (CAWa) project.

Acknowledgements

We thank F. Denzinger, M. Duishonakunov, M. Fischer, A. Ghirlanda, S. Gindraux, A. Kääb, D. Kriegel, M. Kummert, N. Mölg, K. Naegeli, A. Neureiter, D. Petrakov, S. Reisenhofer, H. Rieck, J. Schmale, A. Sharshebaev, L. Sold, P. Schuppli, A. Zubovich for their valuable support in the field. T. Bolch is acknowledged for sharing data. The project was only possible thanks to support of the Federal Office of Meteorology and Climatology MeteoSwiss through the project CATCOS (Capacity Building and Twinning for Climate Observing Systems), Contract no. $7F - 08114.1$ between the Swiss Agency for Development and Cooperation and MeteoSwiss and the project CICADA (Cryospheric Climate Services for improved Adaptation), Contract no. 81049674 between Swiss Agency for Development and Cooperation and the University of Fribourg. The CAWa (Water in Central Asia) project (www.cawa-project.net) was supported by the German Federal Foreign Office (contract no. AA7090002) as a part of the "Berlin Process". This study was also supported by the Swiss National Science Foundation (SNSF), by the two projects: 'Snowline observations to remotely derive seasonal to sub-seasonal glacier mass balance in the Tien Shan and Pamir Mountains' grant 155903 and 'Changing glacier firn in Central Asia and its impact on glacier mass balance' grant 169453. Further support came from the European Research Council (FP/2007-2013, ERC grant agreement no. 320816). We are also grateful to all collaborators of the Central Asian Institute for Applied Geosciences for their continued support of this long-term project.

Chapter 6

Paper II: Re-analysis of seasonal mass balance at Abramov Glacier 1968–2014

Barandun, Martina, Matthias Huss, Leo Sold, Daniel Farinotti, Erlan Azisov, Nadine Salzmann, Ryskul Usubaliev, Alexandr Merkushkin, and Martin Hoelzle. *"Re-analysis of seasonal mass balance at Abramov glacier 1968–2014."* Journal of Glaciology 61, no. 230 (2015): 1103-1117

Abstract

Abramov Glacier, located in the Pamir-Alay, Kyrgyzstan, is a reference glacier within the Global Terrestrial Network for Glaciers. Long-term glaciological measurements exist from 1968 to 1998 and the mass balance monitoring programme has been re-established in 2011. In this study we re-analyse existing mass balance data and use a spatially distributed mass balance model to provide continuous seasonal time series of glacier mass balance covering the period 1968–2014. The model is calibrated to seasonal mass balance surveys and then applied to the period with no measurements. Validation and re-calibration is carried out using snowline observations derived from satellite imagery and, after 2011, also from automatic terrestrial camera images. We combine direct measurements, remote observations, and modelling.

The results are compared to the geodetic glacier volume change over the last decade and to a Ground Penetrating Radar (GPR) survey in the accumulation zone resolving several layers of accumulation. Previously published geodetic mass budget estimates for Abramov Glacier suggest a close-to-zero mass balance for the last decade which contradicts our results. We find a low plausibility for equilibrium conditions over the past 15 years. Instead, we suggest that the glacier's sensitivity to increased summer air temperature is decisive for the substantial mass loss during the last decade.

6.1 Introduction

Strong impacts of atmospheric warming on snow, glaciers and permafrost have been observed in high-mountain regions throughout the past decades (IPCC Climate Change, 2013). Glacier mass balance is directly linked to atmospheric conditions and is thus a valuable indicator for climate change (Braithwaite and Zhang, 2000; Haeberli et al, 2007). The importance of changes in Central Asian glaciers in terms of water resources (Immerzeel et al, 2010; Unger-Shayesteh et al, 2013; Sorg et al, 2012, 2014) and their variations due to climate change (Gafurov et al, 2013; Pieczonka et al, 2013) attract much public and scientific attention. Geodetic observations provide evidences for inhomogeneous glacier response in the Pamir (Gardner et al, 2013; Kääb et al, 2015), but validation data sets are sparse for the recent past. For the downstream areas of the Tien Shan and Pamir, melting glacier ice represents an important contribution to runoff (Kure et al, 2013; Lutz et al, 2013). Especially in late summer, water supply is highly critical for irrigation and, hence, economic development and political stability. To better understand the regional variability of glacier response but also to provide an in-depth understanding of the runoff patterns of this region, long-term glacier mass balance observations are fundamental.

In the former Soviet Union an extensive glacier monitoring network was initiated in the late 1960s and detailed, well-documented mass balance series for selected glaciers are available (e.g. Dyurgerov et al, 2002; WGMS, 2005). After the collapse of the Soviet Union most of the glacier monitoring programmes in Central Asia were abandoned. Consequently, Central Asian glaciers are currently strongly underrepresented in the global databases (WGMS, 2012). As a consequence of climate change and today's water stress, an increased interest in re-establishing the historical glacier monitoring sites in this region has emerged. The multinational cooperation projects Central Asian Water (CAWa) and Capacity Building and Twinning for Climate Observing Systems (CATCOS) include the installation of Automatic Weather Stations (AWS) (Schöne et al, 2013), terrestrial cameras, and the set-up of a new glacier mass balance monitoring programme at Abramov Glacier (Barandun et al, 2013).

Mass balance series for Abramov Glacier, located in the Kyrgyz Pamir, covering the period from 1968 to 1998 have been published in different studies (Suslov et al, 1980;

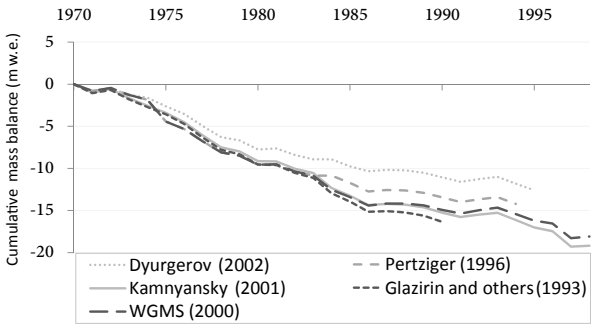

Figure 6.1: Cumulative mass balance series for Abramov Glacier published by different authors (modified after Dyurgerov (2002)).

WGMS, 2005) and the same data has been repeatedly re-analysed (Glazirin et al, 1993; Pertziger, 1996; Kamnyansky, 2001; Dyurgerov et al, 2002) (Fig. 6.1). However, disagreement between the different publications and some data gaps between 1968 and 1998 cause problems in the interpretation of these time series. After 1998 no direct measurements were performed until 2011.

In this study, we re-analyse the historical mass balance data collected at Abramov Glacier to create a consistent and homogeneous time series. Using a distributed mass balance model we reconstruct seasonal glacier mass balance for the period 1968–2014. This allows us to fill the data gap from the mid-1990s to the onset of the newly established monitoring in 2011. Local meteorological measurements and different climate Reanalysis products are used as model input. Observations of the transient snowline derived from satellite images and terrestrial cameras throughout the ablation season are used to independently validate mass balance results. Finally, we compare the reconstructed mass balance series with geodetic mass balance calculations from Gardelle et al (2013) and with estimates of point-based accumulation rates derived from GPR measurements collected in 2013.

6.2 Study site and field data

Abramov Glacier (N39 °36.787′, E71 °33.320′) is located in the Koksu Valley (Amu-Darya River basin) in the Pamir-Alay (North-Western Pamir) in Central Asia (Fig. 6.2). The Pamir range counts over 10'000 glaciers with a total glacierized area of around 9800 km^2 (Khromova et al, 2014). The north to north-west orientated Abramov Glacier has a total area of 24 km^2 (as of 2013) ranging from 3650 m a.s.l. to nearly 5000 m a.s.l. On Landsat images an area reduction of 5% was identified from 1975 to 2014. Even though the glacier tongue advanced by around 0.4 km between 1972 and 1975 (Suslov et al, 1980; Glazirin et al, 1987, 1993), a retreat by almost 1 km has been detected since 1975. The glacier carries a high load of surface impurities considerably lowering the albedo in the ablation area. A debris-covered tributary glacier of an area of about 2 km^2 with strongly reduced melt rates joins the tongue of the glacier (Fig. 6.3b).

6.2.1 Glaciological measurements

In 1967, the Central Asian Hydrometeorological Research Institute (SANIGMI) built a glaciological research station in close vicinity of the glacier front (Fig. 6.3a). We used

Figure 6.2: Location map of Abramov Glacier, Pamir-Alay, Kyrgyzstan.

observations of (1) monthly to seasonal mass balance components (ablation and accumulation), and (2) standard meteorological variables (Tab. 6.1). The observations have been carried out continuously from 1968 until 1998. The glacier monitoring programme of that time included glaciological measurements along 13 profiles (with a total of 165 stakes) and nine snow pits. The 165 stakes were used to measure snow depth at the end of the accumulation season (end of May). At the end of the ablation season (September) these stakes were used to determine the cumulative melt in the ablation area as well as the snow depth in the accumulation area. Monthly snow density and snow depth measurements were carried out at the eight snow pits which were dug down to the last year's end-of-summer horizon (Pertziger, 1996).

A compilation of this exceptional glaciological data is published in Pertziger (1996), which is a reference book including a selection of scientific measurements on Abramov Glacier acquired by the SANIGMI Glaciological Department. Point values of winter and summer balance are not available to us from 1969 to 1970, and from 1995 to 1998 (Tab. 6.1). Annual glacier-wide mass balance data is published from 1968 to 1998 (WGMS, 2005; Kamnyansky, 2001). The data provided by Pertziger (1996) delivers the base for a consistent re-analysis of the entire series and mass balance model calibration performed in this study.

Furthermore, repeated measurements of firn density, layer stratigraphy and a temperature profile in three 30 m firn cores from 1972 to 1975 are available (Suslov et al, 1980; Glazirin et al, 1993). Density, meltwater infiltration and stratigraphy were also determined at two firn pits of up to 17 m depth at an elevation of 4250 m a.s.l. and 4410 m a.s.l., respectively (Suslov et al, 1980) (Fig. 6.3b).

In 2011 a new network of 16 ablation stakes has been set up to represent the previous profile lines and to cover the main features of the surface ablation pattern (Fig. 6.3b). Since 2012, snow depth and density measurements in three to four snow pits per year are carried out to determine the annual accumulation from the previous end-of-summer horizon in August (Tab. 6.1). The snow pits are located in different accumulation basins. Glaciological measurements have been repeated annually between mid- to late-August since 2011. In order to quantify the melt on the strongly debris-covered sections of Abramov Glacier, four stakes have been installed in 2012 (Fig. 6.3b).

Ice ablation is converted to water equivalent (w.e.) by assuming a density of 900 kg m^{-3}

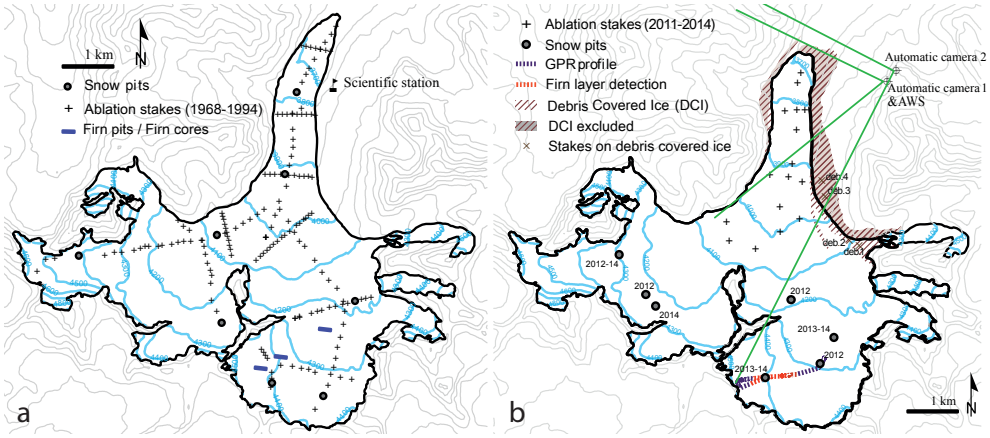

Figure 6.3: (a) Stake and snow pit network on Abramov Glacier during 1968–1998. The firn core and firn pit locations measured in the early 1970's are also indicated. (b) Stake network in 2011 and snow pits measured in the consecutive years. The locations of terrestrial automatic cameras with their view angle (green), the AWS and the GPR profile collected in 2013 are indicated. The red line corresponds to the locations for which a comparison between long-term glaciological measurements, GPR data and geodetically derived elevation changes is performed.

(e.g. Beedle et al, 2014), and through direct density observations in the snow pits for the accumulation zone. An overview of the measurement network is given in Figure 6.3. The number of available mass balance data is summarized in Table 6.1.

6.2.2 Meteorological data

Standard meteorological variables including daily mean air temperature and precipitation sums have been recorded at the glaciological station (3837 m a.s.l., Fig. 6.3a), from 1968 to 1994 (Pertziger, 1996). Solid and liquid precipitation was measured with rain gauges. AWS was installed in summer 2011 (Schöne et al, 2013). The AWS is located at an elevation of 4100 m a.s.l. at a distance of about 1 km to the former glaciological station (Fig. 6.3b).

For years with no meteorological in-situ measurements (1995–2011) we use data from climate Reanalyses. For precipitation, Reanalysis data was also used from 2012 to 2014. Reanalysis data provide global, continuous, and three-dimensional fields of meteorological variables of the past (Bengtsson and Shukla, 1988). Performance is spatially and temporally variable, depending on the number and quality of observations available for the assimilation process. As a result, Reanalyses show typically lower quality at high altitude and in remote regions where observations are sparse (e.g. Trenberth et al, 2001; Duethmann et al, 2013). Furthermore, if there are long-term in-situ observations available and accessible, these have most probably been used in the Reanalysis assimilation process and thus are not an independent source for evaluating the local Reanalyses. Moreover, the performance during the period with observations is also not equal to the period without observations. A reduction and assessment of the uncertainty associated with the use of Reanalysis data in remote mountain areas can be achieved by using a set of different Reanalyses instead of only one product.

Here we use the products NCEP/NCAR R1 (spatial resolution of 2.5 degrees; Kalnay et al, 1996), ERA-interim (spatial resolution of 0.78 degrees, Dee et al, 2011) and MERRA (spatial resolution of about 0.55 degrees; Rienecker et al, 2011), which all provide data since 1979.

6.2.3 Glacier outlines and digital elevation models

Glacier extent is mapped manually based on Landsat Thematic Mapper (TM) / Enhanced Thematic Mapper Plus (ETM+) and Operational Land Images (OLIs) false-colour composites for each year of the study period as far as an appropriate satellite image is available. For 1972 and for 1975 to 1978, we found satisfying scenes with a resolution of 79 m whilst for 1986 to 1988, 1992, and annually since 1998 scenes with a pixel size of 30 m are available.

Debris-covered glacier ice (about 2 km^2) with strongly reduced melt rates (as indicated by ablation measurements) is excluded from the mass balance calculations. Thin debris cover on the glacier, which is supposed to lower melt rates by less than 45%, is mapped and included for modelling (Fig. 6.3b). We adjust the terminus region of the glacier to obtain annual glacier masks for modelling and assume no changes in the outline in the accumulation area. Errors related to glacier outlines digitized manually on remote sensing images depend on atmospheric and topographic corrections, shading, glacier surface characteristics, snow cover and local clouds but mainly on misinterpretation of debris cover (Paul et al, 2013a, 2015). Uncertainties are expected to be in the range of ±5% of the total glacier area (Paul et al, 2013a) resulting in ±1 km^2 for our case.

A digital elevation model (DEM) generated by digitizing contour lines of a topographic map (1:25'000) acquired in 1986 by the Soviet Union-Kyrgyz Office of Geodesy with a cell size of 20 m and a non-void-filled Shuttle Radar Topography Mission (SRTM) DEM from February 2000 are used. We downscaled the SRTM DEM to a regular 20 m grid using cubic interpolation. The topographic map is based on theodolite measurements collected in 1986 by Kuzmichenok (1990). We compared the DEM from 1986 to the theodolite measurements and found a Root-Mean-Square Error (RMSE) of 4 m. To avoid a shift in the two DEMs, we applied a co-registration as proposed by Nuth and Kääb (2011).

6.2.4 Terrestrial camera and satellite images

Two terrestrial cameras (Mobotix M25) have been installed in August 2011. One camera is located next to the AWS, and the other at approximately 500 m distance at an elevation of 4200 m a.s.l. (Fig. 6.3b). The digital cameras allow monitoring the transient snowline on the glacier and take eight oblique photographs per day. Pictures with fresh snowfall are discarded. Due to multiple camera failures and power supply problems, pictures are lacking from the end of the ablation season in 2012 to the end of the ablation season in 2013, and again partly for the summer months in 2014. Six camera images from late August to late September in 2011, and 34 images from June to mid-August in 2012 were used for snowline mapping (Tab. 6.1). In addition to the terrestrial photographs, we use orthorectified and georeferenced Landsat TM/ETM+ and OLIs scenes to repeatedly observe the snowline throughout the melting season (e.g. Fig. 6.4). A total of 71 satellite images with satisfying conditions are available for 1972–2014 (Tab. 6.1). Additional information on historical transient snowline position is given in earlier publications (Suslov et al, 1980; Glazirin et al, 1993). The snowline on 22/23 August 2012 was mapped in the field with handheld GPS.

6.2.5 Ground penetrating radar

In summer 2013, an 800 MHz ground penetrating radar survey (MALÅ Geoscience ProEx System) has been conducted on the eastern tributary to investigate the firn stratigraphy (Fig. 6.3b). The antenna was mounted on a sledge that was pulled at a walking speed of

Table 6.1: Summary of the different measurements available for this study. The number of annual (n_a), summer (n_s) and winter point mass balance measurements (n_w), the snow density observations (ρ) and their date are given (mth indicates monthly frequency). The availability of locally measured air temperature T_{air} and precipitation (P) (y: available) and the number of Landsat (LS) and terrestrial camera (TC) scenes used for snowline observations is stated.

year	n_a	n_s	n_w	ρ	date	T_{air}	P	LS	TC
1968	-	25	59	2	Apr	y	y	-	-
1969	-	-	-	-	-	y	y	-	-
1970	-	-	-	-	-	y	y	-	-
1971	-	119	132	8	mth	y	y	-	-
1972	-	94	133	8	mth	y	y	1	-
1973	-	131	148	8	mth	y	y	-	-
1974	-	88	153	8	mth	y	y	-	-
1975	-	59	114	5	mth	y	y	1	-
1976	-	135	124	8	mth	y	y	1	-
1977	-	153	135	8	mth	y	y	3	-
1978	-	163	161	5	mth	y	y	1	-
1979	-	156	105	8	mth	y	y	-	-
1980	-	156	104	8	mth	y	y	-	-
1981	-	148	78	8	mth	y	y	-	-
1982	-	155	129	8	mth	y	y	-	-
1983	-	132	160	8	mth	y	y	-	-
1984	-	-	99	7	mth	y	y	-	-
1985	-	152	147	8	mth	y	y	-	-
1986	-	154	157	8	mth	y	y	-	-
1987	-	163	156	8	mth	y	y	-	-
1988	-	147	125	8	mth	y	y	1	-
1989	-	149	150	8	mth	y	y	-	-
1990	-	147	142	8	mth	y	y	-	-
1991	-	147	141	8	mth	y	y	-	-
1992	-	148	151	8	mth	y	y	-	-
1993	-	149	151	8	mth	y	y	-	-
1994	-	150	152	8	mth	y	y	-	-
1995	-	-	-	-	-	n	n	-	-
1996	-	-	-	-	-	n	n	-	-
1997	-	-	-	-	-	n	n	-	-
1998	-	-	-	-	-	n	n	3	-
1999	-	-	-	-	-	n	n	4	-
2000	-	-	-	-	-	n	n	2	-
2001	-	-	-	-	-	n	n	1	-
2002	-	-	-	-	-	n	n	3	-
2003	-	-	-	-	-	n	n	1	-
2004	-	-	-	-	-	n	n	3	-
2005	-	-	-	-	-	n	n	3	-
2006	-	-	-	-	-	n	n	5	-
2007	-	-	-	-	-	n	n	4	-
2008	-	-	-	-	-	n	n	3	-
2009	-	-	-	-	-	n	n	4	-
2010	-	-	-	-	-	n	n	3	-
2011	-	-	-	-	-	n	n	5	6
2012	27	-	-	4	Aug	y	n	5	34
2013	24	-	-	3	Aug	y	n	7	-
2014	35	-	-	4	Aug	y	n	8	-

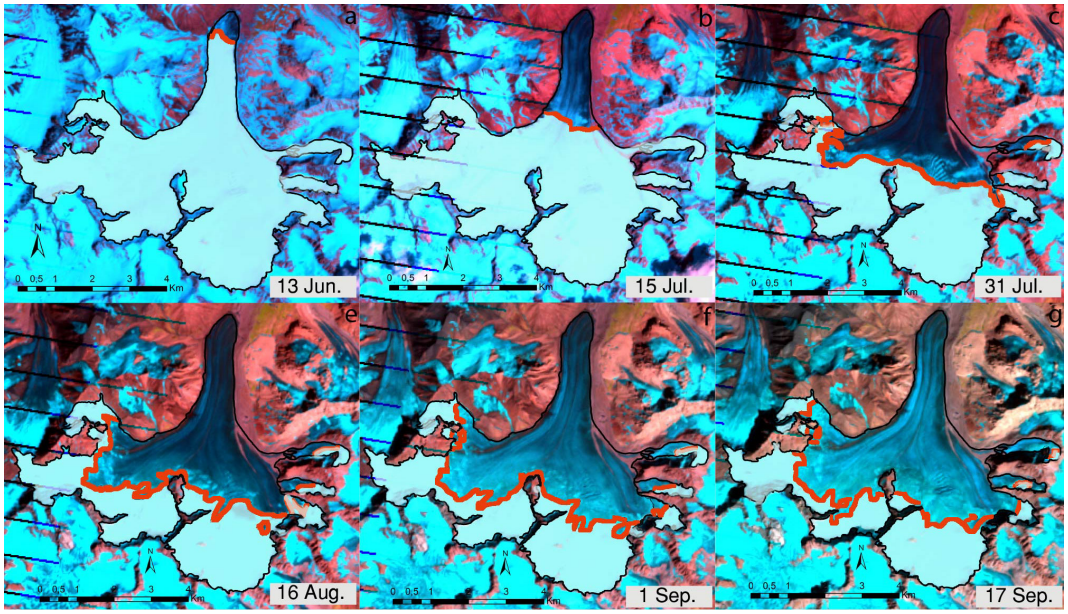

Figure 6.4: False-colour Landsat images for the 2006 ablation season. The snow depletion pattern is well visible. Dark blue areas indicate bare-ice surfaces, white areas are snow-covered. The manually delineated snowline is shown in red.

about $1\,\mathrm{m\,s^{-1}}$ taking two measurements per second. For each measurement, 2048 samples were recorded for a time window of 250 ns. Measurement positions are available from a single frequency GPS receiver. The GPR profile stretched from the top of the eastern tributary across its accumulation area down to an elevation of 4100 m. a.s.l. The entire profile has a length of 2.94 km of which a section of about 1 km was used for the analysis of the firn layers (red line in Fig. 3b). This section was chosen according to the proximity to former glaciological measurements, spatial continuity, good visibility and the regularity of the detected reflectors.

6.3 Methods

This study is structured into three working steps focusing on (1) the period from 1971 to 1994, sustained by detailed seasonal in-situ data for annual optimization and calibration of a mass balance model, (2) the reconstruction of the mass balance for the years 1968 to 1970 and 1995 to 2011, where only limited direct measurements exist, and (3) the analysis of the data collected in 2012 to 2014 from the newly installed monitoring network. All three steps rely on the application of a further developed version of the distributed mass balance model by Huss et al (2009) in combination with a simplified energy-balance approach to calculate melt as proposed by Oerlemans (2001). This model is used for steps (1) and (3) as an interpolation tool to obtain mass balance values for each grid cell at daily temporal resolution based on in-situ field data extrapolating them using physical relations. We aim at the best possible representation of glacier-wide mass balance as documented by the direct point measurements and do not focus on detailed physical process understanding. For (1) and (3) the model is calibrated for each year individually with the field measurements. The spatial mass balance distribution is directly deduced from the in-situ measurements and observed melt and accumulation are related to meteorological input data via tuned parameters. For step (2) the model is driven using the summarized

parameters found for the years with measurements. An additional model optimization strategy is adopted using snowline observation on remote sensing imagery to estimate mass balance in the best possible way. This re-calibration approach is described in more detail in Section Second-order model parameter adjustment.

6.3.1 Surface mass balance model

Snow and ice melt is calculated based on a simplified energy balance approach after Oerlemans (2001). The cumulative melt M_{cum} for each grid cell (x, y) of the glacier and each time step (Δt=1 day) is obtained with

$$M_{\mathrm{cum}}(x, y, t+1) = M_{\mathrm{cum}}(x, y, t) + \Delta t\big(min\big(0; \frac{\Psi_{\mathrm{d}}}{L_{\mathrm{m}}}\big)\big), \tag{6.1}$$

where L_{m} is the latent heat of fusion of ice ($334\,\mathrm{kJ\,kg^{-1}}$). The daily mean surface energy flux Ψ_{d} is parameterized as

$$\Psi_{\mathrm{d}}(x, y, t) = \tau(1-\alpha)Q_{\mathrm{E}} + (C_0 + C_1 \cdot T_{\mathrm{air}}), \tag{6.2}$$

where Q_{E} is the mean daily potential clear-sky solar radiation and α is the albedo of the snow/ice surface. τ is the total transmissivity of the atmosphere including cloud cover. Following Oerlemans (2001) τ is held constant at a value of 0.65 due to a lack of data on cloudiness to constrain this parameter. Furthermore, Machguth et al (2008) showed that, compared to other parameters, mass balance is not highly sensitive to τ. T_{air} is the 2 m air temperature outside the glacier boundary layer. The term $(C_0 + C_1 \cdot T_{\mathrm{air}})$ describes the sum of the long-wave radiation balance and the turbulent sensible heat exchange linearized around the melting point (Oerlemans, 2001). For simplification, we used a constant value of $-50\,\mathrm{W\,m^{-2}}$ for C_0 and only calibrated C_1. We use different values for the albedo of snow, ice, and firn but assume them to be constant over time. The spatial resolution of the model is 20 m. Air temperature is calculated for each grid cell with a constant lapse rate of $-4.8\,^{\circ}\mathrm{C\,km^{-1}}$ (determined from direct measurements after Glazirin et al (1993)). A melt reduction of 45% over debris-covered ice (Fig. 6.3b) is applied after the depletion of the winter snow. This reduction factor has been derived from comparison of observed melt rates over debris and bare-ice surfaces. Q_{E} is calculated for each grid cell and each day of the year, taking into account slope, aspect, topographic shading and a standard atmosphere depending on elevation according to Hock (1999).
Snow accumulation C at any location (x, y) and time t is calculated based on the sum of solid precipitation:

$$C(x, y, t) = P_{\mathrm{ws}}(x, y, t) \cdot C_{\mathrm{prec}} \cdot D_{\mathrm{S}}(x, y). \tag{6.3}$$

Solid precipitation is defined as all precipitation that falls below a threshold temperature set to 1.5 °C, with a linear transition range of ±1°C (e.g. Hock, 1999). The amount of solid precipitation at the weather station P_{ws} is corrected with the parameter C_{prec} in order to account for gauge under-catch, a shift of the measurement location and other systematic differences. C_{prec} is calibrated in order to match direct winter point mass balance measurements as closely as possible. Multiplication with a spatial snow distribution factor $D_{\mathrm{S}}(x, y)$ (Tarboton et al, 1995; Farinotti et al, 2010) allows the approximation of a plausible distribution of winter accumulation, including topographic effects, wind redistribution, and non-altitude dependent small-scale effects. This dimensionless, spatial accumulation map is derived from inverse-distance interpolation of the point winter balance measurements, normalized over the entire glacier area. $D_{\mathrm{S}}(x, y)$ is computed for all years with

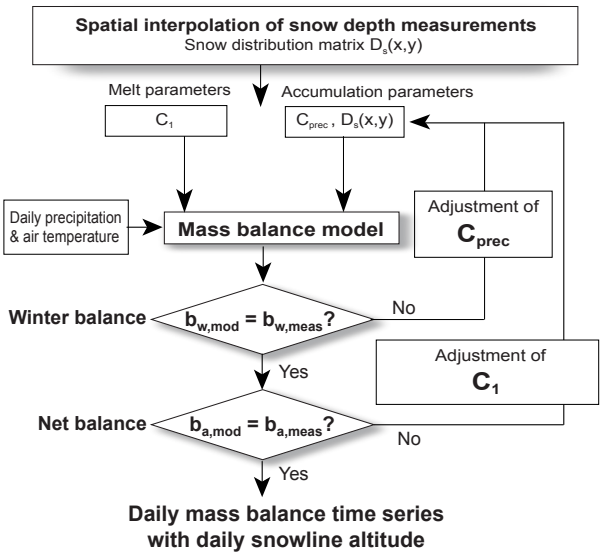

Figure 6.5: Model procedure including the automated optimization of the parameters of the distributed mass balance model (modified after Huss (2010)).

abundant measurements (i.e. 1971-1994). $D_{\mathrm{S}}(x, y)$ for years with no such measurements it is taken from year with rich data, assuming similar spatial accumulation variability from year to year (e.g. Helfricht et al, 2014b).

The combined model for accumulation and melt is calibrated to the point measurements for each year individually in a three-step procedure (Fig. 6.5):

1. The dimensionless accumulation pattern $D_{\mathrm{S}}(x, y)$ is computed from the winter point balance measurements.

2. The winter mass balance is modelled with an initial parameter set. C_{prec} is then adjusted iteratively in order to optimally match the winter snow depth measurements.

3. The model is run over the entire balance year using C_{prec} from step 2 and the melt parameter C_1 is iteratively adjusted to match the annual point measurements.

The final result is a daily mass balance series for every glacierized grid cell, which agrees with all available point measurements. For 1968–1994 a RMSE of 0.152 m w.e. for the winter point balance and 0.484 m w.e for the annual point balance is found. The annually optimized parameters from 1971 to 1994 were averaged (Fig. 6.6). We use this set of summarized parameters to compute the mass balance for the years 1969–1970 and 1995–2011 for which no in-situ point mass balance measurements are available.

Annual glacier-wide mass balances are given in a fixed-date system (Cogley et al, 2011) and correspond to the hydrological year (1 October–30 September). However, field surveys follow a floating-date system, and do not perfectly match the hydrological calendar dates. We use the mass balance model as a tool to correct the measurement period to the hydrological year. A conventional mass balance (Elsberg et al, 2001), i.e. balances are calculated over a changing glacier surface is presented. This allows direct comparison between glaciological and geodetic methods. Here, only the area is adjusted and surface

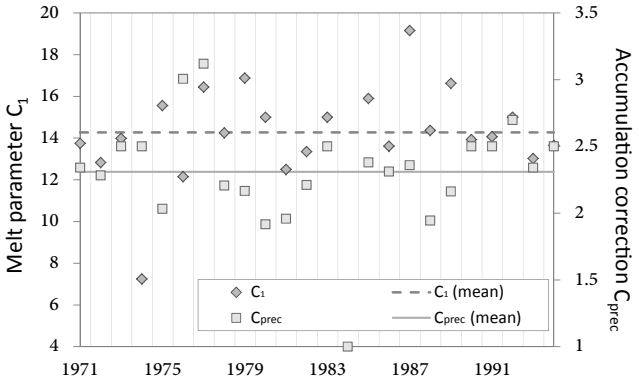

Figure 6.6: Annually calibrated melt and accumulation parameters. Solid lines indicate the average of the annually optimized model parameters.

elevation is updated on an irregular basis. The impact of using the DEM from 1986 instead of that from 2000 on calculated annual mass balances is $+0.02\,\mathrm{m\,w.e.\,yr^{-1}}$ which is not significant at the 5% level. We use the DEM from 1986 for the period 1968 to 1994 and the DEM from 2000 for 1995 to 2014.

6.3.2 Internal accumulation and basal ablation

Whereas on temperate glaciers the mass change is dominated by the surface components, contributions from the internal and basal mass balance might not be negligible on cold and polythermal high-latitude and high-altitude glaciers (Shumskiy, 1964). In order to estimate the internal-basal mass balance of Abramov Glacier, a set of simple models has been developed to quantify the importance of (1) refreezing melt water in firn layers, and (2) basal melting due to geothermal heat flux and friction.

Our estimate of refreezing is based on calculating a temperature profile in firn and ice using the heat conduction equation (see e.g. Pfeffer et al, 1991). The temperature profile is updated in daily time steps driven by surface temperature which, for simplicity, is assumed to equal the air temperature. The one-dimensional model runs separately for each grid cell and is discretized in 0.1 m depth layers. The depth-dependent thermal conductivity is estimated from firn densities as inferred from a simple densification model (Herron and Langway, 1980). The model is coupled with the surface mass balance model that provides the quantity of melt water for every grid cell and day. The latent heat exchange due to the penetration of the surface melt water is then calculated and allows determining the quantity of refrozen water in every layer. To evaluate internal accumulation we are only interested in the refreezing taking place in layers older than one year. We assume the bare ice surface to be impermeable. Internal accumulation is thus restricted to the firn zone (Pelto and Miller, 1990).

The refreezing model is calibrated by adjusting firn temperature at the bottom of the profile at model initialisation to match repeated firn temperature measurements made in three firn cores (Fig. 6.3b) (Glazirin et al, 1993). Finally, we compared our results to direct estimates of internal accumulation based on a method described by Bazhev (1973). These measurements on Abramov Glacier were acquired in two 12–17 m deep firn pits (Suslov et al, 1980). Measurements on Abramov Glacier in the early 1970s showed that 90 to 93% of the infiltrated melt water refreezes typically in the first four annual layers (Suslov et al, 1980). Overall refreezing for the three years ranges between $0.16\,\mathrm{m\,w.e.\,yr^{-1}}$

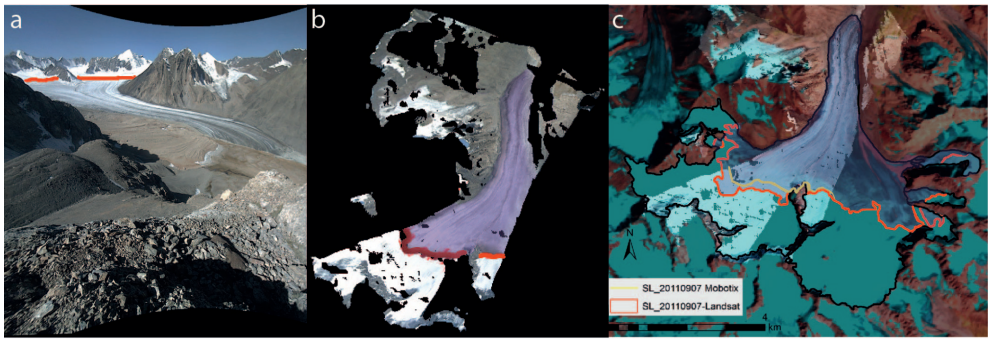

Figure 6.7: (a) Oblique terrestrial image, (b) georeferenced terrestrial camera image and (c) a Landsat image of Abramov Glacier. In (a) and (b) the observed snowline is indicated in red, and the snow-free area is shown in purple. The image refers to the 7 September 2011. In (c) the snowlines detected on a satellite image (red) and on a georeferenced photograph (yellow) for the 7 September 2011 are depicted.

to $0.27\,\mathrm{m\,w.e.\,yr^{-1}}$ at the upper firn pit. The comparison reveals that we overestimate internal accumulation by about $0.03\,\mathrm{m\,w.e.\,yr^{-1}}$ at these locations. We estimate the total contribution of the annual internal accumulation to be about 20% of the total mass balance in the accumulation area, which is in line with findings at Sary-Tor Glacier located in the Central Tien Shan by Dyurgerov et al (1995).

Our quantification of basal melting is based on simple considerations of the heat balance and the assumption of a temperate glacier bed. We adopt a literature value for the geothermal heat flux ($0.05\,\mathrm{W\,m^{-2}}$, Bagdassarov et al, 2011) for the Kyrgyz Tien Shan, and convert it to melt using the latent heat of fusion. Basal friction and strain heating, as two other components of basal-internal mass loss, are approximated by complete dissipation of the potential energy released through gravitational glacier flow. Based on typical values of ice thickness, the bedrock slope and flow velocities of Abramov Glacier (Glazirin et al, 1993), the released energy is estimated and converted to an equivalent melt. The total quantity of basal ablation is estimated as $-0.02\,\mathrm{m\,w.e.\,yr^{-1}}$.

6.3.3 Adjustment of Reanalysis data

For the missing years of the climate record, we use three different climate Reanalyses (NCEP/NCAR, ERA-Interim, MERRA). For each Reanalysis, the four nearest grid points to Abramov Glacier are compared to the in-situ meteorological data during the period covered by both series. In order to enforce consistency between local station data and Reanalysis products for the periods in which both data are available, we adjusted the Reanalysis data by applying mean monthly additive (multiplicative) biases for air temperature (precipitation). From the so-corrected monthly means we generate daily series by superimposing day-to-day variability observed at the meteorological station from 1968 to 1994. Thereby we chose the variability of a corresponding month randomly from a year between 1968 and 1994. We generate air temperature series for 1995 to 2011 and precipitation series for 1995 to 2014.

6.3.4 Model validation

Model validation is performed by using observations of the snow cover depletion pattern on remote imagery. Oblique ground-based photographs are first corrected automatically

for lens distortion with the software PTLens (http://epaperpress.com/ptlens/), then georeferenced and orthorectified after Corripio (2004) in order to associate every pixel of the photograph to the elevation of the DEM (Fig. 6.7a & b). Georeferenced Landsat TM/ETM+/OLI satellite (false-colour composites) and terrestrial camera images provide binary information regarding the surface type (snow/ice) of a pixel located on the glacier. The snow-covered area is manually digitized by visual separation of bare ice and snow (Huss et al, 2013; Hulth et al, 2013). Manual detection allows integrating the knowledge of the observer on snow-cover depletion patterns and is assumed to be less error-prone than an automatic classification (Huss et al, 2013).

The transient snowline separates bare-ice from snow-covered areas during the ablation season (Pelto, 2011). At the end of the balance year and under the precondition that no superimposed ice is present, the mean Snow Line Altitude (SLA) approximately corresponds to the ELA (LaChapelle, 1962; Lliboutry, 1965). The Snow-Covered Area Fraction (SCAF) at a given point in time is the fraction of the total glacier surface which is covered by seasonal snow at that time. This measure is similar to the accumulation area ratio, describing the same quantity at the end of the balance year in a stratigraphic system (Mernild et al, 2013a). We detect the SLA and SCAF on remote-sensed imagery (Landsat, terrestrial camera) and use them as a proxy for sub-seasonal mass balance by comparing them to the corresponding modelled quantities (Pelto, 2011; Huss et al, 2013). The acquisition date on a few satellite images agrees with the terrestrial photographs. This allows comparing the snowline delineation using two different image sources (Fig. 6.7c). The match is satisfying with a slight tendency to a higher mean SLA detected on Landsat images (vertical offset <10 m). The accuracy of the observed SLA and SCAF depends on the uncertainties in (1) the snowline delineation, (2) the DEM, and (3) the georeferencing of the images (Huss et al, 2013). We estimate the uncertainties of the snowline as <100 m (5 pixels) in a horizontal plane on the remote sensing images. From this, a maximal vertical error of 30 m results when using the mean slope of the glacier. This estimate agrees with Wu et al (2014). For the SCAF we assume an uncertainty of ±3% based on the same analysis.

6.3.5 Second-order model parameter adjustment

For the period from 1995 to 2011 for which neither direct meteorological data nor glaciological measurements are available (Tab. 6.1), the calibrated mass balance model is driven with the three different climate Reanalysis data series and is validated with SLA and SCAF observations as described in Section Model validation.

The information provided by snowline observations based on the multiple Landsat scenes (Tab. 6.1) is used to re-calibrate the model parameters for each year from 1998 to 2011. With this second-order adjustment we aim at a better match between modelled and observed SLA and SCAF and thus a better representation of that year's mass balance.

6.3.6 Extracting firn layer water equivalents

A series of processing steps was applied to the GPR data as described in Sold et al (2013) and Sold et al (2015), involving frequency bandpass filtering to reduce noise, background removal, the application of a gain function to compensate for signal attenuation with depth, and spatial interpolation to a 0.5 m equidistant spacing of traces to account for variations in the walking speed. Migration was found not to improve the data quality and was not applied. The vertical resolution of the GPR signal depends on the signal

bandwidth. It is typically estimated as half of the wavelength (Jol, 2009), corresponding to less than 0.13 m for firn densities greater 530 kg m^{-3}.

The processed GPR data revealed a maximum of 13 pronounced Internal Reflection Horizons (IRHs) reaching up to approximately 18 m depth (Fig. 8). For the analyses of the firn layers we only used the sections of the profile with a minimum of seven continuous layers and homogeneous IRHs, which are located in the vicinity of long-term glaciological measurements. A total length of approximately 1 km satisfies these criteria (red line in Fig. 3b). The IRHs were interpreted as high-density or ice layers that formed at previous summer surfaces. The correspondence of density peaks to summer surfaces is supported by the core-based firn stratigraphy published by Glazirin et al (1993) which covers the period 1935–1974. As discussed below, we assumed that all detected layers are of annual origin and that their chronology is given by counting from top to bottom.

In order to extract accumulation rates from IRHs in the GPR profile acquired in summer 2013, an estimate of the firn density is required to obtain the radio-wave velocity and layer water equivalents. We apply a simple transient model for firn compaction (Herron and Langway, 1980; Reeh, 2008) where the change in density is linearly related to the pressure from overlying firn layers. The model is applied in a step-by-step procedure (Sold et al, 2015): For the uppermost layer, representing the accumulation of 2013, density is set to 530 kg m^{-3}, based on the two density field measurements taken on the eastern tributary next to the GPR profile (Fig. 6.8). Using an empirical relation of the dielectric permittivity with snow density (Frolov and Macheret, 1999) we obtain the signal velocity in the snow. Thereby, we assume that the effect of liquid water in the snow pack on the signal velocity is negligible. This is supported by the good agreement found between the depth of the snow density pit (2.40 m) and the GPR-derived snow depth (2.44 m) at the same location. The signal velocity and the snow density is then provided for every GPR measurement location leading to an estimate for the thickness and water equivalent of this layer and, thus, for its weight on the underlying layers at each GPR measurement location. Then, the firn compaction model can be used to obtain the density of the second firn layer. By stepping through the firn layers from top to bottom an estimate for the water equivalent of each layer is derived.

The model is calibrated with repeated density observations in two firn pits in the early 1970s published by Suslov et al (1980) corresponding to the location of melt water infiltration measurements (see Section Internal accumulation and basal ablation). Calibrated parameters are in line with Huss (2013) who found a 6% higher densification rate when fitting the model to a set of density profiles from 19 firn cores for temperate and polythermal mountain glaciers and ice caps around the globe.

The accumulation rates derived from GPR are sensitive to potential perturbations in the chronology of IRHs in the radar profiles. As no reference data such as from firn cores is available to corroborate the dating of IRHs, this is a major drawback to the approach presented here. As stated above, however, the firn stratigraphy record by Glazirin et al (1993) for the period 1935–1974 supports the correspondence of high-density layers to summer surfaces. On the other hand, some annual layers where not present in this record. This is supported by past in-situ measurements which indicate that the ELA sporadically rose over the elevation of the radar profile. As a consequence, we assume that we potentially missed individual accumulation layers but that we did not detect reflectors other than from summer surfaces. Hence, the presented accumulation rates obtained from IRH traveltimes provide an upper limit estimate for the local accumulation rates and the results are interpreted accordingly.

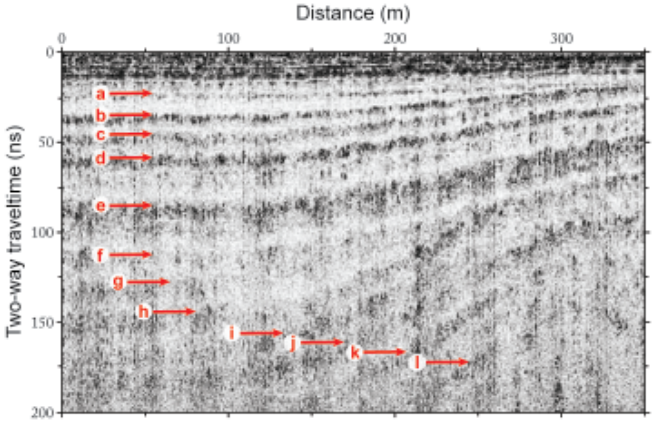

Figure 6.8: A selected section of the processed GPR profile (Figure 3b) acquired in the accumulation area of Abramov Glacier on 17 August 2013. IRHs used to extract accumulation rates are indicated. IRHs were detected to a maximum depth of approximately 18 m. Not all layers are continuous over the entire profile, in particular layers at greater depth.

6.3.7 Uncertainty analysis

The overall uncertainty in the calculated glacier-wide mass balance was assessed through a cross-validation experiment for the periods with available point data (periods 1971–1994, and 2012–2014). We randomly selected 75% of the point measurements for each seasonal survey and re-calibrated our model to these data. The remaining 25% of the measurements were used as a validation subset. This procedure was repeated ten times with different random subsets. Model uncertainty was estimated by computing the RMSE of the difference between modelled and measured mass balance for the points in the validation subset. Under the assumption that (a) the model performance is identical for every point location on the glacier and (b) that the uncertainties of individual years are independent from each other, the calculated mean RMSE for both the winter and annual mass balance is interpreted as the uncertainty in the corresponding glacier-wide mass balance. We found mean uncertainties in winter and annual balance for the above mentioned periods of $\pm 0.21\,\mathrm{m\,w.e.\,yr^{-1}}$ and $\pm 0.47\,\mathrm{m\,w.e.\,yr^{-1}}$, respectively.

The uncertainties for the period from 1969 to 1970 and from 1995 to 2011, i.e. the years for which no direct field measurements are available, primarily depend on (1) the chosen model parameters and (2) the quality of the meteorological input data. In order to quantify the uncertainties for these periods, we run the mass balance model for 1971-1994 (the period with direct glaciological measurements) with average parameters, i.e. those used for 1995–2011. Based on comparison with the annually optimised glacier-wide mass balance we derive a mean RMSE of $0.30\,\mathrm{m\,w.e.\,yr^{-1}}$.

To estimate the uncertainty related to the meteorological input data, we drove the mass balance model with the three different climate Reanalysis products. The differences between the modelled balances and the final glacier-wide balance obtained after the second-order parameter adjustment (i.e. our best estimate) are calculated for each year individually. The RMSE of the differences was $0.43\,\mathrm{m\,w.e.\,yr^{-1}}$, which was interpreted as the error introduced by the uncertainty of meteorological data for the period with no direct measurements. Combining the above uncertainties on quadrature, i.e. assuming independence between individual error sources, the total uncertainty for yearly values during the period with no glaciological data available is $\pm 0.54\,\mathrm{m\,w.e.\,yr^{-1}}$. Note that when calculating the average over a period of n years (e.g. Table 6.4), this value is reduced by a factor

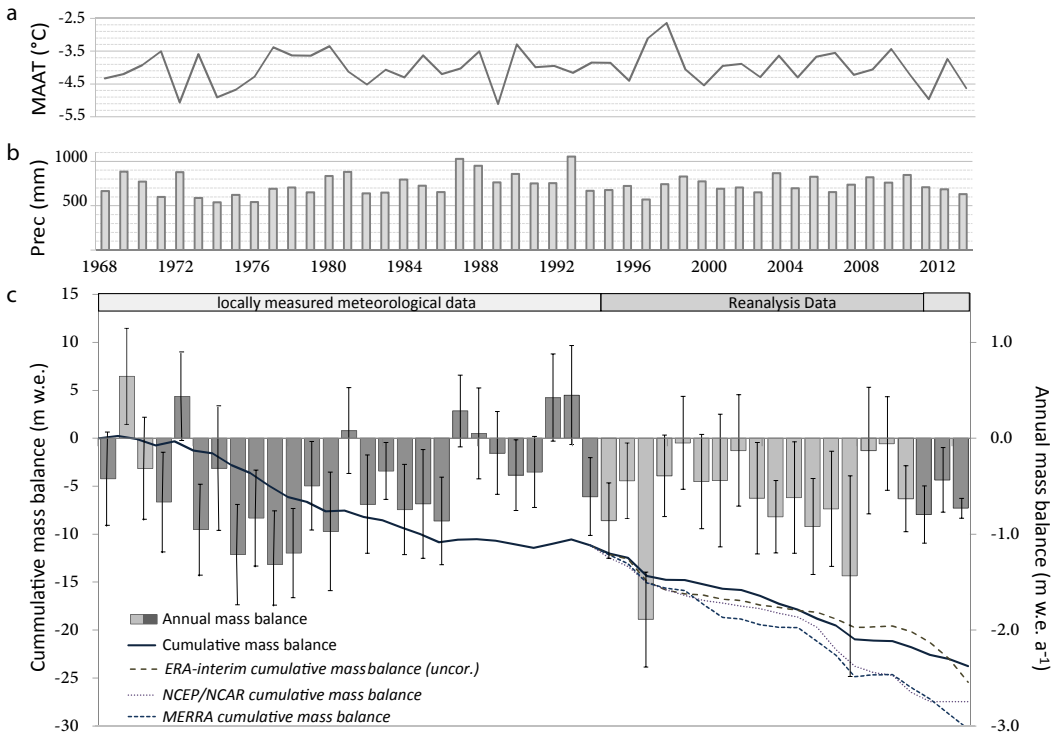

Figure 6.9: (a) Mean Annual Air Temperature (MAAT) and (b) annual precipitation from direct observations and Reanalysis data. (c) Re-analysed annual mass balance (bars) and cumulative balance (lines) for Abramov Glacier from 1968 to 2014. Dark grey bars indicate the years sustained by glaciological measurements and light show are years with no point measurements. After 1995, cumulative mass balances generated from different climate Reanalyses are shown (dashed lines). The thick black line indicates the optimal series found by comparison to SLA and SCAF observations by remote imagery.

$\sqrt{(n)}$, as given by the rule of Gaussian error propagation (Thibert et al, 2008a).

6.4 Results

Availability of in-situ mass balance data between 1971 and 1994 is optimal (Tab. 6.1). Our re-analysed surface mass balances are compared to published series that are based on traditional evaluation techniques such as the profile- and contour-line method (Kaser et al, 2003).

We found an average annual surface mass balance of $-0.46\pm0.06\,\mathrm{m\,w.e.\,yr^{-1}}$ (1971–1994) which is less negative than stated in most of the earlier literature but corresponds to the recalculated series by Dyurgerov et al (2002). The major discrepancies with Pertziger (1996), Kamnyansky (2001) and WGMS (2005) are explained by data gaps (1984) and years with poor data coverage (1974–1976). By using the profile- or contour-line method, large errors in the calculated mass balance propagate with increasing elevation, leading to considerably too negative mass balance. A different glacier surface hypsometry, mainly around the elevation of the ELA, also explains some of the disagreement between the studies. Furthermore, a misinterpretation of the area-altitude distribution causing a shift in the elevation bins has been discovered in some publications. In the past, ablation stakes were grouped together and a mean elevation was attributed for mass balance calculation.

Table 6.2: Summary of re-analysed mean annual surface mass balance from 1971–1994 in comparison with literature-based values.

	period	$\overline{B_{\mathrm{a,\ sfc}}}$ in $\mathrm{m\,w.e.\,yr^{-1}}$
Dyurgerov (2002)	1971–1994	−0.49
Pertziger (1996)	1971–1994	−0.61
WGMS (2000)	1971–1994	−0.64
Glazyrin and others (1993)	1971–1990	−0.82
Kamnyansky (2001)	1971–1994	−0.67
This study	1971–1994	−0.46

Table 6.3: Comparison of mean annual balance ($\overline{B_{\mathrm{a,\ sfc}}}$) and the RMSE for SLA and SCAF when using different Reanalysis products. $\mathrm{ERA_{cor}}$ indicates the result obtained for ERA-interim data and re-adjusted model parameters to match annually the SLA and SCAF.

1995–2011	$\mathrm{RMSE_{SLA}}$ (m)	$\mathrm{RMSE_{SCAF}}$ (%)	$\overline{B_{\mathrm{a,\ sfc}}}$ ($\mathrm{m\,w.e.\,yr^{-1}}$)
ERA	117	13	−0.53
NCEP	172	27	−0.90
MERRA	132	24	−0.87
$\mathrm{ERA_{cor}}$	89	10	−0.63

More recent publications use regular 100 m elevation bins for the same data, which leads to a vertical shift of the hypsometry of up to 100 m.

From 1971 to 1994, the observed transient snowlines on Landsat images are well approximated by the model ($\mathrm{RMSE_{SLA}} = 45\,\mathrm{m}$; $\mathrm{RMSE_{SCAF}} = 6\%$) and the results qualitatively match snowline observations from literature (Suslov et al, 1980; Glazirin et al, 1993). The amount of available remote sensing images with good quality is unfortunately limited for this period, hampering a sound validation.

The three Reanalysis data sets used result in a range of mass balance for 1995-2011. From our validation using SLA and SCAF observed on Landsat scenes and comparison of overlapping periods with both in-situ meteorological and Reanalysis data, we conclude that ERA-interim yields the most plausible results (Tab. 6.3). The applied second-order adjustment on the mass balance model driven with ERA-interim data from 1995 to 2011 noticeably reduces the RMSE of SLA (90 m) and SCAF (10%) (Tab. 6.3). However, years with only a small number of remote sensing images during the ablation season such as in 2001 and 2003 (Tab. 6.1) are problematic for the annual adjustment. For the period 1995–2011, the glacier-wide average surface mass balance for the annually corrected series decreases from −0.53 to $-0.63\,\mathrm{m\,w.e.\,yr^{-1}}$ (Table 6.3) and becomes less negative than the uncorrected values for the years from 1995 to 2000 and vice versa for 2000 to 2011 (Fig. 6.10).

The balance years 2011/12 to 2013/14 show considerable mass loss. Observed SLAs and SCAFs in 2012 to 2014 are reproduced by the model within a range of ±41 m and ±3.4%. With the higher frequency of high-quality images the confidence of the validation increases (Fig. 6.11).

From 1968 to 2014, the glacier-wide mass balance is predominantly negative. We found a mean annual surface mass balance of $-0.51\pm0.10\,\mathrm{m\,w.e.\,yr^{-1}}$ (Fig. 6.9 and Tab. 6.4) and a basal-internal balance of $+0.07\,\mathrm{m\,w.e.\,yr^{-1}}$. Both the components of internal and basal balance are one to two orders of magnitude smaller than the surface mass balance

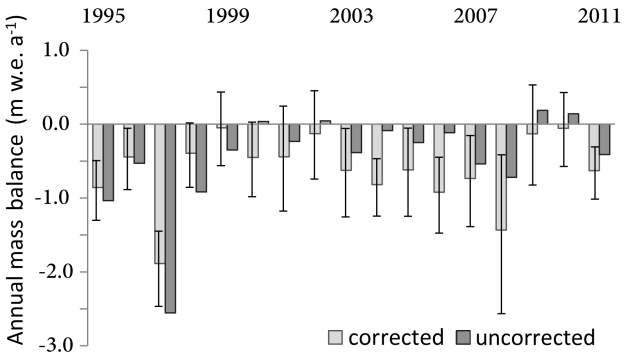

Figure 6.10: Comparison of the calculated annual mass balance 1995–2011 before (uncorrected) and after (corrected) the second-order adjustment of the model parameters to match annual SLA and SCAF observations. The error bars indicate uncertainties calculated as described in Section Uncertainty analysis.

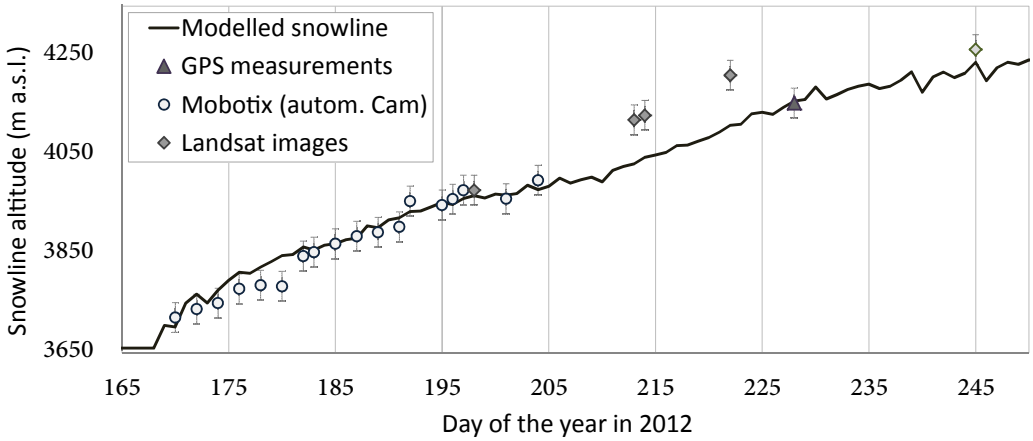

Figure 6.11: Modelled transient snowline altitude during the ablation season of 2012 (from June to the beginning of September) and observations on terrestrial photographs (circles), Landsat images (diamonds) and in-situ GPS measurements (triangle).

but still need to be taken into account for long-term studies of glacier mass change and the comparison to geodetic mass balance.

6.5 Discussion

6.5.1 Climate sensitivity

A prerequisite for the application of empirical positive degree day models for the calculation of snow and ice melt is the correlation between air temperature and the melt rate (see Ohmura, 2001, for the physical background). For Abramov Glacier, we tested the relation between air temperature and melt by comparing the sum of positive degree days (CPDDs) over the summer season to the observed average summer balance at all ablation stakes from 1968 to 1994. For this year to year comparison, we found the squared correlation coefficient of r^2=0.67. The correlation is similar as for glaciers in the European Alps and Scandinavia (Ohmura et al, 2007; Sicart et al, 2008). Additionally, we compared the summer balance of each ablation stake individually to the annual CPDDs calculated for

Table 6.4: Seasonal mass balance of Abramov Glacier from 1968 to 2014 with $B_{\mathrm{w,\ sfc}}$ the winter mass balance (1 Oct–31 May), $B_{\mathrm{a,\ sfc}}$ the annual surface balance over the hydrological year, $B_{\mathrm{i\text{-}b}}$ the internal-basal mass balance and ΔM the total annual glacier mass balance.

[year	Area (km^2)	$B_{\mathrm{w,\ sfc}}$ (m w.e.)	$B_{\mathrm{a,\ sfc}}$ (m w.e.)	$B_{\mathrm{i\text{-}b}}$ (m w.e.)	ΔM (m w.e.)
1967/68	24.64	1.79	-0.42	0.07	-0.35 ± 0.48
1968/69	24.64	1.33	0.65	0.07	0.71 ± 0.53
1969/70	24.13	1.29	-0.32	0.07	-0.24 ± 0.53
1970/71	24.64	1.22	-0.67	0.08	-0.59 ± 0.52
1971/72	24.64	1.30	0.44	0.06	0.50 ± 0.46
1972/73	25.32	1.62	-0.95	0.07	-0.89 ± 0.47
1973/74	25.32	0.65	-0.31	0.08	-0.24 ± 0.65
1974/75	25.32	0.88	-1.21	0.07	-1.14 ± 0.52
1975/76	25.26	0.89	-0.83	0.07	-0.76 ± 0.50
1976/77	25.15	1.45	-1.31	0.06	-1.26 ± 0.49
1977/78	25.12	1.43	-1.20	0.06	-1.13 ± 0.46
1978/79	25.12	1.51	-0.50	0.05	-0.44 ± 0.46
1979/80	25.12	1.13	-0.97	0.07	-0.91 ± 0.62
1980/81	25.12	1.00	0.08	0.06	0.14 ± 0.45
1981/82	25.12	0.89	-0.69	0.08	-0.61 ± 0.51
1982/83	24.66	1.25	-0.34	0.06	-0.28 ± 0.30
1983/84	24.66	1.31	-0.74	0.07	-0.67 ± 0.47
1984/85	24.66	1.41	-0.69	0.07	-0.61 ± 0.57
1985/86	24.66	0.99	-0.86	0.07	-0.79 ± 0.46
1986/87	24.66	1.66	0.28	0.06	0.34 ± 0.37
1987/88	24.64	1.62	0.05	0.07	0.12 ± 0.47
1988/89	24.64	1.16	-0.16	0.07	-0.09 ± 0.43
1989/90	24.64	1.63	-0.39	0.07	-0.32 ± 0.37
1990/91	24.64	1.31	-0.35	0.07	-0.28 ± 0.37
1991/92	24.51	1.63	0.42	0.06	0.48 ± 0.45
1992/93	24.51	1.65	0.45	0.07	0.52 ± 0.51
1993/94	24.51	1.56	-0.61	0.06	-0.55 ± 0.40
1994/95	24.13	1.29	-0.86	0.06	-0.80 ± 0.39
1995/96	24.13	1.43	-0.44	0.07	-0.37 ± 0.40
1996/97	24.13	0.78	-1.89	0.08	-1.81 ± 0.49
1997/98	24.13	1.42	-0.39	0.06	-0.34 ± 0.42
1998/99	24.13	1.50	-0.05	0.06	0.01 ± 0.48
1999/2000	24.03	1.22	-0.45	0.08	-0.38 ± 0.49
2000/01	24.01	1.07	-0.44	0.07	-0.37 ± 0.69
2001/02	24.04	1.26	-0.13	0.07	-0.06 ± 0.58
2002/03	24.08	1.19	-0.63	0.05	-0.57 ± 0.58
2003/04	24.13	0.99	-0.82	0.06	-0.76 ± 0.38
2004/05	24.12	1.37	-0.62	0.06	-0.56 ± 0.58
2005/06	24.12	1.06	-0.92	0.08	-0.84 ± 0.50
2006/07	24.10	1.05	-0.74	0.07	-0.66 ± 0.60
2007/08	24.10	1.04	-1.43	0.08	-1.36 ± 1.04
2008/09	24.10	1.19	-0.13	0.06	-0.07 ± 0.66
2009/10	24.08	1.46	-0.06	0.07	0.02 ± 0.49
2010/11	24.06	1.03	-0.63	0.07	-0.56 ± 0.34
2011/12	23.94	1.18	-0.80	0.05	-0.75 ± 0.30
2012/13	23.91	1.23	-0.44	0.07	-0.36 ± 0.34
2013/14	23.91	1.08	-0.73	0.08	-0.65 ± 0.10
1968–2014	24.50	1.26	−0.51	0.07	−0.44±0.10
2000–2011	24.49	1.16	−0.58	0.07	−0.51±0.17
$\mathrm{B_{n,geod(2000–2011)}}$ (Gardelle et al, 2013)					−0.03±0.14

the corresponding location. This comparison, which excludes a certain effect of elevation, indicates also a satisfying correlation, the average correlation coefficient being r^2=0.57, with 80% of the data having an r^2 between 0.35 and 0.78.

Oerlemans (2001) assessed the sensitivity of Abramov Glacier to changes in temperature and precipitation by using a calibrated energy-balance model of intermediate complexity. According to that study, the mass balance of Abramov Glacier is less sensitive to changing climatological conditions in comparison to glaciers located in more maritime climates such as Nigardsbreen (Norway) or Franz Joseph Glacier (New Zealand), and is more sensitive than continental glaciers such as White Glacier (Canadian Arctic). The sensitivity of Abramov Glacier to temperature changes during the summer months is pronounced; sensitivity to precipitation on the other hand is relatively low and constant throughout the year (Oerlemans, 2001). Rasmussen (2013) used Reanalysis data (NCEP / NCAR products) to investigate the glacier's sensitivity to air temperature and precipitation on selected glaciers in High Asia. For Abramov Glacier a relatively high temperature sensitivity of δB=$-0.47\,\mathrm{m\,w.e.\,^{\circ}C^{-1}}$, and a high correlation between the Reanalysis temperature and interannual variations of glacier-wide summer surface mass balance was found.

6.5.2 Mass balance variations

The evolution of the mass balance distribution with elevation and time (Fig. 6.12) reveals a weak tendency towards more accumulation at higher elevation but also more ablation during the last decades. This indicates a shift in the mass turnover of Abramov Glacier. A similar change in the accumulation and ablation pattern is indicated for the entire Pamir region by Glazirin et al (2002), Khromova et al (2006) and Khromova et al (2014). Kure et al (2013) project an increase in monthly mean precipitation from November through April but simultaneously a reduction in snow fall from February through October for the future. The reduced snow fall in spring and autumn can be linked to a rise of air temperature. Lutz et al (2013) and Wang et al (2014b) support this finding with similar results for entire Central Asia. Studies from the nearby Karakoram region show that increased winter snow fall can compensate for increased melt rates in summer (Gardelle et al, 2013; Mandal et al, 2014; Kääb et al, 2015) for high elevation glaciers that consequently exhibit a reduced sensitivity to air temperature changes.

6.5.3 Comparison of modelled point balance and GPR data

From 2001 to 2013 the GPR observations indicate substantially higher accumulation rates than the modelled point balance (mean difference of $0.5\pm0.36\,\mathrm{m\,w.e\,yr^{-1}}$). As stated above, the GPR-derived layer water equivalents were considered as upper limit estimates of the annual mass balance because one or several previous summer surfaces might be absent in the GPR data. A direct comparison with observations is impeded by the lack of glaciological mass balance measurements in that period. To estimate the contribution of the mass balance model to the encountered difference, we compared the modelled point balance based on the averaged parameter set (i.e. parameters used for 1995 to 2011), thus independent from the stake measurements, to the in-situ measurements available for a location on the radar profile (red dot in Fig. 6.3b). A difference of $+0.36\pm0.31\,\mathrm{m\,w.e\,yr^{-1}}$ was found. This explains two thirds of the disagreement between the modelled and the GPR-based point balance. We conclude that the higher accumulation rates derived from GPR do not conflict with the re-analysed mass balance time series, but can be attributed to local effects at the location for which water equivalents were extracted and the uncertainties in the layer chronology. Because the latter poses a substantial drawback to the GPR-based

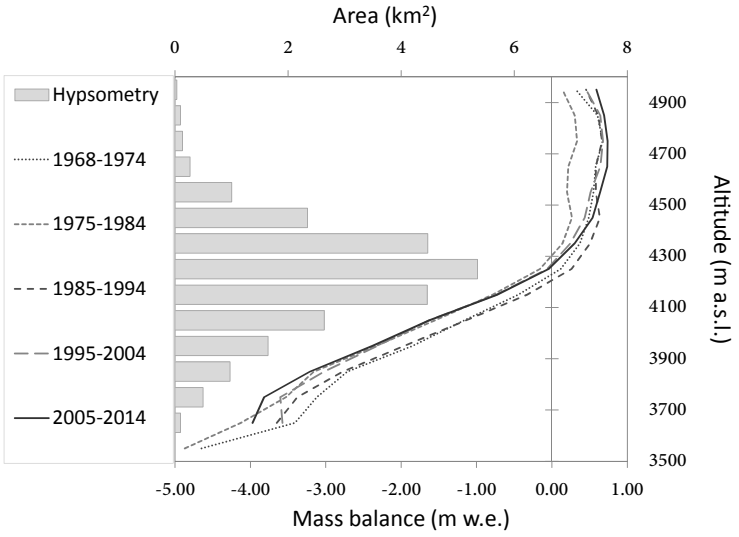

Figure 6.12: Elevation dependence of the mass balance averaged for the indicated periods (lines), and surface hypsometry (as of 2013) of Abramov Glacier (bars).

derivation of annual accumulation, the data was not used to constrain the mass balance model.

6.5.4 Comparison of modelled and geodetic mass balance 2000–2011

Our results on the mass balance evolution between 1971 and 1994 are well constrained by the high number of seasonal in-situ observations. The inferred mass balance between 1995 and 2011 is, however, less certain since it relies on modelling and sparse and temporally inhomogeneous information on snow-covered area. Due to the low quality of the available DEMs, it was not possible to compute a geodetic mass balance from 1986 (topographic map) to 2000 (SRTM DEM). However, Gardelle et al (2013) provide an independent estimate for the mass change of Abramov Glacier. By differencing the SRTM DEM of Feb 2000 and a SPOT5 stereo image from Nov 2011, the authors estimate an average mass balance of $-0.03\pm0.14\,\mathrm{m\,w.e.\,yr^{-1}}$, thus indicating a balanced mass budget. Gardelle et al (2013) report significant positive elevation changes in the accumulation area compensated by surface lowering below the ELA. This is in contrast to our results indicating a total balance of $-0.51\pm0.17\,\mathrm{m\,w.e.\,yr^{-1}}$ from 2000 to 2011.

For verifying the plausibility of surface elevation changes derived by Gardelle et al (2013) we combine the long-term series of accumulation available for several locations in the vicinity of the GPR profile (Fig. 3a and Tab. 1) with the recent accumulation rates inferred from GPR. This is achieved by applying simple considerations of glacier dynamics. The elevation change Δh at a given point in the accumulation area is determined by the local long-term mean of point mass balance b, the change in mass balance Δb relative to a reference period, and the vertical ice flow velocity v_z as

$$\Delta h = \left(\frac{b + \Delta b}{\rho_\mathrm{firn}/\rho_\mathrm{w}} + v_\mathrm{z}\right) \cdot \Delta t, \tag{6.4}$$

where ρ_firn is the firn density and ρ_w the water density. Δt is the time period considered. If we suppose a steady-state over the reference period ($\Delta h = 0$), the local mass change b is balanced by the vertical velocity resulting in an invariant glacier surface (Cuffey and

Paterson, 2010). For any time interval following the reference period we can thus simplify Equation 6.4 into

$$\Delta h = \frac{\Delta b}{\rho_{\text{firn}}/\rho_{\text{w}}} \cdot \Delta t. \tag{6.5}$$

For our case we use $\Delta t = 12\,\text{a}$ (2000–2011) and estimate Δb from the change in local mass balance that has occurred over the last decade (2001–2014) compared to the reference period from 1968 to 1994. ρ_{firn} is inferred from a firn densification model (Herron and Langway, 1980).

For all locations on the GPR profile (Fig. 3b) for which more than seven continuous IRHs have been detected, the data set by Gardelle et al (2013) indicates a mean surface elevation change of $+5.3\pm4.7\,\text{m}$. Such positive elevation change in the accumulation area over only one decade would be likely to result in strong effects on the glacier outlines in the upper reaches of Abramov Glacier. However, no evidences for such behaviour were found in the repeated Landsat images. We calculated the expected elevation change on the profile based on the GPR data and Equation 5. On average we find $\Delta h = +0.6\pm0.7\,\text{m}$ for the period 2000–2011 assuming a steady-state of the glacier prior to 1994. Most probably Abramov Glacier was already out of balance before. Hence, the actual Δh would even be somewhat smaller. Given that a similar difference applies to the entire accumulation area, the geodetic mass balance according to Gardelle et al (2013) would be overestimated substantially. Unfortunately, GPR measurements are limited to a small part of the glacier but comparison at different locations with long-term in-situ measurements in the accumulation area indicates a similar trend.

The geodetic mass balance calculation might be affected by an underestimation of the C-band penetration over snow and firn previously documented for the SRTM DEM (Rignot et al, 2001; Gardelle et al, 2012a; Paul et al, 2015). This would be consistent with an overestimation of positive surface elevation changes in the firn area between 2000 (SRTM DEM) and 2011 (SPOT5). Region-wide mass balance estimates derived from IceSat for 2003 to 2008 were recently published by Kääb et al (2015). They mentioned a highly variable C-band penetration depth in snow and firn, especially for the Pamir Mountains. Kääb et al (2015) estimate the C-band penetration depth of 5–6 m, instead of 1.8 m as used by Gardelle et al (2013). If we adjust the elevation change reported by Gardelle et al (2013) accordingly, their estimate would be reduced to a mean of +1.1 to −2.1 m at the locations described above. This is close to our independent assessment. If we re-calculate the geodetic mass balance Feb 2000 to Nov 2011 for Abramov with a C-band penetration depth of 5–6 m instead of 1.8 m, a glacier-wide mass balance of about $-0.25\,\text{m w.e. yr}^{-1}$ is found. This value lies within the uncertainties of our reconstructed time series. Comparing theodolite measurements from 1986 and the SRTM DEM from 2000, we find an elevation change of +3.7 to +4.7 m. Using the direct measurements and modelling the inferred elevation change is $+4.2\pm1.1\,\text{m}$. Again the good agreement underlines the performance of the mass balance model, also for a period without direct measurements.

A mass balance of $-0.48\pm0.14\,\text{m w.e. yr}^{-1}$ is reported for the Pamir from 2003 to 2008 by Kääb et al (2015). Our model-based reconstruction of mass balance in the first decade of the 21st century allows assessing the temporal dynamics of the mass change of Abramov Glacier indicating $-0.79\pm0.25\,\text{m w.e. yr}^{-1}$ for the same period. According to our assessment, Abramov Glacier thus shows a more negative balance than the mean region-wide mass balance found for the Pamir.

6.6 Conclusions

For the Central Asian countries only little is known regarding seasonal glacier mass balance over the last two decades so far. A re-evaluation of other monitoring programmes on various glaciers during the 1970s and 1980s is urgently needed. Such long-term mass balance data are an important data basis for future evaluations of climate change impacts in a highly vulnerable region, especially in the context of future runoff estimates. With this study we present a first step towards revealing the long-term seasonal mass balance changes for a reference glacier in the Pamir-Alay by combining various sources of historical and modern data.

We aimed at deriving a persistent seasonal mass balance series for Abramov Glacier from 1968 to 2014. Our approach combines seasonal field measurements with distributed modelling at daily temporal resolution. We show that it is possible to validate modelling results with transient snowline observations from satellite images and that these observations provide valuable information on the mass balance of remote glaciers for time periods without direct measurements. The mass balance model is used as a tool to inter- and extrapolate annual or seasonal point data in space and time, allowing the establishment of a continuous mass balance series. Moreover, it allows the interpretation of inter-annual accumulation and ablation characteristics, their typical distribution, and their changes over time.

From our calculations and earlier publications there is no doubt that Abramov Glacier has shown a considerable mass loss from the late 1960s until the end of the 20th century. We found convincing evidence that this trend has been continued in the beginning of the 21st century. We infer a mean annual total mass balance of $-0.44\pm0.1\,\mathrm{m\,w.e.\,yr^{-1}}$ for 1968 to 2014 resulting from a surface mass balance of $-0.51\pm0.1\,\mathrm{m\,w.e.\,yr^{-1}}$ and an internal-basal balance of $+0.07\,\mathrm{m\,w.e.\,yr^{-1}}$.

In our re-evaluation of the mass balance series, we combine direct measurements, remote observations, and modelling following the general monitoring strategy defined by Zemp et al (2014). The importance of long-term point balance measurements and their value for model calibration is highlighted. Snowline observations on remote imagery provided essential information to allow model validation when no other data is available. Mass change calculations based on geodetic methods suggested a balanced mass budget since 2000 (Gardelle et al, 2013) contradicting our results. The disagreement can probably be explained by an underestimation of the C-band penetration depth in the SRTM DEM leading to too positive mass balances. This interpretation is supported by the results of Kääb et al (2015) and our ground-based GPR measurements on Abramov Glacier. Because the latter are prone to uncertainties in the layer chronology, the results are not used to reconstruct mass balances and were interpreted according to its limitations. Altogether, we find a low plausibility for equilibrium conditions over the past 15 years. Instead, we suggest that the glacier's sensitivity to increased summer air temperature is decisive for the strong mass loss assessed for the last decade.

Author contribution

MB, MHo and MHu conceived of the presented idea. MHu provided the mass balance model and instructed and supervised MB in modelling. MB performed the mass balance data analysis, reanalysis and reconstruction, the validation and interpretation with help of MHo, MHu, DF, LS. MB performed the snowline mapping and LS carried out the analysis of the GPR measurements. MB related the mass balance data with the GPR data and NS

provided the meteorological Reanalysis Data sets. MB wrote the manuscript with help from DF, MHu, MHo. AM, RU, EA, DF, MB, MHe, LS organized, helped and performed the field measurements.

Acknowledgments

The project was only possible due to the support of the Federal Office of Meteorology and Climatology MeteoSwiss through the project Capacity Building and Twinning for Climate Observing Systems (CATCOS) Phase 1 & 2, Contract nos. $7F-08114.1$, $7F-08114.02.01$, between the Swiss Agency for Development and Cooperation (SDC) and MeteoSwiss. This study is supported by the Swiss National Science Foundation (SNSF), grant 200021_155903. Additional support by the German Federal Foreign Office in the frame of the CAWa project (http://www.cawa-project.net) is equally acknowledged. We thank J. Gardelle and E. Berthier for providing the elevation change data of Abramov Glacier 2000–2011. J. Corripio is acknowledged for the software to georeference oblique photographs. We additionally thank H. Machguth, W. Hagg, A. Gafurov, M. Kronenberg, J. Schmale, D. Sciboz and everybody else that contributed with field work. We also thank all scientists of the glaciological expedition of the Central Asian Research Hydrometeoroloigcal Institute, who carried out the extensive measurements at Abramov Glacier in the past. We are also grateful to the Central Asian Institute for Applied Geosciences for their collaboration, especially to B. Moldobekov for his continuous support. Detailed comments by two anonymous reviewers were helpful to finalize the manuscript.

Chapter 7

Paper III: Multi-decadal mass balance series of three Kyrgyz glaciers inferred from modelling constrained with repeated snowline observations

Barandun, Martina, Huss Matthias, Berthier Etienne, Kääb Andreas, Azisov Erlan, Bolch Tobias, Usubaliev Ryskul, and Hoelzle Martin. *"Multi-decadal mass balance series of three Kyrgyz glaciers inferred from transient snowline observations"*, The Cryosphere, 12:1899-1919.

Abstract

Glacier surface mass balance observations in the Tien Shan and Pamir are relatively sparse and often discontinuous. Nevertheless, glaciers are one of the most important components of the high-mountain cryosphere in the region as they strongly influence water availability in the arid, continental and intensely populated downstream areas. This study provides reliable and continuous surface mass balance series for selected glaciers located in the Tien Shan and Pamir-Alay. By cross-validating the results of three independent methods, we reconstructed the mass balance of the three benchmark glaciers, Abramov, Golubin and Glacier No. 354 for the past two decades. By applying different approaches, it was possible to compensate for the limitations and shortcomings of each individual method. This study proposes the use of transient snowline observations throughout the melting season obtained from satellite optical imagery and terrestrial automatic cameras. By combining modelling with remotely acquired information on summer snow depletion, it was possible to infer glacier mass changes for unmeasured years. The model is initialized with daily temperature and precipitation data collected at automatic weather stations in the vicinity of the glacier or with adjusted data from climate Reanalysis products. Multi-annual mass changes based on high-resolution digital elevation models and in situ glaciological surveys were used to validate the results for the investigated glaciers. Substantial surface mass loss was confirmed for the three studied glaciers by all three methods, ranging from $-0.30 \pm 0.19\,\mathrm{m\,w.e.\,yr^{-1}}$ to $-0.41 \pm 0.33\,\mathrm{m\,w.e.\,yr^{-1}}$ over the 2004-2016 period. Our results indicate that integration of snowline observations into mass balance modelling significantly narrows the uncertainty ranges of the estimates. Hence, this highlights the potential of the methodology for application to unmonitored glaciers at larger scales for which no direct measurements are available.

7.1 Introduction

Glaciers are important components of the hydrological cycle in Central Asia. In this arid continental region, the intensely populated and irrigated downstream areas strongly depend on a supply of water from the cryosphere such as glaciers and snow (Kaser et al, 2010; Schaner et al, 2012; Duethmann et al, 2014; Chen et al, 2016; Huss and Hock, 2018). The uncertainty of water availability in the context of a changing climate creates a major potential for political tension and builds a complex set of future threats, affecting different sectors such as water management, energy production and irrigation (Varis, 2014; Munia et al, 2016). Climate change poses a manifold challenge for the Central Asian population and will influence natural hazards and threaten future economies and the livelihood of coming generations (Stocker et al, 2013). For this reason, continuous and high-quality data for the different components of the hydrological cycle acquired within established regional and national cryospheric and hydrologic climate services are key for providing accurate predictions which enable sustainable adaptation. As stated by the World Meteorological Organization (GCOS, 2016), large gaps currently exist in the global climate observation system. This refers in equal measure to such remote and unmonitored areas especially in the Pamir, but also in the Tien Shan, where there is a lack of data crucially needed to plan and enhance future development (Sorg et al, 2012; Unger-Shayesteh et al, 2013). Improved temporal and spatial representation of glacier monitoring is thus essential, due to the paramount significance of glaciers in the high-mountain cryosphere.

During the Soviet era, in the 1950s and 1960s, an extensive system of cryospheric monitoring was launched in the Tien Shan and Pamir-Alay. Most programmes stopped abruptly after the breakdown of the USSR in the mid-1990s. Monitoring activities were

maintained only on Tuyuksu Glacier, Kazakhstan, and Urumqi Glacier (No. 1), China. In recent years, different initiatives have aimed at the re-establishment of glacier monitoring in Central Asia (Hoelzle et al, 2017). Surface mass balance (SMB) series are now available for the following glaciers: Abramov (Pamir-Alay), Batysh Sook, Sary-Tor, Karabatkak and Glacier No. 354 (Central Tien Shan), for Urumqi No. 1 (Eastern Tien Shan) and for Golubin and Tuyuksu (Northern Tien Shan) (Fig. 7.1) (WGMS, 2013). However, a significant gap in the data from the mid-1990s to around 2010 hinder the interpretation of long-term trends in glacier behaviour in this region.

Different studies derived continuous mass balance series for selected glaciers based on modelling (e.g., Fujita et al, 2011; Barandun et al, 2015; Kronenberg et al, 2016; Liu and Liu, 2016; Kenzhebaev et al, 2017) and estimated mass balance at a regional scale in the Pamir-Alay and Tien Shan (Farinotti et al, 2015). Modelled mass balance series have a good temporal resolution; however, they are not observation-based and thus strongly depend on model calibration and the quality of the input variables. Several studies use remote sensing techniques to fill the gaps in glacier monitoring and to generate insights into region-wide mass changes covering entire High Mountain Asia within the past two decades (e.g. Gardner et al, 2013; Gardelle et al, 2013; Kääb et al, 2015; Brun et al, 2017; Wang et al, 2017). Furthermore, other authors focused on selected regions of the Central and Northern Tien Shan (e.g., Aizen et al, 2007; Pieczonka et al, 2013; Bolch, 2015; Pieczonka and Bolch, 2015; Goerlich et al, 2017) deriving glacier-specific geodetic mass balances. These studies often cover large areas, but temporal resolution is typically limited to five years or longer periods. Thus, they fail to capture the interannual or even seasonal signals.

The snowline is recognized as a valuable proxy for glacier mass balance (LaChapelle, 1962; Lliboutry, 1965; Braithwaite, 1984b; Kulkarni, 2012; Rabatel et al, 2017). Different methods have been developed to use the end-of-summer snowline observed on air- and spaceborne data, i.e., without direct access to the glacier, to infer glacier mass changes based on a statistical relation between the equilibrium line altitude and the glacier-wide SMB (e.g., Kulkarni, 1992; Dyurgerov, 1996; Rabatel et al, 2005). These methods were applied to glaciers located in a wide range of different regions, such as in Europe (e.g., Hock et al, 2007; Rabatel et al, 2008, 2016), South America (e.g., Rabatel et al, 2012), New Zealand (e.g., Chinn, 1995, 1999), the Arctic (e.g., Mernild et al, 2013b), the Himalayas (e.g., Kulkarni et al, 2004, 2011) and Central Asia (e.g., Dyurgerov et al, 1994; Kamniansky and Pertziger, 1996). Some pioneer studies (e.g., Østrem, 1973, 1975; Young, 1981; Dyurgerov et al, 1994) have identified the value of transient snowline (TSL) observations in connection with subseasonal SMB. Recent studies (e.g., Hock et al, 2007; Pelto, 2010; Pelto et al, 2013; Huss et al, 2013; Hulth et al, 2013) have further developed this concept to improve surface mass balance monitoring and modelling strategies, including information extracted from continuous TSL observations. However, most approaches still rely on long-term glaciological information and are thus not applicable to unmonitored glaciers located in remote and unmeasured regions.

In this study, three pillars of a multi-level strategy for glacier observation are combined, covering the period of the past two decades, to improve the understanding of mass change evolution of Abramov, Golubin and Glacier No. 354, three benchmark glaciers in the Tien Shan and Pamir-Alay. (1) We integrate in situ glaciological measurements, when available, to compute annual SMB using a model-based extrapolation of the measurement points to reach glacier-wide coverage. (2) We calculate geodetic mass changes based on high-resolution digital elevation models (DEMs) on decadal to semi-decadal time scales. (3) We infer daily SMB series using a model approach supported by transient snow-

line observations, as a proxy for glacier mass balance. In this way, a temperature-index model is calibrated with the snow-covered area fraction (SCAF) of the glacier observed on satellite optical imagery and time-lapse photographs throughout the ablation season. This approach represents a new tool for glacier observation at high temporal and spatial resolution. The remote snowline observations provide valuable information, especially for periods for which no direct measurements are available. By combining different independent approaches, we aim to overcome the limitations and shortcomings of each individual method and to deliver a robust mass balance estimate for the three selected glaciers at annual resolution for a period for which only limited data has been available so far.

7.2 Study Site and Data

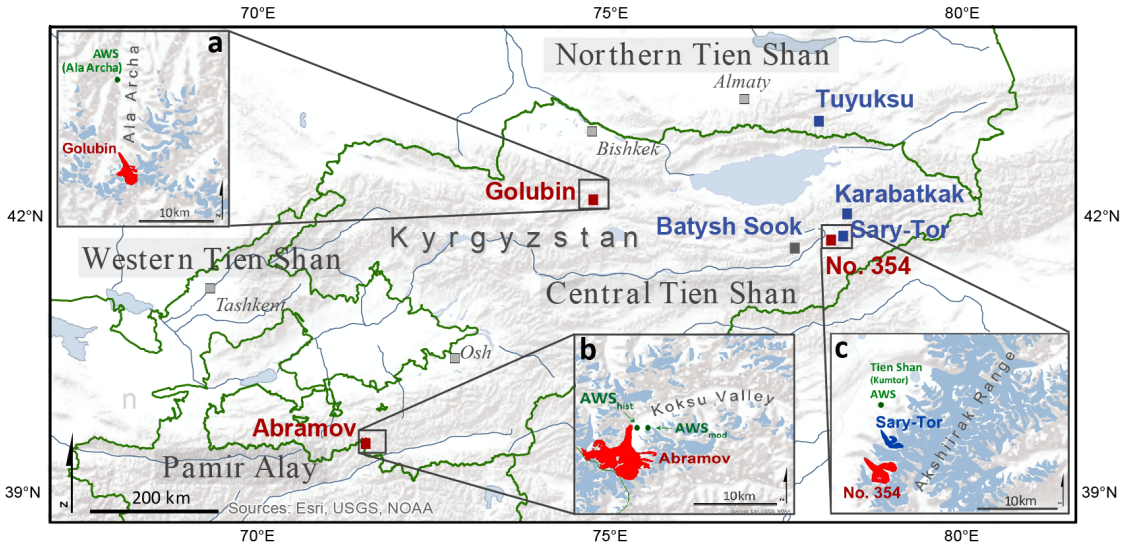

Figure 7.1: Overview map of Central Asia showing the location of glaciers (blue) with available long-term SMB measurements. Glaciers investigated in this study are marked in red. The insets show the position of the automatic weather station (AWS) for (**a**) Golubin, (**b**) Abramov and (**c**) Glacier No. 354. Note that $\mathrm{AWS_{mod}}$ indicates the position of the new AWS installed in 2011 and $\mathrm{AWS_{hist}}$ the old glaciological station at Abramov.

7.2.1 Study sites

In this section we present a brief overview of the study sites. A detailed description of the three selected glaciers and their geographic and climatological settings is given in Hoelzle et al (2017). Table 7.1 summarizes the available data for each glacier.

Abramov Glacier

Abramov Glacier (N 39 °36.78′, E 71 °33.32′) is located in the Pamir-Alay (North-Western Pamir, Fig. 7.1). The north to north-east facing glacier has an extent of about 24 $\mathrm{km^2}$ (as of 2016) and ranges from 3650 m a.s.l. to nearly 5000 m a.s.l. Barandun et al (2015) suggested that the glacier had a mean annual balance of -0.44 ± 0.10 m w.e. $\mathrm{yr^{-1}}$ between 1968 and 2014 and estimated internal accumulation and basal ablation to contribute by

$+0.07\,\mathrm{m\,w.e.\,yr^{-1}}$ to the total mass change of the glacier. Brun et al (2017) indicated a mass loss of $-0.38 \pm 0.10\,\mathrm{m\,w.e.\,yr^{-1}}$ for Abramov from ca. 2002 to 2014.

Mean daily air temperature and total daily precipitation sums were measured at a glaciological station located at 3837 m a.s.l. from 1967 to 1998 (Fig. 7.1). The station was located at a distance of about 0.5 km from the glacier tongue. Air temperature measured at an Automatic Weather Station ($\mathrm{AWS_{mod}}$) was used from 2011 to 2016 (Fig. 7.2a). This station is located at an elevation of 4100 m a.s.l. at a distance of about 1.5 km from the glacier terminus. ERA-interim Reanalysis data with spatial resolution of 0.78 degrees (Dee et al, 2011) were used to fill measurement gaps (Barandun et al, 2015).

The SMB was measured intensively from 1967 to 1998 (Suslov et al, 1980; Glazirin et al, 1993) and the monitoring was re-established in 2011 (Hoelzle et al, 2017). Since then, annual glaciological surveys were continuously carried out in late August. For a re-analyzed and reconstructed mass balance series for Abramov from 1968 to 2014 and a detailed description of the measurement network, see Barandun et al (2015).

Golubin Glacier

Golubin Glacier (N42 °26.94′, E 74 °30.10′) is located in the Ala Archa valley in the Kyrgyz Ala-Too in the Northern Tien Shan (Fig. 7.1). The glacier has an area of $\sim 5\,\mathrm{km^2}$ (as of 2016) and a north to northwestern aspect. The terminus is currently located at an elevation of about 3400 m a.s.l. and the glacier extends to an elevation of about 4300 m a.s.l. Long-term measurements indicated an internal accumulation due to refreezing of meltwater of about $+0.08\,\mathrm{m\,w.e.\,yr^{-1}}$ (Aizen et al, 1997). For Golubin, the geodetic mass loss reported by Bolch (2015) was $-0.28 \pm 0.96\,\mathrm{m\,w.e.\,yr^{-1}}$ from 2000 to 2012, whereas Brun et al (2017) found a geodetic mass balance of $-0.04 \pm 0.19\,\mathrm{m\,w.e.\,yr^{-1}}$ for the period 2002 to 2013.

We used meteorological data from the Alplager station located in the Ala Archa valley, situated at an elevation of 2145 m a.s.l. at a distance of about 10 km from the glacier (Fig. 7.1). There are several other meteorological stations in the valley, however, the Alplager station has the most complete and continuous series at high elevation covering the entire study period.

Intense glacier monitoring started in 1958 and continued until 1994 when the monitoring programme was stopped (Aizen, 1988). In summer 2010, SMB measurements were re-initiated. Figure 7.2b summarizes the monitoring network at Golubin as of 2016, including a SMB measurement network, an AWS ($\approx$3300 m a.s.l.) and two terrestrial cameras installed in 2013. A detailed description of the monitoring strategy is provided in Hoelzle et al (2017).

Glacier No. 354

Glacier No. 354 (N 41 °47.62′, E 78 °9.69′) is situated in the Ak-shiirak range in the Central Tien Shan (Fig. 7.1). The glacier covered a surface area of about $6.4\,\mathrm{km^2}$ in 2016. The accumulation zone comprises three basins and the glacier tongue is oriented to the northwest. The glacier spans an elevation range of 3750-4680 m a.s.l. Mass loss since the mid-1970s was reported by different studies ranging from about -0.8 to $-0.5\,\mathrm{m\,w.e.\,yr^{-1}}$ (Pieczonka and Bolch, 2015; Kronenberg et al, 2016; Brun et al, 2017). Summer snowfall is frequent and fresh snow can cover the entire glacier surface for several days during the melt season, significantly reducing ablation (Kronenberg et al, 2016). Evidence of persistent superimposed ice is found and Kronenberg et al (2016) estimated internal accumulation to be $+0.04\,\mathrm{m\,w.e.\,yr^{-1}}$. An AWS (Tien Shan (Kumtor) AWS) installed at an elevation of $\approx$3660 m a.s.l. and a distance of approximately 10 km to the glacier recorded continuous

meteorological data for the study period (Fig. 7.1). We used daily precipitation sums and mean daily air temperature for modelling.

Since 2010, in situ SMB has been obtained annually in late summer (Fig. 7.2c). Winter measurements exist for May 2014 (Kronenberg et al, 2016). A description of the meteorological input data and the SMB measurement network, as well as a reconstruction of the mass balance series back to 2003 are provided by Kronenberg et al (2016).

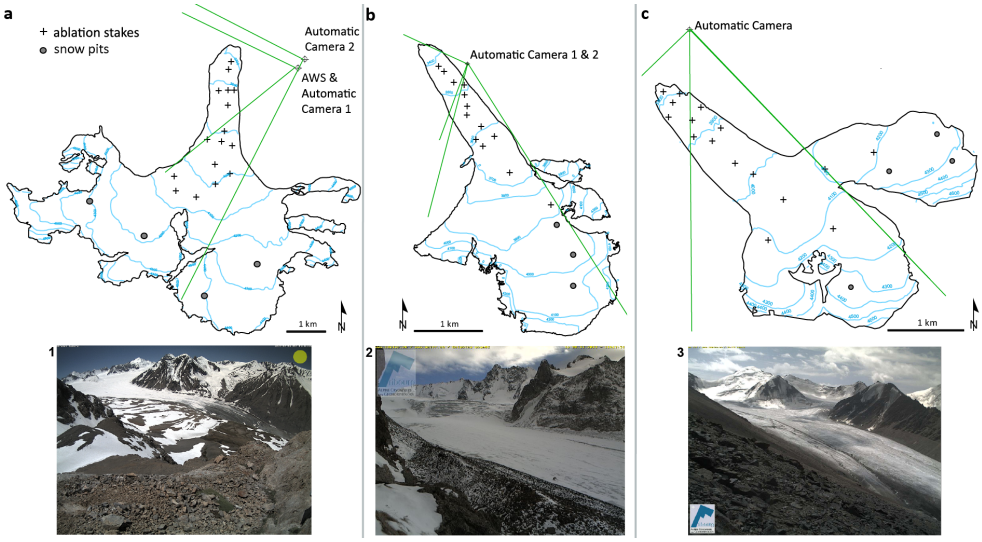

Figure 7.2: Glacier monitoring network at (**a**) Abramov, (**b**) Golubin and (**c**) Glacier No. 354. A photograph taken by the terrestrial cameras is shown for (**1**) Abramov, (**2**) Golubin and (**3**) Glacier No. 354.

7.2.2 High-resolution satellite images and DEMs

To compute geodetic mass balances for Abramov, high-resolution DEMs were used based on Pléiades stereo images acquired in 2015, and on stereo images from 2003 and 2011 from Satellite Pour l'Observation de la Terre (SPOT) 5. For Glacier No. 354, DEMs from 2003 (QuickBird) and from 2012 (GeoEye) were available from Kronenberg et al (2016). In addition, a SPOT6 stereo-pair acquired in 2015 was used to produce an updated DEM. High-resolution stereo images for Golubin are sparse and we had to rely on a SPOT7 tri-stereo scene from November 2014 and on Advanced Land Observing Satellite (ALOS) Prism scenes from 2006 (Table 7.1). Important snow coverage was present on the SPOT5 image from 2011 for Abramov and on the SPOT7 image from 2014 for Golubin. A fine layer of fresh snow covered parts of the SPOT6 image from 2015 for Glacier No. 354. For modelling purposes, the most complete and accurate DEM available of each glacier was used to represent the surface topography (Table 7.1).

7.2.3 Optical satellite and terrestrial camera images

We used freely accessible, orthorectified and georeferenced Landsat TM/ETM+ and OLI, Terra ASTER-L1B and Sentinel-2A scenes to repeatedly observe the glacier outlines and the snowline throughout the melting season for all three glaciers. In addition, we used the snow-free high-resolution optical satellite images as described above for snowline and glacier outline mapping.

Table 7.1: Available data on glacier monitoring for the three glaciers used in this study. The dates marked with an asterisk indicate the DEMs used as a topographic base for the modelling.

	Abramov	Golubin	Glacier No. 354
No. surface mass balance measurements per year	22	14	16
No. annual glaciological surveys (2000-2016)	5	6	6
Total No. snowline observations	122	56	78
High-resolution satellite stereo images	27/08/2003 (SPOT5) 29/11/2011 (SPOT5) 01/09/2015 (Pléiades)*	08/09/2006 (ALOS)* 01/11/2014 (SPOT7)	01/09/2003 (QuickBird) 27/07/2012 (GeoEye)* 01/10/2015 (SPOT6)

Two terrestrial cameras (Mobotix M25) overlooking Abramov were installed in August 2011. One camera was located next to the AWS_{mod}, and the other one at approximately 500 m distance at an elevation of 4200 m a.s.l. (Fig. 7.2a). Due to multiple camera failures and power supply problems, pictures were lacking from the end of the ablation season in 2012 to the end of the ablation season in 2013, and again partly for the summer months in 2014. In 2015, continuous coverage was obtained from Camera 1 but only a few images could be retrieved from Camera 2. A complete set of data was collected from both cameras for the first time in 2016. A similar setup has been installed for Glacier No. 354 in 2014, delivering continuous coverage since implementation (Fig. 7.2c). The camera is located at an elevation of 4145 m a.s.l. Images from the two cameras installed at Golubin were not used here due to limited image quality (Fig. 7.2b). Figure 7.3 illustrates the number of camera and satellite images with satisfying quality that were used to obtain maps of snowlines for the three glaciers. Image availability for snowline mapping prior to 1998 was insufficient for the most part.

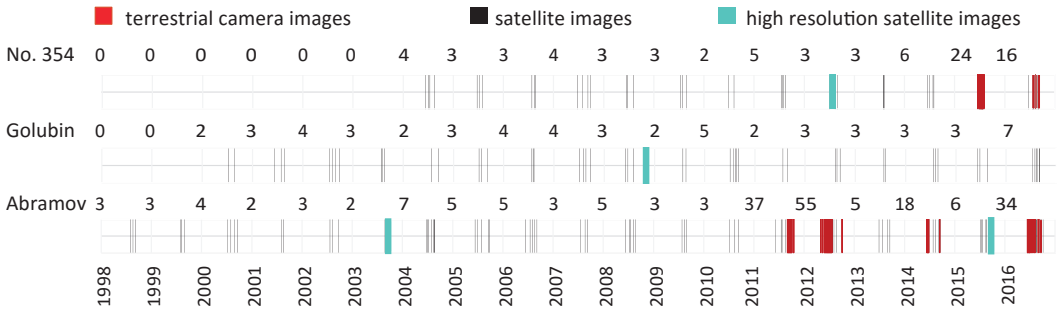

Figure 7.3: Image availability and distribution for snowline mapping. Numbers indicate the total available scenes per year and glacier. Prior to 1998, image coverage is sparse for all three glaciers. For Golubin and for Glacier No. 354, the first summer season for which enough snowline observations could be collected was 2000 and 2004, respectively. Snow-covered high-resolution images have not been used to delineate the snowline and are not shown here.

7.3 Methods

7.3.1 Glacier outlines

Glacier extents were mapped manually based on satellite images for all three glaciers and for each year of the corresponding study period. Only cloud- and snow-free images were

selected. The surfaces of Glacier No. 354 and Golubin are mostly debris-free. We excluded a debris-covered part with strongly reduced melt rates at the western margin of Abramov (Barandun et al, 2015). Annually repeated measurements of the glacier front position using a handheld GPS for all three glaciers were combined with the satellite observations for mapping from 2011 onward. The same extents were used for all three methods. Errors related to glacier outlines digitized manually on remote sensing images depend on atmospheric and topographic corrections, shading, glacier surface characteristics, snow cover and local clouds, but mainly on misinterpretation of debris cover (Paul et al, 2013a, 2015). Uncertainties are expected to be in the range of ±5% of the total glacier area for medium-resolution images such as Landsat TM, and smaller for high-resolution images (Paul et al, 2013a).

7.3.2 Meteorological data

For Abramov, the air temperature data measured at the AWS was adjusted to the elevation of the former glaciological station by applying a constant lapse rate of $-6\,^{\circ}\mathrm{C\,km^{-1}}$ (Suslov et al, 1980). The ERA-interim Reanalysis dataset was adapted by applying mean monthly additive and multiplicative biases for air temperature and precipitation, respectively. The biases were calculated from long-term in situ measurements (Barandun et al, 2015). From the corrected monthly means, daily series were generated by superimposing day-to-day variability, observed at the meteorological station from 1969 to 1994. For Abramov, we generated air temperature series from 1995 to 2011 and precipitation series from 1995 to 2016. More detailed information on data preparation and their suitability is given in Barandun et al (2015).

Mean daily air temperature data measured at the Ala Archa AWS and Tien Shan (Kumtor) AWS were extrapolated to the median elevation of the corresponding glacier with monthly temperature lapse rates for the Northern and Central Tien Shan provided in Aizen et al (1995b).

7.3.3 Snowline delineation

A visual pre-selection of suitable camera and satellite images was taken in order to preclude problems associated with image quality such as fresh snowfall, extensive cloud cover, among others. Oblique ground-based photographs were first corrected automatically for lens distortion, then projected and orthorectified following Corripio (2004). Every pixel on the photograph was associated to the elevation of the DEM. Georeferenced products of satellite scenes were downloaded. On each camera and satellite image, the snow-covered area was digitized manually by means of visual separation of bare ice and snow (Pelto et al, 2013; Mernild et al, 2013b; Huss et al, 2013). Manual detection allowed the observer's knowledge of the snow-cover depletion patterns to be integrated, and was assumed to be less error-prone than an automatic classification (Huss et al, 2013; Rabatel et al, 2013).

Errors occurred due to the pixel size of the images, slope of the terrain, the accuracy of the georeferencing and the quality of the DEM (Rabatel et al, 2012). In view of the fact that the border between ice and snow is not a clearly defined line, operator expertise is desired and beneficial. Contrast becomes rather weak, especially when the snowline rises above the firn line (Rabatel et al, 2013; Wu et al, 2014) for both satellite and terrestrial camera images. In order to estimate the influence of ambiguous transition areas, we conducted extensive experiments on the interpretation of the surface type (see Section 7.4).

Table 7.2: Survey period of glaciological measurement for each glacier and each year

Abramov	Golubin	Glacier No. 354
	10/09/2010–17/08/2011	05/09/2010–12/08/2011
26/08/2011–22/08/2012	17/08/2011–29/08/2012	12/08/2011–14/08/2012
22/08/2012–15/08/2013	29/08/2012–25/08/2013	14/08/2012–23/07/2013
15/08/2013–18/08/2014	25/08/2013–17/08/2014	23/07/2013–03/09/2014
18/08/2014–27/08/2015	27/08/2014–09/08/2015	03/09/2014–14/08/2015
27/08/2015–01/08/2016	09/08/2015–14/09/2016	14/08/2015–29/08/2016

We assumed the spatial depletion pattern to be approximately constant in time so that camera and satellite images with minor invisible sections of the snowline due to shading, cloud cover, Landsat 7 SLC-off void-stripes or due to the terrestrial camera view angle could be included. To fill in those data gaps, we extrapolated the snowline based on information from repeated snowline observations of images with good quality over a ≈15-year period. The effect of a misinterpretation of the snowline on the calculated SMB was investigated in detail and is described in Section 7.4.

7.3.4 Glaciological surface mass balance

Ablation stakes are distributed over the entire ablation zone in order to provide an optimal representation of melt patterns (Fig. 7.2). Each year, they are re-drilled at the initial position. An ice density of $900\,\mathrm{kg\,m^{-3}}$ was assigned. Snow pits were dug to the previous end-of-summer horizon to measure snow density and snow accumulation. Annual field surveys ranged from late July to late August and for logistic reasons, can vary from year to year. Winter snow measurements were carried out to retrieve a detailed snow distribution pattern, and to compute the winter balance for Glacier No. 354 and Golubin in May 2014 (Kronenberg et al, 2016). Winter surveys from 1993 and 1994 were available for Abramov (Pertziger, 1996). A model-based spatial extrapolation of point measurements to the entire glacier surface after Huss et al (2009) was used to retrieve glacier-wide SMB for all years with direct measurements. The model is a combined distributed accumulation (Huss et al, 2008) and temperature-index melt model with daily resolution (Hock, 1999) which was automatically optimized to best represent all collected point data from each seasonal/annual survey. The model is considered as a suitable tool to extrapolate the glaciological point measurements to the glacier surface for the measurement periods.

7.3.5 Geodetic mass balance

For Abramov, the 4-m Pléiades DEM from 1 September 2015 was used as reference. It was created using the AMES stereo-pipeline (Shean et al, 2016) and the processing parameters that were used in Marti et al (2016). The two SPOT5 DEMs (August 2003 and November 2011) were derived from High Resolution Stereoscopic (HRS) images by the French mapping agency (Korona et al, 2009). The steps required to adjust the two SPOT5 DEMs horizontally and vertically to the Pléiades reference DEM are similar to the ones followed in a previous study on the Mont Blanc area (Berthier et al, 2014).

We created DEMs with a spatial resolution of 5 m for Golubin and Glacier No. 354 from the available two/tri-stereo pairs of high-resolution satellite imagery using standard procedures and the software PCI Geomatica (Kronenberg et al, 2016). The two/tri-stereo pairs were connected using common tie points before DEM extraction. For Glacier No.

354, a horizontal shift between the two DEMs was corrected through a DEM co-registration procedure as proposed by Nuth and Kääb (2011). For the data covering Golubin, no horizontal shift was encountered. We thus corrected only for a mean elevation difference of 3.9 m detected over stable ground. For this vertical co-registration, only terrain sections with a slope smaller than 30 ° were selected and areas with parallax-matching problems were avoided. Snow-covered areas were included in the offset correction, in order to correct for fresh snow on the image, assuming similar snow thicknesses on- and off-glacier. The vertical accuracy was thus improved, and the mean absolute difference off-glacier was limited to 1.0 m (2003-2015) and 0.6 m (2011-2015) for Abramov, 0.7 m for Glacier No. 354 and 1.6 m for Golubin (see also Section 7.4). Steep mountain walls and shading caused problems. Areas affected were manually masked out. Unmeasured areas (Abramov: 26% in 2003-2015, and 23% in 2011-2015; Golubin: 30%; Glacier No. 354: 25%) were assumed to have experienced the same elevation change as the measured areas in the same altitude band and the median of the corresponding elevation bin was used for gap-filling. For elevation bins higher than 4300 m a.s.l. at Golubin (9% of total area) and for elevation bins higher than 4500 m a.s.l. at Glacier No. 354 (8% of total area), obvious DEM errors were dominant and not enough realistic values for median elevation-change calculation were available. Thus, the median of the uppermost elevation band with reliable data was used to fill in the gaps. To derive the geodetic mass balance ΔM_{geod}, a density $\rho_{\Delta \mathrm{V}}$ of $850\,\mathrm{kg\,m^{-3}}$ was used for volume-to-mass conversion (Huss, 2013):

$$\Delta M_{\mathrm{geod}} = \frac{\Delta V \cdot \rho_{\Delta V}}{\overline{A} \cdot \Delta t \cdot \rho_w} \tag{7.1}$$

where, $\overline{A}$ is the average glacier area and Δt is the time in years between the corresponding image pairs and ρ_w is the density of water ($1000\,\mathrm{kg\,m^{-3}}$). Uncertainties in the detected elevation changes and the derived geodetic mass balances are described in Section 7.4.

7.3.6 Surface mass balance modelling constrained by snowline observations

An accumulation and temperature-index melt model closely constrained by transient snowline observations was implemented in order to infer glacier-wide SMBs. The applied methodology is a further stage in the approach presented by Huss et al (2013). The principle of the approach is to employ the information given by the temporal change in the position of the transient snowline throughout the ablation season to constrain both the amount of winter snow accumulation and melting by iteratively calibrating a mass balance model. The approach also allows us to temporally extend SMB estimates to the end of the hydrological year although snowline observations do not cover the entire ablation season. The methodological steps are described in more detail in the following.

A surface mass balance model with a spatial resolution of 20 m was driven with daily mean air temperature and precipitation sums measured at nearby meteorological stations or inferred from Reanalysis data (see Section 7.2.1). We used a classical temperature-index melt model (e.g., Braithwaite, 1995; Hock, 2003). Melt M was calculated for each grid cell x, y and time step t based on a linear relation with positive daily mean air temperature $T_{\mathrm{air}}(x, y, t)$ as

$$M_{x,y,t} = \begin{cases} DDF_{\mathrm{ice/snow}} \cdot T_{\mathrm{air}(x,y,t)} & T_{\mathrm{air}} > 0^{\circ} \\ 0 & T_{\mathrm{air}} \leq 0^{\circ} \end{cases} \tag{7.2}$$

Table 7.3: Constant model parameters. The temperature lapse rate for Abramov was adopted from Barandun et al (2015) and for Golubin and Glacier No. 354 from Aizen et al (1995b). $\delta T/\delta z$, $\delta P/\delta z$, Z_{crit} and R_{DDF} are held constant throughout the entire modelling period. The initial parameter ranges of DDF_{snow} and C_{prec} as well as the mean value obtained from annual calibration is given with its standard deviation.

parameter	Abramov	Golubin	Glacier No. 354	unit
$\delta T/\delta z$	-4.8	-6.3	-6.7	$^{\circ}\mathrm{C\,km^{-1}}$
$\delta P/\delta z$	6.4	4.5	1.5	$\%\,10^{-4}\,\mathrm{m^{-1}}$
R_{DDF}	1.57	1.36	1.06	–
$\mathrm{Z_{crit}}$	4400	4000	4500	m a.s.l
annually variable model parameters				
initial range				
DDF_{snow}	3.5 – 5.5	3.0 – 5.5	1.5 – 4.5	$\mathrm{mm\,day^{-1}\,^{\circ}C^{-1}}$
$\mathrm{C_{prec}}$	1.75 – 3.0	1.5 – 3.0	1.0 – 3.5	–
best combination				
DDF_{snow}	4.54 ±0.74	5.09 ±0.46	3.04 ±0.66	$\mathrm{mm\,day^{-1}\,^{\circ}C^{-1}}$
$\mathrm{C_{prec}}$	2.23±0.40	1.46±0.31	2.35 ±0.29	–

Daily air temperatures are extrapolated to each grid cell using a constant temperature lapse rate based on literature values (Table 8.1). Different degree-day factors $DDF_{\mathrm{ice/snow}}$ were chosen for snow and ice surfaces. The surface type over the glacier area was given by the snow depth updated with modelled daily snowfall and melt. The ratio between DDF_{ice} and DDF_{snow}, R_{DDF}, was held constant over time. As a wide range of different ratios can be found in literature (e.g., Hock, 2003; Zhang et al, 2006; Gao et al, 2010; Liu and Liu, 2016), we decided to constrain R_{DDF} by SMB measurements in the Tien Shan and Pamir (Table 8.1). A sensitivity test shows that a variation of R_{DDF} by ±25%, a value exceeding the maximum range found in the literature (±22%), only causes small changes in modelled SMB (Table 7.4) indicating that calibrating R_{DDF} improves model performance to some extent but is not essential to applying the model. For more details see Section 7.4.

Snow accumulation C was calculated for each grid cell x, y and time step t by

$$C_{(x,y,t)} = P_{\mathrm{ws}}(x,y,t) \cdot C_{\mathrm{prec}} \cdot (1 + (z_{(x,y)} - z_{\mathrm{ws}}) \cdot \delta P/\delta z), \tag{7.3}$$

where P_{ws} is the measured precipitation at the meteorological station at elevation z_{ws}. $z(x,y)$ is the elevation of each grid cell. The measured precipitation was extrapolated to every grid cell with a constant precipitation gradient $\delta P/\delta z$ calculated from winter snow surveys (Table 8.1). Solid precipitation occurs at $T_{\mathrm{air}} \leq 1.5\,^{\circ}C$ with a linear transition range of ±1°C (e.g., Hock, 1999). C_{prec} is a scaling factor that accounts for gauge undercatch and other systematic measurement errors of precipitation (e.g., Huss et al, 2009). In order to account for smaller measurement errors during summer related to the type of precipitation (solid/liquid, wet/dry snow), C_{prec} was reduced for the summer months to 25% of its value (Sevruk, 1981). Above a critical elevation Z_{crit}, precipitation is set to no longer increase linearly (Alpert, 1986). Our selected value of Z_{crit} approximated the elevation for which a decrease in accumulation was observed on long-term monitored glaciers situated in the Tien Shan and Caucasus (WGMS, 2013). All parameters used are summarized in Table 8.1.

Model calibration

We calibrated C_{prec} and DDF_{snow}, keeping R_{DDF} constant. C_{prec} and DDF_{snow} were calibrated annually and for each glacier separately to correctly represent the winter snow accumulation and the melt rate. To calibrate C_{prec}, we relied on the fact that, at the position of the transient snowline, icemelt had not yet started but all winter snow was melted. The modelled cumulative melt, calculated at the position of the observed snowline, is thus interpreted as the total amount of accumulated winter snow that melted from the onset of the ablation season until the snowline observation date. Using the melt model, we can infer the winter accumulation at the beginning of the ablation season along each observed snowline. This quantity needs to agree with the directly modelled snow accumulation at the end of the winter season. DDF_{snow} was calibrated to best represent all SCAF observations of one ablation season (Fig. 7.4).

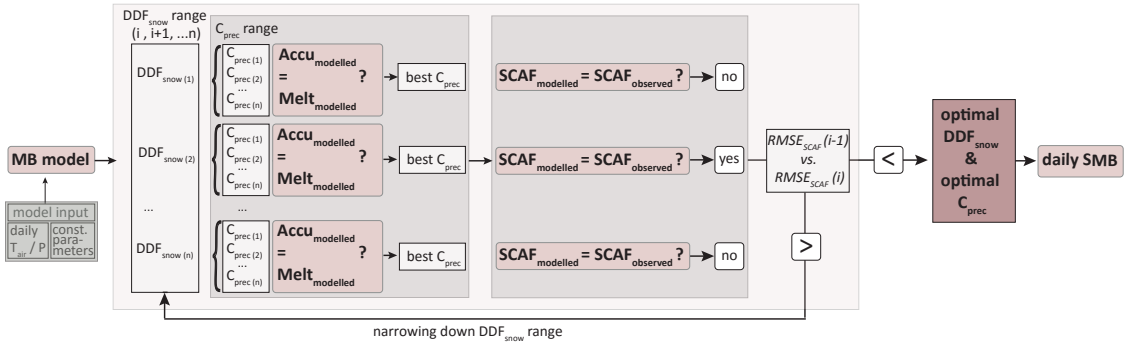

Figure 7.4: Calibration procedure to obtain an ideal combination of DDF_{snow} and C_{prec}. An initial range for DDF_{snow} and C_{prec} was narrowed down through comparison to snowline observations until an optimal solution for both parameters was found. First, for each initial value of DDF_{snow}, the best value of C_{prec} was determined constraining the modelled cumulative melt ($Melt_{\text{modelled}}$) at the snowline position to agree with the modelled winter snow accumulation ($\text{Accu}_{\text{modelled}}$) for the same location. Second, the performance of each DDF_{snow} was evaluated to narrow down the range of DDF_{snow} by comparing the $\text{RMSE}_{\text{SCAF}}$ of the modelled and observed snow-covered area fractions (SCAF). This was repeated until an optimal solution is reached.

As C_{prec} and DDF_{snow} depend on each other, overestimation of DDF_{snow} could cause an overestimation of C_{prec}, and vice versa, without affecting the modelled position of the snowline and the SCAF. To overcome this problem, the values of C_{prec} and DDF_{snow} were constrained to remain within realistic bounds. Through an iterative calibration procedure, we aimed at finding the best possible parameter combination without the need of any additional information.

First, we defined a plausible range for DDF_{snow} and C_{prec} for all three glaciers based on literature (Hock, 2003; Liu and Liu, 2016) (Table 8.1). For each DDF_{snow}, an optimal parameter C_{prec} was calibrated through iteratively narrowing a plausible range of initial values of C_{prec} (Fig. 7.4). In this way, the RMSE between the directly modelled winter snow accumulation $Accu_{\text{modelled}}$ and the modelled cumulative melt from the onset of the ablation season to each observation date $Melt_{\text{modelled}}$ was minimized until no further improvement of the RMSE was observed.

Second, the performance of each DDF_{snow} with its optimal C_{prec} pair, was evaluated based on the $\text{RMSE}_{\text{SCAF}}$ between the observed $SCAF_{\text{obs}}$ and the modelled $SCAF_{\text{modelled}}$ for all available snowline observations within one year (Fig. 7.4). The range of DDF_{snow}

was narrowed around the best solution and the optimization process was restarted until no further significant improvement of the $\mathrm{RMSE}_{\mathrm{SCAF}}$ was observed. The calibration procedure was repeated for each year individually.

A minimum of two images was needed to enable application of our calibration approach. The influence of the image frequency and distribution was assessed in detail with sensitivity experiments described in Section 7.4. In a last step, the calibrated model was re-run with the ideal parameter set. This snowline-constrained mass balance model was thus applied to derive continuous daily SMB series that agreed with the snow depletion patterns observed by remote sensing imagery. In the following, we refer to the methodology described above as *s*nowline approach.

Adjustments to enable comparison of different methods

Geodetic surveys provide an estimate of the total mass change of a glacier ΔM_{geod}, whereas the results inferred from the snowline approach refer to the surface mass balance B_{sfc} and do not account for internal and basal components of the mass balance (Cogley et al, 2011). For comparing the results, we adjusted the modelled SMB constrained by snowline observations, with an estimate of the internal/basal mass balance of $+0.07\,\mathrm{m\,w.e.\,yr^{-1}}$ for Abramov (Barandun et al, 2015), $+0.08\,\mathrm{m\,w.e.\,yr^{-1}}$ for Golubin (Aizen et al, 1997) and $+0.04\,\mathrm{m\,w.e.\,yr^{-1}}$ for Glacier No. 354 (Kronenberg et al, 2016). Values are positive due to a significant amount of refreezing of meltwater in cold firn.

To compare the results of the different methods, the time periods covered by the datasets also needed to be homogenized. We thus adjusted the observation period of the modelled mass balance constrained by snowline observations to exactly match the respective periods of geodetic and glaciological mass balance, respectively. However, the final results $B_{\mathrm{sfc(fix)}}$ derived from the snowline approach are presented for the fixed dates of the hydrological year (1 October to 30 September) and do not include internal/basal mass balance.

7.4 Uncertainties and model sensitivity

7.4.1 Glaciological surface mass balance

Uncertainty σ_{glac} related to the direct glaciological measurements for Abramov was adopted from Barandun et al (2015), and for Glacier No. 354 from Kronenberg et al (2016). Uncertainties concerning the SMB of Golubin were calculated after Kronenberg et al (2016). Uncertainties regarding all three glaciers range between 0.24 and $0.30\,\mathrm{m\,w.e.\,yr^{-1}}$ (Table 7.4). For a sensitivity experiment we artificially shifted temperature and precipitation series used for the model-based extrapolation by $\pm 1°\mathrm{C}$ and $\pm 25\%$, respectively. The resulting glacier-wide SMB indicate a very small sensitivity to the meteorological input data with a Standard Deviation (STD) of $<0.01\,\mathrm{mm\,w.e.\,yr^{-1}}$. We strictly refer to the annual SMB obtained for the measurement dates (table 7.2).

7.4.2 Geodetic mass balance

The total uncertainty of the geodetic mass balance includes a random and systematic error. We followed Brun et al (2017) for computing the random error of the geodetic mass balance estimate but did not assess the systematic error. Uncertainties in elevation differences were quantified by computing the area-weighted mean of the absolute difference off-glacier in 50 m altitude bins. The resulting values for Abramov, 1.0 m for 2003-2015

and 0.6 m for 2011-2015, and for Glacier No. 354, 0.7 m for 2012-2015, are in line with the uncertainty of 1.3 m found over the Mont Blanc area through comparison of similar satellite data to elevation differences measured in situ (Berthier et al, 2014). For Golubin, a value of 1.6 m indicates a slightly lower DEM quality. The uncertainty related to the density assumption for converting volume to mass change was assumed to be $\pm 60\,\mathrm{kg\,m^{-3}}$ for time intervals larger than five years (Huss, 2013). For shorter periods, we used a more conservative estimate of $\pm 120\,\mathrm{kg\,m^{-3}}$. The elevation uncertainty for unmeasured glacier zones was roughly estimated to be five times as large as the uncertainty determined for measured locations. We assumed independence between the different error components and combined them as Root-Sum-Square (RSS) to the total uncertainty for the geodetic mass balance, σ_{geod}.

7.4.3 Surface mass balance modelling constrained by snowline observations

The uncertainty introduced by the mass balance model constrained by transient snowline observations σ_{tsl} depends on (1) the delineation accuracy of the SCAF, σ_{map}, (2) the image frequency and distribution throughout the ablation season, σ_{dis}, (3) the DEM quality, σ_{DEM}, (4) the meteorological input data, σ_{meteo}, and (5) the uncertainty in constant model parameters, σ_{para} (Table 7.4). The individual components were estimated as follows:

(1) The accuracy of the mapped SCAF is dependent on the positioning and the transect of the snowline, the georeferencing of the images, and the extrapolation of the snowline to invisible areas (Huss et al, 2013). The limit between snow- and ice-covered areas is often not a clear line but rather a transition zone, especially for glaciers with superimposed ice. To account for the total uncertainty related to the mapping procedure, we identified an upper- and lowermost position of the surface that could be classified as either snow or ice on each available image. Hence this zone included all ambiguous areas observed, such as cloud-covered regions, shading, superimposed ice or invisibility due to reduced image quality (e.g., Landsat 7 SLC-off void-stripes, invisible areas on photographs). We interpreted the zone to be either entirely snow-covered or entirely snow-free. The standard deviation of the minimal, maximal and optimal SCAF was used as an uncertainty. This uncertainty was calculated for each image individually. To evaluate the corresponding effects on calculated SMB, the model was re-run with the maximal and the minimal possible SCAF. The standard deviation of the SMB, σ_{map}, ranged between 0.06 to 0.09 $\mathrm{m\,w.e.\,yr^{-1}}$ for the three glaciers.

(2) To estimate the effect of varying image availability, we repeated the modelling using different snowline observation frequencies and temporal distributions throughout the summer for calibration. Due to limited image availability, this could only be conducted for the few years when many images were available (Fig. 7.3). We used the results to create a look-up table that linked the image frequency, the distribution over the ablation season and the last observation date of the season to an uncertainty estimate in the calculated annual SMB, σ_{dis}. Tests showed that the model reacts more sensitively to image distribution than to reduced image frequency (Fig. 7.5). A minimum of two images well distributed throughout the ablation season (i.e., at the beginning/middle and at the end) is sufficient to achieve reliable SMB estimates. Greater uncertainties were found if images were concentrated on, for example, a few days at the beginning of the ablation season (Fig. 7.5). In this case, higher image frequency cannot compensate for the missing information on the snow depletion pattern. An image taken towards the end of the ablation season is more important than images from the beginning of the summer. Our assessment of image

availability resulted in smaller uncertainties for Abramov ($\sigma_{\text{dis}} = 0.09\,\text{m w.e. yr}^{-1}$) than for Golubin ($\sigma_{\text{dis}} = 0.16\,\text{m w.e. yr}^{-1}$) and for Glacier No. 354 ($\sigma_{\text{dis}} = 0.18\,\text{m w.e. yr}^{-1}$) (Table 7.4).

(3) To estimate the uncertainty caused by the DEM used for the modelling, we compared our results to those obtained from model runs that used lower-resolution DEMs. For this experiment, we replaced the high-resolution DEM with the SRTM DEM. This enabled us to both investigate the sensitivity of the results to DEM quality and to assess our assumption of unchanged topography during the entire study period. The effects of a reduced DEM quality for all three glaciers were found to be small ($\sigma_{\text{DEM}} < 0.03\,\text{m w.e. yr}^{-1}$).

(4) We investigated the uncertainty related to the meteorological input data, σ_{meteo}, by re-running the model with a climatological average daily temperature and precipitation series for each glacier instead of the actual meteorological series. The test assessment revealed an RMSE of $0.13\,\text{m w.e. yr}^{-1}$ for the annual SMB of Abramov, of $0.23\,\text{m w.e. yr}^{-1}$ for Golubin and of $0.14\,\text{m w.e. yr}^{-1}$ for Glacier No. 354 (Fig. 7.6). These results demonstrate a relatively low sensitivity of our model approach to daily meteorological input data. With the chosen calibration procedure the model parameters DDF_{snow} and C_{prec} are adjusted to best represent the TSL observations for each year and glacier individually. The modelled SMB are thus closely tied to the snowline observations and exhibit a reduced dependence from meteorological input data. This underline the potential of our methodology for regional application based on minimal input data.

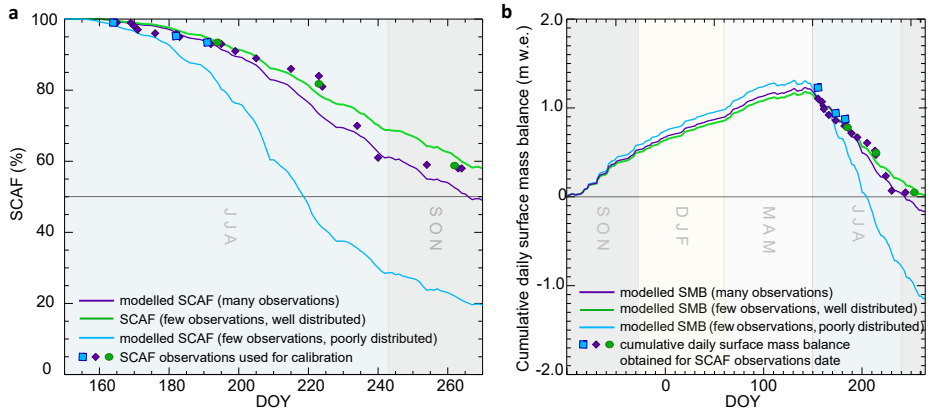

Figure 7.5: Example of the (**a**) daily SCAF and (**b**) cumulative daily SMB obtained with different sets of image frequency and distribution for Abramov in 2016. Snowline observation dates used to calibrate the model are indicated with symbols. The modelled daily SCAF and cumulative daily SMB and their corresponding snowline observations are shown with the same colour. Three images at the beginning of the ablation season (blue), three images well distributed throughout the ablation season (green), or all available images (purple) were used.

(5) To test the uncertainty introduced by the constant (i.e. uncalibrated) model parameters, $\delta T/\delta z$, $\delta P/\delta z$ and the R_{DDF} were varied by ±25% for each glacier and year. A mean standard deviation, σ_{para}, of around $0.17\,\text{m w.e. yr}^{-1}$ was found. We additionally tested the behaviour of the model relative to the individual parameters and identified a higher sensitivity to $\delta T/\delta z$ and R_{DDF}, whereas sensitivities to the other parameters were minor (Table 7.5).

Components 1 to 5 are assumed to be independent of each other and are combined as RSS to represent the total error of the annual SMB σ_{tsl} obtained from the snowline approach. We then averaged the annual error over the different periods to compute overall

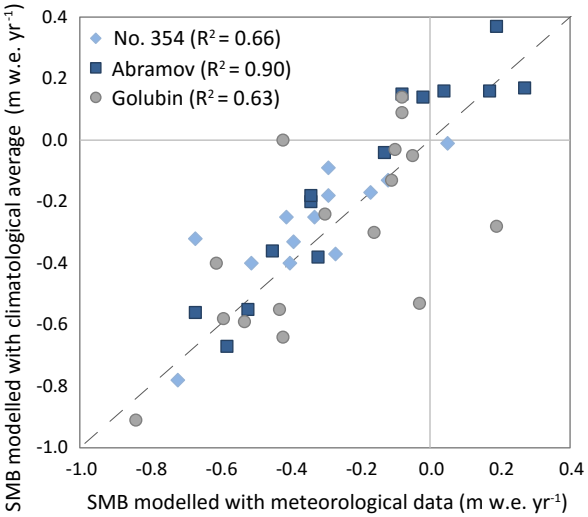

Figure 7.6: Comparison between the annual SMB obtained from the snowline-constrained model when using meteorological and climatological average daily data for Abramov, Golubin, and Glacier No. 354.

Table 7.4: Overall average uncertainties related to the three methods used, namely the glaciological σ_{glac}, geodetic σ_{geod} and snowline-constrained modelled mass balances σ_{tsl} for all three investigated glaciers in m w.e. yr^{-1}. Additionally, the uncertainty for each component of the snowline approach is specified. σ_{map} shows the uncertainty of the snowline delineation, σ_{dis} the uncertainty related to image frequency and distribution, and σ_{DEM} to the DEM. σ_{meteo} indicates the uncertainty introduced by the meteorological input data and σ_{para} the one by the model parameter choice.

Uncertainty in	Abramov	Golubin	Glacier No. 354
Glaciological SMB			
σ_{glac}	0.25	0.30	0.24
Geodetic mass balance			
σ_{geod}	0.16 (2003–15) 0.26 (2011–15)	0.37	0.32
SMB from snowline approach			
σ_{tsl}	0.27	0.32	0.36
σ_{map}	0.05	0.06	0.09
σ_{dis}	0.03	0.16	0.18
σ_{DEM}	0.12	0.03	0.02
σ_{meteo}	0.13	0.23	0.14
σ_{para}	0.20	0.17	0.20

uncertainty.

Table 7.5: Model sensitivity to the different constant input parameters for each glacier in m w.e. yr^{-1}. See text for details on the experiments.

sensitivity in	Abramov	Golubin	Glacier No. 354
$\delta T/\delta z$	0.06	0.14	0.05
$\delta P/\delta z$	0.07	0.08	0.01
R_{DDF}	0.11	0.25	0.06

7.5 Results

7.5.1 Long-term surface mass balances derived from snowline approach

We found that the mass balance model constrained by snowline observations is capable of representing the observed SCAFs on satellite and terrestrial camera images within ±8% for Abramov, ±13% for Golubin and ±9% for Glacier No. 354 (Fig. 7.7). Comparing the SCAF observed on camera and on spaceborne images for the same day reveals a RMSE of 2.5%. However, tests showed that the influence of the image source (terrestrial/spaceborne) on the inferred SMB is negligible.

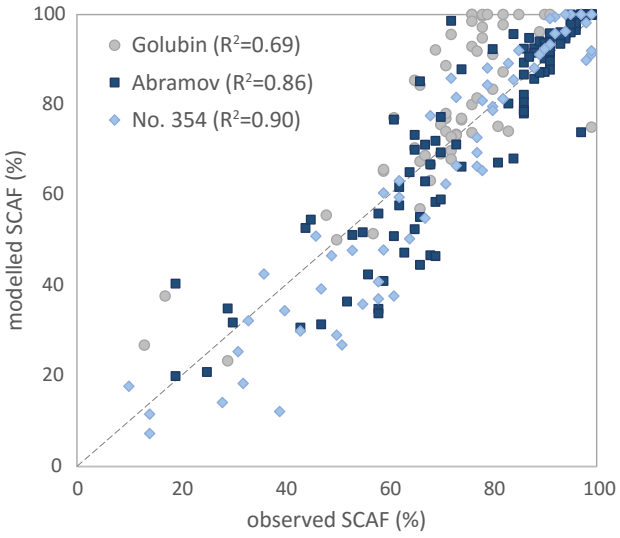

Figure 7.7: Comparison between observed and modelled SCAF for Abramov, Golubin, and Glacier No. 354.

Annual glacier-wide modelled surface mass balances constrained by snowline observations, calculated for Abramov (1998-2016), for Golubin (2000-2016), and for Glacier No. 354 (2004-2016), are predominantly negative (Fig. 7.8 and Table 7.6). Study periods depend on the data availability for each glacier. Abramov exhibited a mean annual SMB of -0.30 ± 0.19 m w.e. yr^{-1} from 2004 to 2016. For Golubin and Glacier No. 354 a slightly more negative annual average balance of -0.41 ± 0.33 m w.e. yr^{-1} and -0.36 ± 0.32 m w.e. yr^{-1}, respectively, was calculated for the same time period (Table 7.6). Length change measurements underline the observed negative balance regime of all three glaciers (Hoelzle et al, 2017). A significant glacier retreat was observed for the last century. A first speed-up of frontal retreat occurred in the 1980s and acceleration was observed in the last decade. However, no clear acceleration of mass loss for the three glaciers was iden-

tified over the investigated periods. Two phases of close-to-zero SMB could be recognized (2002-2005 and 2009-2011) for all glaciers. A lower standard deviation of annual mass balances from 2004 to 2016 is found for Glacier No 354 (0.19 m w.e. yr^{-1}) than for Golubin (0.4 m w.e. yr^{-1}) and Abramov (0.29 m w.e. yr^{-1}), which indicated higher interannual variability for the latter two. Glacier No. 354, receiving lower amounts of total annual precipitation, showed a smaller mass turnover and had a positive balance only in 2009 (Table 7.6). For Golubin most negative values were found in 2012 and 2014. Abramov and Golubin also had strongly negative balances in 2006 and 2008. For Abramov, the snowline observations indicated that the snowline rose close to the upper edge of the glacier already at the end of August. For Golubin, observations of the last image of the season showed that the SCAF decreased to less than 45% already in mid-August in 2006, similar to 2001 and 2015. The ablation season typically stretched until the end of September, and summer snowfalls during this month were rare (Aizen et al, 1995b), likely leading to continued mass loss. Data availability, however, was rather critical for Golubin in 2008, which is also reflected by the larger uncertainties. The last snowline observation dates from as early as the end of July.

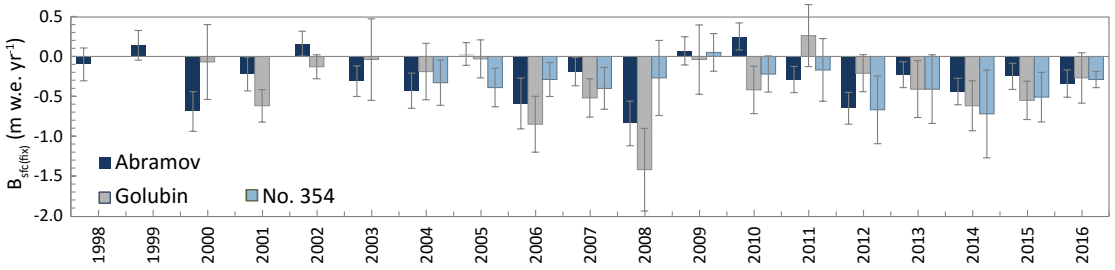

Figure 7.8: Modelled annual SMB $B_{\mathrm{sfc(fix)}}$ constrained by snowline observations for all three glaciers for the hydrological year.

7.5.2 Comparison to glaciological and geodetic mass balances

The glaciological and geodetic surveys delivered two extensive and independent datasets for validation of the modelled mass balance series constrained by snowline observations. Joint analysis of the data sets permitted robust conclusions to be drawn about the mass change and its temporal dynamics over the past two decades. The glaciological SMB measurements showed a good agreement with the SMB inferred using snowline observations for the same time periods (Table 7.7). Exact survey dates are given in table 7.2. Annual glaciological SMB was reproduced with an RMSE of less than ± 0.26 m w.e. yr^{-1} for all three glaciers using the snowline approach (Fig. 7.9). For Golubin and Glacier No. 354, the glaciological SMB was slightly more negative than the modelled SMB (Table 7.7). For Abramov, on the other hand, the glaciological SMB was somewhat less negative than the snowline-constrained model results. In general, a satisfactory agreement was obtained between the two methods for all three glaciers (Fig. 7.9). Squared correlation coefficients between snowline constrained model results and glaciological SMB ranged between r^2=0.63 (Abramov) and r^2=0.90 (Golubin).

Table 7.8 and Figure 7.10 summarize the results obtained from the different geodetic surveys. For the comparison with the geodetic mass change, an estimate for internal/basal mass balance was added to the modelled SMB constrained by snowline observations (see Subsection 7.3.6) and referred to as the modelled total mass change con-

Table 7.6: Annual, glacier-wide SMB for the three glaciers for the hydrological year $B_{\mathrm{sfc(fix)}}$ in m w.e. yr^{-1} inferred from the mass balance model constrained by snowline observations.

year	Abramov	Golubin	Glacier No. 354
1998	-0.10 ± 0.21		
1999	$+0.14 \pm 0.19$		
2000	-0.69 ± 0.25	-0.07 ± 0.47	
2001	-0.22 ± 0.21	-0.62 ± 0.20	
2002	$+0.16 \pm 0.16$	-0.13 ± 0.15	
2003	-0.31 ± 0.19	-0.04 ± 0.51	
2004	-0.43 ± 0.22	-0.19 ± 0.35	-0.33 ± 0.28
2005	$+0.03 \pm 0.14$	-0.03 ± 0.24	-0.39 ± 0.24
2006	-0.59 ± 0.32	-0.85 ± 0.35	-0.29 ± 0.21
2007	-0.19 ± 0.18	-0.52 ± 0.24	-0.40 ± 0.26
2008	-0.84 ± 0.28	-1.42 ± 0.52	-0.27 ± 0.47
2009	$+0.07 \pm 0.18$	-0.04 ± 0.43	$+0.05 \pm 0.24$
2010	$+0.25 \pm 0.17$	-0.42 ± 0.30	-0.22 ± 0.23
2011	-0.29 ± 0.16	$+0.26 \pm 0.39$	-0.17 ± 0.39
2012	-0.65 ± 0.20	-0.21 ± 0.23	-0.67 ± 0.42
2013	-0.23 ± 0.16	-0.41 ± 0.36	-0.41 ± 0.43
2014	-0.44 ± 0.17	-0.62 ± 0.31	-0.72 ± 0.55
2015	-0.25 ± 0.16	-0.55 ± 0.24	-0.51 ± 0.31
2016	-0.34 ± 0.17	-0.27 ± 0.31	-0.29 ± 0.10
2004-2016	-0.30 ± 0.19	-0.41 ± 0.33	-0.36 ± 0.32

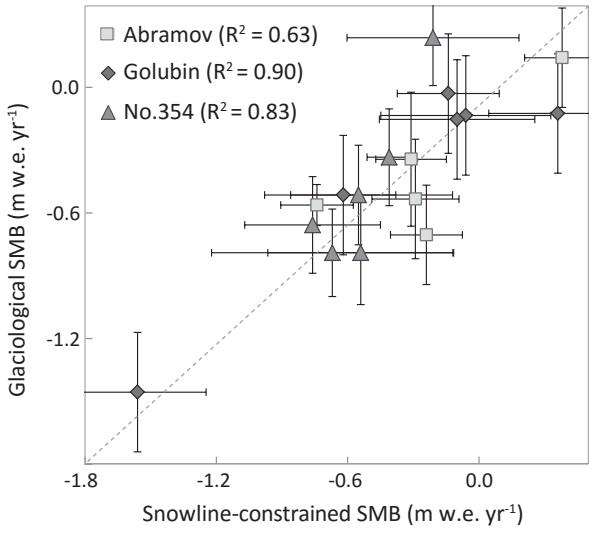

Figure 7.9: Comparison of modelled annual SMB constrained by snowline observations and glaciological SMB for Abramov, Golubin, and Glacier No. 354. Uncertainties in the annual SMB are indicated.

strained by snowline observations. The geodetic method reveals a total mass balance of -0.30 ± 0.37 m w.e. yr^{-1} for Golubin from 8 September 2006 to 1 November 2014 (Fig. 7.10). The corresponding total modelled mass balance constrained by snowline observa-

Table 7.7: Annual SMB $B_{\mathrm{sfc(meas)}}$ for the measurement periods (i.e., exact dates of the surveys (Table 7.2)) based on direct glaciological measurements and on the snowline-constrained model for the three glaciers in m w.e yr^{-1}.

	Abramov		Golubin		Glacier No. 354	
year	glaciological	snowline-constrained	glaciological	snowline-constrained	glaciological	snowline-constrained
2011			-0.06 ± 0.30	-0.05 ± 0.39	-0.21 ± 0.27	$+0.34 \pm 0.39$
2012	-0.29 ± 0.30	-0.47 ± 0.20	-0.14 ± 0.30	$+0.06 \pm 0.23$	-0.52 ± 0.26	-0.74 ± 0.42
2013	-0.31 ± 0.34	-0.27 ± 0.16	-0.10 ± 0.30	-0.07 ± 0.36	-0.54 ± 0.25	-0.45 ± 0.43
2014	-0.74 ± 0.10	-0.50 ± 0.17	-1.56 ± 0.30	-1.44 ± 0.31	-0.68 ± 0.22	-0.74 ± 0.55
2015	-0.24 ± 0.25	-0.65 ± 0.16	-0.62 ± 0.30	-0.45 ± 0.24	-0.68 ± 0.24	-0.60 ± 0.31
2016	$+0.38 \pm 0.25$	$+0.24 \pm 0.17$	$+0.36 \pm 0.30$	-0.04 ± 0.31	-0.41 ± 0.24	-0.26 ± 0.10
2011-2016	-0.24 ± 0.25	-0.33 ± 0.17	-0.35 ± 0.30	-0.33 ± 0.31	-0.51 ± 0.24	-0.41 ± 0.37

Table 7.8: Geodetic mass change $\Delta M_{\mathrm{geod(meas)}}$ and the total annual mass change derived from the snowline approach $\Delta M_{\mathrm{tsl(meas)}}$ for the three glaciers and for the periods corresponding to the geodetic surveys in m w.e. yr^{-1}.

	$\Delta M_{\mathrm{geod(meas)}}$	$\Delta M_{\mathrm{tsl(meas)}}$
Abramov		
2003-2015	-0.39 ± 0.16	-0.25 ± 0.20
2011-2015	-0.36 ± 0.26	-0.43 ± 0.17
Golubin		
2006–2014	-0.30 ± 0.37	-0.38 ± 0.35
Glacier No. 354		
2003-2012	-0.42 ± 0.07	-0.25 ± 0.31
2012-2015	-0.58 ± 0.31	-0.53 ± 0.43

tions was slightly more negative with -0.38 ± 0.35 m w.e. yr^{-1} for the same period (Table 7.8 and Fig. 7.11). Comparison of digital elevation models indicated that Glacier No. 354 had a mass balance of -0.58 ± 0.31 m w.e. yr^{-1} from 27 July 2012 to 1 October 2015 (Fig. 7.10) and -0.42 ± 0.07 m w.e. yr^{-1} from 1 September 2003 to 27 July 2012 (Kronenberg et al, 2016). The total annual mass change for the same time intervals derived from the snowline approach was -0.53 ± 0.43 m w.e. yr^{-1} and -0.25 ± 0.31 m w.e. yr^{-1}, respectively. For the first period, the results are in good agreement, whereas for the second period the mass balance model constrained by snowline observations indicates a significantly less negative mass balance (Fig. 7.11). For Abramov, a geodetic mass balance of -0.39 ± 0.16 m w.e. yr^{-1} from 27 August 2003 to 1 September 2015 and of -0.36 ± 0.26 m w.e. yr^{-1} from 29 November 2011 to 1 September 2015 was calculated. For the same periods, the snowline model reveals a total mass change of -0.25 ± 0.20 m w.e. yr^{-1} and of -0.43 ± 0.17 m w.e. yr^{-1}, respectively. For the first period, the modelled mass balance constrained by snowline observations indicates a less negative mass balance, whereas the second period is in good agreement (Table 7.8 and Fig. 7.11). For all three glaciers and periods studied the differences are within the error margins.

7.6 Discussion

7.6.1 More accurate modelling through integrating snowline observations

In order to demonstrate the advantage of using snowline observations on repeated remote sensing data throughout the melting season for increasing the confidence in mass balance

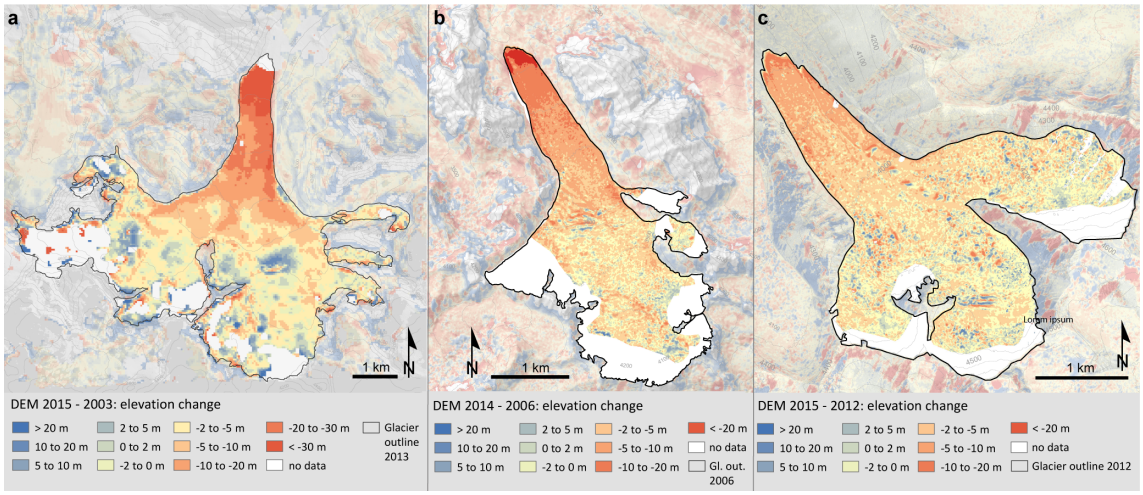

Figure 7.10: Geodetic mass balance for (**a**) Abramov from 2003 to 2015, (**b**) Golubin from 2006 to 2014 and for (**c**) Glacier No. 354 from 2012 to 2015.

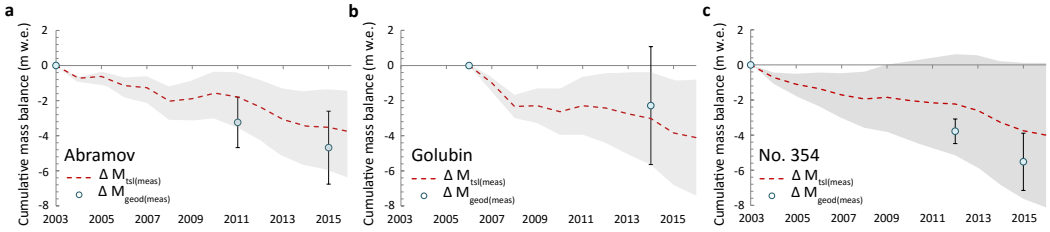

Figure 7.11: Cumulative snowline-constrained modelled mass change $\Delta M_{\mathrm{tsl(meas)}}$ (red) in comparison to the geodetic mass change $\Delta M_{\mathrm{geod(meas)}}$ (circles) for (**a**) Abramov, (**b**) Golubin and (**c**) Glacier No. 354. The shading indicates the uncertainty range of the mass change from the snowline approach.

modelling, we ran the same accumulation and temperature-index model without the use of snowlines or any other direct observations for calibration for all three glaciers from 2004 to 2016 (See Section 7.3.6). The same constant parameters were used (Table 8.1). We chose C_{prec} to account for a 20%-measurement error of observed precipitation (Sevruk, 1981), and a combination for DDF_{ice} ($7.0\,\mathrm{mm\,day^{-1}\,^{\circ}C^{-1}}$) and DDF_{snow} ($5.5\,\mathrm{mm\,day^{-1}\,^{\circ}C^{-1}}$) as recommended by Hock (2003) for the former Soviet territory, for all three glaciers. Similar values were used to model glaciers in the Tien Shan and Himalayas (e.g. Zhang et al, 2006; Wu et al, 2011; Shea et al, 2015). All parameters were held constant over time. Figure 7.12 shows the difference between the cumulative SMB derived from our model constrained by snowline observations, and the results obtained with an unconstrained mass balance model. The results clearly indicate the potential of the snowline approach to infer SMB series of unmeasured glaciers without any additional information. The unconstrained mass balance model overestimates mass loss by almost five times for Abramov and for Glacier No. 354, whereas mass loss for Golubin is about three times higher (Fig. 7.12).

7.6.2 Intercomparison of methods to determine glacier mass balance

A satisfying agreement was found between all three independent methods used to compute glacier-wide mass balance for the three benchmark glaciers in the Central Tien Shan and

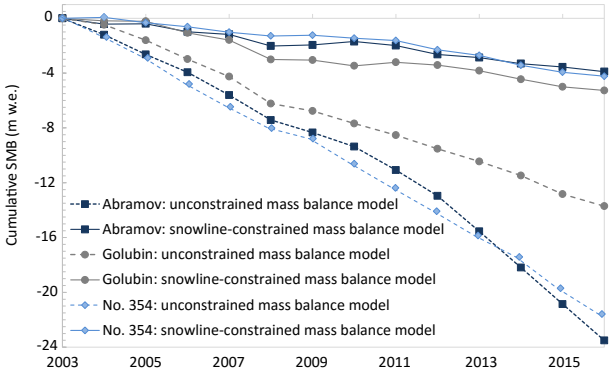

Figure 7.12: Comparison of the cumulative SMB derived from unconstrained mass balance modelling to the results obtained from snowline-constrained modelling from 2004 to 2016.

Pamir-Alay for the past two decades. In the following, we discuss shortcomings and advantages of each method and point out the limitations of the individual approaches.

The snowline model reproduces the direct measurements well and shows a satisfactory performance for all three glaciers (Table 7.8, 7.6 and Fig. 7.13). For Glacier No. 354, a larger misfit between the glaciological SMB and the snowline-constrained model results was found, especially for 2011. A possible reason might be the limited stake network at the initiation of the monitoring programme, errors of the stake readings and an unknown measurement date for some ablation stakes, affecting the calculation of the glaciological SMB for the considered year. Discrepancies between the two approaches are also found for Golubin for 2016 and for Abramov for 2015. For Abramov, summer snowfalls in mid-August 2015 stopped the ablation season early. This pattern is mirrored in the daily SMB derived from the snowline approach. For Golubin, the last snowline observation is from the end of August and matches the field observations. No clear indication of a poor performance of the snowline approach could thus be identified for both glaciers for the considered years.

An important problem is related to the varying measurement periods of the glaciological SMBs for the selected glaciers (Table 7.2). Due to changing period lengths, the data do not always represent a complete mass-balance year, and might thus not be representative, making comparison of the results with other methods, glaciers and regions difficult. Interpretation of the results, their contextualization and application in other study fields, such as in hydrology or climatology, are also hampered through the varying and irregular investigation periods. Based on our methodology, we are now able to derive homogenous SMBs for comparable periods of the hydrological year.

An important factor limiting the applicability of mass balance modelling constrained by snowline observations is the dependence on good satellite imagery to map the snowline throughout the ablation season. However, the sensitivity analysis (Section 7.4) shows that a minimum of only two images that are well distributed throughout the ablation season are sufficient to retrieve reliable results. Image availability is most important close to the end of the ablation season. Taking into account the increasing number of satellite sensors that provide a range of possibilities to observe snowlines in the future will partly resolve this limitation. By comparing the snowline-derived daily SMBs for the years in which seasonal in situ measurements are available, we were able to investigate the effect on the results of the two parameters used for model calibration. The mass balance of Golubin is

slightly underestimated at the beginning of the ablation season, and hence the modelled melt is also too low (Fig. 7.13b). This shortcoming of the calibration procedure cannot be overcome without including additional data, such as e.g. measurements of winter snow accumulation which is difficult on remote glaciers.

SMBs inferred from the snowline approach are closely tied to the representativeness of snowline observations. The method might be able to yield reliable SMB estimates for many glaciers in different climatic regimes, for which the transient snowline is an indicator of the surface mass balance. The relationship between the snowline and the SMB can however be importantly challenged when the position of the transient snowline is blurred by fresh snow or superimposed ice. The applicability of the snowline approach presented here can thus be critical when the transient snowline on remote sensing data cannot unambiguously be identified. This is mainly a problem for glaciers with a summer accumulation regime due to frequent fresh snow falls, and glaciers with a high relevance of superimposed ice.

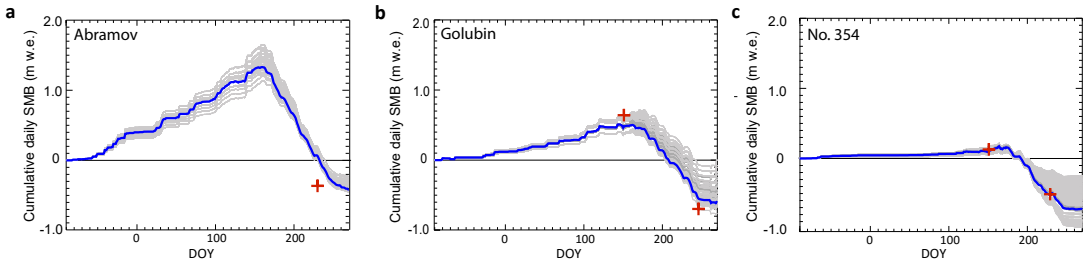

Figure 7.13: Cumulative daily glacier-wide SMBs inferred from the snowline approach for (**a**) Abramov, (**b**) Golubin and (**c**) Glacier No. 354 for the year 2014 (blue line). The grey lines indicate the spread obtained by using different constant parameters to run the model (Section 7.4) and the red cross indicates the measured glaciological SMB for both the winter and the annual period.

The geodetic mass balance and the results obtained from the snowline approach agree well, in particular for the recent years (Fig. 7.11). Overall, a slightly greater mass loss is calculated for Abramov and Glacier No. 354 using DEM differencing. Especially during the earlier part of our study period, the mass balance inferred with the snowline approach seems to be not negative enough. Limitations related to the geodetic approach are mainly connected to the limited stereo acquisitions in the first years of the 21^{st} century. In recent years, image availability strongly increased, but it is still not common to find a suitable scene from the end of the hydrological year for any glacier or region with sufficient quality for a sound geodetic evaluation. Fresh snow or low image contrast (in particular in the accumulation areas) interfere with DEM quality but cannot be avoided and have thus to be corrected for, increasing the uncertainty of the result. We present geodetic mass balances for periods shorter than five years, a critical time interval for an accurate volume-to-mass conversion. Huss (2013) showed a high variability of the volume-to-mass conversion factor for short observation periods ($\leq$ 3 years), especially for glaciers with close-to-zero mass balances in combination with strongly varying mass balance gradients. For the observation periods considered in this study, annual mass balances were predominantly negative but moderate variations of the mass balance gradients have been observed (Barandun et al, 2015; Kronenberg et al, 2016). We identified a rather large elevation change for the short observation periods, and are thus confident that the chosen conversion factor lies within the uncertainty range assigned here (see Section 7.4).

The glaciological and the modelled results constrained by snowline observations re-

fer to surface mass balance components only. The geodetic mass balance, on the other hand, takes into account the total glacier mass change, thus including internal and basal ablation and accumulation. This is a limiting factor for direct comparison. Evidence of refreezing meltwater in cold firn is reported for all three glaciers (Suslov et al, 1980; Aizen et al, 1997; Dyurgerov and Mikhalenko, 1995) and can have a significant effect on the total mass change. The values used in this study to account for internal and basal mass balance are first-order approximations which improve the comparability between the different methods. However, the uncertainties in these estimates are considerable.

7.6.3 Comparison to other studies

We performed a comprehensive comparison of long-term averages of mass balance derived from the snowline approach to independent studies based on geodetic surveys using different sensors and modelling, both for the investigated glaciers as well as for the regional mass budget (Fig. 7.14). Note that the study periods vary between the different studies and results might thus not be directly comparable.

For Abramov, we find mass balances inbetween the results derived by Gardelle et al (2013) and Brun et al (2017) based on the comparison of DEMs, overlapping within the respective uncertainty ranges. Mass changes reported by Gardelle et al (2013) are most likely too positive as SRTM C-Band penetration depth into snow (Kääb et al, 2015; Berthier et al, 2016) might have been underestimated for the cold and dry snow of accumulation areas (Dehecq et al, 2016). The average mass balance for Abramov of $-0.38 \pm 0.10\,\mathrm{m\,w.e.\,yr^{-1}}$ (2002-2014) derived by Brun et al (2017) using multi-temporal optical ASTER DEMs indicates a stronger mass loss than the results obtained with the snowline approach. We note, however, that the start and end dates of their geodetic mass balance assessment represent a mean over a mosaic of different dates, thus hampering direct comparison. In addition, the differences are still within their error bounds. The results by Brun et al (2017) are in line with the geodetic mass balance calculated in the present study for the period 2003 to 2015 based on high-resolution satellite images.

For Golubin, the inferred mass balance is in close agreement with the geodetic mass change reported by Bolch (2015) (Fig. 7.14b). Brun et al (2017) computed a mass balance of $-0.04 \pm 0.19\,\mathrm{m\,w.e.\,yr^{-1}}$ for ≈2002-2013, which is consistently less negative than our estimate but still lies within the respective error bounds. For Glacier No. 354, an excellent agreement between all available mass balance assessments was found (Fig. 7.14c). Brun et al (2017) reported a mass balance of $-0.46 \pm 0.19\,\mathrm{m\,w.e.\,yr^{-1}}$ for ≈2002-2014.

We also compared our results for the investigated glaciers to region-wide assessments in order to investigate their regional representativeness (Fig. 7.14d-f). Brun et al (2017) divided the Pamir-Alay and the Pamir into two different regions, whereas Gardner et al (2013), Gardelle et al (2013), Kääb et al (2015) and Farinotti et al (2015) did not make this distinction. For the Pamir, widely varying mass balance estimates were presented by the different studies, which might be related to important methodological differences and inconsistent time periods considered. Our results for Abramov are close to the average of the regional studies (Fig. 7.14d). The interannual variability and, in particular, a very negative mass balance in 2008 and a positive balance in 2010 for Abramov found in the present study agrees well with modelled mass balance series reported by Pohl et al (2017) for the Pamir from 2002 to 2013. The snowline-constrained modelled mass balance for Golubin agrees with the region-wide estimates by Brun et al (2017) but indicates smaller mass losses than other large-scale studies (Fig. 7.14e). Close agreement between the

different regional studies is found for the Central/Inner Tien Shan, where Glacier No. 354 is located (Fig. 7.14f).

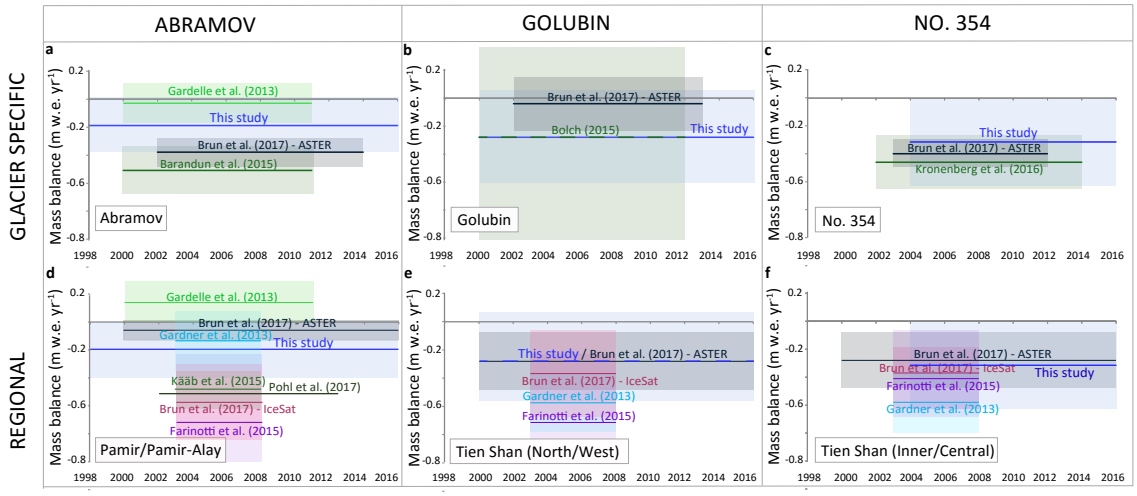

Figure 7.14: Long-term average mass balances from various studies in comparison with the snowline-constrained modelled mass balance for (**a**) Abramov, (**b**) Golubin, (**c**) Glacier No. 354. Results from the snowline approach for the three glaciers are compared to region-wide mass balance estimates for (**d**) the Pamir, for (**e**) Tien Shan (North/West) and for (**f**) the Tien Shan (Inner/Central). Lines indicate the mean annual mass balance over the respective periods for each study, and shaded squares represent the corresponding uncertainty. For the study by Brun et al (2017) results based on ASTER DEMs and IceSat are presented separately.

7.7 Conclusions

In this study we used three independent methods to reconstruct robust mass balance series at high temporal resolution for Abramov, Golubin and Glacier No. 354 located in the Pamir-Alay and Tien Shan mountains for the past two decades – a period for which only little is known about glacier behaviour. We proposed a methodology to derive glacier SMB series for unmeasured glaciers based on mass balance modelling constrained by repeated snowline observations relying either on in situ temperature and precipitation data or climate Reanalysis datasets. We recommend including snowline observations in the glacier monitoring strategy to reduce uncertainty and to increase robustness of the data. We used extensive geodetic and glaciological surveys to validate the results and found satisfying agreement between the independent methods. Our snowline approach reproduced observed annual to decadal SMB for all three glaciers and enabled the calculation of daily SMBs for arbitrary periods, and is, hence, capable of covering the entire hydrological year based on minimal data input. Some of the shortcomings of the glaciological and geodetic surveys could thus be overcome.

The results of all three methods confirm a continuous mass loss of the three glaciers Abramov, Golubin and Glacier No. 354 since ≈2000 but no clear SMB trend could be identified for the time period considered. Our results suggest a slightly less negative SMBs for Abramov of -0.30 ± 0.19 m w.e. yr^{-1} located in the Pamir-Alay than for the Tien Shan glaciers Golubin of -0.41 ± 0.33 m w.e. yr^{-1} and Glacier No. 354 of -0.36 ± 0.32 m w.e. yr^{-1}

from 2004 to 2016. Periods of almost balanced mass budgets were observed from 2002 to 2005 and from 2009 to 2011. The mass balance of 2006 to 2008 was very negative for Abramov and Golubin. Glacier No. 354 showed a weaker interannual variability than the other two glaciers. Model sensitivity experiments revealed a relatively small sensitivity to the input parameters and the meteorological data used, indicating a considerable advantage in comparison to conventional mass balance modelling that does not include direct glacier-specific observations. Our results show that with a minimum of two snowline observations, ideally at the beginning and the end of the ablation season, reliable estimates of the annual SMB can be inferred.

At present, mass balance observations in the Pamir and Tien Shan are relatively sparse but crucially needed to improve understanding of glacier behaviour in the region and its effect on future water availability. Direct measurements are important but costly and laborious and require an immense logistic effort. For remote and unmonitored regions and countries, lacking in financial resources and infrastructure to support such monitoring programmes, our proposed approach delivers a tool for investigating and reconstructing the SMBs of unmeasured and remote glaciers with minimal effort. The integration of snowline observations into conventional modelling is shown to be highly beneficial for filling the gaps in long-term SMB series for periods for which direct glaciological measurements were discontinued or are missing completely.

Data availability

Measurements and detailed model results are available in the Supplementary Material. Model code and raw data are available upon request from the first author (M. Barandun) or be downloaded through official, open-access databases and online portals (see Supplementary Material for more information.

Author contribution

MB, MHo and MHu conceived of the presented idea. MB developed and applied the mass balance model, detected the snowlines and derived the geodetic mass balance for Golubin and No. 354 with support of AK. AK, TB, EB provided the satellite data. EB calculated the geodetic mass balance for Abramov. MB performed the uncertainty analysis, the validation and interpretation with help of MHo, MHu, EB, AK. MB, EA analyzed the mass balance field measurements. MB wrote the manuscript with help from MHu, MHo and EB. MHo, MB, MHu, LS organized, helped and performed the field measurements.

Acknowledgments

This study is supported by the Swiss National Science Foundation (SNSF), grant 200021_155903. Additional support by the German Federal Foreign Office in the frame of the CAWa project (http://www.cawa-project.net) and the support of the Federal Office of Meteorology and Climatology MeteoSwiss through the project Capacity Building and Twinning for Climate Observing Systems (CATCOS) Phase 1 & 2, Contract nos. 7*F*-08114.1, 7*F*-08114.02.01, between the Swiss Agency for Development and Cooperation (SDC) and MeteoSwiss as well as the project CICADA (Cryospheric Climate Services for improved Adaptation), and contract no. 81049674 between Swiss Agency for Development and Cooperation and the University of Fribourg is equally acknowledged. E. Berthier acknowledges support from the French Space Agency (CNES) and the Programme National de Télédétection Spatiale grant PNTS−2016−01. A. Kääb and T. Bolch acknowledges

funding by ESA (Glaciers_cci project 4000109873/14/I-NB), and the European Union Seventh Framework Program (FP7) under European Research Council (ERC) contract 320816. We thank F. Brun for providing the elevation change data of Abramov, Golubin and Glacier No. 354. J. Corripio is acknowledged for the software to georeference oblique photographs. We extend our thanks as well to T. Saks, A. Ghirlanda, A. Gafurov, M. Kronenberg, D. Sciboz and all others who contributed with fieldwork. We are also grateful for the collaboration of Central Asian Institute for Applied Geosciences, especially to B. Moldobekov for his continuous support. The Kumtor Gold Company provided the meteorological data. We thank S. Braun-Clarke for the proofreading and linguistic revision. Constructive comments by the anonymous reviewer and Prof. Dr. M. Pelto were very helpful to finalize the manuscript.

Chapter 8

Paper IV: Region-wide estimate of annual glacier mass balance for the Tien Shan and Pamir from 2000 to 2017

Barandun, Martina, *McNabb Robert, Naegeli Kathrin, Huss Matthias, Bunting Pete, Berthier Etienne and Hoelzle Martin. "Region-wide estimate of annual glacier mass balance for the Tien Shan and Pamir from 2000 to 2017", Frontiers in Earth Science: in preparation.*

Abstract

The Tien Shan and Pamir are among the largest mountain ranges on earth, hosting more than 25,000 glaciers. Most glacier mass balance assessments focus on region-wide, decadal mass changes and only a few address seasonal or annual mass balance series for Central Asia. Hence, the regional annual variability is so far poorly understood. Here, multi-annual glacier mass changes derived from remote sensing were complemented with seasonal to annual mass balance series inferred from modelling closely constrained with repeated transient snowline observations on a regional scale. We calculated geodetic mass loss for the entire Tien Shan and Pamir from 2004 to 2012 and annual surface mass balance time series for the glaciers of the three mountain ranges: the Kyrgyz Ala-Too, the Pamir-Alay and the Akshiirak range from 2000 to 2017. To derive annual time series, transient snowline observations were used to calibrate an accumulation and temperature-index melt model for each year and glacier individually. Then, the modelled decadal mass balance was constrained with glacier specific geodetic mass balances calculated from satellite stereo images. The data set permitted to not only observe decadal changes but also to infer interannual mass balance variability for all investigated glaciers. A geodetic mass loss of $-0.52 \pm 0.53\,\mathrm{m\,w.e.\,yr^{-1}}$ was calculated for the Tien Shan and $-0.24 \pm 0.43\,\mathrm{m\,w.e.\,yr^{-1}}$ for the Pamir from 2004 to 2012. With the transient snowline-constrained modelling, we confirmed the decadal mass loss ranging from -0.36 ± 0.32 to $-0.44 \pm 0.32\,\mathrm{m\,w.e.\,yr^{-1}}$ for 2000 to 2017 for the Kyrgyz Ala-Too, the Pamir-Alay and the Akshiirak range. Our results showed a significant trend to increased mass loss for the Pamir-Alay and the Kyrgyz Ala-Too, accompanied with a moderate increase of the interannual variability. For the Akshiirak, no significant trend was observed but mass balances and interannual vairability showed to have increased in more recent years.

8.1 Introduction

The Tien Shan and Pamir, forming part of High Mountain Asia (HMA), are among the largest mountain ranges on earth, encompassing more than 25,000 glaciers (RGI-Consortium, 2017). Most glaciers around the world are in retreat and mass loss has accelerated during the past decades (Zemp et al, 2015). Glaciers in HMA have been observed to respond heterogeneously to climate change (Scherler et al, 2011; Bolch et al, 2012; Kääb et al, 2012). This is not only connected to diverging climatological settings, including very humid conditions as well as extremely arid, continental environments (Schiemann et al, 2007; Yao et al, 2012; Maussion et al, 2014; Sakai and Fujita, 2017), but also relates to contrasting glacier area-altitude distributions throughout HMA (Fujita and Nuimura, 2011). So far, glacier mass change assessments are sparse for the Central Asian Mountains but a few regional studies reveal a similarly complex and diverse pattern, as observed for remaining HMA (Gardner et al, 2013; Farinotti et al, 2015; Brun et al, 2017; Wang et al, 2017).

The scarcity of reliable and appropriate glaciological datasets, as well as the heterogeneity of both their spatial and temporal extent for the Tien Shan and Pamir, hamper sound synthesis to a regional picture on annual to seasonal time scale (Unger-Shayesteh et al, 2013; Gan et al, 2015). Especially since the late 1990s barely any direct measurements are available until 2010, when several glacier monitoring sites were revived (Hoelzle et al, 2017). Remote sensing techniques have helped to fill such survey gaps and are a powerful tool to study a large number of inaccessible glaciers on a cost-effective basis. This can partly bridge the aforementioned deficit in data availability (e.g., Kääb et al, 2015; Brun et al, 2017; Wang et al, 2017). However, at the current stage of research, remotely

sensed mass change observations are generally limited to decadal / semi-decadal temporal resolution, and, hence, do not allow detailed understanding of the processes driving mass balance changes. Thus, region-wide assessments cannot rely solely on geodetic surveys but also need to be combined with other techniques to investigate glacier mass changes at annual to seasonal time scales.

One of the first to introduce the use of transient snowlines (TSL) in relation with direct mass balance observations was Dyurgerov et al (1994), who used intense direct glaciological and TSL measurements during one summer season to establish a relationship for all possible TSLs with the mass balance. Huss et al (2013) and Hulth et al (2013) used TSLs to infer winter snow accumulation. Whereas Hulth et al (2013) calibrated a melt model using direct ablation measurements and emphasized the use of the remotely sensed TSL to infer a correct winter accumulation, Huss et al (2013) resigned completely from the use of field observations. Huss et al (2013) relied on the combination of a relation between the transient mass balance and the TSL to infer the sub-seasonal mass balances based simply on the information content stored in the rate of change of the TSL and its position on repeated oblique photography. Barandun et al (2018) further developed the approach by Huss et al (2013) and used transient snowlines to constrain a mass balance model on three selected glaciers in the Tien Shan and Pamir. This approach avoids equally the use of in situ glaciological measurements for calibration. Direct measurement and geodetic estimates were used for validation only. Barandun et al (2018) showed that the integration of snowline observations into conventional modelling is highly beneficial for filling the gaps in long-term mass balance monitoring.

Here, we apply this approach by Barandun et al (2018) in combination with multi-annual glacier mass changes derived from remote sensing for almost 80% of all 209 glaciers larger than 2 km^2 located in the Kyrgyz Ala-Too, the Akshiirak massif and the Pamir-Alay, respectively, from 2000 to 2017. With the help of mass balance modelling, we provide, for the first time, annual surface mass balance (SMB) time series, closely tied to TSL observations to complement multi-annual geodetic surveys for data-sparse mountain ranges in Central Asia.

We used semi- to decadal geodetic mass balances calculated from freely available Advanced Spaceborne Thermal Emission and Reflection Radiometer (ASTER) L1A and from High Mountain Asia DEM (HMA DEM) data for the entire Tien Shan and Pamir. The glacier-specific decadal to semi-decadal geodetic mass change are used to constrain the modelled mass balance time series in order to reach agreement between the two estimates. This second-order calibration aims at a combination of different independent methods.

Through combining geodetic assessments with TSL-constrained modelling, we implement a tool for an optimal reconstruction of annual mass balance time series of a large amount of unmeasured and remote glaciers on mountain range scale. The obtained mass balance time series permit to not only observe decadal changes for a large number of glaciers in the Tien Shan and Pamir, but also to infer annual mass balance variability for the investigated glaciers with minimal cost and labour effort through a combination of information from geodetic mass changes and temporal variations of the snow cover. The provided results enable an in depth analysis of the regional and temporal distribution of the mass balance in relation to their topographic characteristics and revealed for the first time detailed insights on temporal changes of the past decades for data sparse regions.

8.2 Study Site and Data

8.2.1 Study sites

The Central Asian mountain ranges Tien Shan (glacierised area:12,385 km^2 RGI-Consortium, 2017) and Pamir (glacierised area:12,083 km^2 RGI-Consortium, 2017) have been separated into seven subregions for the geodetic assessment: Western / Northern Tien Shan, Eastern Tien Shan, Central Tien Shan, Dzhungarsky Alatau, Pamir-Alay, Western Pamir and Eastern Pamir. The subdivision is based on Bolch et al (in press).

Both the Tien Shan and Pamir are known to host numerous surge-type glaciers (Mukherjee et al, 2017; Kotlyakov et al, 2008; Gardelle et al, 2012b). Mukherjee et al (2017) confirmed 9 glaciers of the Central Tien Shan as active surge type glaciers and reported another 13 as very probable to surge. In the Pamir, 215 glaciers have been identified to show signs of repeated surge activity (Kotlyakov et al, 2008). Furthermore, many glaciers of the study area are heavily debris-covered in their ablation areas and debris thickness can range considerably (Kraaijenbrink et al, 2017).

Glaciers in the western part of the Tien Shan and Pamir are characterized by winter accumulation, whereas summer accumulation regimes become more frequent towards the central and eastern part (Dyurgerov et al, 1994), where a combination of low air temperatures and a coinciding summer precipitation maxima is more common (Kutuzov and Shahgedanova, 2009). This is accompanied with a pronounced west to east gradient in seasonal precipitation distribution (Hoelzle et al, 2017) and the glacier area-altitude distribution (RGI-Consortium, 2017). A consistent temperature and precipitation increase throughout the Tien Shan since the 1940s was described by different authors (Aizen et al, 1996; Kutuzov and Shahgedanova, 2009; Kriegel et al, 2013). Pohl et al (2017) reported increasing temperature trends for the Pamir, however did not find a clear precipitation trend.

Region-wide geodetic mass balance assessments agree on a glacier mass loss for the Tien Shan during the past two decades. Results range between about -0.3 to $-0.7\,\mathrm{m\,w.e.\,yr^{-1}}$ for different regions and periods (Gardner et al, 2013; Farinotti et al, 2015; Brun et al, 2017). For the Pamir, reported mass change are far more contradicting, ranging from a close to balanced budget (about $+0.14$ to $-0.13\,\mathrm{m\,w.e.\,yr^{-1}}$, Gardelle et al, 2013; Gardner et al, 2013; Brun et al, 2017) to strongly negative mass balances (about -0.48 to $-0.52\,\mathrm{m\,w.e.\,yr^{-1}}$, Kääb et al, 2015; Pohl et al, 2017) for roughly the past two decades.

During Soviet times, long-term glaciological measurements were carried out on a range of glaciers distributed over the different subregions, but most monitoring programmes abruptly stopped in the mid-1990 (Hoelzle et al, 2017). Only two continuous long-term mass balance series are available for the Tien Shan; one for Tuyuksu Glacier (Kazakhstan) situated in the Western / Northern Tien Shan and one for Urumqi Glacier (China) located in the Eastern Tien Shan. Since 2010, several monitoring sites have been (re-)established and continued until today in the Western / Northern and Central Tien Shan (Fig. 8.1; Hoelzle et al, 2017). In the Pamir, long-term glacier monitoring during Soviet times was concentrated on Abramov Glacier, located in the Pamir-Alay. The direct measurements stopped in 1999 and were re-initiated in 2011 (Barandun et al, 2013). For the remaining part of the Pamir, only a few sporadic direct glacier mass balance observations are available (WGMS, 2017).

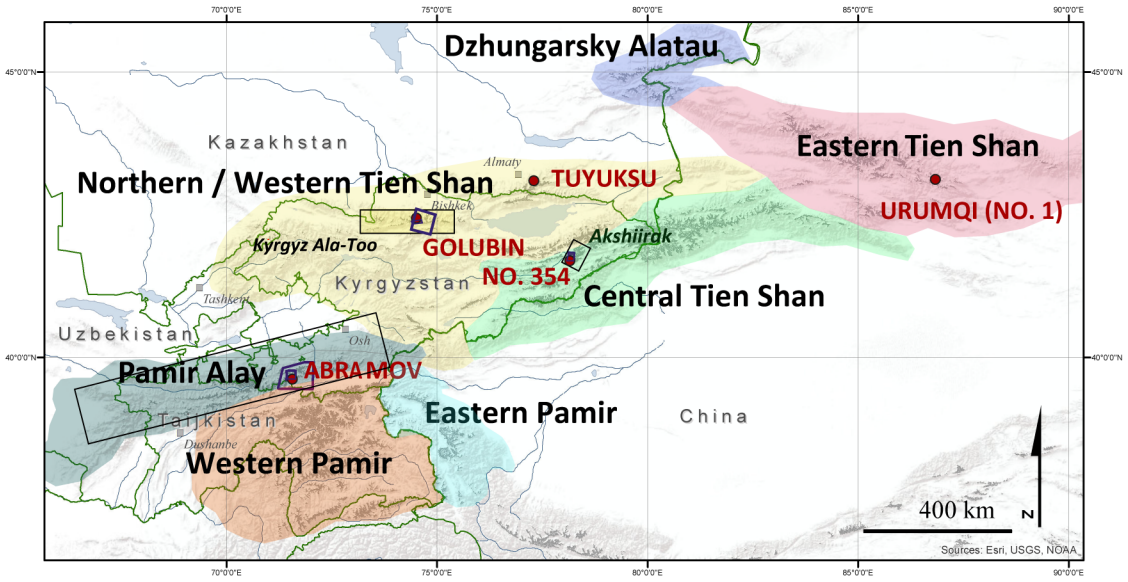

Figure 8.1: Overview map of the study region. The seven subregions of the geodetic assessments are shown in blue (Dzhungarsky Alatau), red (East Tien Shan), yellow (West / North Tien Shan) and in light green (Central Tien Shan) located in the Tien Shan and in dark green (Pamir-Alay), light blue (East Pamir) and orange (West Pamir) in the Pamir. Regions for which annual mass balance has been inferred with the TSL-constrained modelling are indicated with black squares. The location of all glaciers with long-term mass balance series are indicated with red dots. The footprints of the available high-resolution images are indicated in purple.

Study site for TSL-constrained modelling

The TSL-constrained model was applied on three mountain ranges: the Kyrgyz Ala-Too, the Akshiirak range and the Pamir-Alay (Fig. 8.1). The Kyrgyz Ala-Too forms part of the West / North Tien Shan. The mountain range hosts 565 glaciers of which 23 are larger than 2 km^2. The 23 glaciers cover a surface area of 68 km^2. The Akshiirak massif located at the northwestern margin of the Central Tien Shan counts 204 glaciers in total. 31 are larger than 2 km^2 and cover a total surface of 270 km^2. The glaciers receive an important share of their accumulation during summer (Dyurgerov et al, 1994; Ozmonov et al, 2013) and 11 glaciers show a surge-type behaviour (Mukherjee et al, 2017). The Pamir-Alay contains over 3,000 glaciers (1,848 km^2) of which only 151 are larger than 2 km^2, covering 45% of the total glacierised area. Active surges were reported for two glacier of the range (RGI-Consortium, 2017).

8.2.2 Data

A total of 1213 Landsat TM/ETM+ and OLI surface reflectance level-2 science products with cloud cover of less than 50% were collected for automated surface classification. These products consist of six (TM/ETM+) or seven (OLI) individual spectral bands in the wavelength range of around 440 nm to 2300 nm, with slight deviations of the individual band widths for the specific sensors. They are atmospherically corrected but lack a correction for topographic or shadow effects. More detailed information about these level-2 science products can be found in the product guides provided by the U.S. Geological

Survey and Masek et al (2006), Claverie et al (2015) and Vermote et al (2016) provide details concerning their performance compared to other datasets.

To compute geodetic mass balances, we used 1034 individual ASTER L1A scenes and HMA DEMs. We used all available scenes with at most 50% cloud cover, with scenes ranging from 30th of June 2000 to 2nd of November 2017. We relied on DEMs from high-resolution optical satellite data available from other studies (Gardelle et al, 2013; Kronenberg et al, 2016; Barandun et al, 2018) for validation of the ASTER derived terrain models (Fig. 8.1). We used the freely available, void-filled Shuttle Radar Topography Mission (SRTM, Jarvis et al, 2008) DEM as topographic input for each glacier for modelling, to infer altitudinal distribution of the albedo and as reference DEM for the ASTER processing with Mic Mac ASTER (MMASTER) (Girod et al, 2017b). We chose a lower limit in size of 1 km^2 that accounts for around 70% of the total glacierised area as adequate for the geodetic mass change calculations, whereas TSL-constrained mass balance determination (see 8.3) was applied on glaciers larger than 2 km^2. The latter limit is related to the capability of sound TSL detection on satellite images.

Glacier outlines are taken from the RGIv6 (RGI-Consortium, 2017) and are kept unchanged over time.

ERA-interim 2 m-air temperature and total precipitation daily products were downloaded. For each glacier the dataset of the closest grid cell was corrected to the median elevation of the glacier with a constant temperature lapse rate of $-6° \, C \, km^{-1}$.

Long-term mass balance series available for Golubin (Barandun et al, 2018), for Glacier No. 354 (Kronenberg et al, 2016), for Abramov (Barandun et al, 2015, 2018), and for Tuyuksu and Urumqi (WGMS, 2017) were compiled. The locations of the glaciers are indicated in Figure 8.1.

8.3 Methods

8.3.1 Automatic TSL mapping

The mapping of TSLs is carried out automatically on the surface reflectance maps of Landsat TM/ETM+ and OLIs scenes. Thereby, we derive spatially distributed shortwave broadband albedo for the glacierised area of each image to discriminate snow-covered and bare-ice surfaces using an automated, multi-step classification scheme (Naegeli and Huss, 2017; Naegeli et al, 2018). In a first step, the Spectral Angle Mapper (SAM) classification algorithm implemented in ENVI with manually derived, sensor-specific spectral libraries for different cloud signatures was used for cloud detection (Kruse et al, 1993; Naegeli et al, 2018). Hence, for each scene a cloud mask was obtained that was used to exclude cloud-affected pixels from all consecutive analyses. In a second step, we applied the narrow-to-broadband conversion by Liang (2001) to obtain shortwave broadband albedo from the individual spectral bands. The conversion is based on five of the seven individual bands. For Landsat OLIs, the band numbers were adjusted accordingly (Naegeli et al, 2017; Naegeli and Huss, 2017). Naegeli et al (2017) demonstrated the high accuracy of such albedo products.

In order to automatically pre-select the Landsat scenes for the surface-type classification, images with less than 20% information content above and below the median glacier elevation were removed. Most important classification steps according to the albedo values are summarized hereafter and more details can be found in Naegeli et al (2018).

First, two threshold values for *c*ertainly snow (α >0.5) and *c*ertainly ice (α <0.2) were defined based on literature (Cuffey and Paterson, 2010). Critical albedos, for which an

unambiguous assignment of the surface type was not possible, vary between a value of 0.2 and 0.5. Values within this range were evaluated according to their spatial distribution. Therefore, the average albedo in each 30 m-elevation band within the critical albedo range was considered. The mean TSL was defined based on the greatest slope of the albedo-elevation profile. The albedo for this altitude was considered to be the site- and scene-specific albedo threshold (α_{crit}) discriminating snow from ice / firn. The TSL and α_{crit} were used as reference to re-evaluate the surface type within the range of critical albedo values of each scene individually.

In a last step, all grid cells were examined regarding their relative position compared to the TSL in order to reclassify extreme outliers based on a probability-based approach. Thereby an increasing positive / negative vertical distance from the TSL results in a decrease in likelihood of the cell to associate to either class, or grid cells are accordingly reclassified. Additionally, to avoid misclassification of completely snow-covered glacier surfaces, we assume that the median albedo of >0.32 within the lower quarter of the glacier is only exceeded in the case of an entirely snow-covered glacier. After the binary surface classification into snow and ice / firn, the TSL and the snow-covered-area fraction (SCAF), thus the area of the glacier that is snow-covered in relation to the total glacier area, were calculated for each glacier and scene.

The TSLs used for model calibration were filtered automatically to avoid misclassified TSLs due to sporadic fresh snowfall. To this end, a set of different rules were formulated: (1) the SCAF cannot be lower than 50% at the very beginning of the ablation season. (2) The minimum observed SCAF at the end of the summer defines the end of the ablation season, and all following SCAFs are omitted. (3) Fresh snowfall events were discarded.

8.3.2 Geodetic volume change inferred from ASTER L1A and HMA DEM datasets

We produced ASTER DEMs using the MMASTER processing chain (Girod et al, 2017b). To remove the along-track component of the jitter on ASTER L1A data, we used the SRTM DEM as a reference, as it provides a consistent DEM for the entire region. We then masked the final DEMs using the correlation score provided by the MMASTER processing, using a threshold for the correlation score of 70%. We used the corrected ASTER DEMs and HMA DEMs for DEM differencing. The sensor specific DEM differencing pairs, based on at least five years separation, and only with at least 40% scenes overlap, were selected. We co-registered each of the image pairs to each other based on the methods described in Nuth and Kääb (2011) before differencing. This provided a total of 1844 DEM pairs, with most (1604 pairs) covering the Pamir.

To filter the DEM differencing pairs, we employ a filtering procedure, modified after Pieczonka and Bolch (2015) to remove remaining outliers on the glacier area. The introduced filter used the overall standard deviation (STD) of the glacier elevation difference, weighted by an elevation-dependent coefficient, and allowed elevation changes in the ablation and accumulation area in both positive and negative directions. The weighted coefficient for each pixel was determined using a sigmoid function. After a normalization of all pixels on the glacier surface to its elevation range (Eq. 8.1), a weighting coefficient c was calculated using the normalized glacier elevation w (Eq. 8.2). This coefficient was then multiplied with the standard deviation of the glacier elevation change σ_{dh} to indicate the expected maximum change of each pixel on the glacier surface δh_{max}.

$$w = \frac{z_{x,y} - z_{min}}{z_{max} - z_{min}} \tag{8.1}$$

where $z_{x,y}$ is the pixel on the glacier surface, z_{min} and z_{max} the minimum and maximum glacier elevation, respectively.

$$c = \frac{1}{1 - tanh(\frac{\pi}{2} - 3w)} \tag{8.2}$$

$$\delta h_{max} = c \times \sigma_{\mathrm{dh}} \tag{8.3}$$

Because of low correlation due to clouds, shadow, or bright snow, the DEMs (and therefore the elevation change maps) have significant voids over the glaciers, which prevent a straightforward summation of the elevations differences to calculate volume changes. Based on investigations detailed in McNabb et al (2017), we calculate volume change using a hypsometric approach. Thereby, we first estimate the area-altitude distribution for each glacier based on the SRTM DEM, with bins spaced by 50 m or for shorter glacier by 10% of the glacier elevation range. For each DEM differencing scene, we then took the mean elevation difference per elevation bin, iteratively removing remaining outliers that are more than 3 standard deviations away from the mean of the bin, which yields an estimation of the elevation difference as a function of elevation. We then removed all values where the bin is more than 40% void (i.e., nodata). If the elevation curve still covered at least 75% of the glacier area based on the area-altitude distribution, the curve was filled using linear interpolation, setting elevation difference values above and below the glacier elevation range to zero. Finally, we calculated the volume change by multiplying the elevation difference curve by the area-altitude distribution, and summing the result.

8.3.3 Geodetic mass balances for the reference period from 2004 to 2012

The difference in volume changes ΔV for each glacier based on ASTER scenes, were converted into geodetic mass balances ΔM_{geod}, using a density $\rho_{\Delta V}$ of $850\,\mathrm{kg\,m^{-3}}$ (Huss, 2013):

$$\Delta M_{\mathrm{geod}} = \frac{\Delta V \cdot \rho_{\Delta V}}{\overline{A} \cdot \Delta t \cdot \rho_w} \tag{8.4}$$

where, $\overline{A}$ is the glacier area, Δt is the time in years between the corresponding image pairs and ρ_w the density of water ($1000\,\mathrm{kg\,m^{-3}}$).

Due to the use of a large amount of overlapping ASTER scenes for the studied glaciers, a range of different geodetic mass balances with different time stamps was obtained for each glacier. In order to provide a suitable and robust result for comparison with the TSL-constrained modelled SMB, all geodetic mass changes for each individual glacier was homogenized to represent a fixed reference period. We chose the period from 2004 to 2012 as adequate, guaranteeing a good coverage for most studied glaciers with both methods.

To homogenize geodetic mass balances covering arbitrary periods to the reference period, we overlaid the observed annual mas balance variability of glaciers located in the same regions. We thus corrected the geodetic annual mean mass balance from the actual observation period to the reference, using the difference in the average annual glaciological mass balances of the corresponding periods. For the homogenization step, the series of Tuyuksu was used for Dzhungarsky Alatau, Western / Northern Tien Shan, Pamir-Alay and Western Pamir and the one of Urumqi for Eastern and Central Tien Shan and Eastern

Pamir. The median of all geodetic mean annual mass balance values corrected for the reference period was interpreted as the reference geodetic mass balance of the corresponding glacier and used for a second-order model calibration (see Section 8.3.4).

We followed the uncertainty calculations proposed by Brun et al (2017) to estimate the random error of all inferred mass changes. The calculated uncertainty estimate includes three components: (1) the uncertainty related to the elevation change observed over stable ground, (2) the uncertainty of elevation change determination over glacierised areas and (3) the uncertainty in the volume-to-mass conversion. For each glacier, the calculated uncertainties of the mass changes obtained for the different periods are summarized through their arithmetic mean. This value is used to represent the uncertainty of the geodetic mass balance detected for the reference period.

8.3.4 TSL-constrained mass balance modelling

We use the mass balance model constrained by TSL observations as presented in Barandun et al (2018) for inferring daily glacier-specific SMBs. Hereafter, we only provide a short overview of the methodology. For more details, the reader is referred to Barandun et al (2018).

We used a distributed accumulation and classical temperature index model (e.g., Braithwaite, 1995; Hock, 2003) with a daily temporal and a 30 m spatial resolution. Reanalysis daily mean air temperature and precipitation sums were used to drive the model. A constant temperature lapse rate $\delta T/\delta z$ and a linear precipitation gradient $\delta P/\delta z$ was used to extrapolate the daily air temperatures to each grid cell (Table 8.1). In order to calculate melt M, a linear relation with positive daily mean air temperature $T_{\text{air}}(x, y, t)$ was applied for each grid cell x, y and time stamp t as follows:

$$M_{x,y,t} = \begin{cases} DDF_{\text{ice/snow}} \cdot T_{\text{air}(x,y,t)} & T_{\text{air}} > 0^{\circ} \\ 0 & T_{\text{air}} \leq 0^{\circ} \end{cases} \tag{8.5}$$

We used two different degree-day factors for snow DDF_{snow} and ice DDF_{ice} and held their ratio R_{DDF} constant over time.

The snow accumulation C was simulated for each grid cell x, y and time step t by

$$C_{(x,y,t)} = P_{\text{ERA}}(x, y, t) \cdot C_{\text{prec}} \cdot (1 + (z_{(x,y)} - z_{\text{ERA}}) \cdot \delta P/\delta z). \tag{8.6}$$

Solid precipitation occurs at $T_{\text{air}} \leq 1.5\,^{\circ}C$ with a linear transition range of $\pm 1^{\circ}$C (e.g., Hock, 1999). P_{ERA} is the daily precipitation sum provided by the Reanalysis for the closest grid cell, z_{ERA} denotes the mean elevation of the ERA grid cell and $z(x, y)$ gives the elevation of each grid cell. To correct for the Reanalysis precipitation data, P_{ERA} is scaled with a correction factor C_{prec} (Huss et al, 2008, 2009). C_{prec} is assumed to be 25% lower for liquid precipitation (during summer months) (Sevruk, 1981). We based the choice of the constant model parameters on Barandun et al (2018) and adopted the values of Glacier No. 354 for Akshiirak range, of Golubin for Kyrgyz Ala-Too, and of Abramov for the Pamir-Alay (Table 8.1). Precipitation is set to no longer increase linearly after a critical elevation Z_{crit}.

In Barandun et al (2018), C_{prec} and DDF_{snow} were calibrated keeping R_{DDF} constant, and an initial range for DDF_{snow} and C_{prec} was narrowed down until an optimal parameter combination was obtained. In order to limit computation time, the calibration procedure was adjusted. Instead of starting with an initial range, a start value for DDF_{snow} and C_{prec} based on Barandun et al (2018) was selected and iteratively adjusted until no improvement of the model was observed anymore (Fig. 8.2). C_{prec} was adjusted to minimize the

Table 8.1: Constant model parameters used in Barandun et al (2018) were adopted for modelling for Pamir-Alay from Abramov, the Kyrgyz Ala-Too from Golubin and for the Akshiirak range from Glacier No. 354.

	$\delta T/\delta z$ $^{\circ}\mathrm{C\,km^{-1}}$	$\delta P/\delta z$ $10^{-4}\,\mathrm{m^{-1}}$	R_{DDF} –	Z_{crit} m a.s.l
Pamir-Alay	−4.8	6.4	1.57	4400
Kyrgyz Ala-Too	−6.3	4.5	1.36	4000
Akshiirak	−6.7	1.5	1.06	4500

RMSE between the modelled cumulative melt $Melt_{\mathrm{modelled}}$, calculated at the position of the observed snowline, and the total amount of accumulated winter snow $Accu_{\mathrm{modelled}}$ that melted from the onset of the ablation season until the snowline observation date. DDF_{snow} was calibrated to best represent all SCAF observations of one ablation season by reducing the RMSE between modelled and observed SCAF $RMSE_{\mathrm{SCAF}}$. Hereby, C_{prec} and DDF_{snow} were calibrated annually and for each glacier separately to correctly represent the winter snow accumulation and the melt rates (Barandun et al, 2018). The TSL-constrained model was run from 2000 to 2017 for all glaciers greater than $2\,\mathrm{km^2}$ and for which at least two snowline observations in different summer months are available per ablation season. For years with insufficient TSL observations, the calibrated parameters obtained for years with good data availability were averaged.

Uncertainties related to the snowline approach are directly taken from Barandun et al (2018) where an in-depth analysis of the uncertainties and sensitives of the snowline-constrained mass balance model was presented. We thus adopted the mean ($\pm 0.32\,\mathrm{m\,w.e.\,yr^{-1}}$) of the global uncertainties associated with the snowline-constrained mass balance model presented for the three studied glaciers in Barandun et al (2018).

8.3.5 Second-order model calibration of annual mass balance series with geodetic mass changes

In a second step, we constrain the modelled annual SMB by comparing it to the geodetic mean annual mass changes inferred for each glacier for the reference period 2004 to 2012. In case the snowline-constrained SMB series exceeds the error range of the geodetic approach, first R_{DDF} was adjusted within a plausible range (Hock, 2003) and the aforementioned calibration step (see Section 8.3.4) was repeated. If still no agreement was found, but the plausibility limit for R_{DDF} was reached, the precipitation gradient $\delta P/\delta z$ was adjusted within its realistic bounds. Both literature-based parameters are highly variable in space and are not well constrained for the individual glacier, justifying the applied second-order calibration. After each re-adjustment of the parameters, the annual model calibration based on TSL observations was rerun. The second-order calibration was repeated until the absolute difference between the two approaches was smaller than the error range of the geodetic method or both parameters reached their plausibility limits. As a control the mountain range-wide mass balance of both methods were compared. For glaciers for which no geodetic mass balance was available, the subregional arithmetic mean was used. Here, we do not account for internal and basal balance for the modelled series and assume that the related uncertainties do not exceed the calculated error budget.

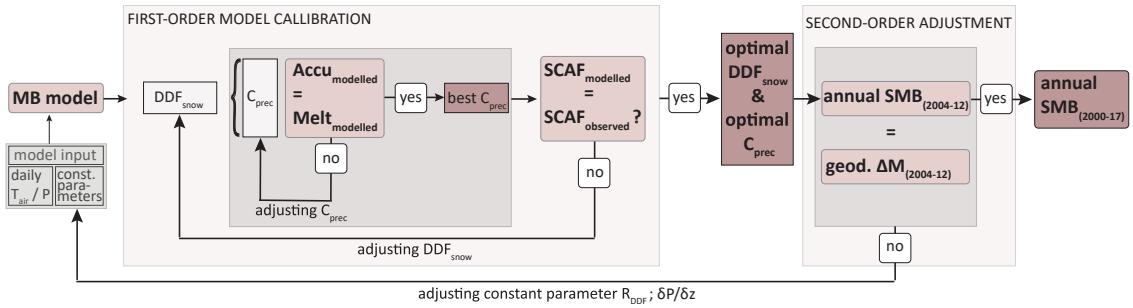

Figure 8.2: Calibration procedure to obtain an ideal combination of DDF_{snow} and C_{prec}. In a first step, DDF_{snow} and C_{prec} are optimized through comparison to snowline observations until a good solution for both parameters was found. First, for the initial value of DDF_{snow}, the best value of C_{prec} was determined constraining the modelled cumulative melt $Melt_{\mathrm{modelled}}$ at the snowline position to agree with the modelled winter snow accumulation $Accu_{\mathrm{modelled}}$ for the same location. Second, the model performance was evaluated to minimize $RMSE_{\mathrm{SCAF}}$ of the modelled and observed snow-covered area fractions (SCAF). This is repeated until an optimal solution is reached. In a second step, the modelled mass balance from 2004 to 2012 is compared to the multi-annual geodetic mass balance and R_{DDF} and $\delta P/\delta z$ were readjusted until the results of both approaches agree within the uncertainty range of the geodetic estimate.

Table 8.2: Number and total area of all glaciers ($> 1\,\mathrm{km}^2$) and of glaciers ($> 1\,\mathrm{km}^2$) with available elevation change data for seven study regions. Numbers are based on RGIv6.0 (RGI-Consortium, 2017).

Study region	total No. of glaciers	No. glaciers with data	total area (in km^2)	area studied glaciers (in km^2)
Western / Northern Tien Shan	583	128	1358	485
Eastern Tien Shan	430	128	1411	511
Central Tien Shan	1012	364	5967	1612
Dzhungarsky Alatau	125	49	293	126
Pamir-Alay	378	160	1147	397
Western Pamir	1464	1339	6422	4714
Eastern Pamir	299	110	1523	305
all	4291	2324	18130	8163

8.4 Results

8.4.1 Geodetic mass change

For the Pamir, we have nearly complete coverage of RGIv6.0 glaciers with an area of at least $1\,\mathrm{km}^2$. 1609 of 2141 glaciers have at least one DEM differencing pair and an average of 11.7 pairs for each of those glaciers (Table 8.2). In the Tien Shan, we have less complete coverage, with only 715 of 2150 glaciers having at least one DEM differencing pair, and 2.7 pairs on average. Hence, a substantial amount of glaciers situated in the Tien Shan could not be included into the here presented analysis.

We calculated a geodetic mass loss of $-0.38\pm0.33\,\mathrm{m\,w.e.\,yr}^{-1}$ from 2004 to 2012 for the entire Tien Shan and Pamir. The results for each region are summarized in Table 8.3. Most negative values are detected for the Easter Tien Shan ($-0.84\pm0.36\,\mathrm{m\,w.e.\,yr}^{-1}$) and the Dzhungarsky Alatau ($-0.73\pm0.63\,\mathrm{m\,w.e.\,yr}^{-1}$) and a positive mean annual mass

Table 8.3: Geodetic and modelled mass balance (m w.e. yr^{-1}) results calculated for the different regions.

Study region	geodetic (2004-2012)	modelled (2000-2017)
Western / Northern Tien Shan	-0.55 ± 0.64	
Eastern Tien Shan	-0.84 ± 0.36	
Central Tien Shan	-0.43 ± 0.68	
Dzhungarsky Alatau	-0.73 ± 0.63	
Western Pamir	-0.37 ± 0.42	
Eastern Pamir	$+0.19\pm1.47$	
Pamir-Alay	-0.13 ± 0.40	-0.34 ± 0.32
Kyrgyz Ala-Too	-0.58 ± 0.63	-0.42 ± 0.32
Akshiirak	-0.40 ± 0.63	-0.39 ± 0.32

balance of $+0.19\pm1.47$ m w.e. yr^{-1} was found for Eastern Pamir (Fig. 8.3). Western Pamir (-0.37 ± 0.42 m w.e. yr^{-1}) and Pamir-Alay (-0.13 ± 0.40 m w.e. yr^{-1}) have a mass loss bellow the region-wide mean. This is in line with literature (e.g., Gardner et al, 2013; Farinotti et al, 2015; Brun et al, 2017) suggesting generally less negative mass balances for the Pamir than for the Tien Shan. Here we calculated a mean geodetic mass balance of -0.24 ± 0.43 m w.e. yr^{-1} for the the Pamir and of -0.52 ± 0.53 m w.e. yr^{-1} for the Tien Shan.

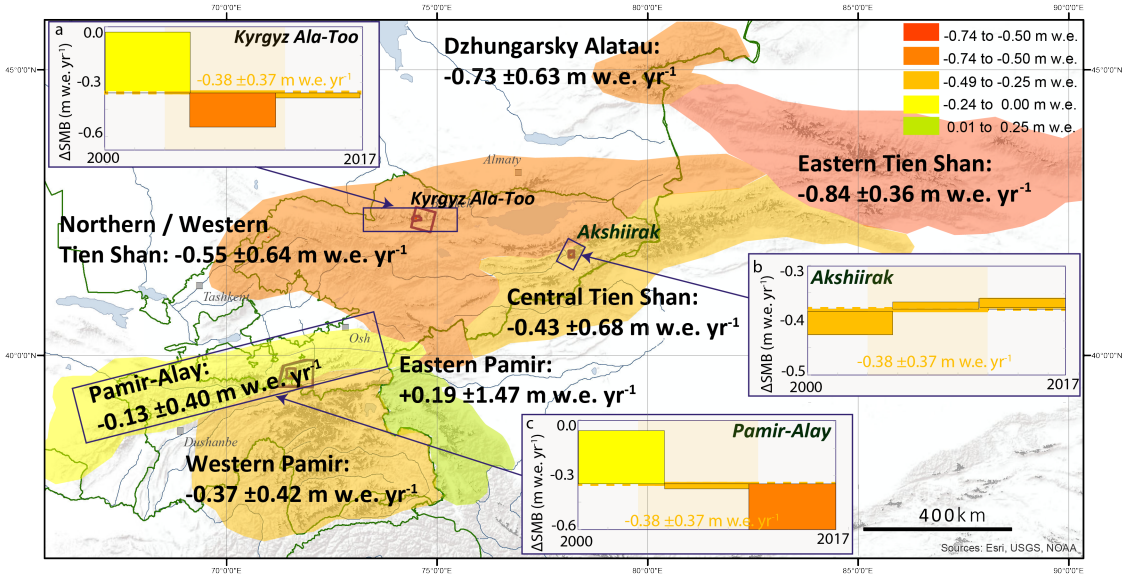

Figure 8.3: The region-wide mean annual mass balance detected from the geodetic assessment based on ASTER data for the seven subregions. The colours of the regions illustrate the mean value of the mass balance for the period 2004 to 2012. Boxes **(a)** to **(c)** illustrate the difference between the SMB derived from TSL-modelling from 2000 to 2017 for six-year periods and the region-wide average from 2004 to 2012 calculated from the ASTER data. **(a)** shows results for the Kyrgyz Ala-too, **(b)** for the Akshiirak range and **(c)** for the Pamir-Alay. The colours of the squares indicate the mean value of the mass balance for each period.

Table 8.4: Number and total area of all glaciers ($> 2\,km^2$) and of glaciers ($> 2\,km^2$) which were included in the modelling study. Numbers are based on RGIv6.0 (RGI-Consortium, 2017).

study region	total No. of glaciers	No. modelled glaciers	total area (in km^2)	area studied glaciers (in km^2)
Kyrgyz Ala-Too	23	23	68	68
Akshiirak	31	27	270	198
Pamir-Alay	151	109	835	685

8.4.2 TSL-constrained mass balance modelling

The TSL-constrained model was applied successfully on all glaciers ($> 2\,km^2$) located in the Kyrgyz Ala-Too, on ≈90% of the glaciers in the Akshiirak range and on ≈70% of the Pamir-Alay glaciers (Table 8.4). The results for the three subregions are summarized and compared to the geodetic mass loss in Table 8.3.

A mean annual SMB of $-0.42\pm0.32\,m\,w.e.\,yr^{-1}$ for the Kyrgyz Ala-Too from 2000 to 2017 was calculated. This added up to a cumulative mass loss of almost $-8\,m\,w.e.$ since 2000 (Fig. 8.4). The region-wide geodetic assessment using ASTER scenes revealed a mass loss of $-0.58\pm0.63\,m\,w.e.\,yr^{-1}$ (Fig. 8.4a), comparing satisfyingly to the modelled results for the same period ($-0.48\pm0.32\,m\,w.e.\,yr^{-1}$). The cumulative mass balance of Golubin, agreed well with the mean cumulative balance on mountain range scale (Fig. 8.4b), and affirmed representative for the surrounding glaciers and suitable for long-term monitoring. We summarised the mass balance of all glaciers for six-year intervals and identified a period of relatively favourable conditions from 2000 to 2005, followed by a sharp decrease in SMB for the consecutive six years with exceptionally high mass loss in 2008 (Fig. 8.3). The mass budget of 2009 was close to balance conditions what is in line with SMB time series inferred for individual glaciers of the Tien Shan (e.g., Kronenberg et al, 2016; Kenzhebaev et al, 2017). From 2012 to 2017, a continuous mass loss with accelerating tendencies after 2013, resulted in a mean annual SMB of $-0.39\pm0.32\,m\,w.e.\,yr^{-1}$ for the 23 modelled glaciers (Fig. 8.4b). This region-wide value is in good accordance to direct measurements for Golubin glaciers ($-0.35\pm0.30\,m\,w.e.\,yr^{-1}$) located in the Kyrgyz Ala-Too for the same period (Hoelzle et al, 2017). Trend analysis underlined the observed acceleration of the mass loss since 2000 with a significance on the 99% level (Mann-Kendall test, n=18).

The mean SMB modelled for the 27 glaciers in the Akshiirak range from 2000 to 2017 was $-0.39\pm0.32\,m\,w.e.\,yr^{-1}$, resulting in a cumulative mass loss of almost $-7\,m\,w.e$ (Fig. 8.5). With the geodetic approach, we detected a region-wide mass loss of $-0.40\pm0.63\,m\,w.e.\,yr^{-1}$ from 2004 to 2012 (Fig. 8.5a). The corresponding modelled SMB of $-0.37\pm0.32\,m\,w.e.\,yr^{-1}$ agreed very well. Figure 8.5a illustrates that the southern edge of the range was prone to enhanced mass loss, similarly observed in (Pieczonka and Bolch, 2015). Further worth noting is the balanced mass budget in 2009 and 2010 observed for most of the glaciers (Fig. 8.5b). The mean annual SMB calculated for the mountain range for periods of six years was relatively constant over time with a mass loss close to the average SMB. A slight tendency to a less negative SMB in recent years might be observed, however, statistical analysis did not show a significant trend. Frequent occurrence of surge-type glaciers, as well as interaction of the glacier response with mining activities hamper sound interpretation of such patterns for the considered mountain range. The mass balance of the monitored glacier No. 354 was observed to be one of the most negative and well below the mean cumulative change (Fig. 8.5b). A glacier with substantially more mass loss

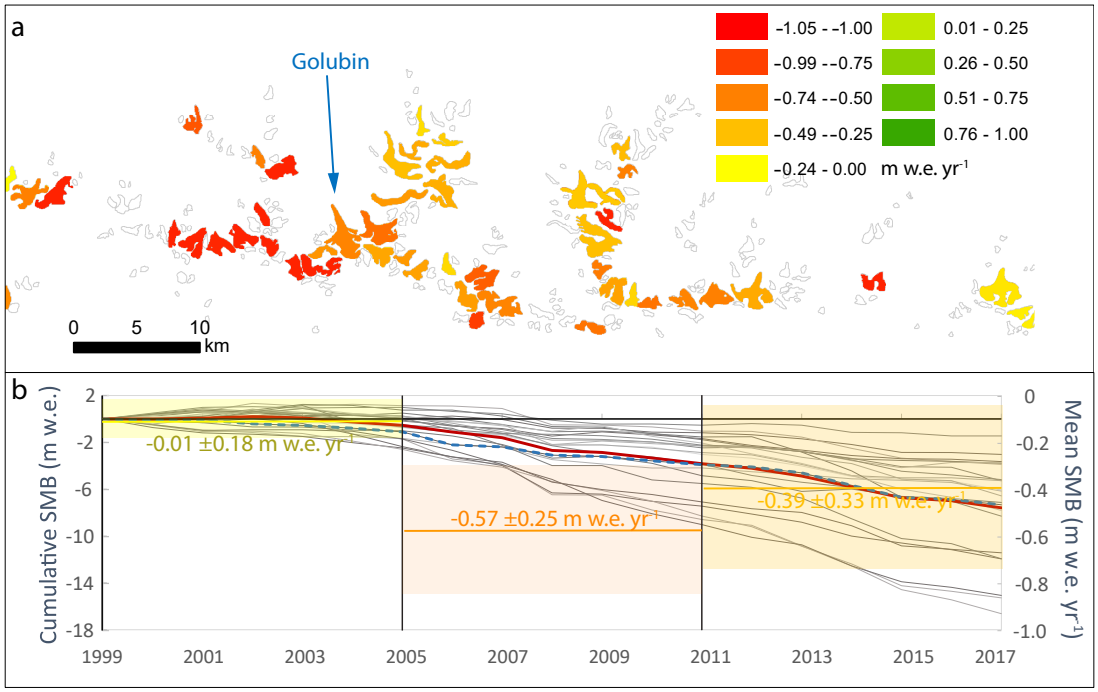

Figure 8.4: Mass balance assessment for the Kyrgyz Ala-Too. **a**) The geodetic mass balance derived from ASTER DEMs summarized for the reference period 2004 to 2012. **b**) The modelled cumulative SMB for all 23 glaciers. The red line indicates the regional mean using all time series and the blue dotted line shows the cumulative balance of Golubin, a glacier included in the glacier monitoring program of Kyrgyzstan. Furthermore, the six-year mean annual SMB derived from TSL-modelling including all 23 glaciers and their standard deviation (given range and shaded area) are given in colours.

than observed in its immediate surroundings is located near a gold mine that might had influenced the glacier response by its activities (Fig. 8.5a). Controversially, on some of the neighbouring glaciers, on which technogenic influences have been shown (Evans et al, 2016), no such elevated mass loss was calculated.

The annual mean SMB calculated for 109 of 151 glaciers located in Pamir-Alay for the period 2000 to 2017 was $-0.36\pm0.32\,\mathrm{m\,w.e.\,yr^{-1}}$, with a few glaciers having positive or close to zero annual balances (Fig. 8.6). The mean cumulative balance totalled to a mass loss of around $-6\,\mathrm{m\,w.e}$ for the same period. The here calculated geodetic mass balance for the Pamir-Alay was substantially less negative with an average of $-0.13\pm0.40\,\mathrm{m\,w.e.\,yr^{-1}}$ from 2004 to 2012 (Fig. 8.6b). The modelled balance of $-0.34\pm0.32\,\mathrm{m\,w.e.\,yr^{-1}}$ for the same period agreed within the uncertainty range of the geodetic estimate. A significant increase in mass loss with time (on the 95% level using a Mann-Kendall test, n=18) was found (Fig. 8.6b) and we could further identify a more favourable period for the earlier half of the study period. 2009 displayed positive / less negative SMBs and 2008, 2012 and 2013 showed most negative mass balances (Fig. 8.6b). The here calculated interannual variability and in particular a very negative mass balance for 2008 and a positive balance in 2010 agreed well with modelled mass balance series reported by Pohl et al (2017) for the entire Pamir from 2002 to 2013. A separation into two different regimes might be adequate: (1) glaciers with a more positive regime especially due to the period from 2000 to 2004, and (2) glaciers under less favourable conditions with pronounced mass loss after

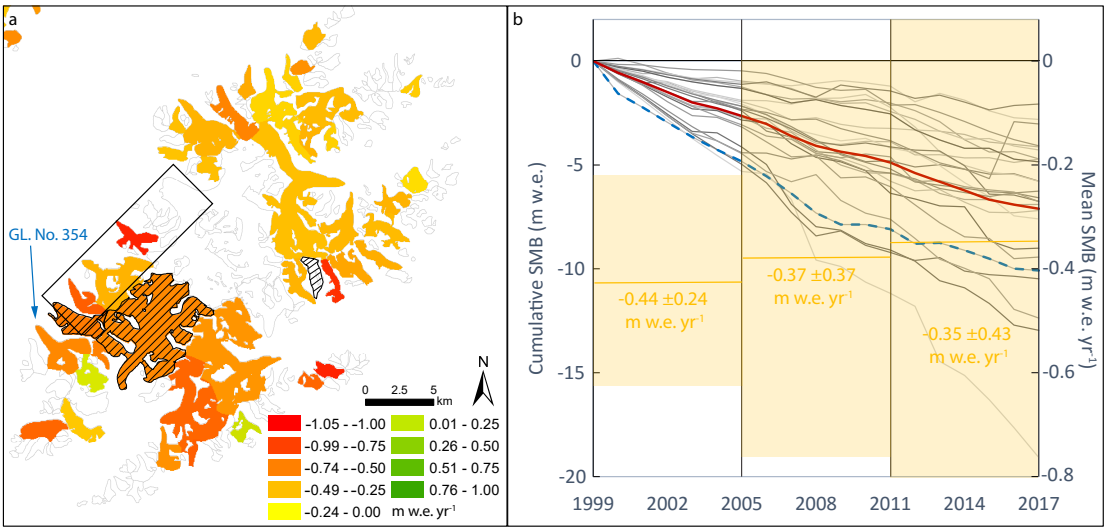

Figure 8.5: **a**) Mean annual mass balance for the Akshiirak range derived from ASTER DEM differencing summarized for the period 2004 to 2012. Indicated are surge-type glaciers based on the RGI-Consortium (2017) (hatched) and glaciers for which technogenic influences have been observed (Evans et al, 2016, black square). Further, the location of Glacier No. 354, for which direct measurements have been collected continuously since 2010 is shown. **b**) The cumulative SMB for the 27 modelled glaciers are plotted from 2000 to 2017. The mean cumulative change is shown in red and the cumulative mass balance for No. 354 is indicated with a dashed blue line. The six-year mean annual SMB derived from TSL-modelling including the 27 glaciers and their standard deviations (given range and shaded area) are given in colours.

2005. Abramov Glacier lies in the middle of the two classes with close to zero SMBs for the first period but with continuous mass loss after 2008. Abramov was slightly more positive than the regional mean, however remains relatively representative (Fig. 8.6b). Contrarily, glaciers in its close vicinity were observed to have less negative mass budgets (Fig. 8.6a).

8.5 Discussion

8.5.1 Automated TSL mapping

We use broadband albedo maps from Landsat satellite images to classify glacier surface characteristics. The separation of snow and ice primary depends on the albedo of the surface classes. It is possible to account for fresh snowfall or changes in other surface characteristics with a physical interpretation of this value. However, the range of albedos for snow and ice / firn can overlap considerably, and a straightforward classification is not always possible (Naegeli et al, 2018). Nonetheless, the transition of the albedo between ice and snow is characterized by a distinct change (e.g., Hall et al, 1987), and the greatest slope of the albedo-elevation profile approximates the limits between snow and bare-ice surfaces well (Naegeli et al, 2018).

Comparison to manually delineated snowlines for Abramov, Golubin and Glacier No. 354 showed satisfying agreement within an RMSE of less than 10% for all mutually observed SCAFs. Mainly for cloud-free images, accurate classification was obtained. The

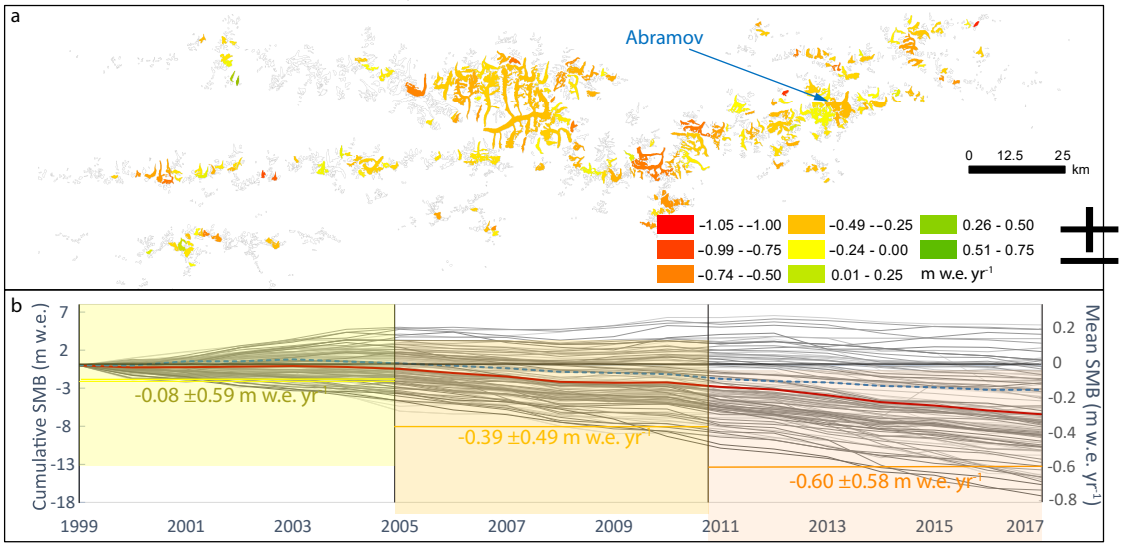

Figure 8.6: **a**) The geodetic mass balance derived from ASTER scenes for the entire Pamir-Alay summarized for the reference period 2004 to 2012. **b**) The cumulative SMB observed for 109 of the 155 glaciers larger than 2 km^2 are shown. The mean cumulative change taking in account all available series is indicated in red and the cumulative mass balance for Abramov Glacier, which has been recently monitored since 2012, is shown with a blue dotted line. The six-year mean annual SMB derived from TSL-modelling including the 109 glaciers and their standard deviation (given range and shaded area) are given in colours.

applied cloud mask using SAM does not filter very thick optical clouds and hence can interfere with automated TSL corrections. Missing out clouds, can lead to considerable misinterpretation of the surface type and often lead to overestimated SCAFs. Such misclassification affect the TSL-constrained model performance and a thorough filtering of TSLs is recommended but often not straightforward or included manual labour.

In the Akshiirak range, summer snowfall and dense cloud cover are frequent and non-optimal performance of the applied cloud filters lead to frequent misclassification of the surface type. In Barandun et al (2018) images have been selected manually, benefiting a proper model functioning. With automatic filtering erroneously classified images are removed to certain degree, but could not be completely eliminated, mirrored in a reduced model performance. To some extent, this illustrates the advantage of using several SCAF observations distributed during the summer months to lower the importance of a single misclassified image.

Thus, despite the advantage of using albedo maps for surface classification, prevalent problems related to limited quality of the surface reflectance data (over-saturation), cloud cover and shading have not entirely been resolved yet and reliable automatic TSL classification on optical multi-temporal satellite scenes still needs improvement.

8.5.2 Comparison between different methods

For validation of the TSL-constrained model on annual temporal resolution, we compared the modelled annual SMBs to available direct observations for Abramov, Golubin and Glacier No. 354 (Barandun et al, 2015; Kronenberg et al, 2016; Hoelzle et al, 2017; Barandun et al, 2018) and to high-resolution geodetic mass balance estimates available for

Table 8.5: Comparison of the here derived SMB with TSL-constrained modelling (B_{snl}) and the geodetic mass change ($B_{\mathrm{geod\ ASTER}}$) with other studies using a combination of modelling and direct measurements $B_{\mathrm{meas/mod}}$ (Barandun et al, 2015; Kronenberg et al, 2016; Barandun et al, 2018) or geodetic survey based on high resolution satellite data ($B_{\mathrm{geod\ HR}}$, Barandun et al, 2018). All values are given in m w.e yr^{-1} and for the period from $\approx$ 2004 to 2012 for individual glaciers and regions.

Glacier	B_{snl}	$B_{\mathrm{meas/mod}}$	$B_{\mathrm{geod\ ASTER}}$	$B_{\mathrm{geod\ HR}}$
Golubin	-0.39 ± 0.32	-0.40 ± 0.30	-0.22 ± 0.33	-0.30 ± 0.37
No. 354	-0.31 ± 0.32	-0.40 ± 0.30	-0.87 ± 0.30	-0.42 ± 0.07
Abramov	-0.32 ± 0.32	-0.64 ± 0.50	-0.33 ± 0.30	-0.36 ± 0.26

parts of the Akshiirak massif (Table 8.5; Kronenberg et al, 2016, the Pamir-Alay and the Ala Archa (Barandun et al, 2018)). The results of the TSL-constrained model agreed with the direct measurement from 2011/12 to 2017 with a RMSE of less than 0.2 m w.e. yr^{-1} for Abramov, of 0.3 m w.e. yr^{-1} for Glacier No. 354, and of less than 0.4 m w.e. yr^{-1} for Golubin. Reconstructed mass balances for the three glaciers available from (Barandun et al, 2015; Kronenberg et al, 2016; Barandun et al, 2018) are also in line with the here presented results and are compared in Table 8.5.

High-resolution geodetic assessments show satisfying agreement with the TSL-modelled time series after second-order adjustment (mean absolute difference of -0.2 m w.e. yr^{-1}, Table 8.5) and indicated no systematic offset with the geodetic results.

We found a tendency of overestimated mass loss using ASTER scenes for all three regions in comparison to the results revealed by the high-resolution datasets of about -0.3 m w.e. yr^{-1} in average.

8.5.3 Mass balance time series from TSL-constrained modelling

We compared the modelled mean annual and cumulative SMBs for 2000 to 2017 for all three regions (Fig. 8.7). The similar year-to-year variability observed for Pamir-Alay ($\sigma = 0.31$ m w.e.) and Kyrgyz Ala-Too ($\sigma = 0.34$ m w.e.) is clearly visible, with slightly more negative balances for the latter. We found a period of close-to-zero or positive mass balance period from 2001 to 2003 / 2004 for the two glaciers. Conversely, for glaciers in the Akshiirak massif, mass balance rates did not change remarkably from year to year. All three regions agree on favourable conditions around 2009 / 2010. Most negative years have been observed coherently for 2008, 2012 and 2013. A significant increase of mass loss with time was found for the Pamir-Alay and the Kyrgyz Ala-Too. For all three regions, interannual variability agreed well with the fluctuation observed for individual glaciers published in previous studies (Barandun et al, 2015; Kronenberg et al, 2016; Barandun et al, 2018). We found a reduced annual mass balance variability for the Akshiirak ($\sigma = 0.12$ m w.e.) in comparison to the other two mountain ranges (Fig. 8.7). This is due to the reduced mass turnover provoked by low precipitation rates and colder mean annual air temperatures. However, a sharp increase of the year-to-year fluctuations was calculated for the massif for recent years (Fig. 8.5b). In Figure 8.3, we show the deviation of the mean SMB observed for six-year periods in comparison to the mean geodetic mass loss calculated for the entire Tien Shan and Pamir. The Kyrgyz Ala-too and the Pamir-Alay experienced a rather favourable period at the beginning of the century with a positive deviation of about $+0.35$ m w.e. yr^{-1}. From 2005 to 2011, glaciers in the Pamir-Alay had SMBs close to the regional mean, whereas the glaciers in the Kyrgyz Ala-Too (-0.22 m w.e. yr^{-1}) tended to lose slightly more mass. For the recent period from 2012 to 2017, Pamir-Alay glaciers

increased their mass loss in comparison to the regional mean by $-0.19\,\mathrm{m\,w.e.\,yr^{-1}}$. The glaciers in the Kyrgyz Ala-Too approximate the regional average well. Fluctuations of the SMB for the Akshiirak are much less pronounced and deviate only within $-0.05\,\mathrm{m\,w.e.\,yr^{-1}}$ to $-0.01\,\mathrm{m\,w.e.\,yr^{-1}}$ from the region-wide geodetic mass balance.

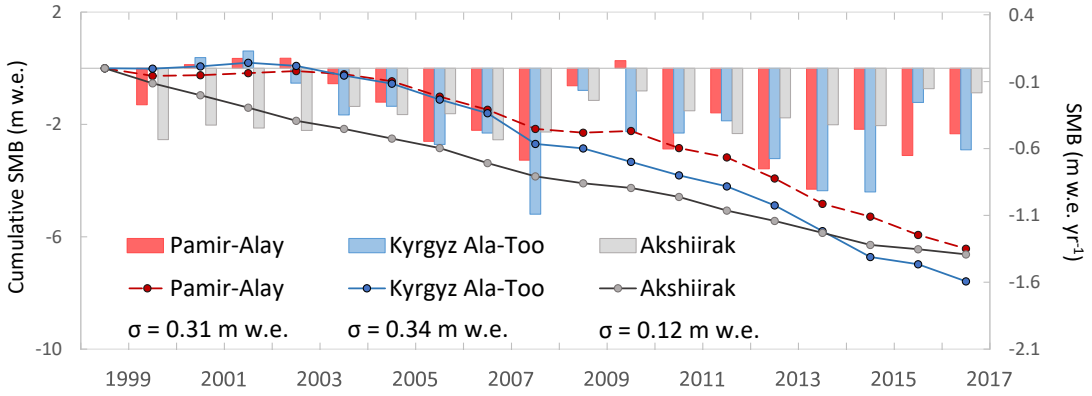

Figure 8.7: The mean annual (bars) and cumulative (lines) SMB obtained from TSL-constrained modelling for each region is shown. The Standard deviation σ denotes the annual mass balance variability for each mountain range.

We evaluated the correlation of the mean annual surface mass balance with the standard deviation of the annual mass balance of all glaciers located in the different regions and could identify a strong negative correlation for the East Pamir-Alay (R^2 = 0.69, n=18), a moderate negative correlation for the Kyrgyz Ala-Too (R^2 = 0.27, n=18; Fig. 8.8) and only a very weak negative correlation for Akshiirak. Surprisingly, we found a very weak positive correlation for the West Pamir-Alay. However, such low correlations might simply be explained through model uncertainties. The negative correlation indicated that with increasingly negative mass balance a more heterogeneous response of the glacier mass balance occurred. Increasing standard deviations with time might thus, be related to more negative mass balances. To investigate temporal trends, we applied a Mann-Kendall test on the mean annual mass balance and standard deviation of the glaciers located in the different regions over the period from 2000 to 2017. Apart from the West Pamir-Alay, we found positive trends for the standard deviation. However, trend analysis showed that none of the trends was significant, and might considerably be influenced by the uncertainty of the applied approach. In general, the standard deviation of the mean annual surface mass balance and the interannual variability is one order of magnitude higher for the Pamir-Alay than for the Kyrgyz Ala-Too and the Akshiirak (Fig. 8.4b, 8.5b, 8.6b). Heterogeneity increased eastwards. A possible reason might be an ongoing regime change from more continental to more maritime climate, following a West-East gradient (Glazirin et al, 1993). Furthermore, we compared the mean mass balances and their standard deviations for the six-year periods (Fig. 8.4b, 8.5b, 8.6b) and indicated an increasing mass loss and greater heterogeneity in more recent periods. Such an increase accompanied with higher interannual variability, especially pronounced for the continental region Akshiirak, might be connected to possible regime shifts from a colder and dry climate to a more maritime environment with higher precipitation rates and air temperatures.

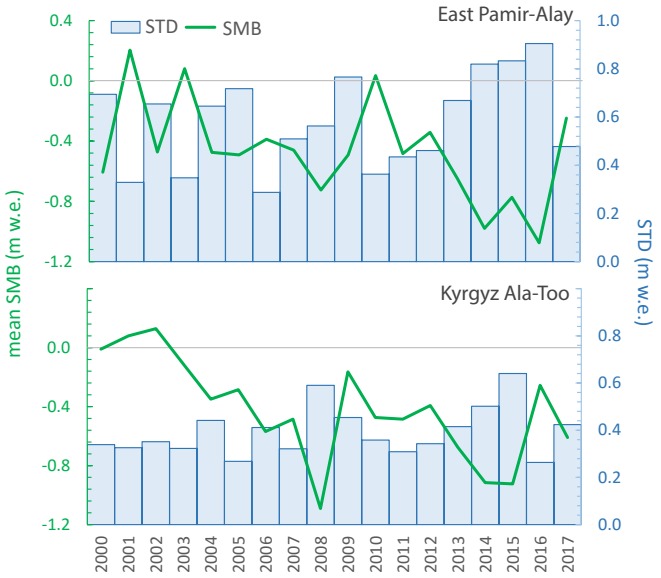

Figure 8.8: Mean annual surface mass balance (SMB) in comparison to their standard deviation (STD) for all the glaciers located in the East Pamir-Alay (top) and the Kyrgyz Ala-Too (bottom).

8.5.4 Comparison to other studies

We calculated a stronger geodetic mass loss for the entire Tien Shan (-0.58 ± 0.53 m w.e. yr^{-1} from 2004 to 2012) than results presented in Brun et al (2017), who reported a mass loss of -0.28 ± 0.20 m w.e. yr^{-1} for ≈2000 to 2017 (Fig. 8.3). Conversely, both Gardner et al (2013) and Farinotti et al (2015) published significantly more negative regional values than Brun et al (2017) that agree well with the here derived geodetic mass changes for the entire Tien Shan and the individual subregions. However, meaningful comparison might be hampered due to varying study periods and spatial divisions between the different studies.

Good agreement was found between the TSL-constrained model results for the Ala Archa Basin, forming part of the Kyrgyz Ala-Too, and the geodetic mass loss presented in Bolch (2015). Their basin-wide average of -0.42 ± 0.66 m w.e. yr^{-1} corresponds well with the here provided modelled results from 2000 to 2012 (-0.44 ± 0.32 m w.e. yr^{-1}) and a RMSE of less than 0.2 m w.e. yr^{-1} between the estimates provided for the individual glacier and further highlights the good agreement between the studies.

The SMB (-0.39 ± 0.32 m w.e. yr^{-1} from 2000-2017) obtained from TSL-constrained modelling for the Akshiirak massif is overall in line with other studies (Gardner et al, 2013; Farinotti et al, 2015; Brun et al, 2017). The here derived geodetic mass balance is slightly more negative (-0.49 ± 0.35 m w.e. yr^{-1} from 2004-2012), however lies well within the uncertainty ranges of the aforementioned publications. Pieczonka and Bolch (2015) inferred a mass change of -0.51 ± 0.36 m w.e. yr^{-1} from 1976 to 1999 and Goerlich et al (2017) encountered a mass loss of -0.40 ± 0.10 m w.e. yr^{-1} from 1964 to 1980 for the same mountain range. We derived similar magnitudes of mass loss for recent periods and, hence no clear trend is identifiable with time.

Mass change published for the entire Pamir vary considerably (Gardner et al, 2013; Gardelle et al, 2013; Kääb et al, 2015; Farinotti et al, 2015), which might be related to the important methodological differences and inconsistent periods. According to the temporal analysis using six-year periods, we identified a close to balanced period from

2000 to 2005. Studies including this period in their assessments reveal clearly less negative values (Gardelle et al, 2013; Brun et al, 2017) than studies focusing on periods after 2004 (Gardner et al, 2013; Kääb et al, 2015; Farinotti et al, 2015). The here obtained region-wide geodetic mass balance for the entire Pamir ($-0.24\pm0.43\,\mathrm{m\,w.e.\,yr^{-1}}$ from 2004 to 2012) lies somewhere in between values in literature.

8.5.5 Limitations and challenges of the presented approaches to assess region-wide glacier mass balance

A limitation of combining different methods for mass balance assessments is related to the inherent difference in the measured quantity. The TSL-constrained modelling calculates the surface mass balance, whereas the geodetic approach examines the total balance, including internal and basal components. The geodetic mass balance uses a simple conversion factor to derive mass from volume change, and does consequentially not account accurately for density changes in the firn pack due to refreezing. The quantification of internal and basal components is for the here applied methods not straightforward and calibration using field data is needed. Such data was not available and modelling internal or basal processes always demand assumptions and simplifications to a certain degree introducing further uncertainties. Here, we avoid such assumption and believe that the provided uncertainties account sufficiently for the generic difference of the measurement quantities.

The TSL-constrained model application might be critical on debris-covered glaciers. The influence of the debris on the glacier mass balance is complex and obscure the climate related reaction of the glacier mass changes. The here applied model does not account for debris-cover, thus might over- or underestimate melt rates of the underlying ice. However, the sub-seasonal TSL variation still reflects the annual variability of the SMB. The model is constrained to decadal geodetic mass changes and the modelled decadal mass change is tied to realistic quantities. Hence, through the applied second-order calibration, the reproduce annual mass balance variability and quantity for debris-covered glaciers by the TSL-constrained model is as accurate as the geodetic estimate and its uncertainty.

To test the influence of debris-cover on the mass balances distribution throughout the seven subregions, we calculated the correlation between the mass balance of debris-free and debris-covered glaciers and found significant correlation on the 99% level. A debris mask provided by Kraaijenbrink et al (2017) was used to distinguish between the two types. From this analysis, we could not identify a significant difference in the mass balance between clean and debris-covered glaciers. We found clearly more negative mean mass balances for debris-covered glaciers for the Eastern Pamir. Mean mass balance for debris-covered and debris-free glaciers for the Western Pamir and the Central Tien Shan however are practically equal, with higher variability encountered for debris-covered glaciers. Only for the Pamir-Alay the mean mass balance is clearly higher for the debris-covered glaciers. No debris-covered glaciers were identified for the other subregions. There are many surge-type glaciers reported for the Tien Shan and Pamir (Mukherjee et al, 2017; Kotlyakov et al, 2008). For surge-type glaciers, mass moves suddenly through hydrological or mechanical triggers from the accumulation to the ablation area (Cuffey and Paterson, 2010). Thus, the mass balance regime of the glacier might change abruptly due to non-climatic reasons. After such pronounced advance, melt rates might increase strongly and uncoupled from current local climate conditions. The TSL-constrained model is capable to predict annual SMBs for surge-type glaciers, if the geometry change is accounted for. At the current stage, outlines are held constant and surge activity is neglected for the here investigated study

period. We could not see strong disagreement between the geodetic and TSL-modelled results and did not observe divergent mass balances from the remaining Central Tien Shan. To estimate the effect of omitted surge activity on the annual mass balance time series, we analysed the relationship between surge-type glaciers and the mass balance for the seven study sites. For the analysis, we used the classification given by the RGIv6.0. From this classification, surge-type glaciers were only reported for the Western Pamir, the Pamir-Alay and the Central Tien Shan. No significant correlation was found. However, slightly more negative mass balances might be observed for glaciers with reported surge activity or signs of surges. Mukherjee et al (2017) reported 11 surge type glacier for the Akshiirak range, much more than identified by the RGIv6.0 (Fig. 8.5a). Underestimated surge activity might influence the here analysed relation.

8.6 Conclusions

In contrast to conventional modelling, the here applied TSL-constrained model is tied to direct sub-seasonal observations for each glacier and year, individually. This improves the results compared to unconstrained modelling significantly. Through a combination of TSL-constrained modelling and multi-annual time series from geodetic estimates, we aim at sound model calibration, integrating independent sub-seasonal and decadal information. The advantage of using multiple DEM differencing pairs from exhaustive ASTER datasets, processed with a new and improved method (MMASTER), in comparison to the use of single pairs derived from medium resolution sensors is shown. We, further, highlight the potential of using broadband albedo maps for surface classification of snow and ice, and thus SCAFs needed for the TSL-constrained model, on region-wide and automatized level. However, thick cloud cover and cast shadow remain an issue, and further development of the present approach would be favourable.

With our approach using multi-annual glacier mass changes derived from remote sensing, complemented with annual mass balance series, derived from modelling closely constrained with repeated TSL observations on a regional scale, we are able to not only observe decadal changes but also to infer annual mass balance variability for all investigated glaciers in data-sparse regions on mountain range scale. A geodetic mass loss of $-0.52 \pm 0.53\,\mathrm{m\,w.e.\,yr^{-1}}$ was calculated for the Tien Shan and of $-0.24 \pm 0.43\,\mathrm{m\,w.e.\,yr^{-1}}$ for the entire Pamir. Heterogeneous behaviour of debris-covered glaciers was found within the seven subregions and surge glaciers are prone to slightly enhanced melt rates in the Central Tien Shan and the Pamir.

With the TSL-constrained modelling, we reached a spatial coverage for glaciers greater than $2\,\mathrm{km^2}$ of 80%, and confirm that the Kyrgyz Ala-Too, the Pamir-Alay and the Akshiirak range show an important decadal mass loss ranging from -0.36 ± 0.32 to -0.44 ± 0.32 $\mathrm{m\,w.e.\,yr^{-1}}$ for 2000 to 2017. A more favourable period was encountered for the early years of the study period and exceptional negative balances were found for most glaciers in 2008. Annual variability is similar for the Kyrgyz Ala-Too and Pamir-Alay and diverges considerably for the Akshiirak massif, having comparably reduced year-to-year variability. We could further show that the annual variability between the glaciers increased for the Kyrgyz Ala-Too and the Akshiirak massif but glacier response became more homogeneous for the Pamir-Alay.

The combination of the two approaches as presented here, for the first time, complements multi-annual geodetic mass balances with modelled annual times series constrained with TSL observations for glaciers in the Tien Shan and Pamir. Such time series annually tied to TSL observations and decadaly tied to the geodetic estimates enable the analysis

of yearly mass balance variability for glaciers in a region with few measurements within the bounds of a multi-annual geodetic estimate and delivers important baseline data for in depth analysis of the glacier response to climate changes on elevated temporal resolution.

Author contribution

MB, MHu, MHo conceived the presented idea and developed the framework. MB developed and applied the model. MB analyzed, interpreted and discussed the results. KN developed the automatic snowline mapping tool that has been applied by MB. PB provided surface reflectance data. RM and MB calculated the geodetic mass balance from ASTER data. MB wrote the manuscript with help of MHu, MHo, MB, RM and KN.

Acknowledgments

This study is supported by the Swiss National Science Foundation (SNSF), grant 200021_15−5903. Additional support by the German Federal Foreign Office in the frame of the CAWa project (http://www.cawa-project.net) and the support of the Federal Office of Meteorology and Climatology MeteoSwiss through the project Capacity Building and Twinning for Climate Observing Systems (CATCOS) Phase 1 & 2, Contract nos. 7F-08114.1, 7F-08114.02.01, between the Swiss Agency for Development and Cooperation (SDC) and MeteoSwiss as well as the project CICADA (Cryospheric Climate Services for improved Adaptation), and contract no. 81049674 between Swiss Agency for Development and Cooperation and the University of Fribourg is equally acknowledged. E. Berthier acknowledges support from the French Space Agency (CNES) and the Programme National de Télédétection Spatiale grant PNTS−2016−01. R. McNabb acknowledges funding by ESA (Glaciers_cci project 4000109873/14/I-NB), and the European Union Seventh Framework Program (FP7) under European Research Council (ERC) contract 320816. We thank Philip Kraaijenbrink to provide debris cover maps for High Mountain Asia. We extend our thanks as well to T. Saks, A. Ghirlanda, A. Gafurov, M. Kronenberg, D. Sciboz and all others who contributed with fieldwork. We are also grateful for the collaboration of Central Asian Institute for Applied Geosciences, especially to B. Moldobekov for his continuous support. The Kumtor Gold Company provided the meteorological data.

Chapter 9

Acknowledgments

I would like to thank all the people involved in my PhD studies that helped and supported me during this time and contributed to the successful termination of this intense and fascinating period of my life:

First, I would like to thank deeply my two supervisors: Martin Hoelzle and Matthias Huss, who gave me the opportunity to work on my thesis but also to participate and lead such incredibly field expeditions. Each of them through their own way matched up to an extraordinary combination from which I benefited enormously, on a professional but also personal level. This kept me on the track to finally successfully complete my PhD. Especially, the endless discussions during the field expeditions about work, life and whatever else you can think of, will stay with me forever. Thank you very much for so many special and extraordinary moments. I cannot think of a better supervision.

Tomas Saks, Alyssa Ghirlanda and Marlene Kronenberg have become my little "Kyrgyz family" during all these years of CATCOS and CICADA. The four of us together make the dream team and without your help, I would never have managed to do all I did for the thesis but also for the CATCOS and CICADA projects. Thank you for the unforgettable moments, we share! From scientific collaborators we became close friends. The relationship, the trust and the friendship that developed with our Central Asian partners, helped me to never lose the motivation and made me feel like going home every summer again.

I have collected so so many nice and impressive memories in Central Asia. Moments I will never forget. These experiences and feeling shaped me to be the person I am today. For all this beautiful, but also sometimes difficult moments, I would like to thank the Central Asian team: Erlan Azisov, Ryskul Usubaliev, Andrey Yakovlev, Maxim Petrov, Dimtry Petrakov, Ruslan Kenzhebaev, Almaz Andashev, Tyinstyik Astanov, Aytshuruk, Avas, Halim, Xorshit, Tokhir, Mokhambad, Pilal, Nurik, Asam, Aman and many more.

Andy Kääb provided me the possibility to work at the Department of Geosciences at the University of Oslo, Norway. During those six months in Oslo, I gained valuable insight into new topics and different scientific approaches, which broadened my scientific horizon and helped to develop my remote sensing skills but also to focus on my thesis. Next to the great personal experience and many friendships built up in Oslo, I also benefited from diverse scientific collaborations and support. I would like to thank all the people from the Department of Geosciences and especially to Bas and Pim.

During my PhD studies I had the opportunity to collaborate with different scientists that have not been directly involved in my thesis but their input, their critical thinking and support were a very valuable contribution to my work: Etienne Berthier for his support with the remote sensing part and also through his impressive way of working and his critical review on my article. Horst Machguth, who pointed out the details and helped me with some programming problems. Kathrin Naegeli, for the moral support, and the scientific input through long, long discussions and phone calls. Nadine Salzmann, who helped me to become more familiar with Reanalysis data. Michael Zemp for the discussion on the perfect mass balance monitoring strategies. And finally, Paul Leclercq giving me a different view on modelling.

I would also like to thank the external experts Antoine Rabatel and Tobias Bolch. First for their time to carefully read my thesis and second for their expertise, helpful comments and critical view on my work.

Very much acknowledged are also to all the people that helped in the field, the capacity building and the twinning. Without you volunteering, we would never have been able to complete the program as smooth and complete as we did. I would also like to mention Govianni Kappenberger thanks to whom I found my passion in glaciology. I would further like to thank all people at the Geography Unit of the University of Fribourg that made my time in Fribourg unforgettable. Especially my office mates that resisted my moods: Leo Sold, Mauro Fischer, Kathrin Naegeli, Marlene Kronenberg, Alyssa Ghirlanda and Cecile Pellet. My gratefulness is also given to the technical staff, that I could bother with many urgent questions and needs. Many thanks for your patience and energy. In Central Asia, women in science are even more seldom than in Europe. I would like to thank deeply all the women involved in the CICADA and CATCOS project. The ones from Europe to show that it is possible and the ones from Central Asia for their energy, their will and their effort to change things. Many thanks to Aytshurok, Merim, Nuria, Mukhlia, Omida, Perizat, Nastia, Sidora, Dilarom, Oythaml, Marlene, Alyssa, Kathrin, Ana-Lena, Desirée, Saskia, Nadine, Julia, Helene. My deepest gratitude is offered to my family and David for their continuous support on my way.

This thesis was financed by the Swiss National Science Foundation (SNSF), grant $200021\_15 - 5903$. Additional support by the German Federal Foreign Office in the frame of the CAWa project (http://www.cawa-project.net) and the support of the Federal Office of Meteorology and Climatology MeteoSwiss through the project Capacity Building and Twinning for Climate Observing Systems (CATCOS) Phase 1 & 2, Contract nos. $7F$-08114.1, $7F$-08114.02.01, between the Swiss Agency for Development and Cooperation (SDC) and MeteoSwiss as well as the project CICADA (Cryospheric Climate Services for improved Adaptation), and contract no. 81049674 between Swiss Agency for Development and Cooperation and the University of Fribourg is equally acknowledged.

Bibliography

Adam S, Pietroniro A, Brugman MM (1997) Glacier snow line mapping using ers-1 sar imagery. Remote Sensing of Environment 61(1):46–54

Ageta Y, Higuchi K (1984) Estimation of mass balance components of a summer-accumulation type glacier in the nepal himalaya. Geografiska Annaler: Series A, Physical Geography 66(3):249–255

Ahlmann H (1922) Glaciers in jotunheim and their physiography. Geografiska Annaler 4(1):1–57

Ahlmann H (1924) Le niveau de glaciation comme fonction de l'accumulation d'humidité sous forme solide: Méthode pour le calcul de l'humidité condensée dans la haute montagne et pour l'étude de la fréquence des glaciers. Geografiska Annaler 6(3-4):223–272

Aizen V (1988) Reconstruktiya balansa massy lednika golubina [golubin glacier mass balance reconstruction]. Mater Glyatsiol Issled 62:119–126

Aizen V, Aizen E, Melack J (1995a) Present and future impact of snow cover and glaciers on runoff from mountain regions - comparison between Alps and Tien Shan. In: Biochemistry of Sesonally Snow-Covered Catchments, IAHS, Boulder, Colorado, USA, vol 228, pp 413–430

Aizen V, Aizen E, Melack J, Martma T (1996) Isotopic measurements of precipitation on central asian glaciers (southeastern tibet, northern himalayas, central tien shan). Journal of Geophysical Research: Atmospheres 101(D4):9185–9196

Aizen V, Surazakov A, Kuzmichenok V, Aizen E (2006) Glacier changes in central and northern Tien Shan during the last 140 years based on surface and remote sensing data. Annals of Glaciology 43:202–213

Aizen VB, Aizen EM, Melack JM (1995b) Climate, snow cover, glaciers, and runoff in the tien shan, central asia. JAWRA Journal of the American Water Resources Association 31(6):1113–1129

Aizen VB, Aizen EM, Melack JM, Dozier J (1997) Climatic and hydrologic changes in the tien shan, central asia. Journal of Climate 10(6):1393–1404

Aizen VB, Kuzmichenok VA, Surazakov AB, Aizen EM (2007) Glacier changes in the tien shan as determined from topographic and remotely sensed data. Global and Planetary Change 56(3):328–340

Alpert P (1986) Mesoscale indexing of the distribution of orographic precipitation over high mountains. Journal of climate and applied meteorology 25(4):532–545

Altena B, Mousivand A, Mascaro J, Kääb A (2017) Potential and limitations of photometric reconstruction through a flock of dove cubesats. International Archives of Photogrammetry, Remote Sensing and Spatial Information Sciences 42(3):7–11

Andreassen LM, Engeset RV (2016) Reanalysis of long-term series of glaciological and geodetic mass balance for 10 norwegian glaciers. The Cryosphere 10(2):535

Arendt A, Sharp M (1999) Energy balance measurements on a canadian high arctic glacier and their implications for mass balance modelling. IAHS Publications pp 165–172

Arendt A, Bliss A, Bolch T, Cogley J, Gardner A, Hagen J, Hock R, Huss M, Kaser G, Kienholz C, Pfeffer W, Moholdt G, Paul F, Radic V, Andreassen L, Bajracharya S, Barrand N, Beedle M, Berthier E, Bhambri R, Brown I, Burgess E, Burgess D, Cawkwell F, Chinn T, Copland L, Davies B, De Angelis H, Dolgova E, Earl L, Filbert K, Forester R, Fountain A, Frey H, Giffen B, Glasser N, Guo W, Gurney S, Hagg W, Hall D, Haritashya U, Hartmann G, Helm C, Herreid S, Howat I, Kapustin G, Khromova T, König M, Kohler J, Kriegel D, Kutuzov S, Lavrentiev I, Le Bris R, Liu S, Lund J, Manley W, Mayer C, Miles E, Li X, Menounos B, Mercer A, Mölg N, Mool P, Nosenko G, Negrete C, Nuth C, Petterson R, Racoviteanu A, Ranzi R, Rastner P, Rau F, Raup B, Rich J, Rott H, Schneider C, Seliverstov Y, Sharp M, Sigurdsson O, Stokes C, Wheate R, Winsvold S, Wolken G, Wyatt F, Zheltyhina N (2015) Randolph glacier inventory: A dataset of global glacier outlines: Version 5.0. Digital media, Global Land Ice Measurements from Space

Aubry-Wake C, Zephir D, Baraer M, McKenzie J, Mark B (2017) Importance of longwave emissions from adjacent terrain on patterns of tropical glacier melt and recession. Journal of Glaciology pp 1–12

Ayala A, Pellicciotti F, MacDonell S, McPhee J, Burlando P (2017) Patterns of glacier ablation across north-central chile: Identifying the limits of empirical melt models under sublimation-favorable conditions. Water Resources Research

Azam M, P W, Berthier E, Vincent C, Fujita K, JS K (2018) Review of the status and mass changes of himalayan-karakoram glaciers. Journal of Glaciology pp 1–14

Azam MF, Wagnon P, Vincent C, Ramanathan A, Linda A, Singh VB (2014) Reconstruction of the annual mass balance of chhota shigri glacier, western himalaya, india, since 1969. Annals of Glaciology 55(66):69–80

Azam MF, Ramanathan A, Wagnon P, Vincent C, Linda A, Berthier E, Sharma P, Mandal A, Angchuk T, Singh V, et al (2016) Meteorological conditions, seasonal and annual mass balances of chhota shigri glacier, western himalaya, india. Annals of Glaciology 57(71):328–338

Bagdassarov N, Batalev V, Egorova V (2011) State of lithosphere beneath tien shan from petrology and electrical conductivity of xenoliths. Journal of Geophysical Research (Solid Earth) 116:1202, DOI 10.1029/2009JB007125

Bahr DB, Dyurgerov M, Meier MF (2009) Sea-level rise from glaciers and ice caps: A lower bound. Geophysical Research Letters 36(3)

Barandun M, Huss M, Azisov E, Gafurov A, M H, Merkushkin A, Salzmann N, Usubaliev R (2013) Re-establishing seasonal mass balance observation at abramov glacier, kyrgyzstan, from 1968-2012. In: EGU General Assembly Conference Abstracts, vol 15, p 5668

Barandun M, Huss M, Sold L, Farinotti D, Azisov E, Salzmann N, Usubaliev R, Merkushkin A, Hoelzle M (2015) Re-analysis of seasonal mass balance at abramov glacier 1968–2014. Journal of Glaciology 61(230):1103–1117

Barandun M, Huss M, Usubaliev R, Azisov E, Berthier E, Kääb A, Bolch T, Hoelzle M (2018) Multi-decadal mass balance series of three kyrgyz glaciers inferred from modelling constrained with repeated snow line observations. The Cryosphere 12(6):1899–1919

Barcaza G, Aniya M, Matsumoto T, Aoki T (2009) Satellite-derived equilibrium lines in northern patagonia icefield, chile, and their implications to glacier variations. Arctic, Antarctic, and Alpine Research 41(2):174–182

Barry RG (1992) Mountain weather and climate. Psychology Press

Bauder A, Funk M, Huss M (2007) Ice-volume changes of selected glaciers in the Swiss Alps since the end of the 19th century. Annals of Glaciology 46:145–149

Bazhev A (1973) Infiltration and run-off of melt water on glaciers. International Association of Scientific Hydrology Publication 95:245–250

Beedle M, Menounos B, Wheate R (2014) An evaluation of mass-balance methods applied to castle creek glacier, british columbia, canada. Journal of Glaciology 60:262–276, DOI 10.3189/2014JoG13J091

Bengtsson L, Shukla J (1988) Integration of space and in situ observations to study global climate change. Bulletin of the American Meteorological Society 69:1130–1143, DOI 10.1175/1520-0477

Benn DI, Lehmkuhl F (2000) Mass balance and equilibrium-line altitudes of glaciers in high-mountain environments. Quaternary International 65:15–29

Berthier E, Arnaud Y, Vincent C, Remy F (2006) Biases of srtm in high-mountain areas: Implications for the monitoring of glacier volume changes. Geophysical Research Letters 33(8)

Berthier E, Schiefer E, Clarke G, Menounos B, Rémy F (2010) Contribution of Alaskan glaciers to sea-level rise derived from satellite imagery. Nature Geoscience 3:92–95

Berthier E, Vincent C, Magnússon E, Gunnlaugsson Á, Pitte P, Le Meur E, Masiokas M, Ruiz L, Pálsson F, Belart J, et al (2014) Glacier topography and elevation changes derived from pléiades sub-meter stereo images. The Cryosphere 8(6):2275–2291

Berthier E, Cabot V, Vincent C, Six D (2016) Decadal region-wide and glacier-wide mass balances derived from multi-temporal aster satellite digital elevation models. validation over the mont-blanc area. Frontiers in Earth Science 4:63

Bhardwaj A, Sam L, Martín-Torres FJ, Kumar R, et al (2016) Uavs as remote sensing platform in glaciology: Present applications and future prospects. Remote sensing of environment 175:196–204

Bippus G (2011) Characteristics of summer snow areas on glaciers observed by means of landsat data. PhD thesis, Leopold Franzens Universit

Bishop MP, Kargel JS, Kieffer HH, MacKinnon DJ, Raup BH, Shroder JF (2000) Remote-sensing science and technology for studying glacier processes in high asia. Annals of glaciology 31:164–170

Bliss AK, Cuffey KM, Kavanaugh JL (2011) Sublimation and surface energy budget of taylor glacier, antarctica. Journal of Glaciology 57(204):684–696

Bojinski S, Verstraete M, Peterson TC, Richter C, Simmons A, Zemp M (2014) The concept of essential climate variables in support of climate research, applications, and policy. Bulletin of the American Meteorological Society 95(9):1431–1443

Bolch T (2007) Climate change and glacier retreat in northern Tien Shan (Kazakhstan/Kyrgyzstan) using remote sensing data. Global and Planetary Change 56(1-2):1–12

Bolch T (2015) Glacier area and mass changes since 1964 in the ala archa valley, kyrgyz ala-too, northern tien shan. Lëd i Sneg 55(1):28–39

Bolch T (2017) Hydrology: Asian glaciers are a reliable water source. Nature 545(7653):161–162

Bolch T, Buchroithner M (2008) Suitability of medium scale topographic maps and the SRTM DEM to estimate glacier volume changes in the Northern Tien Shan. Tech. rep.

Bolch T, Buchroithner MF, Kunert A, Kamp U (2007) Automated delineation of debris-covered glaciers based on aster data. In: Geoinformation in Europe. proceedings of the 27th EARSeL Symposium, pp 4–6

Bolch T, Buchroithner M, Pieczonka T, Kunert A (2008) Planimetric and volumetric glacier changes in the Khumbu Himal, Nepal, since 1962 using Corona, Landsat TM and ASTER data. Journal of Glaciology 54(187):592–600

Bolch T, Yao T, Kang S, Buchroithner M, Scherer D, Maussion F, Huintjes E, Schneider C (2010) A glacier inventory for the western nyainqentanglha range and the nam co basin, tibet, and glacier changes 1976-2009. The Cryosphere 4(3):419

Bolch T, Peters J, Yegorov A, Pradhan B, Buchroithner M, Blagoveshchensky V (2011a) Identification of potentially dangerous glacial lakes in the northern tien shan. Natural Hazards 59(3):1691–1714

Bolch T, Pieczonka T, Benn D (2011b) Multi-decadal mass loss of glaciers in the Everest area (Nepal, Himalaya) derived from stereo imagery. The Cryosphere 5:349–358

Bolch T, Kulkarni A, Kääb A, Huggel C, Paul F, Cogley J, Frey H, Kargel JS, Fujita K, Scheel M, et al (2012) The state and fate of himalayan glaciers. Science 336(6079):310–314

Bolch T, Shea J, Azam F, Liu S, Tahir A, et al (in press) Status and change of the cryosphere. ICIMOD: Hindukush – Himalayan Monitoring and Assessment Programme Report

Braithwaite R, Müller F (1980) On the parameterization of glacier equilibrium line altitude. IAHS Publ 126:263–271

Braithwaite R, Zhang Y (2000) Sensitivity of mass balance of five swiss glaciers to temperature changes assessed by tuning a degree-day model 46(152):7–14, DOI 10.3189/172756500781833511

Braithwaite RJ (1981) On glacier energy balance, ablation, and air temperature. Journal of Glaciology 27(97):381–391

Braithwaite RJ (1984a) Can the mass balance of a glacier be estimated from its equilibrium-line altitude? Journal of Glaciology 30(106):364–368

Braithwaite RJ (1984b) Short notes: Can the mass balance of a glacier be estimated from its equilibrium-line altitude? Journal of Glaciology 30(106):364–368

Braithwaite RJ (1995) Positive degree-day factors for ablation on the greenland ice sheet studied by energy-balance modelling. Journal of Glaciology 41(137):153–160

Braithwaite RJ (2008) Temperature and precipitation climate at the equilibrium-line altitude of glaciers expressed by the degree-day factor for melting snow. Journal of Glaciology 54(186):437–444

Braithwaite RJ, Laternser M, Pfeffer WT (1994) Variations of near-surface firn density in the lower accumulation area of the greenland ice sheet, pâkitsoq, west greenland. Journal of Glaciology 40(136):477–485

Bravo C, Rojas M, Anderson B, Mackintosh A, Sagredo E, Moreno P (2015) Modelled glacier equilibrium line altitudes during the mid-holocene in the southern mid-latitudes. Climate of the Past 11(11):1575

Brückner E (1887) Die höhe der schneelinie und ihre bestimmung. Meteorologische Zeitschrift 4:31–32

Brückner E (1907) Annales de glaciologie, vol 1. Gebrüder Borntraeger.

Brun F, Berthier E, Wagnon P, Kääb A, Treichler D (2017) A spatially resolved estimate of high mountain asia glacier mass balances, 2000-2016. Nature geoscience 10(9):668

Bunting P (2017) Pre-processing of remotely sensed imagery. In: The Roles of Remote Sensing in Nature Conservation, Springer, pp 39–63

Callegari M, Carturan L, Marin C, Notarnicola C, Rastner P, Seppi R, Zucca F (2016) A pol-sar analysis for alpine glacier classification and snowline altitude retrieval. IEEE Journal of Selected Topics in Applied Earth Observations and Remote Sensing 9(7):3106–3121

Callegari M, Marin C, Notarnicola C (2017) Multi-temporal and multi-source alpine glacier cover classification. In: Analysis of Multitemporal Remote Sensing Images (MultiTemp), 2017 9th International Workshop on the, IEEE, pp 1–3

Chapuis A, Rolstad C, Norland R (2010) Interpretation of amplitude data from a ground-based radar in combination with terrestrial photogrammetry and visual observations for calving monitoring of kronebreen, svalbard. Annals of Glaciology 51(55):34–40

Chen Y, Li W, Deng H, Fang G, Li Z (2016) Changes in central asia's water tower: Past, present and future. Scientific reports 6:35,458

Chinn T (1995) Glacier fluctuations in the southern alps of new zealand determined from snowline elevations. Arctic and alpine research pp 187–198

Chinn T (1999) New zealand glacier response to climate change of the past 2 decades. Global and Planetary Change 22(1):155–168

Chinn T, Whitehouse I (1980) Glacier snow line variations in the southern alps, new zealand. World Glacier Inventory International Association of Hydrological Sciences Publication 126:219–228

Chinn T, Salinger J, Fitzharris B, Willsman A (2012) Annual ice volume changes 1976 - 2008 for the New Zealand Southern Alps. Global and Planetary Change 92-93:105–118

Chinn TJ, Heydenrych C, Salinger MJ (2005) Use of the ela as a practical method of monitoring glacier response to climate in new zealand's southern alps. Journal of Glaciology 51(172):85–95

Clarke GK, Jarosch AH, Anslow FS, Radić V, Menounos B (2015) Projected deglaciation of western canada in the twenty-first century. Nature Geoscience 8(5):372

Claverie M, Vermote EF, Franch B, Masek JG (2015) Evaluation of the landsat-5 tm and landsat-7 etm+ surface reflectance products. Remote Sensing of Environment 169:390–403

Cogley J, Hock R, Rasmussen L, Arendt A, Bauder A, Braithwaite R, Jansson P, Kaser G, Möller M, Nicholson L, Zemp M (2011) Glossary of glacier mass balance and related terms, ihp-vii technical documents in hydrology no. 86, iacs contribution no. 2. DOI 10.1657/1938-4246-44.2.256b

Cogley JG (2009) Geodetic and direct mass-balance measurements: comparison and joint analysis. Annals of Glaciology 50(50):96–100

Collins M, Doolittle J, Rourke R (1989) Mapping depth to bedrock on a glaciated landscape with ground-penetrating radar. Soil Science Society of America Journal 53(6):1806–1812

Corripio J (2004) Snow surface albedo estimation using terrestrial photography. International Journal of Remote Sensing 25(24):5705–5729, DOI 10.1080/01431160410001709002

Cox LH, March RS (2004) Comparison of geodetic and glaciological mass-balance techniques, gulkana glacier, alaska, usa. Journal of Glaciology 50(170):363–370

Crawford CJ, Manson SM, Bauer ME, Hall DK (2013) Multitemporal snow cover mapping in mountainous terrain for landsat climate data record development. Remote sensing of environment 135:224–233

Cuffey KM, Paterson WSB (2010) The physics of glaciers. Academic Press

Dahe Q, Shiyin L, Peiji L (2006) Snow cover distribution, variability, and response to climate change in western china. Journal of climate 19(9):1820–1833

De Angelis H, Rau F, Skvarca P (2007) Snow zonation on hielo patagónico sur, southern patagonia, derived from landsat 5 tm data. Global and Planetary Change 59(1-4):149–158

Dee D, Uppala S, Simmons A, Berrisford P, Poli P, Kobayashi S, Andrae U, Balmaseda M, Balsamo G, Bauer P, Bechtold P, Beljaars ACM, van de Berg L, Bidlot J, Bormann N, Delsol C, Dragani R, Fuentes M, Geer AJ, Haimberger L, Healy S, Hersbach H, Hólm E, Isaksen L, Kållberg P, Köhler M, Matricardi M, McNally P, Monge-Sanz B, Morcrette J, Park B, Peubey C, de Rosnay P, Tavolato C, Thépaut J, Vitart F (2011) The ERA-Interim reanalysis: configuration and performance of the data assimilation system. Quarterly Journal of the Royal Meteorological Society 137:553–597, DOI 10.1002/qj.828

Dehecq A, Millan R, Berthier E, Gourmelen N, Trouvé E, Vionnet V (2016) Elevation changes inferred from tandem-x data over the mont-blanc area: Impact of the x-band interferometric bias. IEEE Journal of Selected Topics in Applied Earth Observations and Remote Sensing 9(8):3870–3882

Dozier J (1980) A clear-sky spectral solar radiation model for snow-covered mountainous terrain. Water Resources Research 16(4):709–718

Dozier J, Marks D (1987) Snow mapping and classification from landsat thematic mapper data. Annals of Glaciology 9:97–103

Duethmann D, Zimmer J, Gafurov A, Güntner A, Kriegel D, Merz B, Vorogushyn S (2013) Evaluation of areal precipitation estimates based on downscaled reanalysis and station data by hydrological modelling. Hydrology and Earth System Sciences 17:2415–2434, DOI 10.5194/hess-17-2415-2013

Duethmann D, Peters J, Blume T, Vorogushyn S, Güntner A (2014) The value of satellite-derived snow cover images for calibrating a hydrological model in snow-dominated catchments in central asia. Water Resources Research 50(3):2002–2021

Duethmann D, Bolch T, Farinotti D, Kriegel D, Vorogushyn S, Merz B, Pieczonka T, Jiang T, Su B, Güntner A (2015) Attribution of streamflow trends in snow and glacier melt-dominated catchments of the tarim river, central asia. Water Resources Research 51(6):4727–4750

Dumont M, Sirguey P, Arnaud Y, Six D (2011) Monitoring spatial and temporal variations of surface albedo on saint sorlin glacier (french alps) using terrestrial photography. The Cryosphere 5(3):759–771

Dumont M, Gardelle J, Sirguey P, Guillot A, Six D, Rabatel A, Arnaud Y (2012) Linking glacier annual mass balance and glacier albedo retrieved from modis data. The Cryosphere 6:1527–1539

Dunse T, Schuler TV, Hagen JO, Eiken T, Brandt O, Høgda KA (2009) Recent fluctuations in the extent of the firn area of austfonna, svalbard, inferred from gpr. Annals of Glaciology 50(50):155–162

Dyurgerov M (1996) Substitution of long-term mass balance data by measurements of one summer. Z Gletscherkd Glazialgeol 32:177–184

Dyurgerov M, Dwyer J (2000) Abhandlungen-the steepening of glacier mass balance gradients with northern hemispere warming. with 6 figures. Zeitschrift fur Gletscherkunde und Glazialgeologie 36:107–118

Dyurgerov M, Mikhalenko V (1995) Oledeneniye tien shanya [glaciation of tien shan]. VINITI, Moscow [in Russian]

Dyurgerov M, Kunakhovitch M, Mikhalenko V, Sokalskaya A, Kuzmichenok V (1992) Can the mass balance of the entire glacier area of the tien shan be estimated? Annals of Glaciology 16:173–179

Dyurgerov M, Mikhalenko V, Kunakhovitch M, Ushnurtsev S, Liu C, Xie Z (1994) On the cause of glacier mass balance variations in the tian shan mountains. GeoJournal 33(2):311–317

Dyurgerov M, Liu C, Xie Z (1995) Oledenenie tyan'-shanya [tien shan glaciers]. Publishing House Nauka, Moscow (Russian)

Dyurgerov M, Meier M, Armstrong RL (2002) Glacier mass balance and regime: data of measurements and analysis. Institute of Arctic and Alpine Research, University of Colorado Boulder,, USA

Dyurgerov M, Meier MF, Bahr DB (2009) A new index of glacier area change: a tool for glacier monitoring. Journal of Glaciology 55(192):710–716

Dyurgerov MB, Meier MF (2000) Twentieth century climate change: evidence from small glaciers. Proceedings of the National Academy of Sciences 97(4):1406–1411

Eineder M, Breit H, Fritz T, Schättler B, Roth A (2005) Terrasar-x sar products and processing algorithms. In: IGARSS IEEE International Geoscience and Remote Sensing Symposium, IEEE, vol 7, pp 4870–4873

Elsberg D, Harrison W, Echelmeyer K, Krimmel R (2001) Quantifying the effects of climate and surface change on glacier mass balance 47(159):649–658, DOI 10.3189/172756501781831783

Escher-Vetter H, Kuhn M, Weber M (2009) Four decades of winter mass balance of vernagtferner and hintereisferner, austria: methodology and results. Annals of Glaciology 50(50):87–95

Evans DJ, Ewertowski M, Jamieson SS, Orton C (2016) Surficial geology and geomorphology of the kumtor gold mine, kyrgyzstan: human impacts on mountain glacier landsystems. Journal of Maps 12(5):757–769

Fahnestock M, Abdalati W, Joughin I, Brozena J, Gogineni P (2001) High geothermal heat flow, basal melt, and the origin of rapid ice flow in central greenland. Science 294(5550):2338–2342

Farinotti D, Magnusson J, Huss M, Bauder A (2010) Snow accumulation distribution inferred from time-lapse photography and simple modelling. Hydrological Processes 24(15):2087–2097, DOI 10.1002/hyp.7629

Farinotti D, Longuevergne L, Moholdt G, Duethmann D, Mölg T, Bolch T, Vorogushyn S, Güntner A (2015) Substantial glacier mass loss in the tien shan over the past 50 years. Nature Geoscience 8(9):716–722

Fischer M, Huss M, Kummert M, Hoelzle M (2016) Application and validation of long-range terrestrial laser scanning to monitor the mass balance of very small glaciers in the swiss alps. The Cryosphere 10(3):1279–1295

Forel F (1892) The periodic variations of alpine glaciers

Forel F (1895) Les variations périodiques des glaciers., volume xxxiv. Archives des sciences physiques et naturelles, Geneve

Forel F, Du Pasquier L (1896) Les variations périodiques des glaciers. ier rapport, 1895. Extrait des Archives des Sciences physiques et naturelles 101(2):129–147

Forel FA (1881) Essai sur les variations périodiques des glaciers. Imprimerie Charles Schuchardt

Forster RR, Box JE, van den Broeke MR, Miège C, Burgess EW, van Angelen JH, Lenaerts J, Koenig LS, Paden J, Lewis C, et al (2014) Extensive liquid meltwater storage in firn within the greenland ice sheet. Nature Geoscience 7:95–98

Fountain AG, Hoffman MJ, Granshaw F, Riedel J (2009) The 'benchmark glacier'concept–does it work? lessons from the north cascade range, usa. Annals of Glaciology 50(50):163–168

Frolov A, Macheret Y (1999) On dielectric properties of dry and wet snow. Hydrological Processes 13:1755–1760, DOI 10.1002/(SICI)1099-1085

Fuchs MC, Gloaguen R, Pohl E (2013) Tectonic and climatic forcing on the panj river system during the quaternary. International Journal of Earth Sciences 102(7):1985–2003

Fugazza D, Senese A, Azzoni R, Smiraglia C, Cernuschi M, Severi D, Diolaiuti G, et al (2015) High-resolution mapping of glacier surface features. the uav survey of the forni glacier (stelvio national park, italy). Geografia Fisica e Dinamica Quaternaria 38(1):25–33

Fujita K (2008a) Effect of precipitation seasonality on climatic sensitivity of glacier mass balance. Earth and Planetary Science Letters 276(1-2):14–19

Fujita K (2008b) Influence of precipitation seasonality on glacier mass balance and its sensitivity to climate change. Annals of Glaciology 48:88–92

Fujita K, Ageta Y (2000) Effect of summer accumulation on glacier mass balance on the tibetan plateau revealed by mass-balance model. Journal of Glaciology 46(153):244–252

Fujita K, Nuimura T (2011) Spatially heterogeneous wastage of himalayan glaciers. Proceedings of the National Academy of Sciences 108(34):14,011–14,014

Fujita K, Seko K, Ageta Y, Jianchen P, Tandong Y (1996) Superimposed ice in glacier mass balance on the tibetan plateau. Journal of Glaciology 42(142):454–460

Fujita K, Takeuchi N, Nikitin S, Surazakov A, Okamoto S, Aizen V, Kubota J (2011) Favorable climatic regime for maintaining the present-day geometry of the gregoriev glacier, inner tien shan. The Cryosphere 5(3):539, DOI 10.5194/tc-5-539-2011

Furbish D, Andrews J (1984) The use of hypsometry to indicate long-term stability and response of valley glaciers to changes in mass transfer. Journal of Glaciology 30(105):199–211

Gabbi J, Carenzo M, Pellicciotti F, Bauder A, Funk M (2014) A comparison of empirical and physically based glacier surface melt models for long-term simulations of glacier response. Journal of Glaciology 60(224):1140–1154

Gafurov A, Kriegel D, Vorogushyn S, Merz B (2013) Evaluation of remotely sensed snow cover product in central asia. Hydrology Research 44(3):506–522, DOI 10.2166/nh.2012.094

Gan R, Luo Y, Zuo Q, Sun L (2015) Effects of projected climate change on the glacier and runoff generation in the naryn river basin, central asia. Journal of Hydrology 523:240–251

Gao X, Ye B, Zhang S, Qiao C, Zhang X (2010) Glacier runoff variation and its influence on river runoff during 1961–2006 in the tarim river basin, china. Science China Earth Sciences 53(6):880–891

Gardelle J, Berthier E, Arnaud Y (2012a) Impact of resolution and radar penetration on glacier elevation changes computed from dem differencing. Journal of Glaciology 58(208):419–422, DOI 10.3189/2012JoG11J175

Gardelle J, Berthier E, Arnaud Y (2012b) Slight mass gain of karakoram glaciers in the early twenty-first century. Nature geoscience 5(5):322

Gardelle J, Berthier E, Arnaud Y, Kääb A (2013) Region-wide glacier mass balances over the pamir-karakoram-himalaya during 1999–2011. The Cryosphere 7(4):1263–1286

Gardner A, Moholdt G, Cogley J, Wouters B, Arendt A, Wahr J, Berthier E, Hock R, Pfeffer W, Kaser G, Ligtenberg S, Bolch T, Sharp M, Hagen J, van den Broeke M, Paul F (2013) A Reconciled Estimate of Glacier Contributions to Sea Level Rise: 2003 to 2009. Science 340:852–857, DOI 10.1126/science.1234532

GCOS (2010) Implementation plan for the global observing system for climate in support of the unfccc. GCOS 138p:180

GCOS (2016) The global observing system for climate: Implementation needs. GCOS 325p:180

Gerbaux M, Genthon C, Etchevers P, Vincent C, Dedieu J (2005) Surface mass balance of glaciers in the french alps: distributed modeling and sensitivity to climate change. Journal of Glaciology 51(175):561–572

Girod L, Nuth C, Kääb A, Etzelmüller B, Kohler J (2017a) Terrain changes from images acquired on opportunistic flights by sfm photogrammetry. Cryosphere 11(2)

Girod L, Nuth C, Kääb A, McNabb R, Galland O (2017b) Mmaster: Improved aster dems for elevation change monitoring. Remote Sensing 9(7):704

Glazirin G, Kislov V, Ogudin A (1987) Mechanism of the movement of abramov glacier from 1972-1975. Data of Glaciological Studies 30(1):94–1001

Glazirin G, Kamnyanskii G, Perziger F (1993) Regime of the Abramov glacier. Leningrad: Hydrometeo Publishing

Glazirin G, Braun L, Shchetinnikov A (2002) Sensitivity of mountain glacierization to climatic changes in central asia. with 1 figure. Zeitschrift fur Gletscherkunde und Glazialgeologie 38(1):71–76

Goerlich F, Bolch T, Mukherjee K, Pieczonka T (2017) Glacier mass loss during the 1960s and 1970s in the ak-shirak range (kyrgyzstan) from multiple stereoscopic corona and hexagon imagery. Remote Sensing 9(3):275

Guo Z, Wang N, Kehrwald NM, Mao R, Wu H, Wu Y, Jiang X (2014) Temporal and spatial changes in western himalayan firn line altitudes from 1998 to 2009. Global and Planetary Change 118:97–105

Hadjimitsis DG, Clayton C, Hope V (2004) An assessment of the effectiveness of atmospheric correction algorithms through the remote sensing of some reservoirs. International Journal of Remote Sensing 25(18):3651–3674

Haeberli W (1998) Historical evolution and operational aspects of worldwide glacier monitoring. Studies and reports in hydrology 56:35–51

Haeberli W (2006) Observing systems. Global Change and Mountain Regions: An Overview of Current Knowledge 23:169

Haeberli W, Hoelzle M (1995) Application of inventory data for estimating characteristics of and regional climate-change effects on mountain glaciers: a pilot study with the european alps. Annals of Glaciology 21:206–212

Haeberli W, Cihlar J, Barry RG (2000) Glacier monitoring within the global climate observing system. Annals of Glaciology 31:241–246

Haeberli W, Hoezle M, Paul F, Zemp M (2007) Integrated monitoring of mountain glaciers as key indicators of global climate change: the European Alps. AG 46:150–160, DOI 10.3189/172756407782871512

Hagg W, Braun L, Uvarov V, Makarevich K (2004a) A comparison of three methods of mass-balance determination in the Tuyuksu glacier region, Tien Shan, Central Asia. Journal of Glaciology 50(171):505–510

Hagg W, Braun L, Weber M, Brecht M (2006) Runoff modelling in glacierized Central Asia catchments for present-day and future climate. Nordic Hydrology 37:1–13

Hagg W, Braun L, Kuhn M, Nesgaard T (2007) Modelling of hydrological response to climate change in glacierized Central Asian catchments. Journal of Hydrology 332:40–53

Hagg W, Mayer C, Lambrecht A, Kriegel D, Azizov E (2013) Glacier changes in the big naryn basin, central tian shan. Global and Planetary Change 110:40–50

Hagg WJ, Braun LN, Uvarov VN, Makarevich KG (2004b) A comparison of three methods of mass-balance determination in the tuyuksu glacier region, tien shan, central asia. Journal of Glaciology 50(171):505–510

Hall D, Ormsby J, Bindschadler R, Siddalingaiah H (1987) Characterization of snow and ice reflectance zones on glaciers using landsat thematic mapper data. Annals of Glaciology 9:104–108

Hall D, Williams R, Barton J, Sigurdjsson O, Smith L, Garvin J (2000) Evaluation of remote-sensing techniques to measure decadal-scale changes of hofsjökull ice cap, iceland. Journal of Glaciology 46(154):375–388

Hall DK, Chang AT, Siddalingaiah H (1988) Reflectances of glaciers as calculated using landsat-5 thematic mapper data. Remote Sensing of Environment 25(3):311–321

Hall DK, Riggs GA, Salomonson VV (1995) Development of methods for mapping global snow cover using moderate resolution imaging spectroradiometer data. Remote sensing of Environment 54(2):127–140

Hall M (1895a) A glacial committee for north america and europe. Geological Magazine 2(3):144–144

Hall M (1895b) Ii.—les variations périodiques des glaciers. discours préliminaire. par forel fa, president de la commission internationale des glaciers. archives des sciences physiques et naturelles. genève. vol. xxxiv, p. 209. Geological Magazine 2(12):569–570

Hannah DM, Gurnell AM, McGregor GR (2000) Spatio-temporal variation in microclimate, the surface energy balance and ablation over a cirque glacier. International Journal of Climatology 20(7):733–758

Haritashya U, Bishop M, Shroder J, Bush A, Bulley H (2009) Space-based assessment of glacier fluctuations in the Wakhan Pamir, Afghanistan. Climate Change 94:5–18

Heiskanen J, Kivinen S (2008) Assessment of multispectral,-temporal and-angular modis data for tree cover mapping in the tundra–taiga transition zone. Remote Sensing of Environment 112(5):2367–2380

Helfricht K, Kuhn M, Keuschnig M, Heilig A (2014a) Lidar snow cover studies on glaciers in the otztal alps (austria): comparison with snow depths calculated from gpr measurements. The Cryosphere 8(1):41

Helfricht K, Schöber J, Schneider K, Sailer R, Kuhn M (2014b) Interannual persistence of the seasonal snow cover in a glacierized catchment. Journal of Glaciology 60:889–904, DOI 10.3189/2014JoG13J197

Herron M, Langway C (1980) Firn densification: an empirical model. Journal of Glaciology 25:373–385

Hock R (1999) A distributed temperature-index ice-and snowmelt model including potential direct solar radiation. Journal of Glaciology 45:101–111

Hock R (2003) Temperature index melt modelling in mountain areas. Journal of Hydrology 282(1-4):104–115, DOI 10.1016/S0022-1694(03)00257-9

Hock R (2005) Glacier melt: a review of processes and their modelling. Progress in physical geography 29(3):362–391

Hock R, Jensen H (1999) Application of kriging interpolation for glacier mass balance computations. Geografiska Annaler: Series A, Physical Geography 81(4):611–619

Hock R, Kootstra DS, Reijmer C (2007) Deriving glacier mass balance from accumulation area ratio on storglaciären, sweden. IAHS-AISH publication pp 163–170

Hodge SM, Trabant DC, Krimmel RM, Heinrichs TA, March RS, Josberger EG (1998) Climate variations and changes in mass of three glaciers in western north america. Journal of Climate 11(9):2161–2179

Hoelzle M, Haeberli W, Dischl M, Peschke W (2003) Secular glacier mass balances derived from cumulative glacier length changes. Global and Planetary Change 36(4):295–306

Hoelzle M, Azisov E, Barandun M, Huss M, Farinotti D, Gafurov A, Hagg W, Kenzhebaev R, Kronenberg M, Machguth H, et al (2017) Re-establishing glacier monitoring in kyrgyzstan and uzbekistan, central asia. Geoscientific Instrumentation, Methods and Data Systems 6(2):397

Hoinkes H (1955) Measurements of ablation and heat balance on alpine glaciers: With some remarks on the cause of glacier recession in the alps. Journal of Glaciology 2(17):497–501

Hoinkes HC (1968) Glacier variation and weather. Journal of Glaciology 7(49):3–18

Holzer N, Vijay S, Yao T, Xu B, Buchroithner M, Bolch T (2015) Four decades of glacier variations at muztagh ata (eastern pamir): a multi-sensor study including hexagon kh-9 and pléiades data. The Cryosphere 9(6):2071–2088

Hooke RL (2005) Principles of glacier mechanics. Cambridge university press

Howat IM, de la Peña S, Desilets D, Womack G (2018) Autonomous ice sheet surface mass balance measurements from cosmic rays. The Cryosphere Discussions 2018:1–16, DOI 10.5194/tc-2018-30

Huggel C, Kääb A, Haeberli W, Teysseire P, Paul F (2002) Remote sensing based assessment of hazards from glacier lake outbursts: a case study in the swiss alps. Canadian Geotechnical Journal 39(2):316–330

Huintjes E, Neckel N, Hochschild V, Schneider C (2015a) Surface energy and mass balance at purogangri ice cap, central tibetan plateau, 2001–2011. Journal of Glaciology 61(230):1048–1060

Huintjes E, Sauter T, Schröter B, Maussion F, Yang W, Kropáček J, Buchroithner M, Scherer D, Kang S, Schneider C (2015b) Evaluation of a coupled snow and energy balance model for zhadang glacier, tibetan plateau, using glaciological measurements and time-lapse photography. Arctic, antarctic, and alpine research 47(3):573–590

Huintjes E, Loibl D, Lehmkuhl F, Schneider C (2016) A modelling approach to reconstruct little ice age climate from remote-sensing glacier observations in southeastern tibet. Annals of Glaciology 57(71):359–370

Hulth J, Rolstad Denby C, Hock R (2013) Estimating glacier snow accumulation from backward calculation of melt and snowline tracking. Annals of Glaciology 64:1–7, DOI 10.3189/2013AoG62A083

Humphrey NF, Harper JT, Pfeffer WT (2012) Thermal tracking of meltwater retention in greenland's accumulation area. Journal of Geophysical Research: Earth Surface 117(F1)

Huss M (2010) Mass balance of pizolgletscher. Geographica Helvetica 64:80–92, DOI 10.5194/gh-65-80-2010

Huss M (2012) Extrapolating glacier mass balance to the mountain-range scale: the european alps 1900–2100. The Cryosphere 6:713–727

Huss M (2013) Density assumptions for converting geodetic glacier volume change to mass change. The Cryosphere 7(3):877–887

Huss M, Farinotti D (2012) Distributed ice thickness and volume of all glaciers around the globe. Journal of Geophysical Research DOI 10.1029/2012JF002523

Huss M, Hock R (2015) A new model for global glacier change and sea-level rise. Frontiers in Earth Science 3:54

Huss M, Hock R (2018) Global-scale hydrological response to future glacier mass loss. Nature Climate Change p 1

Huss M, Bauder A, Funk M, Hock R (2008) Determination of the seasonal mass balance of four alpine glaciers since 1865. Journal of Geophysical Research: Earth Surface 113(F1)

Huss M, Bauder A, Funk M (2009) Homogenization of long-term mass-balance time series. Annals of Glaciology 50(50):198–206

Huss M, Hock R, Bauder A, Funk M (2010) 100-year mass changes in the swiss alps linked to the atlantic multidecadal oscillation. Geophysical Research Letters 37(10)

Huss M, Sold L, Hoelzle M, Stokvis M, Salzmann N, Farinotti D, Zemp M (2013) Towards remote monitoring of sub-seasonal glacier mass balance. Annals of Glaciology 53:278–286, DOI 10.3189/2012JoG11J216

Huss M, Bookhagen B, Huggel C, Jacobsen D, Bradley R, Clague J, Vuille M, Buytaert W, Cayan D, Greenwood G, et al (2017) Toward mountains without permanent snow and ice. Earth's Future 5(5):418–435

Immerzeel W, Wanders N, Lutz A, Shea J, Bierkens M (2015) Reconciling high-altitude precipitation in the upper indus basin with glacier mass balances and runoff. Hydrology and Earth System Sciences 19(11):4673

Immerzeel WW, Van Beek LP, Bierkens MF (2010) Climate change will affect the asian water towers. Science 328(5984):1382–1385

IPCC Climate Change (2013) The physical science basis. working group i contribution to the fifth assessment report of the intergovernmental panel on climate change. Cambridge, United Kingdom and New York, USA DOI 10.1017/CBO9781107415324.005

Irish RR (2000) Landsat 7 automatic cloud cover assessment. In: Algorithms for Multispectral, Hyperspectral, and Ultraspectral Imagery VI, International Society for Optics and Photonics, vol 4049, pp 348–356

Jackson LP, Grinsted A, Jevrejeva S (2018) 21st century sea-level rise in line with the paris accord. Earth's Future 6(2):213–229

Jarvis A, Reuter HI, Nelson A, Guevara E, et al (2008) Hole-filled srtm for the globe version 4. available from the CGIAR-CSI SRTM 90m Database (http://srtm csi cgiar org) 15

Joerg PC, Zemp M (2014) Evaluating volumetric glacier change methods using airborne laser scanning data. Geografiska Annaler: Series A, Physical Geography 96(2):135–145

Joerg PC, Morsdorf F, Zemp M (2012) Uncertainty assessment of multi-temporal airborne laser scanning data: A case study on an alpine glacier. Remote Sensing of Environment 127:118–129

Jóhannesson T, Raymond C, Waddington E (1989) A simple method for determining the response time of glaciers. In: Glacier fluctuations and climatic change, Springer, pp 343–352

Johannesson T, Sigurdsson O, Laumann T, Kennett M (1995) Degree-day glacier mass-balance modelling with applications to glaciers in iceland, norway and greenland. Journal of Glaciology 41(138):345–358

Jol H (2009) Ground penetrating radar theory and applications. Elsevier Ltd.

Kääb A (2005a) Remote sensing of mountain environment. Projecting global change impacts and sustainable land use and natural resources management in mountain biosphere reserves p 92

Kääb A (2005b) Remote sensing of mountain glaciers and permafrost creep, vol 48. Geograph. Inst. d. Univ.

Kääb A, Huggel C, Paul F, Wessels R, Raup B, Kieffer H, Kargel J (2002) Glacier monitoring from aster imagery: accuracy and applications. In: Proceedings of EARSeL-LISSIG-Workshop Observing our Cryosphere from Space, vol 2, pp 43–53

Kääb A, Huggel C, Fischer L, Guex S, Paul F, Roer I, Salzmann N, Schlaefli S, Schmutz K, Schneider D, et al (2005a) Remote sensing of glacier-and permafrost-related hazards in high mountains: an overview. Natural Hazards and Earth System Science 5(4):527–554

Kääb A, Reynolds JM, Haeberli W (2005b) Glacier and permafrost hazards in high mountains. In: Global change and mountain regions, Springer, pp 225–234

Kääb A, Berthier E, Nuth C, Gardelle J, Arnaud Y (2012) Contrasting patterns of early twenty-first-century glacier mass change in the himalayas. Nature 488(7412):495

Kääb A, Treichler D, Nuth C, Berthier E (2015) Brief communication: Contending estimates of 2003–2008 glacier mass balance over the pamir–karakoram–himalaya. The Cryosphere 9(2):557–564, DOI 10.5194/tc-9-557-2015

Kääb A, Treichler D, Nuth C, Berthier E (2015) Contending estimates of 2003-2008 glacier mass balance over the Pamir, Karakoram, Himalaya. The Cryosphere 9:557–564

Kääb A, Altena B, Mascaro J (2017) Coseismic displacements of the 14 november 2016 m w 7.8 kaikoura, new zealand, earthquake using the planet optical cubesat constellation. Natural Hazards and Earth System Sciences 17(5):627

Kalnay E, Kanamitsu M, Kistler R, Collins W, Deaven D, Gandin L, Iredell M, Saha S, White G, Woollen J, Zhu Y, Leetmaa A, Reynolds B, Chelliah M, Ebisuzaki W, Higgins W, Janowiak J, Mo K, Ropelewski C, Wang J, Jenne R, Joseph D (1996) The NCEP/NCAR 40-Year Reanalysis Project. Bulletin of the American Meteorological Society 77:437–472, DOI 10.1175/1520-0477(1996)077$⟨$0437:TNYRP$⟩$2.0.CO;2

Kamniansky G, Pertziger F (1996) Optimization of mountain glacier mass balance measurements. Zeitschrift für Gletscherkunde und Glazialgeologie 32:167–75

Kamnyansky G (2001) Abramov glacier mass balance observations resume (1967–1998). Proceedings of SANIGMI 161(242):122–131

Kaser G, Georges C (1997) Changes of the equilibrium-line altitude in the tropical cordillera blanca, peru, 1930–50, and their spatial variations. Annals of Glaciology 24:344–349

Kaser G, Ames A, Zamora M (1990) Glacier fluctuations and climate in the cordillera blanca, peru. Annals of Glaciology 14:136–140

Kaser G, Fountain A, Jansson P (2003) A manual for monitoring the mass balance of mountain glaciers, ihp-vi technical documents in hydrology no. 59

Kaser G, Cogley J, Dyurgerov M, Meier M, Ohmura A (2006) Mass balance of glaciers and ice caps: consensus estimates for 1961–2004. Geophysical Research Letters 33(19)

Kaser G, Großhauser M, Marzeion B (2010) Contribution potential of glaciers to water availability in different climate regimes. Proceedings of the National Academy of Sciences 107(47):20,223–20,227

Kasser P, Muller F (1967) Fluctuations of Glaciers: 1959-1965, vol 1. International Association of Scientific Hydrology, IASH

Kaur R, Saikumar D, Kulkarni AV, Chaudhary B (2009) Variations in snow cover and snowline altitude in baspa basin. Current Science (00113891) 96(9)

Kenzhebaev R, Barandun M, Kronenberg M, Chen Y, Usubaliev R, Hoelzle M (2017) Mass balance observations and reconstruction for batysh sook glacier, tien shan, from 2004 to 2016. Cold Regions Science and Technology 135:76–89

Khromova T, Dyurgerov M, Barry R (2003) Late-twentieth century changes in glacier extent in the ak-shirak range, central asia, determined from historical data and aster imagery. Geophysical Research Letters 30(16)

Khromova T, Osipova G, Tsvetkov D, Dyurgerov M, Barry R (2006) Changes in glacier extent in the eastern pamir, central asia, determined from historical data and aster imagery. Remote sensing of environment 102(1):24–32, DOI 10.1016/j.rse.2006.01.019

Khromova T, Nosenko G, Kutuzov S, Muraviev A, Chernova L (2014) Glacier area changes in Northern Eurasia. Environmental Research Letters 9(1):015003, DOI 10.1088/1748-9326/9/1/015003

Kienholz C, Hock R, Truffer M, Bieniek P, Lader R (2017) Mass balance evolution of black rapids glacier, alaska, 1980–2100, and its implications for surge recurrence. Frontiers in Earth Science 5:56

Kislov B, Nozdryukhin J (1975) Natural contamination of the firn-ice layer of the abramov glacier, according to core drilling. Soviet Hydrology, Selected Papers 3

Kislov B, Nozdrukhin V, Pertziger F (1977) Temperature regime of the active layer of Lednik Abramov (in Russian). Materialy Glyatsiologicheskikh Issledovaniy = Data of Glaciological Studies 30:199–204

Klein AG, Isacks BL (1999) Spectral mixture analysis of landsat thematic mapper images applied to the detection of the transient snowline on tropical andean glaciers. Global and Planetary Change 22(1-4):139–154

Klok EL, Greuell W, Oerlemans J (2003) Temporal and spatial variation of the surface albedo of morteratschgletscher, switzerland, as derived from 12 landsat images. Journal of Glaciology 49(167):491–502

König M, Winther JG, Isaksson E (2001) Measuring snow and glacier ice properties from satellite. Reviews of Geophysics 39(1):1–27

Kononova NK, Pimankina NV, Yeriskovskaya LA, Li J, Bao W, Liu S (2015) Effects of atmospheric circulation on summertime precipitation variability and glacier mass balance over the tuyuksu glacier in tianshan mountains, kazakhstan. Journal of Arid Land 7(5):687–695

Konovalov V, Desinov L (2007) Remote sensing monitoring of the long-term regime of the Pamirs glaciers. In: Remote Sensing for Environmental Monitoring and Change Detection, IAHS, Proceedings of Symposium HS3007, vol 316, pp 149–156

Konovalov V, Shchetinnicov A (1994) Evolution of glaciation in the pamiro-alai mountains and its effect on river run-off. Journal of Glaciology 40(134):149–157

Konz M, Uhlenbrook S, Braun L, Shrestha A, Demuth S (2007) Implementation of a process-based catchment model in a poorly gauged, highly glacierized himalayan headwater. Hydrology and Earth System Sciences Discussions 11(4):1323–1339

Korona J, Berthier E, Bernard M, Rémy F, Thouvenot E (2009) Spirit. spot 5 stereoscopic survey of polar ice: reference images and topographies during the fourth international polar year (2007–2009). ISPRS Journal of Photogrammetry and Remote Sensing 64(2):204–212

Kotlyakov V, Osipova G, Tsvetkov D (2008) Monitoring surging glaciers of the pamirs, central asia, from space. Annals of Glaciology 48:125–134

Kraaijenbrink P, Bierkens M, Lutz A, Immerzeel W (2017) Impact of a global temperature rise of 1.5 degrees celsius on asia's glaciers. Nature 549(7671):257

Kriegel D, Mayer C, Hagg W, Vorogushyn S, Duethmann D, Gafurov A, Farinotti D (2013) Changes in glacierisation, climate and runoff in the second half of the 20th century in the naryn basin, central asia. Global and planetary change 110:51–61

Kronenberg M, Barandun M, Hoelzle M, Huss M, Farinotti D, Azisov E, Usubaliev R, Gafurov A, Petrakov D, Kääb A (2016) Mass-balance reconstruction for glacier no. 354, tien shan, from 2003 to 2014. Annals of Glaciology 57(71):92–102

Kruse FA, Lefkoff A, Boardman J, Heidebrecht K, Shapiro A, Barloon P, Goetz A (1993) The spectral image processing system (sips)—interactive visualization and analysis of imaging spectrometer data. Remote sensing of environment 44(2-3):145–163

Kuhn M (1979) On the computation of heat transfer coefficients from energy-balance gradients on a glacier. Journal of Glaciology 22(87):263–272

Kuhn M (1984) Mass budget imbalances as criterion for a climatic classification of glaciers. Geografiska Annaler: Series A, Physical Geography 66(3):229–238

Kuhn M (1989) The response of the equilibrium line altitude to climate fluctuations: theory and observations. In: Glacier fluctuations and climatic change, Springer, pp 407–417

Kuhn M (1990) Energieaustausch atmosphäre-schnee und eis. Mitteilungen der Versuchsanstalt fur Wasserbau, Hydrologie und Glaziologie an der Eidgenossischen Technischen Hochschule Zurich 108:21–32

Kuhn M (1993) Methods of assessing the effects of climatic changes on snow and glacier hydrology. IAHS Publications-Publications of the International Association of Hydrological Sciences 218:135–144

Kuhn M, Markl G, Kaser G, Nickus U, Obleitner F, Schneider H (1985) Fluctuations of climate and mass balance: different responses of two adjacent glaciers. Zeitschrift für Gletscherkunde und Glazialgeologie

Kuhn M, Dreiseitl E, Hofinger S, Markl G, Span N, Kaser G (1999) Measurements and models of the mass balance of hintereisferner. Geografiska Annaler: Series A, Physical Geography 81(4):659–670

Kulkarni AV (1992) Mass balance of himalayan glaciers using aar and ela methods. Journal of Glaciology 38(128):101–104

Kulkarni AV (2012) Monitoring himalayan cryosphere using remote sensing techniques. Journal of the Indian Institute of Science 90(4):457–469

Kulkarni AV, Rathore B, Alex S (2004) Monitoring of glacial mass balance in the baspa basin using accumulation area ratio method. Current science pp 185–190

Kulkarni AV, Rathore B, Singh S, Bahuguna I (2011) Understanding changes in the himalayan cryosphere using remote sensing techniques. International journal of remote sensing 32(3):601–615

Kumar AK (2013) Significance of risat-1 in isro's earth observation programme. Current Science(Bangalore) 104(4):444–445

Kure S, Jang S, Ohara N, Kavvas M, Chen Z (2013) Hydrologic impact of regional climate change for the snow-fed and glacier-fed river basins in the republic of tajikistan: statistical downscaling of global climate model projections. Hydrological Processes 27:4071–4090, DOI 10.1002/hyp.9536

Kutuzov S, Shahgedanova M (2009) Glacier retreat and climatic variability in the eastern terskey–alatoo, inner tien shan between the middle of the 19th century and beginning of the 21st century. Global and Planetary Change 69(1):59–70

Kuzmichenok V (1990) Topographicheskaya s' emka rel'efa lozha lednikov radiolokacionnim metodom [method of the glaciers surface and bedrock topography measurements by radioecho sounding]. Geodesiya i Kartogrphiya 11:18–23

Kuzmichenok V (2009) Monitoring of water, snow and glacial resources of kyrgyzstan. Assess Snow Glacier Water Resources Asia 8:84–99

LaChapelle E (1962) Assessing glacier mass budgets by reconnaissance aerial photography. Journal of Glaciology 4(33):290–297

Laha S, Kumari R, Singh S, Mishra A, Sharma T, Banerjee A, Nainwal HC, Shankar R (2017) Evaluating the contribution of avalanching to the mass balance of himalayan glaciers. Annals of Glaciology pp 1–9

Lang H (1986) Forecasting meltwater runoff from snow-covered areas and from glacier basins. In: River flow modelling and forecasting, Springer, pp 99–127

Lazarev A A Turchaninova, Y S (2018) Evaluation of snow avalanches contribution into glacier accumulation. EGU General Assembly 2018

Lebourgeois V, Bégué A, Labbé S, Mallavan B, Prévot L, Roux B (2008) Can commercial digital cameras be used as multispectral sensors? a crop monitoring test. Sensors 8(11):7300–7322

Letréguilly A (1988) Relation between the mass balance of western canadian mountain glaciers and meteorological data. Journal of Glaciology 34(116):11–18

Letréguilly A, Reynaud L (1989) Spatial patterns of mass-balance fluctuations of north american glaciers. Journal of Glaciology 35(120):163–168

Li C, Su F, Yang D, Tong K, Meng F, Kan B (2018) Spatiotemporal variation of snow cover over the tibetan plateau based on modis snow product, 2001–2014. International Journal of Climatology 38(2):708–728

Li J, Li Zw, Zhu Jj, Li X, Xu B, Wang Qj, Huang Cl, Hu J (2017) Early 21st century glacier thickness changes in the central tien shan. Remote sensing of environment 192:12–29

Li Z, Li H, Chen Y (2011) Mechanisms and simulation of accelerated shrinkage of continental glaciers: a case study of urumqi glacier no. 1 in eastern tianshan, central asia. Journal of Earth Science 22(4):423–430

Liang S (2001) Narrowband to broadband conversions of land surface albedo i: Algorithms. Remote sensing of environment 76(2):213–238

Lin H, Li G, Cuo L, Hooper A, Ye Q (2017) A decreasing glacier mass balance gradient from the edge of the upper tarim basin to the karakoram during 2000–2014. Scientific reports 7(1):6712

Liu Q, Liu S (2016) Response of glacier mass balance to climate change in the tianshan mountains during the second half of the twentieth century. Climate dynamics 46(1-2):303–316

Lliboutry L (1965) Traité de glaciologie, vol 1. Masson, Paris

Lutz A, Immerzeel W, Gobiet A, Pellicciotti F, Bierkens M (2013) Comparison of climate change signals in cmip3 and cmip5 multi-model ensembles and implications for central asian glaciers. Hydrology and Earth System Sciences 17:3661–3677, DOI 10.5194/hess-17-3661-2013

Maas HG, Schwalbe E, Dietrich R, Bässler M, Ewert H (2008) Determination of spatio-temporal velocity fields on glaciers in west-greenland by terrestrial image sequence analysis. International Archives of Photogrammetry, Remote Sensing and Spatial Information Science 37(Part B8):1419–1424

Machguth H (2008) On the use of rcm data and gridded climatologies for regional scale glacier mass balance modeling in high mountain topography: the example of the swiss alps. PhD thesis, University of Zurich

Machguth H, Eisen O, Paul F, Hoelzle M (2006a) Strong spatial variability of snow accumulation observed with helicopter-borne gpr on two adjacent alpine glaciers. Geophysical research letters 33(13)

Machguth H, Paul F, Hoelzle M, Haeberli W (2006b) Distributed glacier mass-balance modelling as an important component of modern multi-level glacier monitoring. Annals of Glaciology 43:335–343

Machguth H, Purves R, Oerlemans J, Hoelzle M, Paul F (2008) Exploring uncertainty in glacier mass balance modelling with monte carlo simulation. The Cryosphere 2(2):191–204, DOI 10.5194/tc-2-191-2008

Machguth H, Haeberli W, Paul F (2012) Mass-balance parameters derived from a synthetic network of mass-balance glaciers. Journal of Glaciology 58(211):965–979

Machguth H, MacFerrin M, van As D, Box JE, Charalampidis C, Colgan W, Fausto RS, Meijer HA, Mosley-Thompson E, van de Wal RS (2016) Greenland meltwater storage in firn limited by near-surface ice formation. Nature Climate Change 6(4):390

Male D, Granger R (1981) Snow surface energy exchange. Water Resources Research 17(3):609–627

Man Q, Guo H, Liu G, Dong P (2014) Comparison of different methods for monitoring glacier changes observed by landsat images. In: IOP Conference Series: Earth and Environmental Science, vol 17

Mandal A, Ramanathan A, Angchuk T (2014) Assessment of lahaul-spiti (western himalaya, india) glaciers-an overview of mass balance and climate. Journal of Earth Science & Climatic Change 11:2, DOI 10.4172/2157-7617.S11-003

Marti R, Gascoin S, Berthier E, De Pinel M, Houet T, Laffly D (2016) Mapping snow depth in open alpine terrain from stereo satellite imagery. The Cryosphere 10(4):1361

Martinec J, Rango A (1981) Areal distribution of snow waterequivalent evaluated by snow cover monitoring. Water Resources Research 17(5):1480–1488

Marzeion B, Kaser G, Maussion F, Champollion N (2018) Limited influence of climate change mitigation on short-term glacier mass loss. Nature Climate Change 8(4):305

Masek JG, Vermote EF, Saleous NE, Wolfe R, Hall FG, Huemmrich KF, Gao F, Kutler J, Lim TK (2006) A landsat surface reflectance dataset for north america, 1990-2000. IEEE Geoscience and Remote Sensing Letters 3(1):68–72

Maussion F, Scherer D, Mölg T, Collier E, Curio J, Finkelnburg R (2014) Precipitation seasonality and variability over the tibetan plateau as resolved by the high asia reanalysis. Journal of Climate 27(5):1910–1927

McNabb R, Nuth C, Kääb A, Girod L (2017) The effects of void handling on geodetic mass balances. In: EGU General Assembly Conference Abstracts, vol 19, p 7570

Meier M (1961) Mass budget of south cascade glacier, 1957-60. US Geological Survey Professional Paper 424:206–21

Meier M, Post A (1962) Recent variations in mass net budgets of glaciers in western north america. IASH Publ 58:63–77

Meier MF, Dyurgerov MB, Rick UK, O'neel S, Pfeffer WT, Anderson RS, Anderson SP, Glazovsky AF (2007) Glaciers dominate eustatic sea-level rise in the 21st century. Science 317(5841):1064–1067

Melvold K, Rolstad CE (2000) Subglacial topography of jutulstraumen outlet glacier, east antarctica, mapped from ground-penetrating radar, optical and interferometric synthetic aperture radar satellite data. Norsk Geografisk Tidsskrift 54(4):169–181

Mercanton P (1916a) Les variations des glaciers à la lumière des travaux récents. Le Globe Revue genevoise de géographie 55(1):72–75

Mercanton P (1916b) Vermessungen am rhonegletscher, mensurations au glacier du rhone, 1874-1915. Neue Denkschriften der Schweizerischen Naturforschenden Gesellschaft 52

Mercanton P (1932) Les variations périodiques des glaciers des Alpes Suisses. Staempfli & Cie

Mercanton P (1948) Rapport sur les variations de longueur des glaciers de 1935 a1946. Alpes francßaises, suisses, italiennes et autrichiennes Variations des glaciers en Suede, Islande et Norvege IAHS 30:233–261

Mercanton P, Renaud A (1951) Les variations des glaciers des alpes suisses. Die Alpen (Ztschr, siehe [878], Fortsetzung derselben)

Mernild S, Lipscomb W, Bahr D, Radić V, Zemp M (2013a) Global glacier changes: a revised assessment of committed mass losses and sampling uncertainties. The Cryosphere 7(5):1565–1577, DOI 10.5194/tc-7-1565-2013

Mernild S, Pelto M, Malmros JK, Yde JC, Knudsen NT, Hanna E (2013b) Identification of snow ablation rate, ela, aar and net mass balance using transient snowline variations on two arctic glaciers. Journal of Glaciology 59(216):649–659

Mernild SH, Liston GE, Hasholt B, Knudsen NT (2006) Snow distribution and melt modeling for mittivakkat glacier, ammassalik island, southeast greenland. Journal of Hydrometeorology 7(4):808–824

Mertes JR, Gulley JD, Benn DI, Thompson SS, Nicholson LI (2017) Using structure from motion to create glacier dems and orthoimagery from historical terrestrial and oblique aerial imagery. Earth Surface Processes and Landforms

Mikhalenko VN (1990) The base glacier use for mass balance studies of glacier systems. summary of the doctoral dissertation, moscow. PhD thesis, Moscow

Miles ES, Pellicciotti F, Willis IC, Steiner JF, Buri P, Arnold NS (2016) Refined energy-balance modelling of a supraglacial pond, langtang khola, nepal. Annals of Glaciology 57(71):29–40

Miller MM, Pelto MS (1999) Mass balance measurements on the lemon creek glacier, juneau icefield, alaska 1953–1998. Geografiska Annaler: Series A, Physical Geography 81(4):671–681

Mittaz C, Imhof M, Hoelzle M, Haeberli W (2002) Snowmelt evolution mapping using an energy balance approach over an alpine terrain. Arctic, Antarctic, and Alpine Research 34(3):274–281

Moholdt G, Nuth C, Hagen JO, Kohler J (2010) Recent elevation changes of svalbard glaciers derived from icesat laser altimetry. Remote Sensing of Environment 114(11):2756–2767

Mölg N, Bolch T (2017) Structure-from-motion using historical aerial images to analyse changes in glacier surface elevation. Remote Sensing 9(10):1021

Mölg T, Cullen NJ, Kaser G (2009) Solar radiation, cloudiness and longwave radiation over low-latitude glaciers: implications for mass-balance modelling. Journal of Glaciology 55(190):292–302

Mölg T, Großhauser M, Hemp A, Hofer M, Marzeion B (2012) Limited forcing of glacier loss through land-cover change on kilimanjaro. Nature Climate Change 2(4):254

Mölg T, Maussion F, Scherer D (2014) Mid-latitude westerlies as a driver of glacier variability in monsoonal high asia. Nature Climate Change 4(1):68

Molotch NP, Margulis SA (2008) Estimating the distribution of snow water equivalent using remotely sensed snow cover data and a spatially distributed snowmelt model: A multi-resolution, multi-sensor comparison. Advances in Water Resources 31(11):1503–1514

Mukherjee K, Bolch T, Goerlich F, Kutuzov S, Osmonov A, Pieczonka T, Shesterova I (2017) Surge-type glaciers in the tien shan (central asia). Arctic, Antarctic, and Alpine Research 49(1):147–171

Muller FB, Kasser P, et al (1977) Fluctuations of glaciers, 1970-1975 (vol. III). International Commission on Snow and Ice

Munia H, Guillaume J, Mirumachi N, Porkka M, Wada Y, Kummu M (2016) Water stress in global transboundary river basins: significance of upstream water use on downstream stress. Environmental Research Letters 11(1):014,002

Muret E (1900) Les variations périodiques des glaciers, spécialement en ce qui concerne les glaciers du valais. Bulletin de la Murithienne (29):43–65

Naegeli K, Huss M (2017) Sensitivity of mountain glacier mass balance to changes in bare-ice albedo. Annals of Glaciology pp 1–11

Naegeli K, Damm A, Huss M, Schaepman M, Hoelzle M (2015) Imaging spectroscopy to assess the composition of ice surface materials and their impact on glacier mass balance. Remote Sensing of Environment 168:388–402

Naegeli K, Damm A, Huss M, Wulf H, Schaepman M, Hoelzle M (2017) Cross-comparison of albedo products for glacier surfaces derived from airborne and satellite (sentinel-2 and landsat 8) optical data. Remote Sensing 9(2):110

Naegeli K, Huss M, Hoelzle M (2018) Darkening swiss glacier ice? The Cryosphere Discussions 2018:1–21, DOI 10.5194/tc-2018-18

Nagler T, Rott H (2000) Retrieval of wet snow by means of multitemporal sar data. IEEE Transactions on Geoscience and Remote Sensing 38(2):754–765

Nagler T, Rott H, Malcher P, Müller F (2008) Assimilation of meteorological and remote sensing data for snowmelt runoff forecasting. Remote sensing of environment 112(4):1408–1420

Naito N (2011) Summer accumulation type glaciers. In: Encyclopedia of Snow, Ice and Glaciers, Springer, pp 1107–1108

Narama C, Kääb A, Duishonakunov M, Abdrakhmatov K (2010) Spatial variability of recent glacier area changes in the tien shan mountains, central asia, using corona (˜ 1970), landsat (˜ 2000), and alos (˜ 2007) satellite data. Global and Planetary Change 71(1-2):42–54

Neckel N, Kropacek J, Bolch T, Hochschild V (2014) Glaciermass changes on the Tibetan Plateau 2003?2009 derived from ICESat laser altimetry measurements. Environment Research Letters 9:014,009

Niederer P, Bilenko V, Ershova N, Hurni H, Yerokhin S, Maselli D (2007) Tracing glacier wastage in the Northern Tien Shan (Kyrgyzstan/Central Asia) over the last 40 years. Climatic Change 86(1-2):227–234

Nussbaumer SU, Hoelzle M, Hüsler F, Huggel C, Salzmann N, Zemp M (2017) Glacier Monitoring and Capacity Building: Important Ingredients for Sustainable Mountain Development. Mountain Research and Development 37(1):141–152

Nuth C, Kääb A (2011) Co-registration and bias corrections of satellite elevation data sets for quantifying glacier thickness change. The Cryosphere 5:271–290, DOI 10.5194/tc-5-271-2011

Nye J (1960) The response of glaciers and ice-sheets to seasonal and climatic changes. Proceedings of the Royal Society of London Series A(256):559–584

Oerlemans J (1991) A model for the surface balance of ice masses: Part i: alpine glaciers. Zeitschrift für Gletscherkunde und Glazialgeologie 27:63–83

Oerlemans J (2001) Glaciers and climate change. CRC Press

Oerlemans J, Fortuin J (1992) Sensitivity of glaciers and small ice caps to greenhouse warming. Science 258(5079):115–117

Oerlemans J, Klok EL (2004) Effect of summer snowfall on glacier mass balance. Annals of Glaciology 38:97–100

Ohmura A (2001) Physical basis for the temperature-based melt-index method. Journal of Applied Meteorology 40:753–761, DOI 10.1175/1520-0450(2001)040$\langle$\$0753:PBFTTB\$$\rangle$\$2.0.CO;2

Ohmura A, Kasser P, Funk M (1992) Climate at the equilibrium line of glaciers. Journal of Glaciology 38(130):397–411

Ohmura A, Bauder A, Müller H, Kappenberger G (2007) Long-term change of mass balance and the role of radiation. Annals of Glaciology 46:367–374, DOI 10.3189/172756407782871297

Østby TI, Schuler TV, Hagen JO, Hock R, Kohler J, Reijmer CH (2017) Diagnosing the decline in climatic mass balance of glaciers in svalbard over 1957-2014. The Cryosphere 11(1):191–215

Østrem G (1959) Ice melting under a thin layer of moraine, and the existence of ice cores in moraine ridges. Geografiska Annaler 41(4):228–230

Østrem G (1973) The transient snowline and glacier mass balance in southern british columbia and alberta, canada. Geografiska Annaler Series A Physical Geography pp 93–106

Østrem G (1975) Erts data in glaciology—an effort to monitor glacier mass balance from satellite imagery. Journal of Glaciology 15(73):403–415

Østrem G, Brugman M (1991a) Glacier mass-balance measurements: a manual for field and office work

Østrem G, Brugman M (1991b) Mass balance measurement techniques. A manual for field and office work, Environment Canada, Saskatoon

Otsu N (1979) A threshold selection method from gray-level histograms. IEEE transactions on systems, man, and cybernetics 9(1):62–66

Ozmonov A, Bolch T, Xi C, Wei J, Kurban A (2013) Glaciers characteristics and changes in the sary-jaz river basin (central tien shan) 1990–2010 remote sensing letters. Remote Sensing Letters 4:725–734

Parajka J, Haas P, Kirnbauer R, Jansa J, Blöschl G (2012) Potential of time-lapse photography of snow for hydrological purposes at the small catchment scale. Hydrological Processes 26(22):3327–3337

Parry V, Nienow P, Mair D, Scott J, Hubbard B, Steffen K, Wingham D (2007) Investigations of meltwater refreezing and density variations in the snowpack and firn within the percolation zone of the greenland ice sheet. Annals of Glaciology 46:61–68

Paul F (2008) Calculation of glacier elevation changes with SRTM: Is there an elevation dependent bias? Journal of Glaciology 55(188):945–946

Paul F, Kääb A, Maisch M, Kellenberger T, Haeberli W (2002) The new remote-sensing-derived swiss glacier inventory: I. methods. Annals of Glaciology 34:355–361

Paul F, Huggel C, Kääb A (2004) Combining satellite multispectral image data and a digital elevation model for mapping debris-covered glaciers. Remote sensing of Environment 89(4):510–518

Paul F, Machguth H, Hoelzle M, Salzmann N, Haeberli W (2008) Alpinewide distributed glacier mass balance modeling. Darkening peaks: glacier retreat, science, and society p 111

Paul F, Barrand N, Baumann S, Berthier E, Bolch T, Casey K, Frey H, Joshi S, Konovalov V, Le Bris R, et al (2013a) On the accuracy of glacier outlines derived from remote-sensing data. Annals of Glaciology 54:171–182, DOI 10.3189/2013AoG63A296

Paul F, Bolch T, Kääb A, Nagler T, Nuth C, Scharrer K, Shepherd A, Strozzi T, Ticconid F, Bhambri R, Berthier E, Bevan S, Gourmelen N, Heid T, Jeong S, Kunz M, Lauknes T, Luckman A, Merryman Boncori J, Moholdt G, Muir A, Neelmeijer J, Rankl M, VanLooy J, Van Niel T (2013b) The glaciers climate change initiative: Methods for creating glacier area, elevation change and velocity products. Remote Sensing of Environment

Paul F, Bolch T, Kääb A, Nagler T, Nuth C, Scharrer K, Shepherd A, Strozzi T, Ticconi F, Bhambri R, et al (2015) The glaciers climate change initiative: Methods for creating glacier area, elevation change and velocity products. Remote Sensing of Environment 162:408–426

Paul F, Bolch T, Briggs K, Kääb A, McMillan M, McNabb R, Nagler T, Nuth C, Rastner P, Strozzi T, et al (2017) Error sources and guidelines for quality assessment of glacier area, elevation change, and velocity products derived from satellite data in the glaciers_cci project. Remote Sensing of Environment 203:256–275

Pellicciotti F, Brock B, Strasser U, Burlando P, Funk M, Corripio J (2005) An enhanced temperature-index glacier melt model including the shortwave radiation balance: development and testing for haut glacier d'arolla, switzerland. Journal of Glaciology 51(175):573–587

Pellikka P, Rees WG (2009) Remote sensing of glaciers: techniques for topographic, spatial and thematic mapping of glaciers. CRC Press

Pelto M (2010) Satellite identification of transient snowline variation during the melt season for mass balance assessment taku and brady glacier, alaska. In: 67th Eastern Snow Conference Jiminy Peak Mountain Resort, Hancock, MA, USA, pp 51–60

Pelto M (2011) Utility of late summer transient snowline migration rate on taku glacier, alaska. The Cryosphere 5:1127–1133, DOI 10.5194/tc-5-1127-2011

Pelto M, Miller M (1990) Mass balance of the taku glacier, alaska from 1946 to 1986. Northwest Science 64(3)

Pelto M, Higgins S, Hughes T, Fastook J (1990) Modeling mass-balance changes during a glaciation cycle. Annals of Glaciology 14:238–241

Pelto M, Kavanaugh J, McNeil C (2013) Juneau icefield mass balance program 1946–2011. Earth System Science Data 5(2):319–330

Pertziger F (1996) Abramov Glacier data reference book: climate, runoff, mass balance. Central Asian Regional Research Hydrometeorological Institute named by VA Bugaev, Tashkent, Republic of Uzbekistan, 279p

Petrakov D, Lavrientiev I, Kovalenko N, Usubaliev R (2014) Ice thickness, volume and current changes of the sary-tor glacier area (ak-shyirak massif, inner tian shan). Cyosphere Assembly XVIII, No.3:83–91

Petrakov D, Shpuntova A, Aleinikov A, Kääb A, Kutuzov S, Lavrentiev I, Stoffel M, Tutubalina O, Usubaliev R (2016a) Accelerated glacier shrinkage in the ak-shyirak massif, inner tien shan, during 2003–2013. Science of the Total Environment 562:364–378

Petrakov D, Shpuntova A, Aleinikov A, Kääb A, Kutuzov S, Lavrentiev I, Stoffel M, Tutubalina O, Usulbajev R (2016b) Accelerated glacier shrinkage in the Ak-Shyirak massif, Inner Tien Shan, during 2003 to 2013. Science of the Total Environment 562:364–378

Petrakov DA, Tutubalina O, Schpuntova A, Kovalenko N, Usubaliev R, Azisov E, Mikhailyukova P (in review) An assessment of glacier albedo in the ak-shyirak massif (inner tian shan) basing on ground data and landsat satellite images. Earth's Cryosphere

Pfeffer WT, Meier MF, Illangasekare TH (1991) Retention of greenland runoff by refreezing: implications for projected future sea level change. Journal of Geophysical Research: Oceans 96(C12):22,117–22,124

Pieczonka T, Bolch T (2015) Region-wide glacier mass budgets and area changes for the central tien shan between˜ 1975 and 1999 using hexagon kh-9 imagery. Global and Planetary Change 128:1–13

Pieczonka T, Bolch T, Buchroithner M (2011) Generation and evaluation of multitemporal digital terrain models of the Mt. Everest area from different optical sensors. ISPRS Journal of Photogrammetry and Remote Sensing 66:927–940

Pieczonka T, Bolch T, Junfeng W, Shiyin L (2013) Heterogeneous mass loss of glaciers in the aksu-tarim catchment (central tien shan) revealed by 1976 kh-9 hexagon and 2009 spot-5 stereo imagery. Remote Sensing of Environment 130:233–244, DOI 10.1016/j.rse.2012.11.020

Piermattei L, Carturan L, Guarnieri A (2015) Use of terrestrial photogrammetry based on structure-from-motion for mass balance estimation of a small glacier in the italian alps. Earth Surface Processes and Landforms 40(13):1791–1802

Pohl E, Gloaguen R, Andermann C, Knoche M (2017) Glacier melt buffers river runoff in the pamir mountains. Water Resources Research 53(3):2467–2489

Pope A, Willis IC, Pálsson F, Arnold NS, Rees WG, Björnsson H, Grey L (2016) Elevation change, mass balance, dynamics and surging of langjökull, iceland from 1997 to 2007. Journal of Glaciology 62(233):497–511

Popkin G (2017) Earth-observing companies push for more-advanced science satellites. Nature News 545(7655):397

Pritchard H, Ligtenberg S, Fricker H, Vaughan D, Van den Broeke M, Padman L (2012) Antarctic ice-sheet loss driven by basal melting of ice shelves. Nature 484(7395):502

Rabatel A, Dedieu JP, Vincent C (2005) Using remote-sensing data to determine equilibrium-line altitude and mass-balance time series: validation on three french glaciers, 1994–2002. Journal of Glaciology 51(175):539–546

Rabatel A, Dedieu JP, Thibert E, Letreguilly A, Vincent C (2008) 25 years (1981–2005) of equilibrium-line altitude and mass-balance reconstruction on glacier blanc, french alps, using remote-sensing methods and meteorological data. Journal of Glaciology 54(185):307–314

Rabatel A, Bermejo A, Loarte E, Soruco A, Gomez J, Leonardini G, Vincent C, Sicart JE (2012) Can the snowline be used as an indicator of the equilibrium line and mass balance for glaciers in the outer tropics? Journal of Glaciology 58(212):1027–1036

Rabatel A, Letréguilly A, Dedieu J, Eckert N (2013) Changes in glacier equilibrium-line altitude in the western alps from 1984 to 2010: evaluation by remote sensing and modeling of the morpho-topographic and climate controls. The Cryosphere 7(5):p–1455

Rabatel A, Dedieu JP, Vincent C (2016) Spatio-temporal changes in glacier-wide mass balance quantified by optical remote sensing on 30 glaciers in the french alps for the period 1983–2014. Journal of Glaciology 62(236):1153–1166

Rabatel A, Sirguey P, Drolon V, Maisongrande P, Arnaud Y, Berthier E, Davaze L, Dedieu JP, Dumont M (2017) Annual and seasonal glacier-wide surface mass balance quantified from changes in glacier surface state: A review on existing methods using optical satellite imagery. Remote Sensing 9(5):507

Racoviteanu AE, Williams MW, Barry RG (2008) Optical remote sensing of glacier characteristics: a review with focus on the himalaya. Sensors 8(5):3355–3383

Radić V, Hock R (2006) Modeling future glacier mass balance and volume changes using era-40 reanalysis and climate models: A sensitivity study at storglaciären, sweden. Journal of Geophysical Research: Earth Surface 111(F3)

Ragettli S, Bolch T, Pellicciotti F (2016) Heterogeneous glacier thinning patterns over the last 40 years in langtang himal, nepal. The Cryosphere 10:2075–2097

Rango A (1983) A survey of progress in remote sensing of snow and ice. Citeseer

Rasmussen L (2013) Meteorological controls on glacier mass balance in high asia. Annals of Glaciology 54:352–359, DOI 10.3189/2013AoG63A353

Reeh N (2008) A nonsteady-state firn-densification model for the percolation zone of a glacier. Journal of Geophysical Research (Earth Surface) 113:3023, DOI 10.1029/2007JF000746

Reid HF (1895) The variations of glaciers. The Journal of Geology 3(3):278–288

Reid HF (1911) The variations of glaciers. xvi. The Journal of Geology 19(5):454–461

Reid TD, Brock BW (2010) An energy-balance model for debris-covered glaciers including heat conduction through the debris layer. Journal of Glaciology 56(199):903–916

Reijmer CH, Hock R (2008) Internal accumulation on storglaciären, sweden, in a multi-layer snow model coupled to a distributed energy-and mass-balance model. Journal of Glaciology 54(184):61–72

RGI-Consortium (2017) Randolph glacier inventory – a dataset of global glacier outlines: Version 6.0: Technical report. Digital Media

Rienecker M, Suarez M, Gelaro R, Todling R, Bacmeister J, Liu E, Bosilovich M, Schubert S, Takacs L, Kim G, et al (2011) Merra: Nasa's modern-era retrospective analysis for research and applications. Journal of Climate 24:3624–3648, DOI 10.1175/JCLI-D-11-00015.1

Rignot E, Echelmeyer K, Krabill W (2001) Penetration depth of interferometric synthetic-aperture radar signals in snow and ice. Geophysical Research Letters 28:3501–3504, DOI 10.1029/2000GL012484

Rosenthal W, Dozier J (1996) Automated mapping of montane snow cover at subpixel resolution from the landsat thematic mapper. Water Resources Research 32(1):115–130

Rott H (1984) Synthetic aperture radar capabilities for snow and glacier monitoring. Advances in space research 4(11):241–246

Rott H, Nagler T, Malcher P, Bippus G (2007) Modelling mass balance of glaciers using satellite data. In: Proceeding of Envisat Symposium, ESA SP-634

Round V, Leinss S, Huss M, Haemmig C, Hajnsek I (2017) Surge dynamics and lake outbursts of kyagar glacier, karakoram. The Cryosphere 11(2):723

Sakai A, Fujita K (2017) Contrasting glacier responses to recent climate change in high-mountain asia. Scientific reports 7(1):13,717

Sakai A, Nuimura T, Fujita K, Takenaka S, Nagai H, Lamsal D (2015) Climate regime of asian glaciers revealed by gamdam glacier inventory. The Cryosphere 9(3):865–880

Salzmann N, Huggel C, Rohrer M, Silverio W, Mark B, Burns P, Portocarrero C (2013) Glacier changes and climate trends derived from multiple sources in the data scarce Cordillera Vilcanota region, southern Peruvian Andes. The Cryosphere 7:103–118

Sarno S, Graziano MD, Fasano G, D'Errico M (2018) Very-low altitude parasitic radar distributed on small satellites. Advances in Space Research

Schaner N, Voisin N, Nijssen B, Lettenmaier DP (2012) The contribution of glacier melt to streamflow. Environmental Research Letters 7(3):034,029, DOI 10.1088/1748-9326/7/3/034029

Schaper J, Martinec J, Seidel K (1999) Distributed mapping of snow and glaciers for improved runoff modelling. Hydrological Processes 13(12-13):2023–2031

Schär C, Vasilina L, Pertziger F, Dirren S (2004) Seasonal runoff forecasting using precipitation from meteorological data assimilation systems. journal of Hydrometeorology 5:959–973

Scherler D, Bookhagen B, Strecker MR (2011) Spatially variable response of himalayan glaciers to climate change affected by debris cover. Nature geoscience 4(3):156

Schiemann R, Glazirina MG, Schär C (2007) On the relationship between the indian summer monsoon and river flow in the aral sea basin. Geophysical Research Letters 34(5)

Schiemann R, Lüthi D, Vidale PL, Schär C (2008) The precipitation climate of central asia—intercomparison of observational and numerical data sources in a remote semiarid region. International Journal of Climatology 28(3):295–314

Schmidli J, Frei C, Schä C (2001) Reconstruction of mesoscale precipitation fields from sparse observations in complex terrain. Journal of Climate 14:3289–3306

Schneider T, Jansson P (2004) Internal accumulation in firn and its significance for the mass balance of storglaciären, sweden. Journal of Glaciology 50(168):25–34

Schöne T, Zech C, Unger-Shayesteh K, Rudenko V, Thoss H, Wetzel HU, Gafurov A, Illigner J, Zubovich A (2013) A new permanent multi-parameter monitoring network in central asian high mountains–from measurements to data bases. Geoscientific Instrumentation, Methods and Data Systems 2(1):97–111

Semakova E, Gunasekara K, Semakov D (2016) Identification of the glaciers and mountain naturally dammed lakes in the pskem, the kashkadarya and the surhandarya river basins, uzbekistan, using alos satellite data. Geomatics, Natural Hazards and Risk 7(3):1081–1098

Sevruk B (1981) Methodische untersuchungen des systematischen messfehlers der hellmann-regenmesser im sommerhalbjahr in der schweiz. PhD thesis

Shangguan D, Liu S, Ding Y, Ding L, Xiong L, Cai D, Li G, Lu A, Zhang S, Zhang Y (2006) Monitoring the glacier changes in the muztag ata and konggur mountains, east pamirs, based on chinese glacier inventory and recent satellite imagery. Annals of Glaciology 43:79–85

Shea J, Menounos B, Moore RD, Tennant C (2012) Regional estimates of glacier mass change from modis-derived equilibrium line altitudes. The Cryosphere Discussions 6:3757–3780

Shea J, Immerzeel W, Wagnon P, Vincent C, Bajracharya S (2015) Modelling glacier change in the everest region, nepal himalaya. The Cryosphere 9(3):1105–1128, DOI 10.5194/tc-9-1105-2015

Shean DE, Alexandrov O, Moratto ZM, Smith BE, Joughin IR, Porter C, Morin P (2016) An automated, open-source pipeline for mass production of digital elevation models (dems) from very-high-resolution commercial stereo satellite imagery. ISPRS Journal of Photogrammetry and Remote Sensing 116:101–117

Shumskiy P (1964) Principles of structural glaciology: the petrography of fresh-water ice as a method of glaciological investigation, vol 1307. Dover Publications Inc.

Sicart J, Hock R, Six D (2008) Glacier melt, air temperature, and energy balance in different climates: The bolivian tropics, the french alps, and northern sweden. Journal of Geophysical Research Atmospheres 113(D24113), DOI 10.1029/2008JD010406

Siegfried T, Bernauer T, Guiennet R, Sellars S, Robertson A, Mankin J, Bauer-Gottwein P, Yakovlev A (2012) Will climate change exacerbate water stress in central asia? Climate Change 112:881–899, DOI 10.1007/s10584-011-0253-z

Sirguey P, Mathieu R, Arnaud Y (2009) Subpixel monitoring of the seasonal snow cover with modis at 250 m spatial resolution in the southern alps of new zealand: Methodology and accuracy assessment. Remote Sensing of Environment 113(1):160–181

Sirguey P, Still H, Cullen NJ, Dumont M, Arnaud Y, Conway JP (2016) Reconstructing the mass balance of brewster glacier, new zealand, using modis-derived glacier-wide albedo. The Cryosphere 10(5):2465

Sold L, Huss M, Hoelzle M, Andereggen H, Joerg P, Zemp M (2013) Methodological approaches to infer end-of-winter snow distribution on alpine glaciers. Journal of Glaciology 59:1047–1059, DOI 10.3189/2013JoG13J015

Sold L, Huss M, Eichler A, Schwikowski M, Hoelzle M (2015) Unlocking annual firn layer water equivalents from ground-penetrating radar data on an alpine glacier. The Cryosphere 9(3):1075–1087, DOI 10.5194/tc-9-1075-2015

Sold L, Huss M, Machguth H, Joerg PC, Leysinger Vieli G, Linsbauer A, Salzmann N, Zemp M, Hoelzle M (2016) Mass balance re-analysis of findelengletscher, switzerland; benefits of extensive snow accumulation measurements. Frontiers in Earth Science 4:18

Sorg A, Bolch T, Stoffel M, Solomina O, Beniston M (2012) Climate change impacts on glaciers and runoff in tien shan (central asia). Nature Climate Change 2(10):725–731, DOI 10.1038/nclimate1592

Sorg A, Huss M, Rohrer M, Stoffel M (2014) The days of plenty might soon be over in glacierized central asian catchments. Environmental Research Letters 9(10):4018, DOI 10.1088/1748-9326/9/10/104018

Stocker TF, Qin D, Plattner GK, Tignor M, Allen SK, Boschung J, Nauels A, Xia Y, Bex B, Midgley B (2013) Ipcc, 2013: climate change 2013: the physical science basis. contribution of working group i to the fifth assessment report of the intergovernmental panel on climate change

Straub J (2012) Cubesats: A low-cost, very high-return space technology. In: Proceedings of the 2012 Reinventing Space Conference

Stumm D (2011) The mass balance of selected glaciers of the Southern Alps in New Zealand. PhD thesis

Surazakov A, Aizen V (2006) Estimating volume change of mountain glaciers using SRTM and map-based topographic data. IEEE Geoscience and Remote Sensing Letters 44(10):2991–2995

Suslov V, Akbarov A (1973) Hydrological regime of glaciers in the Alay Range, Central Asia. In: Symposium on the hydrology of glaciers, International Union of Geodesy and Geophysics International Association of Scientific Hydrology Commission of Snow and Ice, vol 95, pp 235–238

Suslov V, Akbarov A, Yemelyanov J (1980) Abramov glacier. Hydrometeoizdat, Leningrad

Takeuchi N, Fujita K, Aizen VB, Narama C, Yokoyama Y, Okamoto S, Naoki K, Kubota J (2014) The disappearance of glaciers in the tien shan mountains in central asia at the end of pleistocene. Quaternary Science Reviews 103:26–33

Tang Z, Wang X, Wang J, Wang X, Li H, Jiang Z (2017) Spatiotemporal variation of snow cover in tianshan mountains, central asia, based on cloud-free modis fractional snow cover product, 2001–2015. Remote Sensing 9(10):1045

Tangborn W (1999) A mass balance model that uses low-altitude meteorological observations and the area–altitude distribution of a glacier. Geografiska Annaler: Series A, Physical Geography 81(4):753–765

Tangborn WV, Fountain AG, Sikonia WG (1990) Effect of area distribution with altitude on glacier mass balance–a comparison of north and south klawatti glaciers, washington state, usa. Annals of Glaciology 14:278–282

Tarboton D, Chowdhury T, Jackson T (1995) A spatially distributed energy balance snowmelt model. In: Tonnessen K, Williams M, Tranter M (eds) Biogeochemistry of seasonally snow-covered catchments, Proceedings of a Boulder Symposium, IAHS Publication number 228, pp 141–155

Tawde SA, Kulkarni AV, Bala G (2017) An estimate of glacier mass balance for the chandra basin, western himalaya, for the period 1984–2012. Annals of Glaciology pp 1–11

Thakur PK, Aggarwal S, Arun G, Sood S, Kumar AS, Mani S, Dobhal D (2017) Estimation of snow cover area, snow physical properties and glacier classification in parts of western himalayas using c-band sar data. Journal of the Indian Society of Remote Sensing 45(3):525–539

Thibert E, Vincent C (2009) Best possible estimation of mass balance combining glaciological and geodetic methods. Annals of Glaciology 50(50):112–118

Thibert E, Blanc R, Vincent C, Eckert N (2008a) Instruments and methods glaciological and volumetric mass-balance measurements: error analysis over 51 years for glacier de sarennes, french alps. Journal of Glaciology 54:522–532

Thibert E, Vincent C, Blanc R, Eckert N (2008b) Glaciological and volumetric mass balance measurements: an error analysis over 51 years, sarennes glacier, french alps. Journal of Glaciology 50(186):522–532

Toutin T (2004) Geometric processing of remote sensing images: models, algorithms and methods. International journal of remote sensing 25(10):1893–1924

Treichler D, Kääb A (2017) Snow depth from icesat laser altimetry—a test study in southern norway. Remote Sensing of Environment 191:389–401

Trenberth K, Stepaniak D, Hurrell J, Fiorino M (2001) Quality of reanalyses in the tropics. Journal of Climate 14:1499–1510, DOI 10.1175/1520-0442

Trusel LD, Frey KE, Das SB, Karnauskas KB, Munneke PK, Van Meijgaard E, Van Den Broeke MR (2015) Divergent trajectories of antarctic surface melt under two twenty-first-century climate scenarios. Nature Geoscience 8(12):927

Tuffen H, Pinkerton H, McGarvie D, Gilbert J (2002) Melting of the glacier base during a small-volume subglacial rhyolite eruption: evidence from bláhnúkur, iceland. Sedimentary Geology 149(1-3):183–198

Turpin O, Ferguson R, Clark C (1997) Remote sensing of snowline rise as an aid to testing and calibrating a glacier runoff model. Physics and Chemistry of the Earth 22(3-4):279–283

Unger-Shayesteh K, Vorogushyn S, Farinotti D, Gafurov A, Duethmann D, Mandychev A, Merz B (2013) What do we know about past changes in the water cycle of central asian headwaters? a review. Global and Planetary Change 110:4–25, DOI 10.1016/j.gloplacha.2013.02.004

Ushnurtsev S (1991) Mass balance fluctuations of the sary-tor glacier in inner tien shan and its reconstruction for the period 1930–1988. Data Glaciol Stud 71:70–79

Van Pelt W, Oerlemans J, Reijmer C, Pohjola V, Pettersson R, Van Angelen J (2012) Simulating melt, runoff and refreezing on nordenskiöldbreen, svalbard, using a coupled snow and energy balance model. The Cryosphere 6(3):641–659

Van Pelt W, Kohler J, Liston G, Hagen JO, Luks B, Reijmer C, Pohjola VA (2016) Multidecadal climate and seasonal snow conditions in svalbard. Journal of Geophysical Research: Earth Surface 121(11):2100–2117

Varis O (2014) Curb vast water use in central asia. Nature 514(7520):27–30

Vermote E, Justice C, Claverie M, Franch B (2016) Preliminary analysis of the performance of the landsat 8/oli land surface reflectance product. Remote Sensing of Environment 185:46–56

Vincent C (2002) Influence of climate change over the 20th century on four french glacier mass balances. Journal of Geophysical Research: Atmospheres 107(D19)

Voloshina A (1988) Climate and meteorological features of glacier covered area in the Akshiirak massif. Data of Glaciological Studies 62:184–193

Vuille M, Kaser G, Juen I (2008) Glacier mass balance variability in the cordillera blanca, peru and its relationship with climate and the large-scale circulation. Global and Planetary Change 62(1-2):14–28

Wagnon P, Ribstein P, Kaser G, Berton P (1999) Energy balance and runoff seasonality of a bolivian glacier. Global and planetary change 22(1-4):49–58

Wang P, Li Z, Li H, Wang W, Yao H (2014a) Comparison of glaciological and geodetic mass balance at urumqi glacier no. 1, tian shan, central asia. Global and Planetary Change 114:14–22

Wang Q, Yi S, Chang L, Sun W (2017) Large-scale seasonal changes in glacier thickness across high mountain asia. Geophysical Research Letters

Wang S, Zhang M, Pepin N, Li Z, Sun M, Huang X, Wang Q (2014b) Recent changes in freezing level heights in high asia and their impact on glacier changes. Journal of Geophysical Research (Atmospheres) 119:1753–1765, DOI 10.1002/2013JD020490

Warren SG (1982) Optical properties of snow. Reviews of Geophysics 20(1):67–89

Westoby M, Brasington J, Glasser N, Hambrey M, Reynolds J (2012) 'structure-from-motion'photogrammetry: A low-cost, effective tool for geoscience applications. Geomorphology 179:300–314

WGMS (1993) Fluctuations of Glaciers 1985-1990, Fluctuations of Glaciers, vol VI. IAHS (ICSI), UNEP, UNESCO, Zürich

WGMS (2001) Glacier mass balance bulletin no. 6, Glacier Mass Balance Bulletin, vol 6. IAHS(ICSI) / UNEP / UNESCO / WMO, World Glacier Monitoring Service, Zürich

WGMS (2005) Fluctuations of Glaciers, 1995–2000, Vol. VIII. Tech. rep., IAHS(ICSI)–UNEP–UNESCO, World Glacier Monitoring Service, Zurich, Switzerland

WGMS (2012) Fluctuations of Glaciers, 2005–2010, Vol. X. Tech. rep., ICSU(WDS)/ IUGG(IACS)/ UNEP/UNESCO/ WMO, World Glacier Monitoring Service, Zurich, Switzerland, DOI 10.5904/wgms-fog-2012-11

WGMS (2013) Glacier mass balance bulletin no. 12, Glacier Mass Balance Bulletin, vol 12. ICSU (WDS) / IUGG(IACS) / UNEP / UNESCO / WMO, World Glacier Monitoring Service, Zürich, DOI 10.5904/wgms-fog-2013-11

WGMS (2017) Global Glacier Change Bulletin No. 2 (2014-2015), Global Glacier Change Bulletin, vol 2. ICSU (WDS) / IUGG(IACS) / UNEP / UNESCO / WMO, World Glacier Monitoring Service, Zürich, DOI doi:10.5904/wgms-fog-2017-10

Williams RS, Hall DK, Benson CS (1991) Analysis of glacier facies using satellite techniques. Journal of Glaciology 37(125):120–128

Winsvold SH, Andreassen LM, Kienholz C (2014) Glacier area and length changes in norway from repeat inventories. The Cryosphere 8:1885–1903

Winsvold SH, Kääb A, Nuth C (2015) Regional glacier mapping from time-series of landsat type data. In: Analysis of Multitemporal Remote Sensing Images (Multi-Temp), 2015 8th International Workshop on the, IEEE, pp 1–4

Winsvold SH, Kääb A, Nuth C, Andreassen LM, van Pelt WJ, Schellenberger T (2018) Using sar satellite data time series for regional glacier mapping. The Cryosphere 12(3):867

WMO (1997a) GCOS/GTOS Plan for terrestrial climate related observations, vol 796. World Meteorological Organization, Geneva

WMO (1997b) GHOST Global Hierarchical Observing Strategy, vol 862. World Meteorological Organization, Geneva

WMO (2010) Implementation plan for the global observing system for climate in support of the UNFCCC (2010 update), vol 1523. World Meteorological Organization, Geneva

Woodward J, Sharp M, Arendt A (1997) The influence of superimposed-ice formation on the sensitivity of glacier mass balance to climate change. Annals of Glaciology 24:186–190

Wu L, Li H, Wang L (2011) Application of a degree-day model for determination of mass balance of urumqi glacier no. 1, eastern tianshan, china. Journal of Earth Science 22(4):470–481, DOI 10.1007/s12583-011-0201-x

Wu Y, He J, Guo Z, Chen A (2014) Limitations in identifying the equilibrium-line altitude from the optical remote-sensing derived snowline in the tien shan, china. Journal of Glaciology 60(224):1093, DOI 10.3189/2014JoG13J221

Yao T, Thompson L, Yang W, Yu W, Gao Y, Guo X, Yang X, Duan K, Zhao H, Xu B, et al (2012) Different glacier status with atmospheric circulations in tibetan plateau and surroundings. Nature climate change 2(9):663

Yemelyanov Y (1973) Accumulation, ablation and run-off on Lednik Abramov (Alay range, USSR). In: Symposium on the hydrology of glaciers, International Union of Geodesy and Geophysics International Association of Scientific Hydrology Commission of Snow and Ice, vol 95, p 239

Young G (1981) The mass balance of peyto glacier, alberta, canada, 1965 to 1978. Arctic and Alpine Research pp 307–318

Zemp M, Hoelzle M, Haeberli W (2007) Distributed modelling of the regional climatic equilibrium line altitude of glaciers in the european alps. Global and Planetary Change 56(1-2):83–100

Zemp M, Thibert E, Huss M, Stumm D, Denby CR, Nuth C, Nussbaumer S, Moholdt G, Mercer A, Mayer C, et al (2013) Reanalysing glacier mass balance measurement series. The Cryosphere 7(4):1227–1245

Zemp M, Armstrong R, Gärtner-Roer I, Haeberli W, Hoelzle M, Kääb A, Kargel J, Khalsa S, Leonard G, Paul F, Raup B (2014) Introduction: Global glacier monitoring—a long-term task integrating in situ observations and remote sensing. In: Global Land Ice Measurements from Space, Springer, pp 1–21, DOI 10.1007/978-3-540-79818-7_1

Zemp M, Frey H, Gärtner-Roer I, Nussbaumer SU, Hoelzle M, Paul F, Haeberli W, Denzinger F, Ahlstrøm AP, Anderson B, et al (2015) Historically unprecedented global glacier decline in the early 21st century. Journal of Glaciology 61(228):745–762

Zhang Q, Kang S (2017) Glacier snowline altitude variations in the pamirs, tajikistan, 1998-2013: insights from remote sensing images. Remote Sensing Letters 8(12):1220–1229

Zhang Y, Liu S, Xie C, Ding Y (2006) Application of a degree-day model for the determination of contributions to glacier meltwater and runoff near keqicar baqi glacier, southwestern tien shan. Annals of Glaciology 43(1):280–284

Zhu Z, Woodcock CE (2012) Object-based cloud and cloud shadow detection in landsat imagery. Remote sensing of environment 118:83–94

Zhu Z, Wang S, Woodcock CE (2015) Improvement and expansion of the fmask algorithm: Cloud, cloud shadow, and snow detection for landsats 4–7, 8, and sentinel 2 images. Remote Sensing of Environment 159:269–277

Part III

Appendix

Appendix A

Supplementary Material

Apart of the measurements and research accomplished in direct relation to the objectives of this thesis, a range of supplementary surveys and studies enriching the glacier monitoring in Central Asia have been attained through collaborative efforts with different scientists and research institutions within the framework of the CATCOS, CAWa and CICADA projects. A short summary and a link to the leading scientists or connected publications can be found hereafter. First, studies related to the glaciological measurement programme of the aforementioned projects that led to two additional peer-reviewed publications are summarized. Secondly, a brief description on unpublished materials on glacier mass balance surveys as well as on other variables of the conducted cryospheric research follows. A data is available at the Department of Geoscience at the University of Fribourg.

A.1 Mass Balance reconstruction for Glacier No. 354, Tien Shan, from 2003 to 2014

Kronenberg, Marlene, **Martina Barandun**, Martin Hoelzle, Matthias Huss, Daniel Farinotti, Erlan Azisov, Ryskul Usubaliev, Abror Gafurov, Dmitry Petrakov, and Andreas Kääb. *"Mass-balance reconstruction for Glacier No. 354, Tien Shan, from 2003 to 2014."* Annals of Glaciology 57, no. 71 (2016): 92-102.

The article presents an analysis and reconstruction of the seasonal SMB of Glacier No. 354 from 2003 to 2014 following the strategy presented in Paper I by combining glaciological modelling and various in situ and remotely acquired data. A distributed accumulation and TI-model was calibrated with direct measurements collected from 2011 to 2014. A detailed winter accumulation survey from May 2014 was used for parameter optimization purposes, and to deduce detailed snow distribution patterns. SMB time series from 2003 to 2010 were reconstructed using the calibrated model.

The observed snow cover depletion pattern using satellite imagery provided additional independent information on the dynamics of mass change throughout the melting season. Two DEMs derived from high-resolution satellite stereo images acquired in 2003 and 2012 were used to calculate glacier volume change for the corresponding period. The modelled results showed good agreement with (1) independent geodetic ice volume changes and (2) observations of the SCAF throughout the melting season based on Landsat imagery. For the period 2003 to 2014, a modelled cumulative SMB of -0.43 ± 0.09 m w.e. yr^{-1} was found. A similar mass loss was deduced from the independent geodetic method. By combining in situ glaciological observations and geodetic surveys with modelling it was possible to downscale the decadal mass loss to modelled daily time series. Such increased temporal resolution helps to track inter-annual to seasonal changes of the SMB and to address the underlying processes in more detail.

A.2 Mass balance observations and reconstruction for Batysh Sook Glacier, Tien Shan, from 2004 to 2016

Kenzhebaev, Ruslan, **Martina Barandun**, Marlene Kronenberg, Yaning Chen, Ryskul Usubaliev, and Martin Hoelzle. *"Mass balance observations and reconstruction for Batysh Sook Glacier, Tien Shan, from 2004 to 2016."* Cold Regions Science and Technology 135 (2017): 76-89.

The paper examines the measured annual SMBs of Batysh Sook for the period 2011 to 2016 using three different methods. The profile method, the contour-line method and a model-based extrapolation approach were used to obtain glacier-wide SMB from in situ point measurements. The suitability of the different methods in the context of the Central Asian monitoring program was evaluated. Further, the seasonal SMB from 2004 to 2010 for Batysh Sook was reconstructed. Similarly to Paper II, a distributed mass balance model was calibrated with annual glaciological measurements from 2011 to 2016 and used for the reconstruction. Sub-seasonal model performance was validated based on the TSL observed on satellite images during the summer months from 2004 to 2016.

For Batysh Sook an average annual mass balance of -0.39 ± 26 m w.e. yr^{-1} was found for the period 2004 to 2016. The reconstructed cumulative surface mass balance is in agreement with several remote sensing studies, which report an overall mass loss for glaciers in the Tien Shan, and thus delivered support for the indicated imbalance of glaciers in the region.

Especially at the beginning of the re-established mass balance monitoring program, deviations between the different extrapolation methods were important with a range of 0.40 m w.e. yr^{-1}. With the improvement of the measurement network in consecutive years, the results showed better conformity (range of 0.10 to 0.22 m w.e. yr^{-1}). Overall, all three methods agreed within their uncertainty range. The profile method was judged the least suitable and most sensitive to a limited stake network. The contour-line method proofed particularly beneficial due to its straightforwardness without losing the competence of involving expert knowledge to integrate unmeasured spatial patterns. The model-based extrapolation was less user-friendly, however brought the advantage to increase the temporal resolution and allowed, once calibrated, reconstructing the past SMBs.

This study provided a further step toward a comprehensive glacier monitoring program, helped to increase the understanding of glacier response to climate change for a data-sparse region and marked an important achievement for the capacity building and twining component of the CATCOS project.

A.3 Mass balance reconstruction for Golubin Glacier, Tien Shan, from the early 20th century to present

Azisov, Erlan, **Martina Barandun**, Saks Tomas, Esenamanov Muhammed, Vorogushyn Sergiy, Martin Hoelzle and Ryskul Usubaliev *"Mass balance reconstruction for Golubin Glacier, Tien Shan, from the early 20th century to present"*, (in preparation)

Following the outlined strategies in Paper I and the work accomplished in Paper II, this study aims on the combination of an extensive historical mass balance series of Golubin with the data collected since the re-establishment of the monitoring network in 2010. Similarly, to the aforementioned publications on Glacier No. 354 and Batysh Sook a distributed accumulation and TI-model has been used to analyse existing point measurements and to reconstruct the SMBs back to the early 20th century. Meteorological measurements are available from a close by meteorological station from 1980 to present, and seasonal mass balances are provided by the WGMS from 1969 to 1994. Front variation measurements reach back to the late 19th century. The measured meteorological data was used to adjust climate Reanalysis datasets and to run the mass balance model. The adjusted Reanalysis data cover the period from 1900 to 2010. The modelled seasonal mass balances were compared to the historical mass balance observations and the model parameters underwent a second-order adjustment if necessary. The re-calibrated model was applied to provide daily mass balance series from 1900 to present (Fig. A.1).

Secular mass balances from length change, as well as TSL observations and available geodetic mass balances were used for validation. Golubin lost $-0.17 \pm 45\,\mathrm{m\,w.e.\,yr^{-1}}$ for the entire period of 1901-2016. Mass loss increased in the second half of the century with an average mass balance of $-0.21 \pm 42\,\mathrm{m\,w.e.\,yr^{-1}}$ from 1950-2018 with the most negative value simulated for 2008. Direct measurements for the past decade confirm this tendency with a mass loss of $-0.28 \pm 17\,\mathrm{m\,w.e.\,yr^{-1}}$ (2011-2018). Comparison with long-term mass balance measurements from glaciers located in the Kyrgyz Tien Shan and Pamir show similar values and interannual variability since the early 1960 to present.

With this study, a unique, almost 100 year-long mass balance time series for Golubin glacier on daily resolution, combining meteorological re-analysis data, modern and historical glaciological measurements as well as length change observations was provided. Such data sets are sparse for the Tien Shan, however are indispensable to enhance our understanding on the glacier changes of High Mountain Asia.

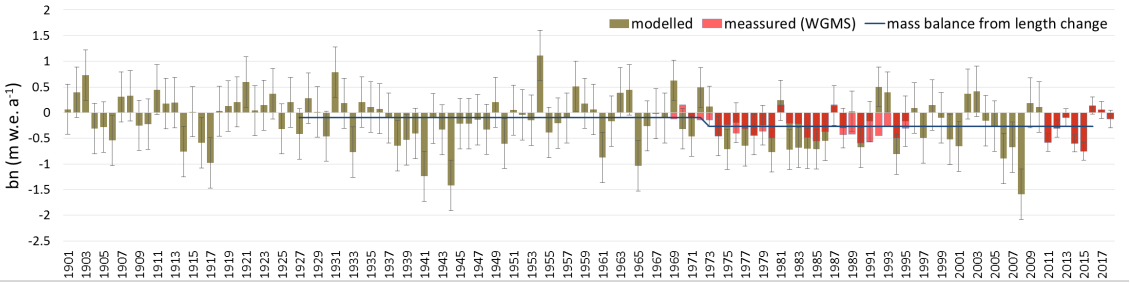

Figure A.1: Reconstruction and re-analysis of mass balance of Golubin Glacier from 1901 to 2018. Modelled mass balance is compared to geodetic estimates based on Bolch (2015) and on Barandun et al (2018) as well as to historical and modern glaciological measurements and secular mass balances derived from length change observations.

A.4 Mass balance monitoring on Glacier No. 599 and Glacier No. 182

Mass balance monitoring was initiated on Glacier No. 599 located in the Issyk Kuul range in 2015 (Fig. A.7) and on Glacier No. 182 situated in the At-Bashy range in 2017 through independent efforts of local scientists of the CAIAG institute, and partly in cooperation with international institutions. The monitoring programs are subject of two Kyrgyz PhD Thesis with focus to apply the collected baseline data in the sector of water resource management. The local scientists have been trained within the framework of the CATCOS and CICADA projects, and submit regularly and independently the collected data to the WGMS. Data analysis of the glaciological measurements, as well as related research is carried out under close support of scientists from the University of Fribourg. The monitoring strategy follows the recommendation outlined in Paper I and aims at combining direct glaciological measurements with geodetic mass change assessments and numerical modelling.

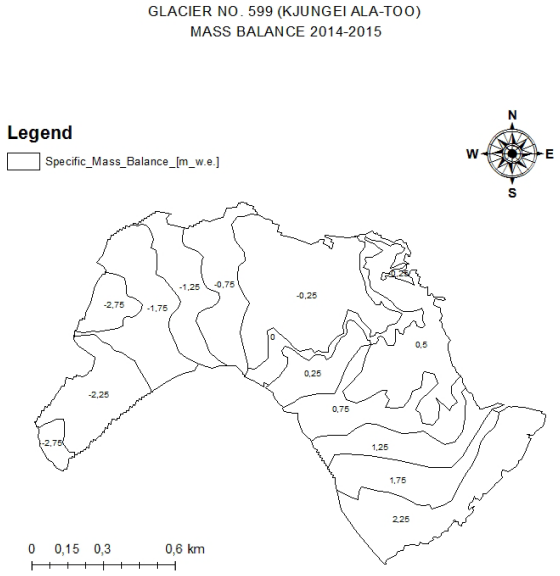

Figure A.2: Overview of the measured network established at Glacier No. 599 in 2015 (*Image Courtesy: Erlan Azisov)*.

A.5 Further research

A.5.1 Surface elevation point measurements

Measurement positioning systems during the Soviet Union relate to a local, independent coordinate system. Thereby, a triangulation network was measured with theodolites to assign x, y and z coordinates to each point of interest, such as the in situ measurements on the glacier surface. These surveys were regularly repeated during the station operation. Data is available for Abramov Glacier from 1986 and 1998 for most of the ablation stakes (in total 166) of the monitoring network. To relate the historical data to the modern measurement locations a transformation to a global coordinate system was necessary. During the field campaign on Abramov in 2014, six reference points on stable ground distributed on the orographic right flank of the glacier, for which the coordinates of the local system were available, have been re-measured with a TopCon Differential Global Positioning System (dGPS). During summer 2015, an additional set of reference points were measured with a Trimble device. During this survey an extended set of measurement profiles on the glacier surface, approximating the historical measurement network locations was carried out with a three-fold aim: (1) a better georeferencing of the theodolite surveys, (2) the validation of the DEM derived from a simultaneously recorded Pleiades stereo-pair (Fig. A.3) and (3) comparison of the dataset to the theodolite measurements to detect a possible elevation change.

A range of unpublished results emerged from combining the historical and modern positioning surveys. After an improved georeferencing, the theodolite measurements have been compared to evaluate the quality of a manually digitized topographic map acquired in 1986 which was used to calculate the geodetic mass balance through DEM differencing with the SRTM DEM (Fig. A.4). A mass loss of -0.33 ± 0.20 m w.e. yr^{-1} was detected for Abramov from 1986 to 2000. Additionally, a plausibility analysis of the penetration depth correction for the SRTM used for Abramov provided in (Gardelle et al, 2013) was examined

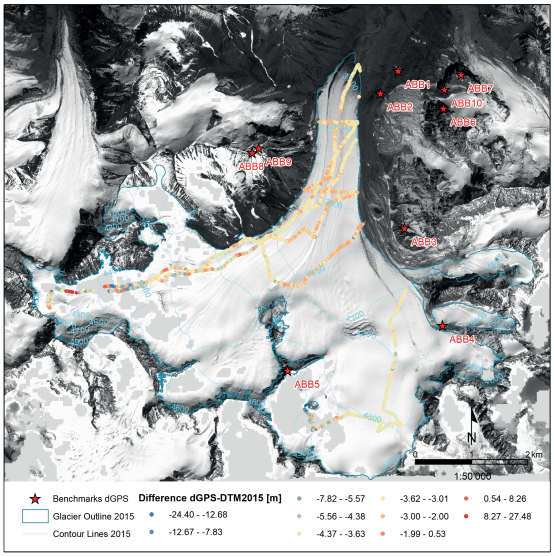

Figure A.3: Overview of the measured reference points on stable ground (red stars) and dGPS measurement profiles on the glacier surface. The coloured points indicate the difference to the DEM produced from a Pleiades stereo-pair. A mean deviation of 0.35 m was found off-glacier and of ≈3 m on glacier (*Image Courtesy: Florian Denzinger)*.

through comparison with the point elevation measurements from 1998. However clear statements were impeded through the time difference in acquisition and the uncertainties in the georeferencing of the point data.

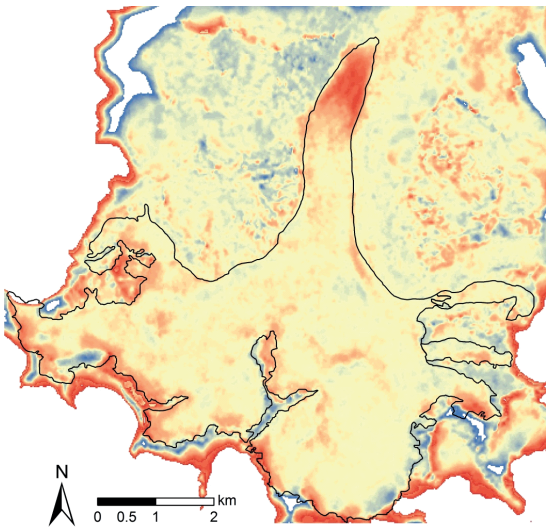

Figure A.4: Geodetic mass balance derived from a corrected topographic map with theodolite measurements and the SRTM DEM (corrected for a C-band penetration depth of 5 m after (Kääb et al, 2015).

A.5.2 Structure-from-Motion using historical aerial images to analyse changes in surface elevation and volume on Abramov Glacier, Kyrgyzstan

Denzinger, Florian. *"Structure from Motion using historical aerial images to analyse changes in surface elevation and volume on Abramov Glacier, Kyrgyzstan"*. MSc Thesis, Department of Geography, University of Zurich, Switzerland and Department of Geology, (2018): 85pp.

Within the framework of a Master Thesis, previously unreleased Soviet aerial imagery was processed using SfM to derive high-resolution DEMs for the years 1975 and 1986. Volume and area changes were detected through comparison to a high-resolution DEM from 2015 based on a Pleiades Stereo-pair. Area loss of 8.18% and a mean annual thickness change of -0.41 ± 0.01 m yr^{-1} were detected over the period 1975 to 2015. The results suggest a considerable loss in volume (-0.43 ± 0.08 km^3) and mass (-0.36 ± 0.07 m w.e. yr^{-1}) and are in the same order of magnitude as glaciological mass balance time series (Fig. A.5). The aerial photographs represent a unique and extremely valuable dataset to detect multi-decadal mass changes for over four decades, and provide an independent source for a multi-level strategy for long-term glacier monitoring. During the Soviet Union, exhaustive airborne survey campaigns to reach territory-wide coverage on semi- to decadal repeat cycles were conducted. Today the data is mostly under restricted access or lost. However, a similar dataset is available for Golubin but has not yet been processed.

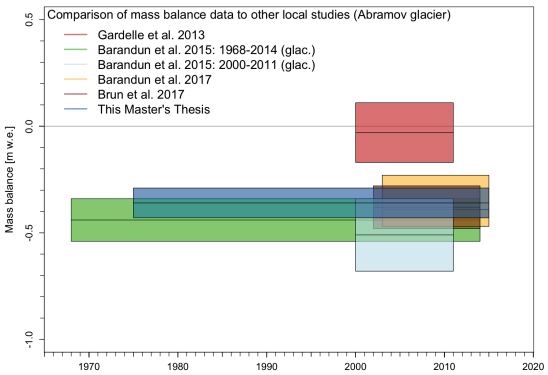

Figure A.5: Comparison between mass balance estimates for Abramov Glacier based on different studies and methods (*Image Courtesy: Florian Denzinger)*.

A.5.3 Firn and ice temperature measurements

Detailed firn information available for Abramov from the 1970s indicated a polythermal state of the glacier (Kislov and Nozdryukhin, 1975; Suslov et al, 1980). Firn temperatures below 0° C enable refreezing in the firn and snowpack that can contribute significantly to the mass balance of a glacier. In 2013, two thermistor chains were installed approximately at the location of the historical firn observation sites at an elevation of 4250 m a.s.l. and 4410 m a.s.l., respectively (Fig. 6.3). The firn temperature was converted from annually repeated resistivity measurements. The upper chain was lost in 2015 and no measurements

are available for 2014 for both chains. Both chains indicated close to zero temperatures throughout the firn profile below the seasonal horizon (Fig. A.6) and preliminary results from recent GPR measurements and firn core analysis indicate temperate conditions (personal communication M. Kronenberg, H. Machguth and I. Lavrentiev). A change in firn structure is thus likely to have occurred during the past four decades and will be investigated in detail within the framework of the project "Changing glacier firn in Central Asia and its impact on glacier mass balance", grant 169453 (SNFS). An additional thermistor chain has been installed at the tongue Batysh Sook and delivers continuous measurements of cold ice since 2013 (Fig. A.7).

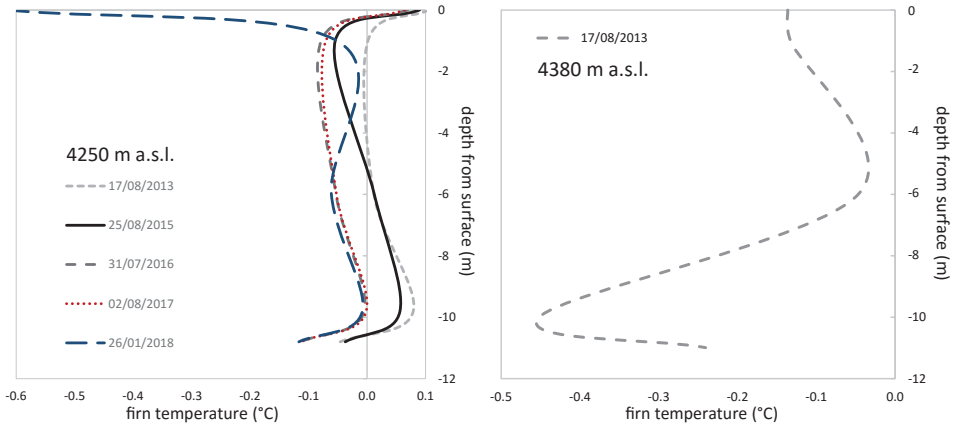

Figure A.6: Firn temperature measurements at two locations in the accumulation area at Abramov. (a) Firn temperatures below the surface measurements approximate 0° C. Measurements indicating higher temperatures than 0° C are most likely associated to a measurement error in earlier years. (b) the firn temperature measured in summer shows the penetration of the winter cold in about 10 m depth but temperature do not decrease to lower than -0.50° C.

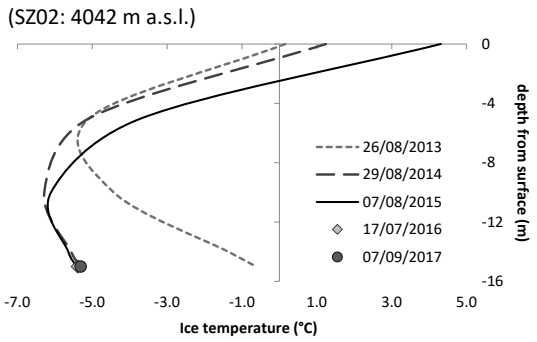

Figure A.7: Ice temperature measurement at the tongue of Batysh Sook indicate clearly a cold glacier tongue.

A.5.4 Ground surface temperature measurements

A collection of temperature loggers (i-Buttons) have been distributed at the location of the modern AWS at Abramov and on the side moraines and rock walls at Golubin. The data has been collected annually and confirmed the presence of permafrost (Fig. A.8).

Additional measurements have been carried out at the location of four ablation stakes on debris covered sections on Abramov (Fig. 6.3). Temperature measurements were accomplished at the ice-debris interface and at the debris-air interface if possible (Fig. A.9).

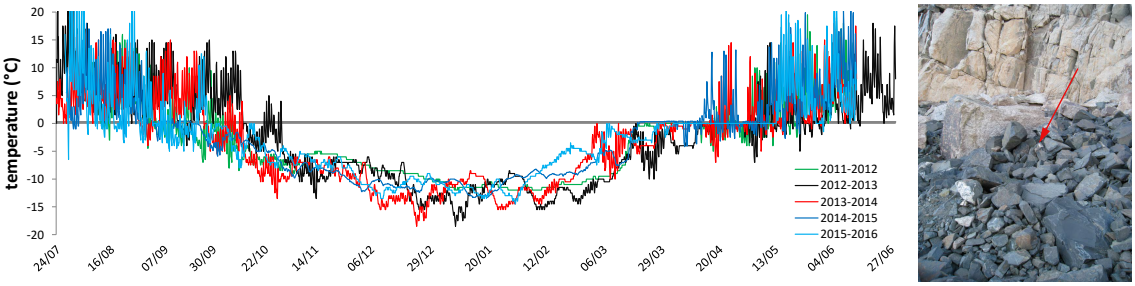

Figure A.8: Example of ground surface temperature measured on the side moraine of Golubin from 2011 to 2016. The location of the i-button is indicated in the photo.

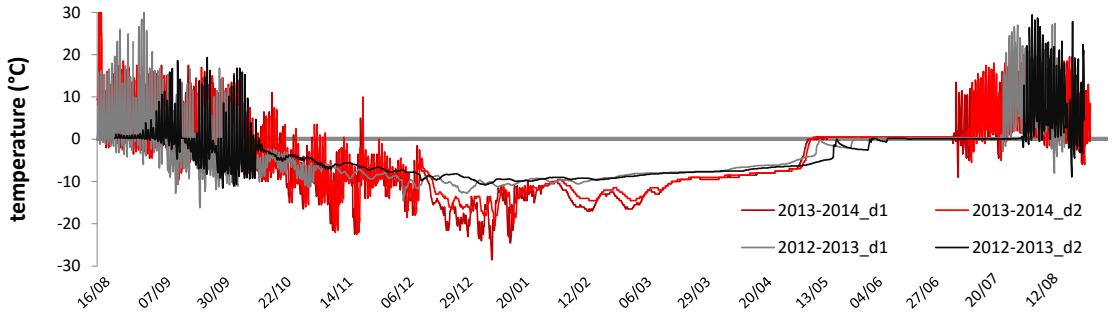

Figure A.9: Example of temperature measurement at the location of the stakes installed on the debris covered part at Abramov (see Fig. 6.3 (deb. 1)) at the ice-debris interface (d1) and the debris-air interface (d2).

A.5.5 Evaluation of snow avalanches contribution into glacier accumulation

Lazarev, Anton. *"Evaluation of snow avalanche contribution into glacier accumulation estimate"*, BsC Thesis, Faculty of Geography, Lomonosov Moscow State University, Moscow, Russian Federation, (2017).

In summer 2016, an UAV survey on Batysh Sook Glacier aimed on the creation of a precise DEM for a glacier for which until today only limited high-resolution satellite images are available. The survey was conducted under joint efforts with the University of Central Asia, the CAIAG, the Eidgenössische Forschungsanstalt für Wald, Schnee und Landschaft (WSL), the Moscow State University and the Kyrgyz National University. After standard data processing, a 0.5 m resolution DEM with a standard deviation of 0.2 m to the measured ground control points was produced (unpublished results by: Saskia Gindraux, WSL, Switzerland; Fig. A.10).

The data was used in combination with detailed snow depth surveys, glaciological measurements and a numerical model to evaluate the avalanche contribution to the total mass balance of Batysh Sook for the balance year 2016 (Lazarev and Y, 2018). The study has been conducted within the framework of a Bachelor thesis at the Lomonosov Moscow State University. The estimated total volume of avalanche drifted snow deposited was estimated to 75,000 m^3 and the snow avalanche accumulation was found to contribute with 13 $\pm$4% to the total accumulation of the glacier for the season 2015/2016 (Lazarev and Y, 2018).

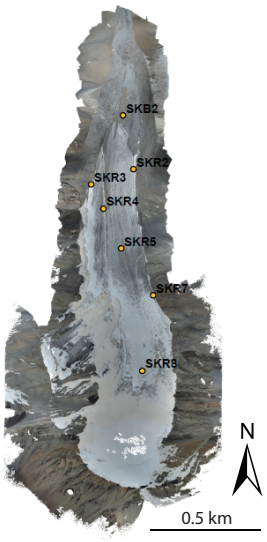

Figure A.10: Orthoimage derived from UAV survey on Batysh Sook in 2016. Points indicate ground control point locations. (*Image Courtesy: Saskia Gindraux)*

A.5.6 Surface reflectance and albedo measurements

During summer 2015, NADIR measurements of pure surface materials were obtained using an ASD FieldSpec Pro (Analysis Spectral Device, Boulder, USA) field spectrometer to compile a site-specific spectral library for Glacier No. 354 with the aim of comparison to historical data and for validation of remotely assessed albedo values. The field spectrometer, measuring in the spectral range between 350–2500 nm, has a spectral sampling interval of 1.4 nm (350–1000 nm) and 2 nm (1000–2500 nm), and a full width half maximum of 3 nm at 700 nm and 10 nm at 1400 nm (Naegeli et al, 2015). In total, 14 targets in the glacier forfield and on the lower most glacier tongue were measured using a standard measurement procedure of 5 white reference measurements followed by 5x5 target measurements and again 5 white reference measurements. For each individual target, the 25 measurements were averaged to obtain a reference spectrum per target.

During joint field work, additional ground based albedo measurements have been carried out with a Sp Lite 2 Kipp & Zonen albedometer on Gl. 354 and Batysh Sook by scientists of the Faculty of Geography of the Moscow State University and the CAIAG who compared the measured data to albedo values assessed on Landsat scenes (Petrakov et al, in review). In combination with a model, the authors evaluated the albedo changes since the 1990s and detected possible technogenic impact due to nearby mining activities.

They did not observe a decrease of glacier albedo in the Akshiirak massif, however the possibility of albedo reduction in local spots of reduced area cannot be ruled out.

A.5.7 Constraining hydrological model parameters using water isotopic compositions in a glacierized basin, Central Asia

He, Zhihua, Unger-Shayesteh Katy, Vorogushyn Sergiy, Gafurov Abor, Weise Stephan, Kalashnikova Olga, Duethmann Doris, **Barandun Martina**, Merz Bruno. *"Constraining hydrological model parameters using water isotopic compositions in a glacierized basin, Central Asia"*, Journal of Hydrology. (in review)

Consecutive sampling of streamflow at the Ala-Archa and Alplager hydrologic stations since 2013 and event groundwater, snow melt and glacier melt samples were collected in the melt season from August 2012 to March 2017 for water stable isotope analysis in the Ala Archa valley and on Golubin within the CAWa project. The data was used in combination with the glaciological measurements from Golubin Glacier and snow depletion patterns observed on MODIS to calibrate a hydrological model for runoff prediction of the Ala-Archa basin. The study is one of the first attempts to integrate the simulation of water stable isotopic composition into hydrological model in glacierised basins and showed promising results.

Appendix B

Curriculum Vitae

Personal details

Name:	Martina Barandun
Citizenship:	Swiss

Educational background

01/2014-present	**PhD student**, University of Fribourg, Department of Geosciences, Switzerland
01/2017-07/2017	**Research stay**, SNFS Mobility Grant, University of Oslo, Department of Physical Geography, Norway
04/2016	**Geoscience Communication School**, Castiglione del Lago, Italy supported by Marie Curie Alumni Association, European Geosciences Union, Agenzia Spaziale Italiana and AXA Research Fund
09/2011-07/2013	**Master of Science in Physical Geography** Global Change and Sustainability - Module in physical Geography, University of Fribourg, Department of Geosciences, Switzerland Thesis Supervision: Prof. Dr. Martin Hoelzle
19/2010-09/2011	**Universidad Nacional de España a Distancia (UNED)**, Department of Physics and Chemistry, Madrid, Spain

Fundamentos de Fisica I & II (12 ECTS)
Matematicas I & II (12 ECTS)

09/2005-04/2010 **Bachelor of Science in Geosciences**, University of Fribourg, Department of Geosciences, Switzerland
Degree: Major in Geography and Minor in Geology (bilingual: German/French)

08/2007-05/2008 **Exchange program (ERASMUS)**, University of Iceland, Department of Geology, Reykjavik, Iceland
Earth science program for foreign students; 2 semesters (66 ECTS)

Professional experience

01/2012-10/2013 **Scientific Under-Assistant**, University of Fribourg, Department of Geosciences, Switzerland
Main project: CATCOS,
http://www.meteoswiss.admin.ch/home/research-and-cooperation/international-cooperation/international-projects.subpage.html/en/data/projects/2011/catcos.html

01/2012-31/2012 **Scientific Under-Assistant**,University of Fribourg, Department of Geosciences, Switzerland
Main project: PERMOS Project, *http://www.permos.ch/*

01/2011-04/2011 **Scientific Internship in Glaciology**, Gateway Antarctica, University of Canterbury, Christchurch, New Zealand
Glaciology Group led by Dr. W. Rack

01/2010-06/2010 **Scientific Internship in Glaciology**, Centro de Estudios Científicos (CECS), Valdivia, Chile.
Glaciology and Climate Change Group led by Dr. A. Rivera

09/2009-11/2009 **Scientific Internship in Climate Science**, Laboratoire de la Glaciologie et Geophysique de l'Environnement (LGGE), Grenoble, France
Position: IPY CONCORDIASI project and Europe's FP7 ICE2SEA project , supervised by Dr. Ch. Genthon

09/2009-10/2009 **Scientific Research Assistant**, University of Fribourg, Department of Geosciences, Fribourg, Switzerland in cooperation with Mountain Railway Graechen, Wallis, Switzerland

02/2009-07/2009 **Internship at INTERGRAPH AG Switzerland**, Dietikon, Switzerland
Technical support and project managing

Teaching experience

Bachelor Level	**Quantitative Methods I**, University of Fribourg Exercises
CICADA/CATCOS	**Project management** for CATCOS and CICADA projects (http://www.unifr.ch/geoscience/geographie/en/research/integrated-themes/international-cooperation-capacity-building) **Summer School on Mass Balance** Measurements and Analysis in Central Asia **Supervision of Kyrgyz MSc and PhD students**
Master Level	**Excursion to Central Asia**, University of Fribourg **Guest lecture** at CAWa Summer School, Tashkent
others	**WINS** (Women in Science and Technology), University of Fribourg Leading of day-long stage for a group of female high school students

Appendix C

Personal Bibliography

As part of the Thesis

Barandun, M, McNabb, R, Naegeli, K, Huss, M, Berthier, E, Bunting P, and Hoelzle, M (in preparation). Region-wide estimate of annual glacier mass balance for the Tien Shan and Pamir Mountains, Frontiers in Earth Science.

Barandun, M, Huss, M, Berthier, E, Kääb, A, Azisov, E, Bolch, T, Usubaliev, R, and Hoelzle, M (accepted). Multi-decadal mass balance series of three Kyrgyz glaciers inferred from transient snowline observations, The Cryosphere.

Hoelzle, M, Azisov, E, **Barandun, M**, Huss, M, Farinotti, D, Gafurov, A, Hagg, W, Kenzhebaev, R, Kronenberg, M, Machguth, H, Merkushkin, A, Moldobekov, B, Petrov, M, Saks, T, Salzmann, N, Schöne, T, Tarasov, Y, Usubaliev, R, Vorogushyn, S, Yakvlev, Y and Zemp, M (2017). Re-establishing glacier monitoring in Kyrgyzstan and Uzbekistan, Central Asia. Geoscientific Instrumentation Methods and Data Systems, 6: 397-418.

Barandun, M, Huss, M, Sold, L, Farinotti, D, Azisov, E, Salzmann, N,Usuabliev, R, Merkushkin, A and Hoelzle, M (2015). Re-analysis of seasonal mass balance at Abramov glacier 1968-2014. Journal of Glaciology, 61(230), 1103-1117.

Others

Kenzhebaev, R, **Barandun, M**, Kronenberg, M, Yaning, C, Usubaliev, R, Hoelzle, M (2017). Mass balance observations and reconstruction for Batysh Sook Glacier, Tian Shan, from 2004 to 2015. Cold Regions Science and Technology, 135: 76–89

Kronenberg, M, **Barandun, M**, Hoelzle, M, Huss, M, Farinotti, D, Azisov, E, Usubaliev, R, Gafurov, A, Petrakov, D, and Kääb, A (2016). Mass-Balance Reconstruction for Glacier No. 354, Tien Shan, from 2003 to 2014. Annals of Glaciology, 57 (71): 92–102.

Conference abstracts

POLAR, Davos, Switzerland, 2018 (Talk)

Alpine Glaciology Meeting, Chamonix, France, 2018 (Talk)

Swiss Geoscience Meeting, Davos, Switzerland, 2017 (Poster)

Water Resources of Central Asia and Their Use, Almaty, Kazakhstan, 2016 (Talk)

XVI Glaciological Symposium, St. Petersburg, Russia, 2016 (Talk)

General Assembly European Geosciences Union (EGU) Conference, Vienna, Austria, 2016 (Poster)

Alpine Glaciology Meeting, Munich, Germany, 2016 (Poster)

Swiss Geoscience Meeting, Geneva, Switzerland, 2016 (Poster)

International Symposium on Glaciology in High Mountain Asia, Kathmandu, Nepal, 2015, (Poster, young scientist award)

Remote and Ground-based Earth Observations in Central Asia, Bishkek, Kyrgyzstan, (Talk)

General Assembly European Geosciences Union (EGU) Conference, Vienna, Austria, 2014 (Poster)

Swiss Geoscience Meeting, Fribourg, Switzerland, 2014 (Talk)

MountainHazards2013-Conference, Colpon Ata, Kyrgyzstan, 2013 (Talk)

Davos Atmosphere and Cryosphere Assembly DACA-13, Davos, Switzerland, 2013 (Talk).

General Assembly European Geosciences Union (EGU) Conference, Vienna, Austria, 2013 (Poster).

Snow and Ice Research Group (SIRG) NZ, Annual Workshop, Fox Glacier Township, New Zealand, 2012 (Talk).

International Polar Year Oslo Science Conference, Oslo, Norway, 2011 (Poster).